STRUCTURE - PROPERTY BEHAVIOR OF FREE RADICAL SYNTHESIZED POLYDIMETHYLSILOXANE-POLYSTYRENE BLOCK POLYMERS AND POLYTETRAMETHYLENEOXIDE BASED IONENE ELASTOMERS

by

Daan Feng

Dissertation submitted to the Faculty of the
Virginia Polytechnic Institute and State University
in partial fulfillment of the requirements for the degree of
DOCTOR OF PHILOSOPHY
in
Chemical Engineering

APPROVED:

Garth L. Wilkes, Chairman

Mark E. Davis

Wolfgang G. Glasser

James E. McGrath

James P. Wightman

April 1989

Blacksburg, Virginia

STRUCTURE - PROPERTY BEHAVIOR OF FREE RADICAL SYNTHESIZED POLYDIMETHYLSILOXANE-POLYSTYRENE BLOCK POLYMERS AND POLYTETRAMETHYLENEOXIDE BASED IONENE ELASTOMERS

by

Daan Feng

Garth L. Wilkes, Chairman

Chemical Engineering

(ABSTRACT)

Structure-property behavior of free radical synthesized polydimethylsiloxane (PDMS) - polystyrene and PDMS-styrene derivative block polymers have been studied. The block polymers were provided by Dr. J. V. Crivello from GE. Two different type of segmented polytetramethyleneoxide (PTMO) based ionene elastomers were also investigated. The PTMO-dihalide ionenes were obtained through the courtesy of Dr. C. M. Leir in 3M, while the PTMO-dipyridinium ionenes were synthesized by Dr. B. Lee in Prof. McGrath's research group at VPI&SU.

In the free radical synthesized PDMS-PS block polymers, the molecular weight (MW) and the molecular weight distribution (MWD) of the PS blocks varied with the PDMS block length (block MW) comprising the macroinitiators, and the styrene conversion level. As the PDMS block length or the conversion level increased, the average PS block MW increased, and the molecular weight distribution of the PS block became broader. Multi-modal molecular weight distribution of the PS blocks was observed on the high conversion polymers with large PDMS blocks. As the MW and the MWD of the PS blocks changed, the morphology, the degree of phase mixing, and bulk properties of these PDMS-PS block polymers were altered as expected.

At constant conversion level, the morphology of these block polymers changed from spherical PS domains in the PDMS matrix to a lamellar structure as the PDMS block length increased. As expected, their mechanical properties were also changed as morphology varied. At constant PDMS

content, the systems with shorter PDMS blocks displayed elastomeric properties, while the polymers having large PDMS blocks behaved like a plastic due to a continuous lamellar morphology. The degree of phase mixing also decreased with an increase of the PS block length because of the increased incompatibility between the two block components. For a constant PDMS block length, the PS block length increased and the MWD of the PS blocks became broader when the styrene conversion level increased. Consequently, the morphology, the degree of phase mixing as well as the bulk properties of the block polymer also varied with conversion level.

Addressing the segmented PTMO based ionene elastomers, these materials displayed excellent elastomeric properties which result from the ion clustering or ionic domain formation in a continuous PTMO matrix. The morphology and bulk properties of these ionene systems were strongly dependent on the strength of ionic association. By varying the ion content, the type of counter ion or hard segment, the ionic association was changed. Therefore, the morphology and the bulk properties were also altered. Morphological textures of these ionene systems were studied by Transmission Electron Microscopy (TEM) and Small Angle X-ray Scattering (SAXS). Due to the strong ion clustering, a ionene rod-like morphology was observed in the PTMO-dihalide ionene elastomers by both TEM and SAXS at low volume fraction of ionene content ($<$ 7 vol%). It is the first time that these two analytical methods have distinctly led to the same end result for any ionomer system! This morphological structure is not predicted by any of existing theories of ion clustering in ionomers nor the classical theories of block/segmented polymers. Finally, the morphology of these ionene systems was altered with ion content. When the ion content was decreased by increasing the PTMO segment length, the long range ordered structure disappeared as well as the rod-like microphase structure.

A very unique phenomenon, a highly reversible modulus "jump" with increasing temperature, has been observed for these ionene materials which has not been reported before. This "jump" is directly related to the ion content, type of counter ion and the hard segment. Based on experimental evidence, the "jump" is tentatively speculated to be caused by a conformational change in the ionene hard segments. However, further investigations are needed to support or disprove this speculation.

Dedicated to the memory of my mother

Mrs. Feng

Acknowledgements

I wish to express my sincere appreciation and deep gratitude to Professor Garth L. Wilkes for his guidance, support and understanding throughout the course of this dissertation. His energetic approach to research is something that I can only strive to achieve. It has been pleasure to work with him, and I look forward to our continuing friendship. I am also grateful to M.E. Davis, W.G.Glasser, J.E. McGrath, and J. P. Wightman for serving on my advisory committee.

I would like to thanks Dr. J. V. Crivello of RPI, Dr. C. M . Leir of 3M, and Dr. B. Lee of Mobay for providing the polymers utilized in this investigations and for very helpful discussions.

Dr. Chin Choi was very involved in the TEM studies of ionene elastomers. I am very grateful to her contributions, support and friendship.

My colleagues, and , have been very helpful in assistance and discussions in thermal analysis and x-ray scattering techniques.

was very helpful in assistance in TEM. Their assistance are certainly appreciated.

Deep appreciation also goes to all my colleagues and friends that made graduate school a wonderful experience.

My heartfelt thanks go to my parents, and , for their ever present love and support and for teaching me the value of education and how to conduct myself in society. My sisters, and , and their families have constantly taken care of my parents during the period of my study abroad, and my uncles and aunts, ; and , have also been very loving and supportive throughout this period, without their supports, I would not able to reach this personal milestone. I certainly appreciate their devotion. Finally, a special thank goes to for her love, support, and understanding.

Table of Contents

List of Illustrations

List of Tables

CHAPTER I

INTRODUCTION

The use of rubber can be traced back to the eleventh century. Since the industrial revolution in the end of the last century, rubber has become one of the most important industrial materials, especially today due to the widespread use of tires etc. Uncrosslinked rubbers or elastomers, both natural and synthetic, have poor mechanical properties, therefore, most rubber or elastomeric based products used today must be made into networks generally by chemically crosslinking (vulcanization). The vulcanization processes is a slow and irreversible process, thus, vulcanized rubber has a disadvantage that it can not be reprocessed again. One way to solve this problem is to develop a reversible network which yet still retain elastomeric behavior at the "use" temperature. Thermoplastic elastomers (TPE) are one of the solutions to this quest.

Since 1960's, numerous new TPE materials have been developed. These materials generally are block or segmented polymers. In only about three decades, block polymers have emerged from being laboratory curiosities to commercial products being produced at a rate of millions of tons per year. In 1987, the total consumption of rubber products was 11.4 million metric tons. Forty percent of this figure, or 4.1 million metric tons were block polymers. The meteoric rise in the production and utilization of block polymers has been due to the advances in polymer synthesis, which allow the creation of well-defined molecular structure, to new knowledge concerning the relation-

ships between polymer structure and properties, and to an improved understanding of how processing can be used as a tool to develop desirable morphological features.

Block polymers are polymers composed of two or more chemically distinguishable species having at least one long sequence of like monomer units attached to another sequence or block of different monomer units. There are four basic types of block polymers; diblock, triblock, multiblock, and star block polymers. Diblock polymers contain two segments or blocks only. Triblock polymers consist of three blocks with ABA, BAB, or ABC arrangements. Multiblock polymers or segmented polymers contain many blocks. but typically the degree of polymerization of the segments is low, i.e. 1 - 15 units. Finally, star or radial block polymers are polymers which have three of more diblock polymers coupled at a single or near single (core) junction point. The architecture of these four basic types of block polymers are shown in Figure 1 on page 3 where A and B denote chemically dissimilar repeat units.

The unique feature of block polymers is their development of a microphase separation morphology of the block or "segment" components at the service condition. It is widely accepted that the unique thermoplastic elastomeric behavior of block polymers (TPE) is directly related to their microphase separated structure. Due to this microphase separation, the block polymers have the ability to achieve a network structure by physical rather than chemical cross-linking. Thus, these materials can have elastomeric characteristics while retaining thermoplastic processibility. At the service temperature, one of the component is viscous or rubbery (soft segment) while the other is glassy or semicrystalline (hard segment). The hard segments associate to form hard domains which serve as a reinforcing filler and physical multifunctional crosslink sites. These sites are thermally reversible. Therefore, this type of phase separated system can be thermally processed at temperatures above the hard block T_g or T_m. However, only architectural forms that contain two or more hard blocks per polymer chain are capable of producing this physical network effect. Hence, all thermoplastic elastomeric block polymers are tri- or multi-block polymers[1].

To improve the subambient temperature properties of these phase separated block polymers, one way is to use a much lower T_g material as the soft segments to reduce the desired application temperature. In the past two decades, polydimethylsiloxane (PDMS) has received considerable

diblock polymer

AAAAAAAAAAAAA--BBBBBBBBBBBB

triblock polymer

AAAAAAAA--BBBBBBBBB--AAAAAAAA

multiblock polymer

-[-AAAAAAAA--BBBBBBBB-]-$_m$

star block polymer

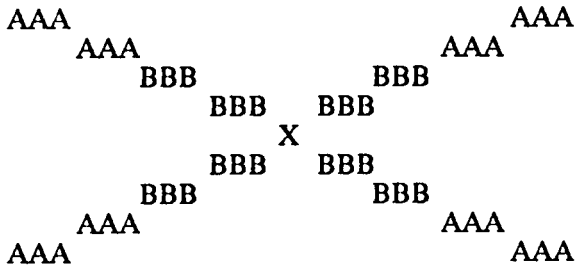

Figure 1. Type of block polymers.

attention as a potential soft segment or block[2]. PDMS displays a number of very desirable properties for many applications: excellent thermal stability, high oxidative stability, high lubricity, excellent gas permeability and electrical properties. It is quite unique in that PDMS has the lowest T_g (-125°C) among all common existing polymers. However, the crystallization of long PDMS chains (Mn > 4000, T_m is ca. -55°C) will affect the low temperature properties of PDMS. Another disadvantage of PDMS is that PDMS homopolymer - crosslinked or not - has relatively poor tensile strength and often lacks solvent resistance[2]. Incorporating PDMS blocks with other proper incompatible monomers into block polymer materials might retain many of the advantages of the special properties of the PDMS while alleviating some of its shortcomings. Indeed, block polymers utilizing PDMS as the soft segments have displayed several of the features stated above. While there are several possible hard segments that could be utilized in conjunction with PDMS, polystyrene (PS) seems to offer economics suited for potential commercial production[3].

In the synthesis of PDMS-vinyl block polymers, anionic as well as condensation polymerization routes have been used[3–7]. The anionic method has been regarded as the best "technical" route since it provides a high control on molecular weight and molecular weight distribution of each block. Hence, a well defined linear structure block polymer can be produced. However, the anionic method requires high purity of reactants and has less synthesis flexibility. Thus, the anionic method is not the most economic method for the commercial production. The free radical approach provides a great variety of potential block polymers because a large number of monomers can be polymerized by the free radical mechanism, especially for many polar monomers which can not be polymerized by the anionic mechanism [8–12] . In general, the free radical route has the major disadvantage of producing a substantial amount of homopolymer thereby resulting in a large variation of the properties of the final products depending on the homopolymer production. Also, the free radical route does not produce a narrow molecular weight block polymer. Hence, the free radical route has not been used in the synthesis of PDMS-vinyl block polymers until the recent work done by Crivello and his colleagues[13,14]. Their method provides an almost pure block polymer by a new free radical polymerization without producing homopolymers. For further development in the synthesis, the processing, and the ap-

plications for these new materials, a detailed structure-property study is needed. This is one of the main topics within this dissertation.

Besides block polymers, most ion containing polymers also display a "two phase" structure[15]. Some of the ionomers such as sulfonated ethylene-propylene-diene terpolymers also posses excellent TPE behavior. Recently, a new kind of elastomeric ionomer based on the ionene chemistry has been developed[16-22]. Segmented ionene polymers are polymers in which the macromolecules contain cationic quaternary amines as integral links in the polymeric chain[23]. By using a polymeric segment of low T_g interconnected with these "ammonium links", a ionene elastomer can be prepared. Several ionene elastomers with polytetramethyleneoxide (PTMO) as the soft segments have been reported[16-22]. Due to the fact that these elastomeric ionene polymers contain ionene units consisting of positively charged ammonium salts with negatively charged counter ions, strong electrostatic or coulombic forces result. These forces promote stronger interchain interactions. The properties of these ionene elastomers are improved due to strong ionic association. These PTMO ionene elastomers have a potential to develop a new class of TPE. To date, there has been no detailed structure-property study on these ionene elastomers. Indeed, this topic is addressed as one of the main focal points of this research.

In this research, detailed structure-property behavior of free radical synthesized PDMS-PS multiblock polymers as well as two different types of segmented PTMO based ionene elastomers has been studied. The research emphasizes the relationship between the molecular structure, morphology and bulk properties. The free radical synthesized PDMS-PS block polymers were kindly supplied by Dr. J. V. Crivello from GE. A series of segmented PTMO-dihalide ionene polymers were obtained through the courtesy of Dr. C. M. Leir in 3M. Segmented PTMO-bipyridinium ionene polymers were prepared by Dr. B. Lee in Professor McGrath's research group at VPI& SU.

CHAPTER II

LITERATURE REVIEW

The literature review will be given in three sections. In the first section, the morphological texture of block polymers and ionomers will be reviewed. The second section will review the structure-property behavior of anionic synthesized PDMS-vinyl block polymers. A detailed review on the free radical synthesis method for the PDMS-vinyl block polymers developed by Crivello et. al. will be also given in this section. Finally, the previous studies of ionene polymers are discussed with an emphasis on aliphatic ionenes.

2.1 MORPHOLOGY OF BLOCK POLYMERS AND IONOMERS

2.1.1 Morphology of Block Polymers

2.1.1.1 Morphological Texture of Block Polymers

The unique character of block polymers is their microphase separated morphology, the key to many of the valuable mechanical properties of these systems. In general, the size of the micro-

phase or domain is in a range of a few nanometers up to several hundred nanometers depending on the segment molecular weight or block length. These domains can be arranged in a very regular fashion with the domain identity period (interdomain spacing) depending on the total molecular weight of the polymer. The actual equilibrium morphology depends on the relative volume fraction of the block components. Figure 2 shows a generalized scheme of the solid state equilibrium morphology of block polymers with change of volume content of the A component[24]. When the volume percent of A (or B) is less than 20%, the morphology is A (B) spherical domains in a B (A) matrix. In a range of 20 to 40 vol% of A (B), the morphology is expected to be display A (B) cylindrical domains in a B (A) matrix. Between 40 to 60 vol% of A (B), an alternating lamellar morphology is formed[25]. Under non-equilibrium condition, the morphology may be changed, e.g., phase inversion may occur.

2.1.1.2 Thermodynamics of Microphase Separation in Block Polymers

In a block polymer, microphase separation and the potential for domain formation is governed by the free energy of mixing ΔG_{mix}. If ΔG_{mix} is positive, the system has a tendency to form a phase separated domain morphology. The value of ΔG_{mix} depends on three energies; the repulsive interaction between the A and B segments, the loss of conformational entropy, and the loss of replacement entropy. Therefore, the equilibrium domain morphology such as size, shape, spatial arrangement of the domains, and the interfacial structure should be determined by a balance of these three energies. In block polymers, two different segments, A and B, are, of course, chemically connected. If the interaction between the A and B segments is repulsive, this will serve as the driving force toward the growth of the domains and to reduce the surface-to-volume ratio of a given domain if possible. When the domain grows, it tends to create a density difference toward the center of the domain. It is a energetically unfavorable process because the polymeric solid is highly incompressible. Thus, only those conformations of the chains which fill the space in the center of the domain are allowed to satisfy the demand of uniform space filling. This process involves

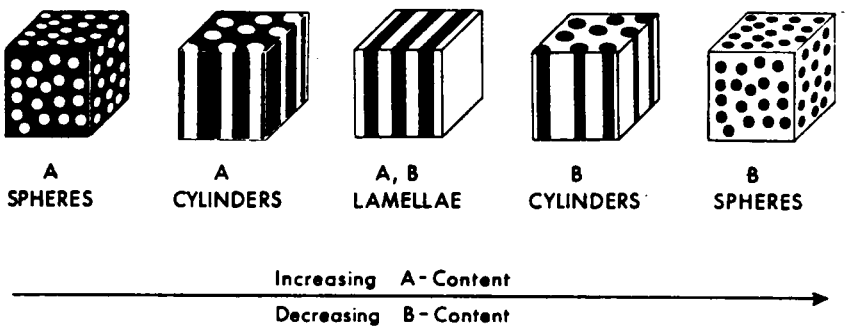

Figure 2. Scheme of block polymer morphology. (Ref.24)

the loss of conformational entropy which increases with increased domain size, and it acts as an opposing force toward domain growth. The placement entropy loss is the entropy loss which confines the junction points somewhere in the interphase and it also increases with the growth of the domain because the volume fraction of the interphase decreases as the domain grows. This entropy loss is also against the domain growth. These three energetic forces are a function of molecular weight, chemical composition, the interaction parameter, and the molecular architecture of the block polymer. Hence, the morphological texture of a block polymer is strongly dependent on the chemical parameters of the block polymer.

Many theories[26-35] have been proposed to describe the equilibrium domain morphology. The theories proposed by Meier[26-28] and by Helfand et. al.[29,30] are the most detailed and capable of describing the domain structure quantitatively. Both theories are similar and are based on the statistical mechanics of random flight chains in the limited "domain space" subjected to the requirement of the uniform space-filling.

For example, Helfand and Wasserman[30] have calculated ΔG_{mix} to form lamellar domains of a diblock polymer by employing the narrow interphase approximation - the result being:

$$\frac{\Delta G_{mix}}{NkT} = \frac{2\gamma}{k} T\left(\frac{Z_A}{\rho_A} + \frac{Z_B}{\rho_B}\right)\frac{1}{d} - \ln\frac{2a_I}{d}$$

$$+0.141\,\frac{(Z_A^{1/2}/b_A\rho_A)^{2.5} + (Z_B^{1/2}/b_B\rho_B)^{2.5}}{[(Z_A/\rho_A) + (Z_B/\rho_B)]^{2.5}}\,d^{2.5}$$

$$-\alpha\,\frac{(Z_A/\rho_A)(Z_B/\rho_B)}{Z_A/\rho_A + Z_B/\rho_B} \qquad (1)$$

where k is the Boltzmann constant, N is the number of chains incorporated in the domain formation, d is the domain identity period or interdomain spacing, i.e., the sum of the A and B lamellar thickness, Z_i is the degree of polymerization of the i block chain, b_i is Kuhn's statistical segment length, and ρ_i is the number density of the segment in pure polymer. The interfacial tension γ can be obtained either from experimental results or given by

$$\gamma = kT\alpha^{1/2}[\frac{\beta_A + \beta_B}{2} + \frac{1}{6}\frac{(\beta_A - \beta_B)^2}{\beta_A + \beta_B}] \quad (2)$$

the interfacial thickness a_I is given by

$$a_I = 2\left(\frac{\beta_A^2 + \beta_B^2}{2\alpha}\right)^{1/2} \quad (3)$$

and

$$\beta_i = \rho_i b_i^2/6, \qquad b_i^2 = <R_i^2>_o/Z_i \quad (4)$$

The interaction parameter α is defined by

$$\alpha = (\delta_A - \delta_B)^2/kT \quad (5)$$

where, the δ_i is the solubility parameter for the i-chain.

The first term on the right hand side of Eq.(1) is associated with the interfacial free energy. This term is composed of the interaction energy of mixing A and B segments and the loss of conformational entropy to maintain uniform density in the interphase. The second term is the loss of the placement entropy. The third term is associated with the loss of the conformational entropy due to the constrained volume effect and to uniform space-filling. The last term is the entropy of demixing. As shown in the Eq.(1), all the energy terms are depended on the value of d except the last one. Therefore, the equilibrium value of d can be obtained by minimizing ΔG_{mix} with respect to d.

Both the theories of Meier and Helfand et. al. are developed for only diblock or triblock polymers, and hence, the effect of the number of segments can not be taken into account. Thus, the application of these theories to multiblock or segmented polymers is limited.

Krause analyzed microphase separation from a strictly thermodynamic approach based on macroscopic variables[31-35]. By assuming complete phase separation with a sharp interface between the domains, she was able to express ΔS_{mix} by:

$$\frac{\Delta S_{mix}}{k} = \phi_A \ln \phi_A + \phi_B \ln \phi_A - 2(n-1)\left(\frac{\Delta S_{dis}}{R}\right) - \ln(n-1) \qquad (6)$$

In this equation, $\Delta S_{dis}/R$ is a disorientation entropy change gained on fusion per segment. This term has a value of approximately 1. The value of **n** represents the number of blocks per polymer chain. This theory allows neither a prediction of morphology nor a calculation of domain size, but it is very useful in demonstrating the influence of the number of blocks per chain on phase separation. The model predicts that the phase separation becomes more difficult as the number of blocks increases in a block polymer chain of a given length. Furthermore, this model suggests that phase separation occurs more easily for a system having a 50/50 volume percent of each component when other parameters are kept constant. Finally, all else remaining the same, phase separation is improved by an increase of the difference between two solubility parameters as would be expected.

2.1.1.3 Domain Size in Block Polymer

Based on the statistical mechanics of random flight chains, the domain size and the interdomain spacing can be related to molecular weight of polymer chains or the molecular weight of the blocks by a simple power law relationship given by

$$d \propto M^z, \text{ or } R \propto M_A^z \qquad (7)$$

where, d is the interdomain spacing, M is the total molecular weight, R is the radius of a spherical domain and M_A is the molecular weight of the spherical domain forming block. For a chain which follows random walk statistics (the unperturbed chain in the bulk), the scaling factor z has a value of 1/2. In practice, the value of z is greater than 1/2. According to self avoiding random walk

statistics (SAW) which refers to a gaussian coil with the excluded volume effect, the value of z is 0.6. Due to the constrained volume and to the chain perturbation required to maintain a uniform segment density, the chains in the domain would expand, and the scaling factor will be greater than 0.6. Helfand and Wasserman[30] have theoretically predicted a scaling factor of 0.643 for a diblock polymer with very high molecular weight, which is commonly referred to as the 2/3 power law. Hashimoto et. al.[36–41] have measured the interdomain spacing d and spherical domain size R for an S-I system with lamellar and spherical morphologies by TEM and SAXS. They also calculated d and R using both theories of Meier and Helfand & Wasserman. They reported that the absolute values of d and R for the spherical domains were found to be consistently about 1/2 of the predicted values by Helfand's theory, however, the experimental values scaled in excellent agreement with the 2/3 power law as predicted by both theories. Recently, York[43] also reported that the TEM and SAXS data from a PDMS-PS graft or block system were well described by the 2/3 power law.

Besides the 2/3 power law, the domain size or lamellar thickness can also be calculated from the root-mean-square (RMS) end-to-end distance of the domain formed segments if the polymer chains behave in a gaussian manner. Experimental results on PS-PI diblock polymers [42] indicated that the PS lamellar thickness was in agreement with the RMS end-to-end distance of the PS chains. The RMS end-to-end distance for flexible gaussian chains has been expressed by Flory[44] as

$$\langle r_o^2 \rangle = Cnl^2 \tag{8}$$

where **n** is the number of segments in the chain, **l** is the segment length, and **C** is the characteristic ratio. Tyagi et. al.[45] found that the PDMS segments in a PDMS-urea segmented polymer system did behave in a near gaussian manner even when the PDMS segment molecular weight was as low as 900 in Mn. The predicted values of the interdomain spacing by Eq.(8) were in a good agreement with the SAXS data.

2.1.2 Morphology of Ionic Polymers

2.1.2.1 Ion aggregation in Ionomers

The morphology of ionomers is of interest because the addition of a few ionizable groups into an otherwise ionic polymer produces a remarkably beneficial change in polymer physical properties. Over the last two decades, there has been much interest to verify the morphology of ion containing polymers. There is a general agreement that some form of ion clustering and/or ionic domain formation occurs in these materials even at relatively low ion contents, i.e. low volume percentages of the ion containing specimens. Two basic types of ion aggregates have been proposed: multiplets and clusters[46,47]. Multiplets are viewed by Eisenberg to be groupings of generally less than eight ion pairs randomly dispersed throughout the polymer matrix. A cluster, however, represents a larger scale aggregation of multiplets to form a rich region of ionic species with a somewhat depleted zone of the ionic species surrounding these former regions[46].

The stability of the multiplets and the clusters in ionomer had been tested theoretically by Eisenberg [46], who considered ion aggregation to occur in two steps. First, ions (most probably ion pairs) form spherical multiplets, up to a maximum of eight ion pairs, with a radius of 0.3 to 0.5 nm. These multiplets can further aggregate to form larger clusters. The clusters are assumed to be stable below a critical temperature T_C. The governing factors of cluster formation are the entropy increase due to the chain elasticity and the free energy decrease caused by coulombic interaction as the multiplets approach each other to form the clusters. By balancing the elastic and electrostatic forces at T_C, the cluster size can be calculated theoretically. The cluster size relates the number of ion pairs in the cluster, the intercluster distance, the spacing of ionic group along the chain, the density, the dielectric constant, the root-mean-square end-to-end distance of the polymer chain, the size of the ions, the average multiplet size above the T_C, and a constant which depends on the cluster geometry. Assuming the spheroid clusters, Eisenberg[46] calculated that the equilibrium intercluster spacing would be about 5 nm and each cluster should contain 100 pairs for ethylene methacrylic acid ionomers by using T_C = 50 °C as obtained from dynamic mechanical studies.

Experimental evidence indicating the presence of isolated ion pairs, multiplets, and clusters was first found by Meyer and Pineri[48] on iron complexes of butadiene-styrene-vinylpyridine terpolymers. Direct support for the concept of multiplets and clusters also come from Raman studies. Neppel et. al.[49,50] studied the styrene sodium methacrylate and sodium-carboxstyrene and for ethyl acrylate ionomers. They found two weak Raman bands at 250cm^{-1} and 170cm^{-1} which were assigned to the multiplets and to the clusters respectively. Neither band was present in the corresponding acid form, but with increasing ionic content, the 250cm^{-1} band appeared with increasing intensity. At a concentration dependent on the dielectric constant of the backbone, the matrix apparently saturated with the multiplets, and the 170cm^{-1} band began to grow as the ionic content increased further.

2.1.2.2 Scattering Studies on the Structure of Ionomers

The concepts of the multiplets and the clusters remain well recognized today. But the shape, size, and spatial distribution of the clusters is still a unsolved puzzle. Experimental evidence based on the scattering techniques of SAXS and SANS have provided the most direct information on the cluster structure. In 1968, Wilson et. al.[51] observed a SAXS maximum at a spacing of ca. 2nm for metal salts of ethylene methacrylic acid copolymer which was absent in the acid form. A similar SAXS peak in butadiene ionomers was observed by Marx, Caulfield and Cooper[52]. MacKnight et. al.[53] found that the ionic peak intensity and the location were directly related to the type of ions and the ionic concentration in ethylene-methacrylic ionomers. They reported that the intensity of the peak was much higher for the cesium salt than for sodium or lithium. The peak moved to high angles with increasing ionic content for a given salt and the spacing was greater for the cesium than sodium. Based on the scattering data, two basic models for the ionic aggregation, the shell-core model and hard sphere model, have been proposed to explain the scattering data.

The shell-core model (Figure 3a) is proposed by MacKnight et. al.[53], who assume that the central spherical cluster of 0.6-2.6nm diameter is surrounded by an ion depleted shell. The thick-

ness of the shell is controlled by the average distance between ionic groups along the chain and the balance between the coulombic and rubber elasticity forces. The clusters are distributed randomly throughout a matrix consisting of isolated ion pairs and multiplets. Thus, the matrix has a higher electron density than the shell but lower than the cluster.

The hard sphere model (Figure 3b) has been proposed by Cooper's group[52,54] which consists of spherical clusters of ca. 1nm in diameter. The clusters are either distributed on a randomly disordered paracrystalline lattice[52] or arranged in a liquid-like order[54]. Each of the ionic clusters is coated with an attached layer of hydrocarbon material which has the same electron density as the matrix. This layer would provide a steric limitation on the relative positions of two ionic clusters.

Both models are quite similar. But the main difference between two models is that the scattering peak is produced by intraparticle scattering in the shell-core model but by interparticle scattering in the hard-sphere model. Both models have been used to fit the scattering data obtained from both systems, unperturbed and perturbed by swelling or deformation.

SAXS studies on the swelling of different ionomers with water have been carried out by Hashimoto et. al. and Cooper et. al.[55,56]. In general, as the water uptake increases, the SAXS maximum shifts toward a smaller angle while the scattering intensity increases. Both models have been tested. It is found that if there is neither rearrangement of the ionic species nor the change in the number of ionic clusters during swelling, and the shell-core model fits the scattering data better [55,57]. However, if the ionic species can rearrange and the number of the ionic cluster can change during the swelling, the hard sphere model fits better[57]. Because there is not enough knowledge about what happens to the ionic cluster upon water adsorption, therefore, the swelling approach can not be used to judge either model.

Deformation studies of various ionomers have been carried out by Fujimura et. al [55] and by Roche et. al.[58]. As the extension ratio (λ) increases, the SAXS pattern becomes elliptical with the long axis of the ellipse orientated perpendicular to the stretching direction (SD). Parallel to the SD direction, the SAXS maximum shifts to smaller angles and decreases in intensity. Perpendicular to the SD, the scattering maximum shifts toward a larger angle and increases in intensity. Both studies show that the microscopic deformation obtained form the shifts of the SAXS maximum is less than

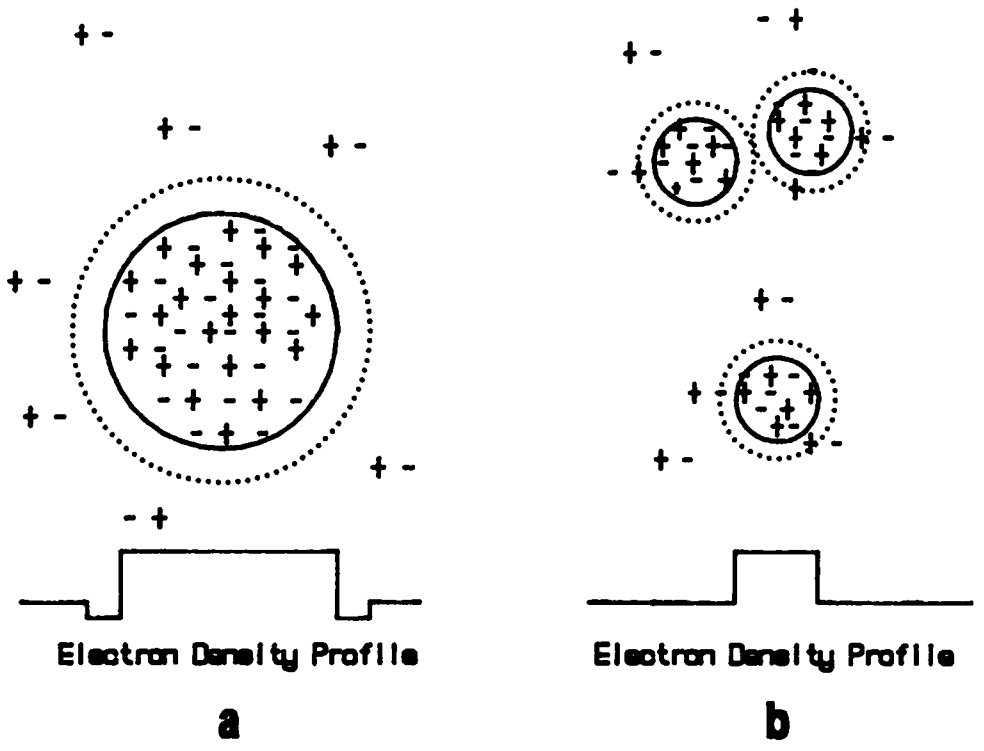

Figure 3. Structural models of ionomers: (a). Shell-core model. (b). Hard-sphere model.

that predicted by the affine deformation under constant volume. Since the affine deformation better fits in the hard sphere model, therefore both authors[55,58] suggested that the shell-core model fits the data adequately. Again, the conclusions drawn from both studies are based on the assumption that no rearrangement of ionic species occurs or no changes in the ionic clusters occurs during the deformation.

The major inability of both models is that neither model can predict the low angle upturn in the SAXS scattering intensity. Therefore, controversy still continues as to their validity and application. Recent studies of Galambos et. al.[59] on solution cast films of sulfonated polystyrene have suggested that the excess low angle behavior attributes to random ion pairs (multiplet) which have not organized into cluster regions. This was based on the observations of the SAXS behavior of these systems as a function of specific thermal history. Very recently, Ding et. al.[60] have proposed a modified hard sphere model. In this model, the ions which have not incorporated into the ionic clusters are distributed inhomogeneously through the matrix. By combining the Debye-Bueche random-two-phase model with the liquid-like hard sphere model, the modified hard sphere model does fit the SAXS data from sulfonated polystyrene ionomers very well in the low angle upturn region, the scattering peak, and tail region.

2.1.2.3 Electron Microscopic Studies on the Structure of Ionomers

As discussed in previous section, It is difficulty to distinguish the morphological texture by the scattering techniques alone, the only available and the most direct method would be electron microscopy. In the past, attempts to image an ionic domain directly by transmission electron microscopy (TEM) have yielded various results[48,61-65] depending on the particular ionomer. Marx et. al.[61] observed that the ionic diameters had diameters of 1.3 to 2.6 nm in solution cast films of acid and salt forms of butadiene methacrylic acid polymers. Phillips[62] observed 5 to 8 nm ionic domains as well as 80nm hydrogen bonded clusters in microtomed sections of a polyethylene with phosphonic acid side groups. Pineri et. al. [48] found the ionic clusters which have sizes in a range

from less than 10nm to 150 nm with most clusters having diameter less than 10 nm in ferric salts of a butadiene-styrene-4-vinylpyridine terpolymer. In polysilane dizwitterionomers, Graiver et. al. [63] found that the lamellar morphology was formed in the ionomer with only 5 mol% of ionic monomers. These results apparently do not fit any of the existing models, and they also disagree with each other even though the materials used having similar SAXS patterns. Therefore, the exact arrangement of the ionic clusters in the matrix is still largely unknown. These various results of the past TEM investigations may be caused by the resolution limits of the electron microscopes used and related focus problems in view of the small dimensional scale of the represented cluster size [64,65].

2.1.3 Summary

The microphase separation and domain formation in block polymers is governed by the free energy of mixing. This energy depends on the chemical nature of each component, the block molecular weight or block length of each block, and the number of blocks per polymer chain. Both theoretical and experimental works indicate that the domain size and the interdomain spacing are strongly dependent on the block length of the domain forming blocks and the molecular weight of the polymer respectively. This relation appears to be described by the 2/3 power law in the case of narrow molecular weight diblock or triblock polymers. The type of the domain is directly related to the composition of the block polymer only at the equilibrium state.

Unlike the block polymers, the morphology of ionomers is still a mystery to date. While considerable progress has been made in utilizing scattering methods to decipher the morphological texture of many different types of ionomers, there remains considerable needs for further clarification. Besides the scattering techniques, the most direct and the only available method is electron microscopy. However, previous TEM studies yield various results which may be caused by the instrumental limitations or by the mis-use of the instruments. With new developments in high re-

solution electron microscopy, the morphological texture of ionomers likely will be able solved in the near future.

2.2 POLYDIMETHYLSILOXANE(PDMS)-VINYL BLOCK POLYMERS

2.2.1 Synthesis of Polydimethylsiloxane-Polystyrene (PDMS-PS) block polymers

2.2.1.1 Basic Synthesis Methods of Block Polymers

Generally, the bulk properties of block polymers are governed by the nature of the components, the relative composition of the components, the molecular weight and the molecular weight distribution of each block, and the final architectural form of the block polymers. In order to obtain specific properties from a block system, it is necessary to synthesize well-defined molecular structure. Regarding the nature of synthesis, there are two general methods to synthesize block polymers[1], chain addition and step growth polymerization.

In the chain addition method, active sites on a macromolecular chain are created which initiate the polymerization of a monomer. The polymerization can be carried out by free radical, anionic or cationic methods. The sequential anionic addition or ring opening polymerization routes are the most common methods. These methods allow the control of block integrity and the sequential architecture of block polymers. However, these methods can only apply on certain monomers. The free radical approach, however, provides a great variety of potential block polymers because of the large number of monomers that can be polymerized by this mechanism. It is especially useful for many polar monomers which can not be polymerized by either an anionic or cationic mechanism. The disadvantages of the common free radical method, however, are

that it generally leads to a polydisperse block molecular weight, a non-uniform composition, and a significant fraction of homopolymer.

In the step growth method, reactions occur between the chemical functional groups of the terminal points of the blocks. With difunctional species, the condensation reaction leads to linear multiblock polymers. Condensation techniques for preparing block polymers are relatively simple to carry out, and they can be applied to a large variety of polymeric species especially to the formation of multiblock polymers. The principal limitation is that increasing the molecular weight of the precursor polymer decreases the concentration of the end groups. As a consequence, the reaction rate decreases. Also, problems often remain with regard to obtaining a well defined structure, and low polydispersity of the block polymers depending on experimental conditions.

2.2.1.2 Synthesis of PDMS-PS Block Polymers

The synthesis of PDMS-PS diblock polymers was first reported by Minoura et. al.[66]. The block polymers were prepared by initiating the polymerization of the cyclic tetramer of dimethylsiloxane with living polystyrene. However, well defined block polymers were not obtained because of the slow propagation rate of dimethylsiloxane tetramers which allowed an additional side reaction. Later, by using the cyclic trimer as the DMS monomer, Saam et. al. [3] prepared diblock PDMS-PS block polymers by initiating cyclic trimer polymerization with polystyrene anions and lithium counterions. In this case, a well defined chain structure was obtained. Products obtained by this method only contained a small percentage of homopolymer and cyclic tetramer.

Most PDMS-PS multiblock polymers have been synthesized by the anionic method[5,6,67,68], which is based upon the generation in solution of terminated dianion "living" polystyrene initiated with a difunctional organolithium agent. Then, the cyclic trimer (D_3) is added. The resulting disilanolate terminated PDMS-PS-PDMS triblock polymers are then coupled with an appropriate reagent such as the dialkyldichlorosilane of diphenyldiaceloxysilane to produce -(-B-A-)$_n$- multi-block polymers. This anionic route is shown in Figure 4 on page 21.

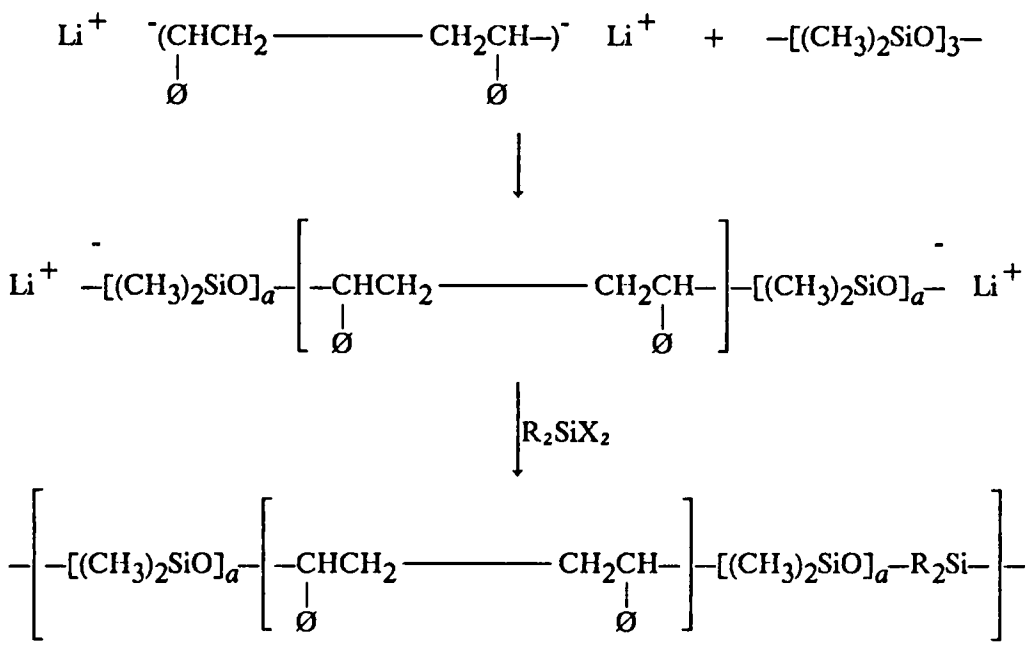

Figure 4. Anionic synthesis of polydimethylsiloxane-polystyrene (PDMS-PS) multiblock polymers.

The condensation polymerization of α,ω-hydrogen terminated PDMS with α,ω-vinylsilane terminated styrene oligomers has also been applied to prepare PDMS-PS multiblock polymers by Rempp et. al.[7]. By this method, the reaction is essentially free of side reactions and the macromolecules obtained are linear with up to 10 blocks.

2.2.2 Properties of Anionic Synthesized PDMS-PS block polymers

2.2.2.1 Phase Separation in PDMS-vinyl Block Polymers

The anionically synthesized PDMS-PS block polymers display microphase separation character as denoted by two T_g's as expected. For example, the modulus-temperature behavior of a diblock PDMS-PS polymer obtained by torsional braid analysis indicates two glass transition temperatures (Figure 5 on page 23) One T_g at about -120°C due to the PDMS blocks and the other at ca. 50°C arises from the PS blocks [69]. The DSC and TMA studies[5,70] also show two glass transitions on diblock and triblock PDMS-PS polymers. Crystallization of the PDMS blocks has also been observed when the PDMS block length exceeded 4000 [5].

2.2.2.2 Morphological Texture of the PDMS-vinyl Block Polymers

The morphological texture of PDMS-PS block polymers is often dependent on the type (di, tri, or multi block) of block polymer, the overall molecular weight, the composition and the block length of each component. Figure 6 on page 25 shows the effect of block length on morphological textures of PDMS-PS diblock polymers cast from toluene [71]. In these polymers, the PS content was about 70wt%. As the overall molecular weight of the polymers decreases from 47,600 to 28,600 to 7,000, the morphology of these materials changes from a spaghetti-like structure

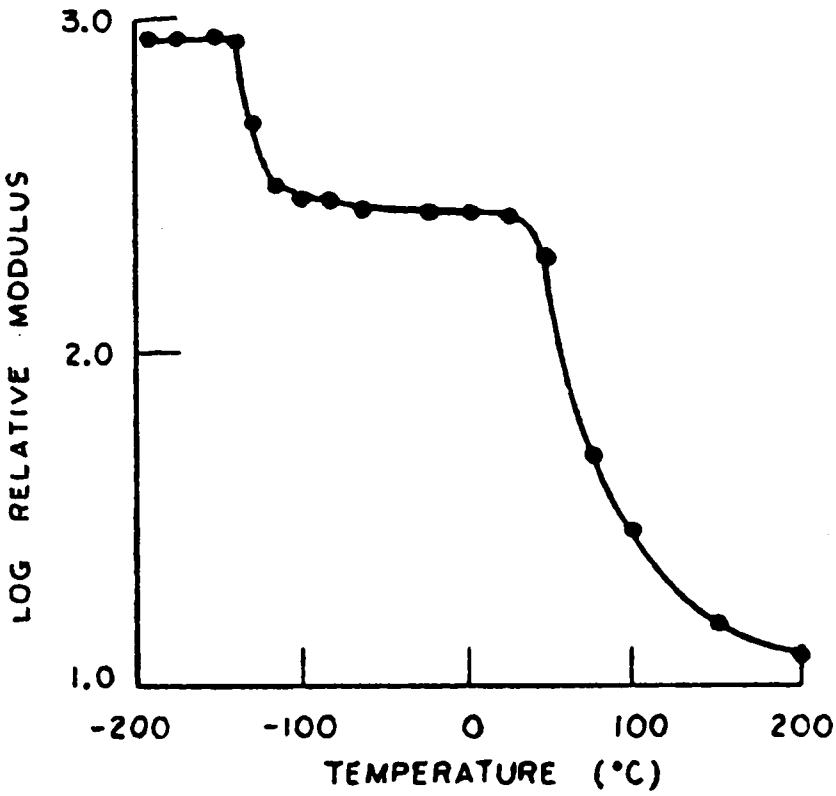

Figure 5. Temperature-modulus curve of PDMS-PS multiblock polymer. (Ref.27)

to lamellar to an ill-defined spherical-like texture. The Mn of 7,000 seems to be the lower limit of the molecular weight for phase separation.

As stated above, the composition also influences the morphology as Saam et. al.[68] reported. For PDMS- PS diblock polymers with a Mn of 48,000, they found that when the PDMS content changed from 35wt% to 62wt% to 82wt%, an inversion in phase behavior occurs from an initial morphology of PDMS domains in a PS continuous matrix at 35wt% of PDMS to PS domains in a PDMS matrix at 82 wt% of PDMS[68]. This kind of behavior is consistent with previous observations of the analogous diene-styrene block polymer systems. The situation is different, however, for PDMS-PS multiblock systems. For these systems, the morphology does not change as drastically over a broad range of composition[68]

Due to the difference in solubility parameters of the blocks, the solid state morphology of a block system is very often dependent on the nature of the casting solvent, i.e. its relative solvent power for the respected block. For a PDMS-PS diblock polymer having a Mn of 48,800 containing 33 mol% of polystyrene [3], the morphology obtained from bromobenzene (a good solvent for the PS phase) leads to spherical PDMS domains in a PS matrix. When the same polymer is cast by cyclohexane (a good solvent for the PDMS phase), the morphology is changed to PS spherical domains in a PDMS matrix. Using toluene, which is a good solvent for both phases, cast films of the same polymer provide a spaghetti-like morphological texture. Also toluene cast films always give the sharpest microscopy contrast which is an indication of sharp phase separation. Similar results for PDMS-PS-PDMS triblock polymers have also been reported[5]. These changes in morphology caused by the casting solvent is believed due to the aggregated or micellar structure that initially forms in solution.

2.2.2.3 Mechanical Properties of the PDMS-vinyl Block Polymers

Mechanical properties, modulus, tensile strength (stress at break), and ultimate elongation, are also strongly dependent on the block length, the composition, and the number of blocks per

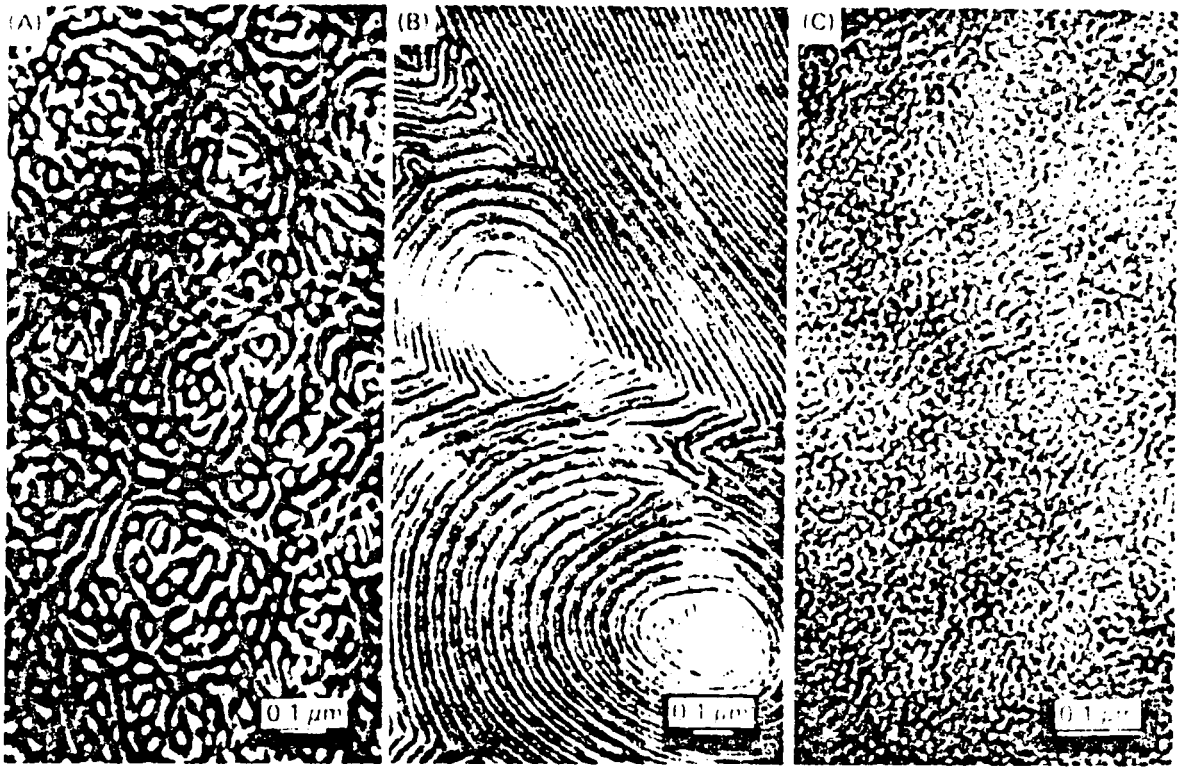

Figure 6. Morphological texture of PDMS-PS constant composition diblock polymers of varied molecular weight: (A) Mn 47,600, 68wt% PS; (B) Mn 28,600, 70.9wt% PS; (C) Mn 7,100, 71.6wt% PS. (Ref.71)

polymer chain. Saam et. al.[69] showed that with other processing variable constant, as the PDMS content of a PDMS-PS multiblock system increased from 50wt% to 70wt%, the polymer became more elastomeric and the high initial modulus as well as the yield point became less significant. The tensile strength of a PDMS-PS system also increased dramatically with the number of blocks per chain, **n** (Figure 7 on page 27). When **n** exceeded 8, there was only a slight improvement in tensile strength[72]. The tensile strength also changed with block length. For a PDMS-PS multiblock system with 30wt% polystyrene, the tensile strength increased from 1.6 MPa to 7.1 MPa as the PS block length increased from 4,000 to 13,550[72].

Depending on the casting solvent, the mechanical properties vary. Films cast from a good solvent for the PDMS phase (e.g. cyclohexane) usually lead to a more elastomeric behavior as compared to the same polymer cast from a good solvent for the PS phase such as bromobenzene [5,69]. This difference is due to the changes in solid state morphological texture of the polymers as discussed above. The mechanical properties of a thermal molded film of a PDMS-PS block polymer have also been studied[5,69]. Its mechanical properties were similar to toluene cast film of the same polymer. However, a dynamic mechanical analysis of this polymer indicated that the phase separation in the thermally molded film was higher than that of the toluene cast film[5].

2.2.3 Free Radical Synthesis of the PDMS-PS Multiblock Polymers

Recently, Crivello et al.[13,14] have developed a unique free radical synthetic method to prepare PDMS-vinyl block polymers. Their method consists of the preparation of a bis(silyl pinacolate) initiator; the use of the pinacolate to prepare a high molecular weight polydimethylsiloxane macroinitiator and, use of these macroinitiators in conjunction with proper vinyl monomers to prepare the multiblock polymers by a free radical block polymerization. By using pinacolate initiators, a high blocking efficiency was achieved and the probability of the formation of homopolymers is essentially reduced to zero if proper selection of a comonomer is made.

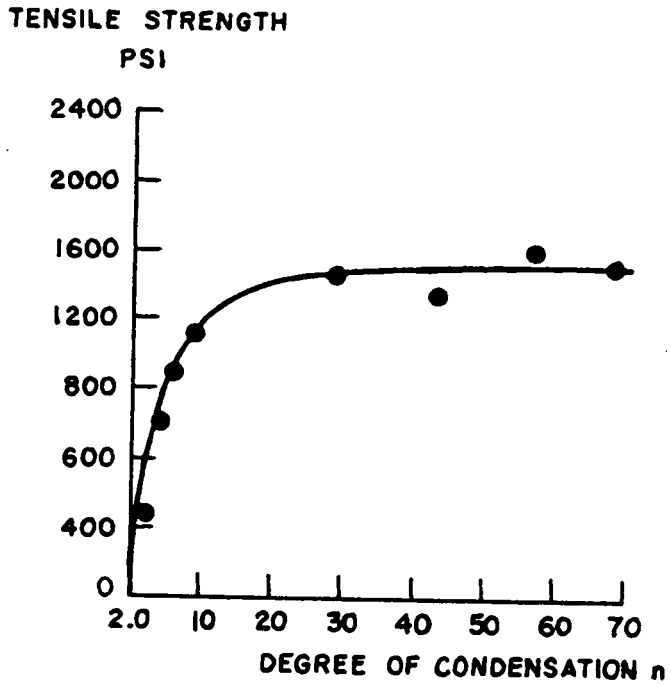

Figure 7. Effect of condensation number (number of blocks per chain) on tensile strength of PDMS-PS multiblock polymers: These polymers contain 30wt% of polystyrene. Mn of ABA diblock polymer is 45,100, and films cast from toluene. (Ref.69)

The silyl pinacolate initiators are prepared by the reduction of diaryl ketones with magnesium metal in the presence of dimethylchlorovinyl silane with THF (tetrahydrofuran) as the solvent and TMU (tertramethylurea) as a promoter[13] (Figure 8 on page 29)

There are two reasons for using the silyl pinacolate as an initiator. First, vinyl silanes are extremely sluggish toward free-radical polymerization even with the most active free radical initiators. Hence, the vinyl double bonds can be retained during the initiator preparation and later serve as sites for attachment of the PDMS blocks under more active conditions. Second, the silyl pinacolate initiator can undergo facile thermolysis at low temperatures (60-80°C) to give dimethylvinyl silyl ketyl radicals. However, the "carbon-centered" free radical which is formed during thermolysis is of low reactivity due to the resonance delocalization of two neighboring aromatic rings and the steric hindrance provided by the two aryl groups. The low reactivity of this free radical means a longer life time. During the later free radical block polymerization with vinyl monomers, the steric hindrance of these carbon center free radicals can reduce the probability of recombination of the macroinitiators.

The PDMS macroinitiators are prepared by the hydrosilylation of vinyl containing bis(silyl pinacolate) with α,ω-hydrogen functional polydimethylsiloxane oligomers. These oligomers are prepared by cationic ring opening polymerization of octamethylcyclotetrasilane (D_4), in the presence of tetramethylsiloxane as a chain stopper (Figure 8 on page 29). By using this synthesis method, the final molecular weight of the α,ω-hydrogen oligomers can be well controlled.

These PDMS macroinitiators can yield a high portion of polydimethylsiloxane macrodiradicals on thermally induced fragmentation. These PDMS di-radicals can then undergo chain extension at both ends in the presence of vinyl monomers and form block polymers. The overall reaction is shown in Figure 8 on page 29.

Analysis of the products has shown that only block polymers are found in the final products by the synthesis just outlined by Crivello et. al.[14]. During the later stage of polymerization, intense iridescence has been developed which indicated the occurrence of microphase separation in these materials. As expected, the mechanical properties of these block systems, utilizing styrene as the vinyl monomer, are highly dependent on the composition of the polymer and the film casting sol-

Synthesis of Pinacolate Initiator

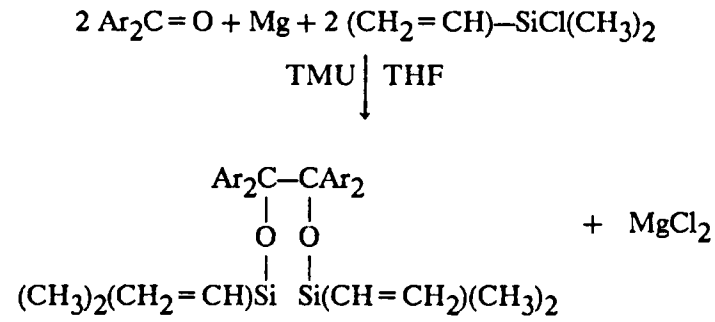

Synthesis of PDMS Macroinitiator

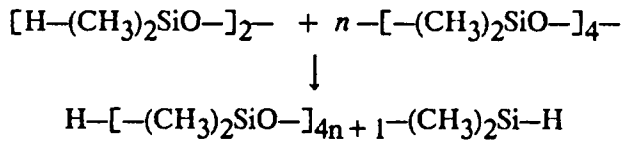

Free Radical Synthesis of PDMS-PS Block Polymers

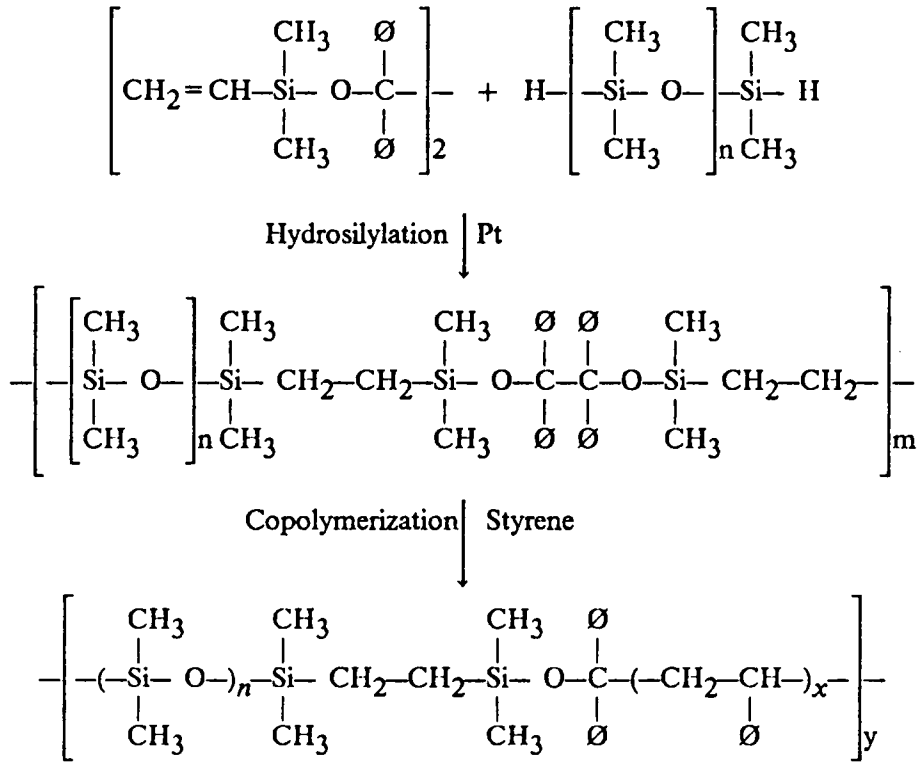

Figure 8. Free radical synthesis of PDMS-PS multiblock polymers.

vent if solution casting is used. Depending on the block length and the relative portion of the hard polystyrene (PS) and soft (PDMS) segments, either thermoplastic elastomers or rubber-modified thermoplastics can be produced.

2.2.4 Summary

The morphological texture of the PDMS-PS block polymers strongly depends on the composition of the polymer, the architecture of the polymer chain, and the molecular weight of each block (block length) and the total molecular weight of the polymer. For the PDMS-PS di- or triblock polymers, the morphological texture changes with the changes in the composition and the block length. But for PDMS-PS multiblock systems, the morphological texture is less sensitive to the change in the composition. The mechanical properties of the PDMS-PS block polymers are directly related to the morphology of the polymers. The ultimate properties of the PDMS-PS block polymers also depend on the number of blocks per polymer chain. Depending on the film preparation method or the type of casting solvent, the solid state morphology of the PDMS-PS block polymers is also changed. The changes in solid state morphology are reflected by the changes in the polymer-polymer interaction or polymer-solvent interaction during the film preparation. Therefore, the final bulk properties of the polymers are altered.

In previous structure-property studies, all of the PDMS-PS block polymers have been prepared by anionic methods. None of PDMS-PS block polymers have been made by free radical synthesis before that recently developed by Crivello and co-workers. They developed a unique free radical synthesis method which produces pure PDMS-vinyl multiblock polymers while eliminating the production of the homopolymers. However, the molecular weight and the molecular weight distribution of each block as well as the architecture of the polymer chains in these free radical systems can not be well controlled due to the nature of the free radical synthesis. Hence, the morphology and the bulk properties of these materials in turn will be influenced. However, no detailed structure-property studies have been carried out on these materials. For further improve-

ment and utilization of this free radical synthesis, it is important to understand the relationship between the synthesis variables and the chemical structure of the final block polymers along with their morphology and the bulk properties. Therefore, a systematic study on the structure-property behavior of these polymers was undertaken, as will be discussed later in this dissertation.

2.3 IONENE POLYMERS

2.3.1 Synthesis and Chemical Structure of Ionenes

Ionenes are cationic ionomers in which macromolecules contain cationic quaternary amines as integral links in the polymer chain. In the 1930's, Marvel et. al.[73] synthesized low molecular weight ionene polymers by polycondensation of some dimethylamino-N-alkylhalides. However, the details of the mechanism and methods of formation of this type of polymer were lacking. In 1968, Rembaum prepared some high molecular weight aliphatic ionenes by the Menschutkin reaction[23], and defined the term "ionene" as used above. Within the last several years, ionene polymers have received increasing attention as for water treatment flocculants, antimicrobials, antistates, and as components of photovoltatic cells, cosmetics, and conductive polymers. However, most of the previous studies have focused on aliphatic ionenes and their solution and electrical properties. Only a very few publications on the synthesis of elastomeric ionene polymers are available[16–21,74,75]. Furthermore, there has been no detailed studies on the structure-property behavior of these novel materials.

The synthesis of an aliphatic ionene is shown in Figure 9 on page 33. In the figure, R_1 and R_2 are alkyl groups which can be the same or different. In the backbone of an aliphatic ionene, n can be one or larger, and m can be the same as n or different. The backbone of the ionene may also represent aromatic moieties yielding structure such as shown in Figure 9 on page 33. The counter ions can be Br^- or Cl^- or other types. In this review section, aliphatic ionenes will be

designated as a "n,m-X ionene" in which "n" and "m" are the numbers of methylene units in the segments and the "X" is the type of counter ion. Side groups R_1 and R_2 will be specified unless they are methyl groups.

2.3.2 Properties of Aliphatic Ionenes

2.3.2.1 Solution Properties

Rembaum et al.[76,77] studied the solution properties of aliphatic ionenes with Br^- or Cl^- counter ions. The water-ionene solution displayed a typical polyelectrolyte behavior; the solution viscosity increased as the ionene concentration decreased (Figure 10). By adding a simple salt, KBr, into the water-ionene solution, the viscosity of the solution decreased as the salt concentration increased. For a 0.4M KBr solution, viscosity became a linear function of ionene concentration over a wide range (Figure 10). Based on the experimental data, the Mark-Houwink parameters were calculated for the 3,4 and 6,6-bromine and 6,6-chlorine ionenes [77]. The changes in solution properties of such ionenes were attributed to their ionic nature. In a salt free dilute electrolyte solution, the charges on the backbone of ionenes led to strong repulsion between segments which caused the polymer to expand, and as a result, the viscosity increased. When the concentration of the polymer decreased, the positive charges in the ionene backbone became less shielded by the negative counterions, therefore, the polymer chain became more extended, and the viscosity increased. By adding a simple salt into a water-ionene solution, the resulting electrostatic screening of the charged segments by the electrolyte caused a marked reduction in the repulsive potential between segments. Hence, the ionene chains contracted and as a result, the viscosity decreased[77].

The dielectric constant of the solvent also affects the solution properties of ionene. Knapick et al.[56] reported that in a water-ethanol-ionene solution, the viscosity of a 4,4-bromine ionene with methyl (R_1) and ethyl (R_2) side groups decreased with the increasing volume percent of ethanol increased, and the polyelectrolyte characteristics of the solution became less pronounced. Buruiana

Synthesis of Aliphatic Ionenes

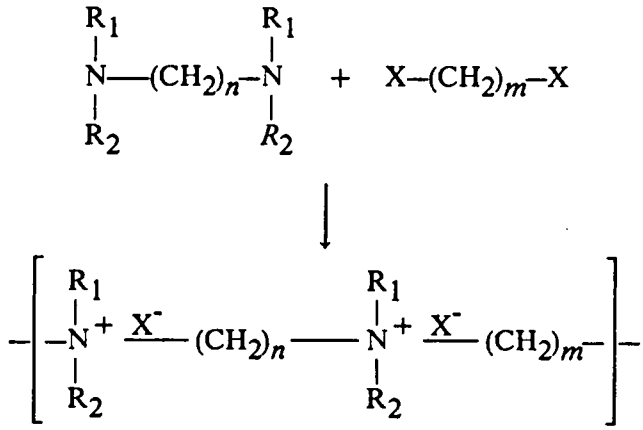

Structure of Aromatic Ionenes

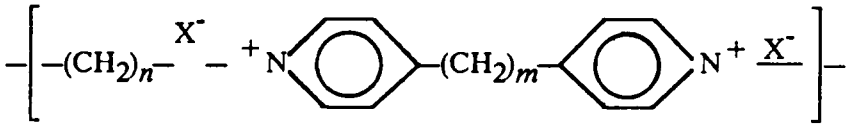

Figure 9. Synthesis of Aliphatic Ionenes and the Structure of Aromatic Ionenes

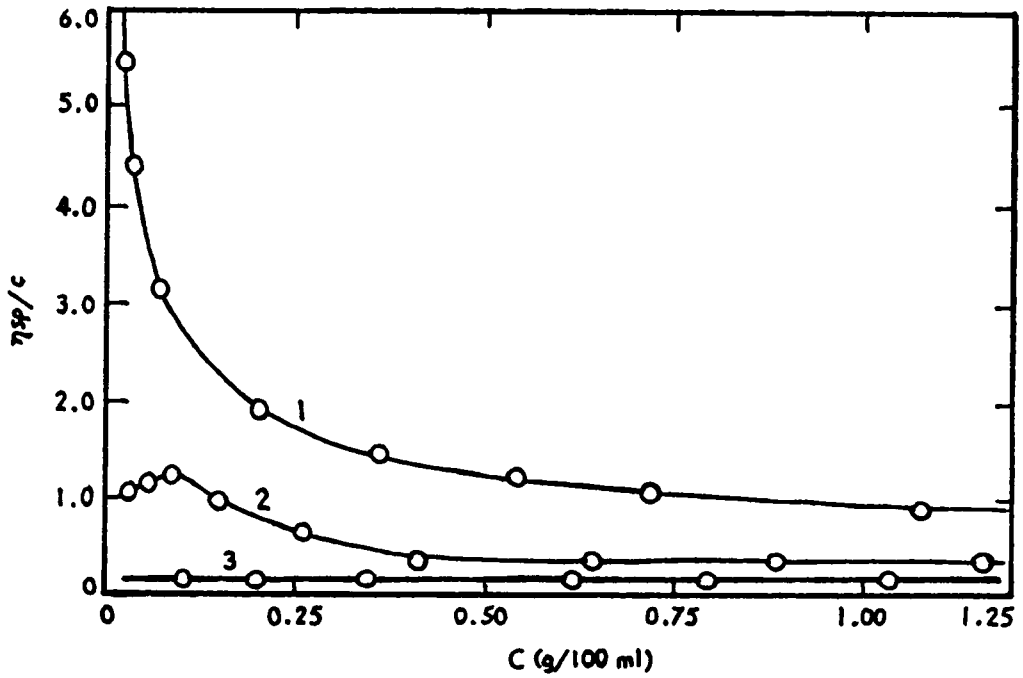

Figure 10. Reduced viscosity behavior of 6,6 Br ionene.: Solvents: (1) H_2O, (2) 0.05M KBr, and (3) 0.40M KBr. (Ref.42).

et. al.[78,79] also studied the dilute solution properties of 2,4′-dibenzyldiisocynate ionenes in the none polar solvents of THF and 1,4-dioxan. The system behaved as a none ionic polymer. When small quantities of a highly polar solvent (water or DMF) were added into the system, the system displayed a polyelectrolyte behavior.

The chemical structure of an ionene polymer also has a strong influence on the dilute solution properties. For a 4,4-bromine ionene, the viscosity of the system with 50/50 water-ethanol solution is high and the system displays polyelectrolyte behavior. By replacing the methyl groups with ethyl, n-hexyl or n-octyl groups, the viscosity decreases as the number of carbon atoms in the side group increases. Also, the polyelectrolyte characteristics becomes less pronounced as would be expected. The 4,4-bromine ionene with n-octyl side groups has the lowest viscosity and a nonionic polymer behavior[56].

2.3.2.2 Crystal Structure of Aliphatic Ionenes

Because of the short regular aliphatic chain structures used to date, most aliphatic ionenes have often been highly crystalline materials. Dominques et. al.[80] have studied the crystallinity of 6,6 and 10,10-ionenes by X-ray diffraction. The degree of crystallinity of the ionenes was influenced by the type of counter ions, the side groups, and the segment length. The degree of crystallinity decreased as the segment length m increased from 6 to 10. The ionene having CH_2CH_3 side groups had a higher crystallinity than the equivalent ionene with CH_3 side groups. The melting point of these ionenes increased with decreasing segment length as expected. The 6,6 ionene with CH_3 side groups could be crystallized from the melt, but the 10,10 ionene and the ionene with CH_2CH_3 side groups could only by crystallized in solution. The superstructure of these ionene was also affected by the type of counter ion. The 6,6 bromide ionene had a spherulitic morphology, but the 6,6 $ZnBr_4$-ionene behaved like an inorganic salts by forming needle-like or plate-like single crystal domains.

2.3.2.3 Glass Transition Behavior of Aliphatic Ionenes

Due to the crystallinity of aliphatic ionenes, a direct determination of the glass transition by DSC is limited. Ionenes are generally hydrophilic but can be dried completely without serious decomposition. Since water can plasticize an ionene, this adds more difficulties in the T_g determination. One approach to measure the T_g of a ionene is to plasticize the ionene to various contents, and measure the T_g as a function of composition, which may extrapolate to zero plasticizer content. Eisenberg et. al.[81] have studied the T_g behavior of several aliphatic ionenes with different solvents as plasticizers. The T_g was calculated by the Gordon-Taylor equation:

$$T_g = w_1 T_{g1} + w_2 T_{g2} - k w_1 w_2 \qquad (9)$$

where w is the weight fraction, T_{g1}, and T_{g2} are the glass transition temperature of the ionene and dilute, and k is a constant. Solvents used to plasticize ionenes have a significant effect on the T_g values as might be expected. Depending on the dielectric constant of the solvent, the T_g of a 6,8 ionene was changed from -4°C with water to -82°C with glycerine. The T_g of a 6,8 ionene obtained with various plasticizers is shown in Figure 11 on page 37. The figure illustrates dramatic changes in T_g by the solvent utilized. These changes may relate to conformational changes of the ionene structures in different solvents. By using a different approach, torsional braid analysis, Tsutsui and co-workers[82] have found that the T_g of aliphatic ionenes is in the range from 90°C to 140°C depending on the spacing, n and m, of the ionene. They have also found that there is no significant difference between the data obtained by both "plasticizer" and the torsional braid method except at extremely low water content (< 5wt%) where the torsional braid method yielded a much higher T_g at zero water content (Figure 11 on page 37).

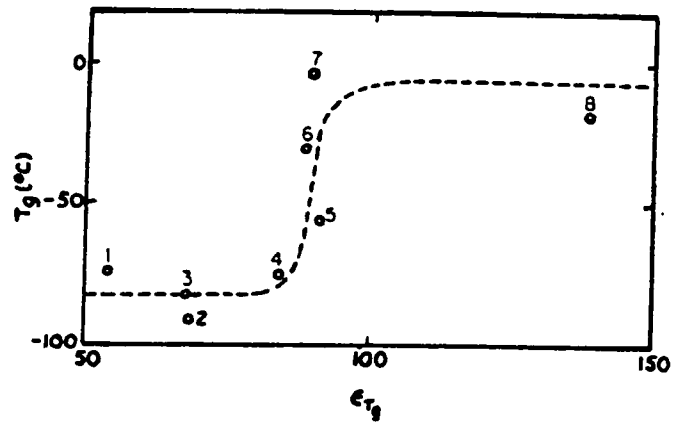

a

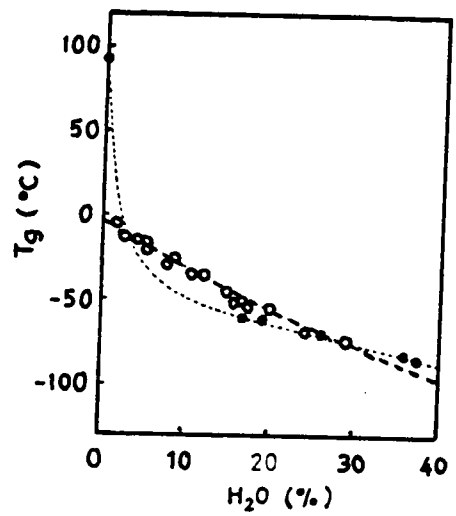

b

Figure 11. Glass transition of a 6,8 ionene: (a). T_g obtained by using various plasticizers versus dielectric constant of the plasticizers. (Ref.81). (b). T_g obtained by the torsional braid method, open circles are the data from Eisenberg by plasticizer method. (Ref.82).

2.3.3 Elastomeric Ionene Polymer

2.3.3.1 Ionene Elastomers

The first ionene elastomer was synthesized by Takahashi et. al.[83]. This material was a 3,3-chloride ionene - polytetramethyleneoxide (PTMO) triblock polymer with PTMO as the center block. The molecular weight of 3,3-ionene ranged from 5000 to 30000. Both ends of polytetramethyleneoxide diol (Mn = 5660) were brominated by the reaction with $SOBr_2$ in benzene with pyridine as catalyst. Then the 3,3-ionene-PTMO-3,3-ionene triblock polymer was prepared by a quaternization reaction. According to their results on molecular weight and composition of the final polymer determined by osmometry and elemental analysis, they reported that the desired triblock polymer was formed. The viscosity behavior of these triblock ionene polymer was similar to that of the ionenes. However, no solid state properties for these interesting materials were reported nor was there any description of the polymers.

Watanabe and co-workers[74,75] studied elastomeric ionene-TCNQ salts. Their system were characterized by an alternating structure of rigid polycation segments that contained 4,4′-bipyridinium rings and flexible polypropyleneoxide (PPO) segments. The dynamic mechanical analysis showed that these materials had two glass transitions corresponding to the T_g's of PPO and the polycation segments. These results were a strong indication that these elastomeric ionenes formed a micro-heterogeneous structure. Wide angle X-ray scattering result showed that these materials were amorphous.

2.3.3.2 Polytetramethyleneoxide (PTMO)-dihalide Ionene Elastomers

The first PTMO-dihalide ionene polymer was synthesized by Kohjiya et. al.[16,17] in 1981. These PTMO-dihalide ionenes were synthesized from dimethylamino-terminated polytetrahydrofuran (PTMO) and 1,4-bis(chloromethyl) benzene by using the Menschutkin re-

action[16–18] as shown in Figure 12 on page 40. The dimethylamino terminated PTMO was synthesized by the method of Smith and Hubin[84]. Unlike the aliphatic ionenes, these PTMO-ionenes did not dissolve in water unless the PTMO segment molecular weight was less than 1160[16,17]. These materials dissolved in $CHCl_3$ and CH_2OH. In $CHCl_3$, these materials displayed a ordinary viscosity concentration behavior whereas they behaved as a polyelectrolyte in methanol. The polyelectrolyte behavior was enhanced as the PTMO segment length decreased. The type of counter ions also influenced the solution behavior of these ionenes. As the Cl^- ions were exchanged by the $CH_3(CH_2)_6SO_3^-$, the polyelectrolyte behavior was less pronounced. When the counter ions were $^-O_3SCH_2CH_2SO_3^-$, the polyelectrolyte behavior vanished[17].

These PTMO-ionene polymers displayed good elastomeric behavior; low modulus, high tensile stress (27MPa) and ultimate elongation (> 1000%) [17]. The mechanical properties of these ionenes were governed by the type of the counter ion and the PTMO segment length. The modulus of these ionenes increased as the size of the counter ion decreased or the charge of the counter ion increased. The tensile strength increased as the PTMO segment length decreased while the ultimate elongation of the ionenes increased with an increase of the PTMO segment length.

More recently, Klun et. al.[19] prepared numerous ionene systems from diamines and dihalides by the Menschutkin reaction. Some of their ionenes displayed good elastomeric behavior; high elongation (> 1000%) and high tensile strength. Depending on the dihalide moieties, the so called "melting point" or softening point of these ionenes varied from 120°C to 220°C. Thermal analysis, DSC, DTA, and dynamic mechanical analysis indicated a phase separated structure of these ionene elastomers.

A major problem in the synthesis of the specific PTMO-ionenes being discussed is that when the molecular weight of the functionalized PTMO is high, the concentration of reactive chain ends is low at the onset and continues to decrease during the polymerization. Thus, the overall rate and the ultimate degree of polymerization can be greatly reduced. Without a high "degree of polymerization", these materials will not display good elastomeric behavior such as low creep and hysteresis properties. This may be one of the reasons that only a few publications on these type of ionene exist.

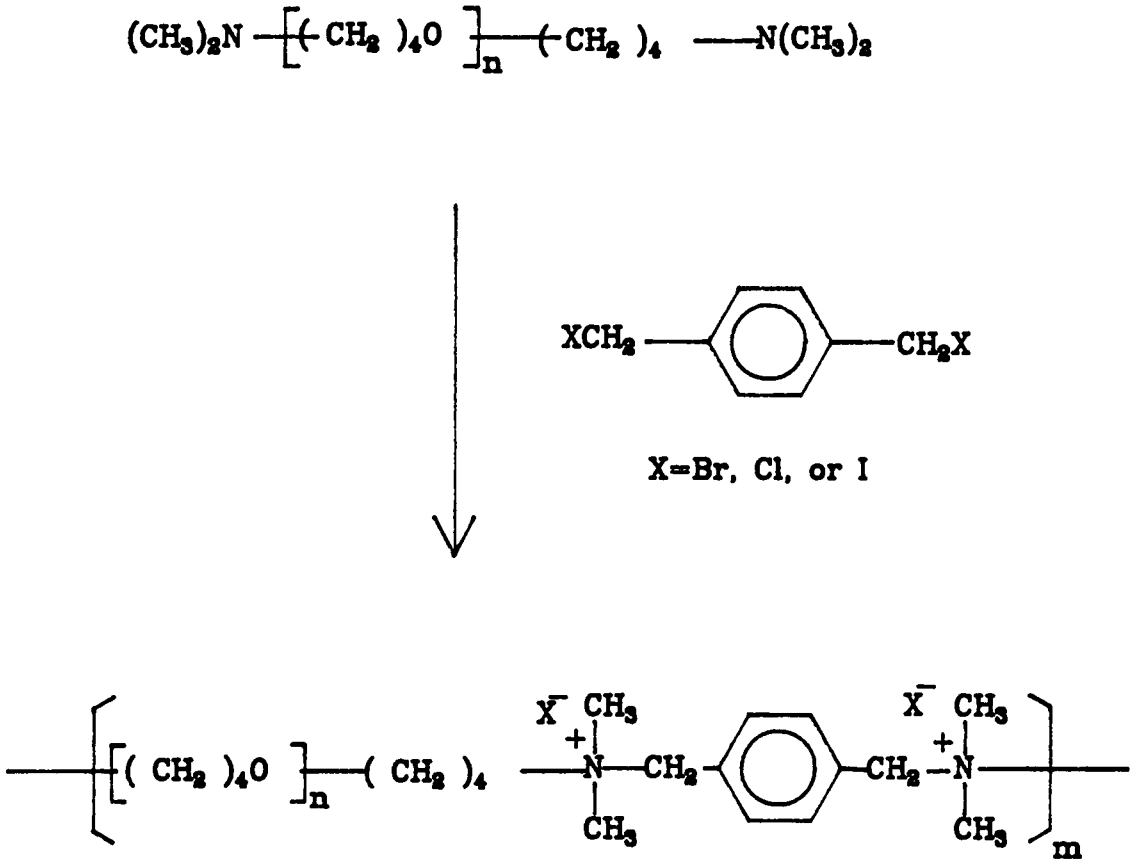

Figure 12. Synthesis of polytetramethyleneoxide (PTMO)-dihalide ionene elastomers.

Recently, Leir et. al.[20] have been successful in synthesizing high molecular weight PTMO-ionenes with long segments of PTMO (segment length is up to 10,000) by a similar method shown in Figure 12 on page 40. They have also prepared different dihalides as hard segments. These materials display excellent elastomeric behavior in all respects. They also show a drastically reduced solution viscosity when the polymer is heated to its softening temperature (> 150°C). After cooling down, the solution viscosity of these materials almost resumes its original level although not completely. This phenomenon may relate to a depolymerization-repolymerization process taking place during the heating and cooling cycle. In general, quaternary tetraalkylammonium salts can undergo decomposition when they are heated to high temperatures and yield the original alkylhalides and tertiary amines, i.e. a reverse Menschutkin reaction. The solution viscosity behavior of the PTMO-dihalide ionenes described above may relate to this reversed process. If this is the case, these PTMO-chlorine ionenes could potentially provide a unique character for thermal processing. This character may lead these PTMO-ionenes to become an important TPE material. But as will be discussed later, there seems to be some limits to the thermal reversibility.

2.3.3.2 PTMO-dipyridinium Ionene Elastomers

Besides the dihalides, 4,4′-bipyridine has been also used to prepare PTMO-ionene elastomers. In 1985, Kohjiya et. al.[21] first utilized 4,4′-dipyridine to terminate living PTMO dioxonium ions. At that time, they were only interested in both polyelectrolyte and photochromic behavior of these materials. No systematic study of the structure property behavior of these materials was reported yet. Until recently, it is the only study on such PTMO-dipyridinium ionenes.

Recently, Dr. B. Lee[22] in Professor J. E. McGrath's group at VPI also developed the same type of PTMO-dipyridinium ionenes without an awareness of the work of Kohjiya et. al. by the same synthesis routine (Figure 13 on page 43) His NMR results confirmed the formation of segmented ionene polymers. Thermal analysis, DSC and TMA, indicated that a well defined microphase separation was developed in these materials. The mechanical properties of these

PTMO-dipyridinium ionene were also similar to that of the PTMO-dihalide ionenes. In addition, TGA results indicated that these PTMO-dipyridinium ionenes had a much higher softening temperature (ca. 210°C) than the PTMO-dihalide ionenes (ca. 175°C).

2.3.4 Summary

PTMO based ionenes are a new type of segmented elastomer. These materials display some unusual properties such as polyelectrolyte - nonpolyeletrolyte solution properties and possess quite excellent mechanical properties. Due to the potential useful polymerization - depolymerization mechanism of these ionene materials, the ionene elastomers may have some strong potential to be a new type of TPE material. Furthermore, these materials are suitable for model studies because of the well defined ionene chemistry. As stated earlier, no structure-property study of these ionene materials has yet been carried out. Therefore, a systematic structure-property study on these novel materials is necessary to assist future developments and applications of these materials. This indeed is one of the major focal points of this dissertation.

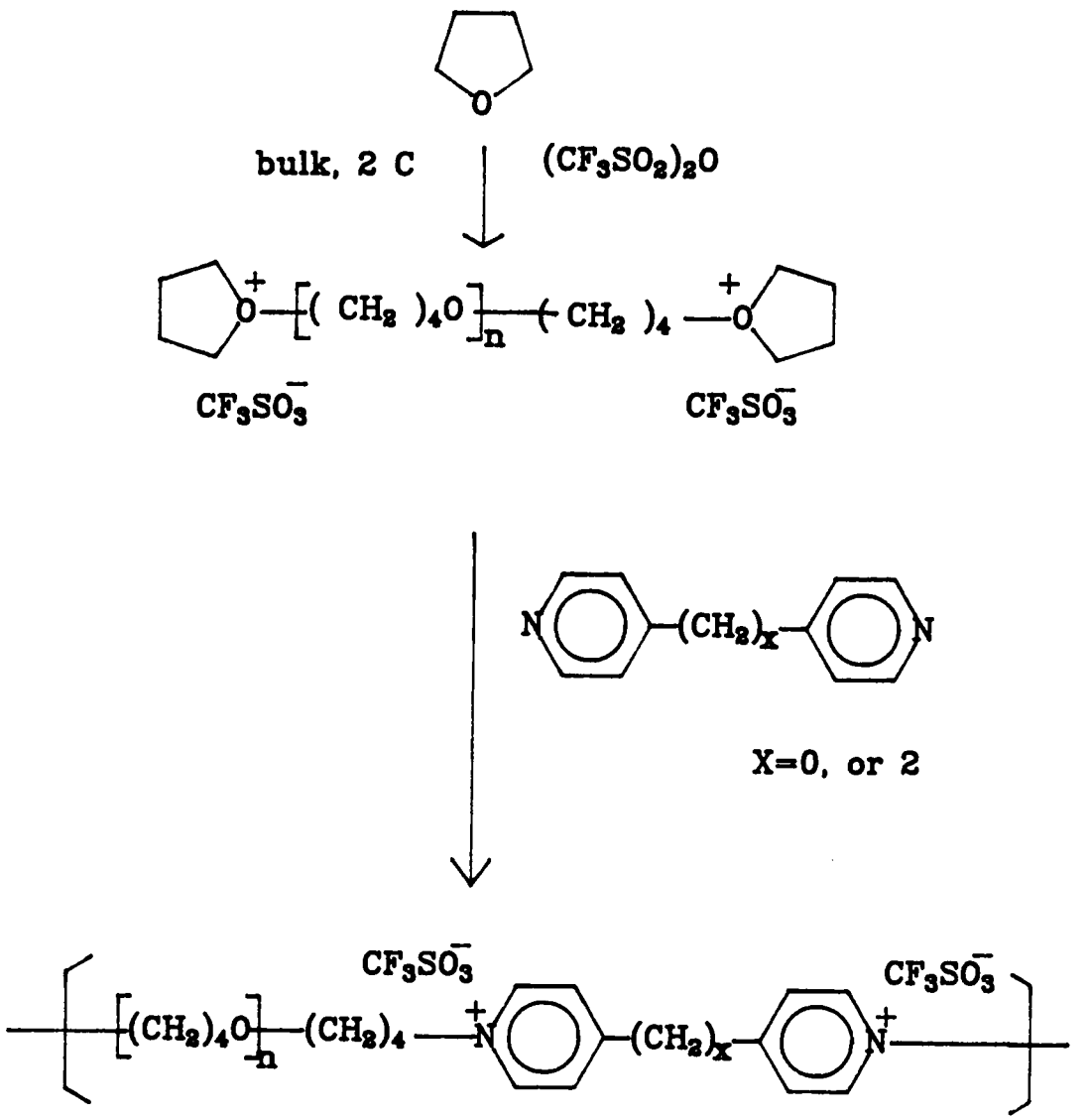

Figure 13. Synthesis of PTMO-dipyridinium ionene elastomers.

CHAPTER III

PURPOSE AND SCOPE OF PRESENT RESEARCH

As was discussed in the previous literature review sections, no structure-property studies on free radical synthesized PDMS-PS block polymers and segmented PTMO based ionene elastomers have been done. It is therefore of interest to study the structure - property behavior of these materials in order to develop a better understanding of these unique materials. This knowledge will be very helpful in the further development of the synthesis, the processing and the applications of these materials. In this work, systematic studies on the structure-property behavior of these materials are presented. These studies have emphasized the chemical structure of these novel materials and how it influences the final solid state morphology and bulk properties of these materials. The studies are carried out by means of thermal analysis, mechanical and dynamic mechanical analysis, X-ray scattering techniques, and electron microscopy. The details of the research scope will be given in two parts. The first part (section 3.1) deals with the free radical synthesized PDMS-PS block polymers while the second one (section 3.2) concerns the segmented PTMO-ionene elastomers.

3.1 FREE RADICAL SYNTHESIZED PDMS-PS BLOCK POLYMERS

In the structure-property study of the free radical synthesized PDMS-PS block polymers, the emphasis will be on the relationship between the reaction parameters, the morphology and the bulk properties. In order to minimize the reaction variables, the PDMS content in these free radical PDMS-PS block polymers has been maintained in the range of 42 to 50 mol%. The main reaction parameters concerning in this study are the PDMS block molecular weight (block length), the conversion level of the styrene monomer, and the type of derivative styrene monomers. Besides the reaction parameters, the effect of film preparation method will also be investigated. Solution casting and thermal compression molding methods have been used to prepare polymer films.

3.1.1 Studies on the Effect of Reaction Parameters

3.1.1.1 Molecular Weight of the PDMS Macroinitiator

Due to the reaction mechanism as shown in Figure 8 on page 29, the block length of the PDMS component in the final polymer is determined by the molecular weight of the PDMS oligomers which are used to prepare the macroinitiators. These PDMS oligomers are prepared by an anionic method[13,14], the molecular weight and the molecular weight distribution of these oligomers are relatively well controlled. Therefore, the chemical structure of the PDMS blocks in the final polymers are well defined. The PS blocks, however, are formed by free radical synthesis, therefore, the block length and the molecular weight distribution of the PS blocks will vary depending on the concentration of the initiator. At constant conversion level of styrene, the PS block length would decrease as the initiator concentration increases, and the number of the PS blocks per chain would increase. Changes in the block length of the PS blocks and the number of blocks per

chain can induce a great variation in the solid state morphology and the bulk properties of the final polymer.

During the block polymerization of all high conversion samples, the same weight ratio of the PDMS macroinitiator to styrene monomers are used[14]. One would expect that the initiator concentration would decrease as the molecular weight of the PDMS segment in the macroinitiators increases. Therefore, by changing the molecular weight of the PDMS segments in the macroinitiator, the PS block length and the number of blocks per polymer chain will be altered. As a result, the solid state morphology and the bulk properties of the final polymer will be changed.

3.1.1.2 Conversion Level of the Styrene Monomer

The free radical polymerization has some features of a conventional free-radical behavior but it also has certain features more consistent with a "living polymer" polymerization[14]. Specifically, the molecular weight of the polymer is directly related to the conversion level of styrene. The higher the conversion level is, the higher the molecular weight should be. Since the PDMS block length is fixed by the PDMS segments in the macroinitiator, only the PS block length would in principle be changed during polymerization. As the conversion level increases, the PS block length increases. By varying the conversion level, the PS block length can be altered. Thus, the morphology and the final properties of the block polymer will be influenced.

3.1.1.3 Type of Vinyl Monomers

In general, the degree of phase separation of a block system is dependent on the difference between the solubility parameters of two chemically dissimilar components. As the type of vinyl monomer changes, the degree of phase separation in the PDMS-vinyl block polymer may be changed. Thus, the bulk properties of the block polymer are also expected to vary. Depending on the glass transition temperature of the blocks of individual vinyl species and the degree of phase

mixing of the component blocks, the T_g's of the block system components may be altered. Therefore, the width of the rubber plateau can change. In this study, three different styrene derivatives: 4-methoxystyrene, 4-t-butylstyrene, and 4-methylstyrene, will be utilized as the "hard segment" in PDMS-styrene block polymers. Due to the changes in chemical structure, the T_g's of these monomers are different from that of the styrene, i.e. the T_g of homopolymer 4-t-butylstyrene is 144°C. Also the solubility parameters of these monomers are different from that of styrene (Table 1). Therefore, the degree of phase separation and the width of the rubbery plateau of these PDMS-vinyl block polymers would be expected to be different from that of the PDMS-PS block polymers.

3.1.2 Effects of Film Preparation Methods

In solution cast films, the morphological texture of a block polymer depends on the interaction between the two different block components (A-B interaction) and the polymer-solvent interactions. There are two types of polymer-solvent interaction: A-S or B-S interaction which is due to the interaction between the block component (A or B) and the solvent. By choosing different solvents with different solubility parameters, the polymer-solvent interaction will be changed. Therefore, the morphological texture and the degree of phase mixing will also be changed as will the final properties of the resulting solid. In this study, three different solvents, methylene chloride, toluene, and cyclohexane were used to cast PDMS-PS block polymer films, and the solubility parameters of these solvents are also listed in Table 1 on page 48. Methylene chloride is a good solvent for the PS blocks while cyclohexane is a good solvent for the PDMS blocks, and toluene is a good solvent for both components. By using these three different solvent as the casting solvent, the morphology and the bulk properties of the solution cast films would be expected to be different, because of the changes in polymer-solvent interactions during the film casting.

In the thermal compression molding process, the morphological texture and the degree of phase separation is only dependent on the A-B interactions between two chemically dissimilar

Table 1. Solubility parameters of polymers and solvents used within this study.

Sample	δ (cal/cc)$^{1/2}$
PDMS	7.3
Styrene	9.3
4-t-butylstyrene*	8.9
4-methoxystyrene*	9.3
4-methylstyrene*	9.3
Methylene Chloride	9.7
Toluene	8.9
Cyclohexane	8.2

* Calculated by group contribution method.

components. Therefore, the morphology and the bulk properties of thermal molded films will differ from that of the solution cast films.

In the next section, the variables studied for the structure property behavior of the ionene elastomers will be discussed.

3.2 SEGMENTED PTMO-IONENE POLYMERS

Segmented PTMO ionenes are a new type of elastomer. Some of the unique character of these materials discussed with the literature review sections have drawn the attention of both academic and industrial researchers. Since the synthesis of these PTMO-ionene elastomers is relatively simple, the PTMO soft segment length can be easily varied as well as the coupling agents which serve as the ionene hard segments. Therefore, these materials are well suited for model structure - property studies. The objective of the research on these ionene materials is to explore the driving forces for microphase separation and the relationship between the chemical structure and the bulk properties of these systems. Another more challenging objective is to verify the morphological texture of these new materials. To achieve these goals, several important chain structure variables of these materials and the effects of film preparation methods have been studied and will be discussed.

3.2.1 Chain Structure Variables of the Ionene Elastomers and Their Importance

3.2.1.1 The Molecular Weight or Segment Length of the PTMO Soft Segments

In ionene polymers, the ion content plays a very important role on the final properties of the polymer. Due to the structure of the chain, the ion content decreases as the PTMO segment length

increases. By changing the PTMO segment length, the ionic concentration as well as the volume fraction of the hard segment is systematically altered, and the resulting polymer is expected to have different final properties. Also, as the PTMO segment length changes, the crystallization of the PTMO segments may occur depending on its chain length. The crystallinity of the soft segment will also change the final properties of the polymer. In this study, the PTMO segment molecular weight (segment length) was in the range from 550 to 10,000 in Mw.

3.2.1.2 Type of Counter Ions

In the segmented PTMO ionene polymers, the strength of the interchain interaction may strongly depend on the ionic nature of the counter ions. By changing different counter ions with different electronegativity, the interchain interaction strength may be changed, thus, the final properties of the polymer will be altered. Besides the electronegativity of the ions, the size of the counter ion has also been considered. For example, a bromine ion has a diameter of 3.90 angstroms which is similar to the size of a benzene ring. Therefore, the size of the counter ion could strongly affect the packing in the "hard domains". Hence, the morphology of the ionene may vary with the type of counter ion. In this research, three different counter ions, chlorine (3.62Å), bromine (3.90Å), and iodine (4.32Å), were used for the PTMO - dihalide ionene elastomers.

3.2.1.3 Type of Hard Segment

Different types of hard segments can change final properties of the ionene polymers depending on their size and chemical character. For example, a short rigid hard segment such as dibromo xylene can likely provide a stronger interchain association than a longer or a more flexible type of ionene hard segment. In such a case, the temperature sensitivity of the rubbery plateau may be reduced and the softening temperature may be altered. Also, the nature of the microphase separation will likely be affected. All of these features will be considered and discussed.

3.2.2 Preparation Methods

The preparation methods of the final films often change the bulk properties. Two film preparation methods of solution casting and thermal molding were used to prepare films. In solution casting, chloroform were used to cast PTMO dihalide ionene elastomer films. For PTMO-dipyridinium ionene elastomers, methanol and acetone were used as casting solvents. However, the bulk properties of PTMO ionene elastomer films were been affected by the type of casting solvent[Lair,Bin].

For thermal compression molding, the major consideration is the thermal stability of the PTMO soft segment and the ionene linkages. Therefore, the thermal molding temperature used was only be 10°C higher than the softening point of the ionene elastomers determined by TMA technique. Also a short molding time (ca. 5 minutes) was used to minimize thermal degradation.

CHAPTER IV

EXPERIMENTAL METHODOLOGY

4.1 Film Preparation

4.1.1 Free Radical Synthesized PDMS-PS Block Polymers

The free radical synthesized PDMS-PS block polymers have been kindly supplied by Dr. J. V. Crivello. In this study, two film preparation methods, solution casting and thermal compression molding, have been used. Three different solvents, methylene chloride, toluene, and cyclohexane, have been used to cast films. Before film casting, the as received polymers were dried in vacuo at 60°C for 24 hours. Then 2 grams of polymer were dissolved into 20cc of the selected casting solvent and stirred for 2 hours until all polymer was completely dissolved. Films were cast on a teflon surface at room temperature. The solvent was allowed to evaporate slowly over a period of two or three days. These films were then dried at 80°C for an additional four hours. The films were further dried in vacuo at 80°C for 24 hours to remove any last trace of solvent.

Some PDMS-PS block polymer films were prepared by compression molding. The polymers were heated at 150°C for 20 minutes and then were pressed at 15000 Psi for 20 minutes at the same

temperature. The PDMS-PS polymer films were stored in vacuo at ambient temperature before using.

3.1.2 Ionene Elastomers

Two types of PTMO-ionene elastomers, the PTMO-dihalide ionene elastomers supplied by Dr. C. M. Leir from 3M and the PTMO-dipyridinium ionene elastomers synthesized by Dr. B. Lee of Professor J. E. McGrath's group in VPI, were investigated in this study. The ionene elastomer films were prepared from either solution casting or thermal compression molding.

Solution cast films of dihalide ionenes were cast from chloroform. For the dipyridinium ionenes, films were cast from either methanol or acetone. The ratio of 1 gm polymer to 10cc solvent was used for the casting. The casting was performed at ambient temperature on a teflon surface over a period of 2-3 days. The films were dried at 80°C in vacuo for 24 hours after casting.

Some ionene elastomer films were also prepared by compression molding. In order to prevent the dissociation of the PTMO soft segments, the molding was carried out at a temperature of 10°C higher than the softening point of the ionene elastomers for only 10 minutes. After the thermal molding, the polymer films were quenched to room temperature. All of the ionene films were stored in a vacuum desiccator until used.

4.2 Experimental Methodology

4.2.1 Mechanical Properties

4.2.1.1 Stress-Strain Measurements

The tensile stress-strain behavior of the PDMS-PS block polymers and ionene elastomers were measured on an Instron 1122 tester at ambient temperature (23 - 25 °C). Dogbone specimens with dimensions of 2.8mm in width and 10mm in length were cut from the films. For the PDMS-PS block polymer, the tensile tests were carried out at a crosshead speed of 5 mm per minute. Cyclic-tensile stress-strain measurements were also carried out on some selected samples cast from cyclohexane at the same crosshead speed for hysteresis behavior. For the ionene elastomers, a crosshead speed of 50mm per minute was used for all samples. The hysteresis behavior of these materials was also measured at the same crosshead speed.

4.2.1.2 Stress-Relaxation Tests

Stress-Relaxation tests were performed on a Tensilon (Model UTM-II) at ambient temperature. The same sample dimension was the same as the samples for the stress-strain measurements. The crosshead speed was 20mm per minute for all the measurements. The strain level was 0.1 for the PDMS-PS block polymers and 0.25 for the ionene elastomers.

4.2.1.3 Creep Tests

Creep experiments on the ionene elastomers were conducted at room temperature by applying a specified load. The samples had the same dimensions as the samples in the tensile tests. In order

to keep essentially a constant stress during the experiments, the maximum strain level was about 0.1. Since the ionene samples containing longer PTMO segments (Mw > 3400) could slowly crystallize at room temperature, it was necessary to limit the experiment period to be within two weeks. Therefore, the initial stress level was chosen to allow the strain of the softest sample to reach a value 0.10 in a period of 4-5 days. For all ionene samples, and the initial stress of 0.15 MPa was used for the creep experiments. The initial strain was less than 0.06 depending on the samples. During the creep experiment, the sample length was monitored by a LVDT (linear voltage displacement transformer). The tensile creep compliance, D(t), was calculated from these data.

4.2.2 Differential Scanning Calorimetric Analysis

The differential scanning calorimetric (DSC) measurements were carried out using a Perkin-Elmer DSC-4 or a DSC-2 differential scanning calorimeter. For the high temperature range (above 25°C), the DSC-4 calorimeter was used whereas for the low temperature measurement range (-150°C to 25°C) the DSC-2 was used.

The DSC-4 was calibrated using a standard indium sample. At the scanning rate of 10°C per minute, the temperature deviation was $\pm$0.5°C and the deviation for the specific heat was $\pm$0.5%. The sample weight of all samples for for the DSC studies was 10$\pm$0.1mg and the samples were sealed in an aluminum sample cell. Standard polystyrene samples purchased from Scientific Polymer Products Co., were used for heat capacity analysis. These PS samples have a ratio of Mw/Mn < 1.06 and the Mw of these PS samples ranged from 1,940 to 100,000.

For the high temperature DSC studies, all the PDMS-PS block polymer samples were heated to 140°C for 30 minutes then quenched to room temperature before DSC data were obtained. The DSC measurement was carried out at a heating rate of 10°C per minute and a cooling rate of 320°C per minute under a constant stream of nitrogen. Data were collected during the heating part of the cycle. The glass transition temperature, Tg, was defined as the temperature at which the heat capacity of the sample was between that of the glassy and rubbery states (midpoint method).

For the low temperature range DSC studies (-150°C - 25°C), the PDMS-PS samples were annealed at 100°C for 30 minutes then quenched to room temperature. The samples were further cooled down to -150°C by liquid nitrogen at a cooling rates of 320°C per minute. For the ionene elastomers, the samples were quenched down to -150°C by liquid nitrogen. The DSC data were collected during heating at a rate of 10°C per minute.

4.2.3 Dynamic Mechanical Thermal Analysis

The dynamic mechanical studies of PDMS-PS block polymers and ionene elastomers were performed on an automated dynamic viscoelastometer model Rheovibron DDV-II-C, (Imass). The temperature range utilized was from -150°C to 200°C. The sample strips were cut from polymer films and cooled to -150°C at a cooling rate of 2-3°C per minute. The measurements were carried out at frequencies of 110, 11, and 1.1 Hz with a heating rate of *ca.* 2°C per minute. All measurements were performed under a purging dry nitrogen stream to minimize moisture condensation.

4.2.4 Thermomechanical Analysis (TMA)

The TMA studies were carried out on a Perkin-Elmer TMS-2 Thermomechanical Analyzer using the penetration probe. The temperature range utilized was from -150°C to 150°C for the PDMS-PS block polymers and -150°C to 250°C for the ionene elastomers. The loading was 10 grams and the heating rate was 10°C per minute. All the measurements were performed in a nitrogen atmosphere.

4.2.5 X-Ray Scattering

The microphase structure of the PDMS-PS block polymers and ionene elastomers was also investigated by using small angle X-ray scattering (SAXS). An automated Kratky slit collimated small angle X-ray camera was utilized for the SAXS intensity measurements. The X-ray source was a Siemens AG Cu 40/2 tube, operated at 40 kV and 20 MA by a GE XRD-6 generator. A Cu Kα-radiation of wavelength 0.154 nm was obtained by Ni-foil filtering. The scattered intensity was monitored by a one dimensional position sensitive detector (M. Braun-Innovative Technology Inc.). In all the SAXS intensity measurements performed on the Kratky camera, the incident x-ray beam was parallel to the normal of the surface of the polymer films (refer to scheme 3). In addition, a simple Warhus camera with pinhole collimation utilizing a flat plate film cassette was also used. With this device, the beam was passed either parallel or perpendicular to the normal of the film surface with an appropriate exposure time to provide direct recording of the intensity under vacuum.

The SAXS measurements on the PDMS-PS block polymers were carried out at ambient temperature on the Kratky camera. For the ionene elastomers, the SAXS studies were performed on both the Kratky and Warhus cameras at ambient and elevated temperatures.

Wide angle X-ray scattering (WAXS) had also been used to study the structure of the PTMO ionenes. The WAXS studies were also carried out on the Warhus camera at ambient and elevated temperatures.

4.2.6 Transmission Electronic Microscopy (TEM)

In all TEM studies, cryomicrotomed ultrathin sections (< 50nm) of polymer films were used. The ultrathin sections were cryo-ultramicrotomed on a Reichert-Jung ULTRAVUTE system (model FC4). The ultramicrotoming temperature was -100°C and -80°C for the PDMS-PS block polymer and the ionene elastomers respectively. The sections were taken from a liquid surface with

copper grids. The liquid was methanol for the PDMS-PS block polymer and was isopropanol for the ionene elastomer. The ultrathin sections were microtomed in the directions both parallel and perpendicular to the film surface. Due to the high electron density differences of the blocks or segments in both PDMS-PS system and the ionene systems, sufficient contrast existed without the need for selective staining.

A Philips EM 420 Scanning Transmission Electron Microscopy (STEM) was used to examine the morphological texture of the PDMS-PS block systems. The STEM was operated in the TEM mode at an accelerating voltage of 100kV.

The TEM studies of ionene elastomers were performed on a JEOL 2000EX high resolution transmission electron microscope with an accelerating voltage of 200kV. The high accelerating voltage provides a higher penetration capability and reduces spherical aberration and multi-scattering. Therefore, a higher resolution can be obtained. A small objective aperture (20μm) was used in the TEM studies. The small objective aperture helps to eliminate some high frequency artifacts.

Both microscopes, Phillips and JEOL, were operated at optimum adjustment to minimized astigmatism.

CHAPTER V

STRUCTURE-PROPERTY BEHAVIOR OF FREE RADICAL SYNTHESIZED PDMS-PS AND PDMS-STYRENE DERIVATIVE BLOCK POLYMERS

The free radical synthesized PDMS-PS and PDMS-styrene derivative block polymers used in this study have been supplied by Dr. J. V. Crivello. The polymer films have been prepared by either solution casting or thermal compression molding. Based on the type of vinyl monomers, the PDMS block length, the styrene conversion level, and the type of sample preparation method, the samples have been designated as following:

S14 - 62 - M
| | | | |
| | | | **Type of casting solvent**
| | | | M = Methylene Chloride, T = Toluene, C = Cyclohexane,
| | | | and P = Thermal Molding film.
| | | |
| | | **Reaction Conversion % (styrene)**
| | |
| | **PDMS block length Mn/100**
|
Type of vinyl monomer
S = Styrene, B = t-Butylstyrene, M = Methylstyrene, and O = Methoxystyrene.

Composition of these materials are listed in Table 2 on page 60.

Table 2. Composition of polydimethylsiloxane(PDMS)-vinyl block polymers.

Sample	PDMS Block Mn	PDMS (wt%)	Conversion (%)	Mn (g/mol.)
S14-95	1360	37	95	85,400
S26-58	2634	40	58	99,400
S26-91	2634	41	91	161,000
S45-25′	4520	50	3	116,000
S45-35′	4520	58	5	155,000
S45-45′	4520	61	7	146,000
S45-45	4520	52	45	254,000
S45-95	4520	42	95	148,000
S89-34	8940	49	34	162,100
S99-95	9894	42	95	290,100
S193-95	19300	41	95	310,000
B99-95	9894	50	95	196,900
M99-95	9894	42	95	171,800
O99-95	9894	48	95	199,000

Note: S45-25′, S45-35′, and S45-45′ samples are designated by the reaction time in minutes. The conversion of these samples are estimated numbers.

5.1 FEATURES OF MICROPHASE SEPARATION FOR PDMS-PS BLOCK POLYMERS

5.1.1 Indication of Formation of the PDMS-PS Block Polymers

Earlier studies of the same PDMS-PS systems have shown that only block polymers were formed by the free radical polymerization developed by Crivello et. al.[13,14]. This is supported by the composite GPC chromatogram shown in Figure 14 on page 62. In this case, three different detectors were employed: a refractive index detector to monitor the elution volume of any species, a UV detector (at 254nm) to sample the aromatic content from the PS block, and an IR detector (at 2.9 μm) to measure the Si-O-Si content from the PDMS block. As shown in Figure 14, the responses of these three detectors are nearly identical which indicates that the composition of a polymer is homogeneous throughout the entire range of molecular weights. Results from NMR analysis[14] also supported the GPC data regarding only the formation of block polymers. Besides the GPC and NMR results, other evidence such as the occurrence of intense iridescence in the later stages of the reaction, solvent dependent mechanical properties, and occurrence of two glass transition regions also confirmed phase separation occurs in these polymers and indirectly supports block polymer formation.

5.1.2 Bulk Properties of the PDMS-PS Block Polymers

5.1.2.1 Thermal Properties of the PDMS-PS Block Polymers

Indeed results from DSC, dynamic mechanical analysis, TMA and TEM all support that block polymers are formed by this free radical synthesis and that microphase separation occurs. As one example, Figure 15 on page 64 shows the DSC thermograms of these PDMS-PS block

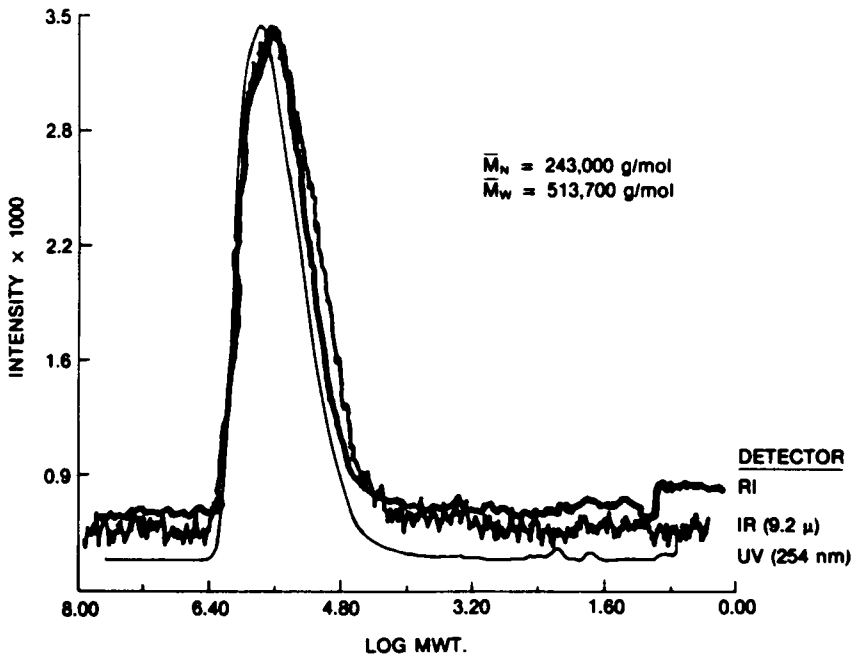

Figure 14. GPC curves for sample S26-58 polymer using IR, UV and refractive index (RI) detectors. (Ref. 14)

polymers. The transition temperatures and other thermal characteristics have been listed in Table 3 on page 65.

The DSC results show that the T_g of the PDMS block decreases as the PDMS block length increases. For example, the PDMS T_g is *ca.* -100°C for S14-95-M and -125°C for S193-95-M (Figure 15 & Table 3). The latter T_g is almost the same as the T_g of homopolymer PDMS with a similar molecular weight[70,85-87]. For PDMS homopolymers, the T_g increases from -130°C to -125°C as the the number average molecular weight, Mn, increases when the Mn is less than 2460 [85]. When the number average molecular weight is greater than 2460, the T_g is around -124°C and only increases very slightly with an increase in molecular weight[85]. Therefore the distinctly higher T_g of the shorter PDMS blocks in these free radical PDMS-PS block polymers is believed due to some degree of styrene mixing within the PDMS block phase. It is also possible that since the PDMS blocks would, on the average, be connected to glassy PS blocks, some restriction of mobility at the chain ends would also conceivably slightly enhance the PDMS T_g values. Such postulations have been made by others with experimental support[88,89]. For example, the T_g of a aminopentyl terminated PDMS oligomers with the Mn of 1550 has been found to be -120°C[88] which is 7°C higher than the T_g of linear PDMS having similar molecular weight[85]. The higher T_g was attributed to the restrictions imposed on the soft PDMS segments by the polar end-groups[88].

When the PDMS block length is greater than 4500, both an exothermic peak and an endothermic peak are observed in addition to its glass transition. The exothermic peak corresponds to the crystallization of PDMS blocks and the endothermic peak is the corresponding crystalline melting peak of these same blocks. The crystallization and melting peaks have not been seen for the shorter PDMS blocks (Mn less than 4500) samples because of the very small length of the siloxane chain involved[88]. Similar observations have been noted in PDMS-PS diblock polymers[90] and in PDMS-urea segmented polymers prepared using oligomeric PDMS species[85,88,90]. While often a dual melting point may be observed in homopolymer PDMS[85,88,90], the results from these free radical PDMS-PS block polymers displayed only a single somewhat broadened melting peak. These observations are consistent with earlier results obtained on PDMS - urea segmented copolymers studied by Tyagi[88]. All melting peaks range from -51°C to -43°C and increase with the

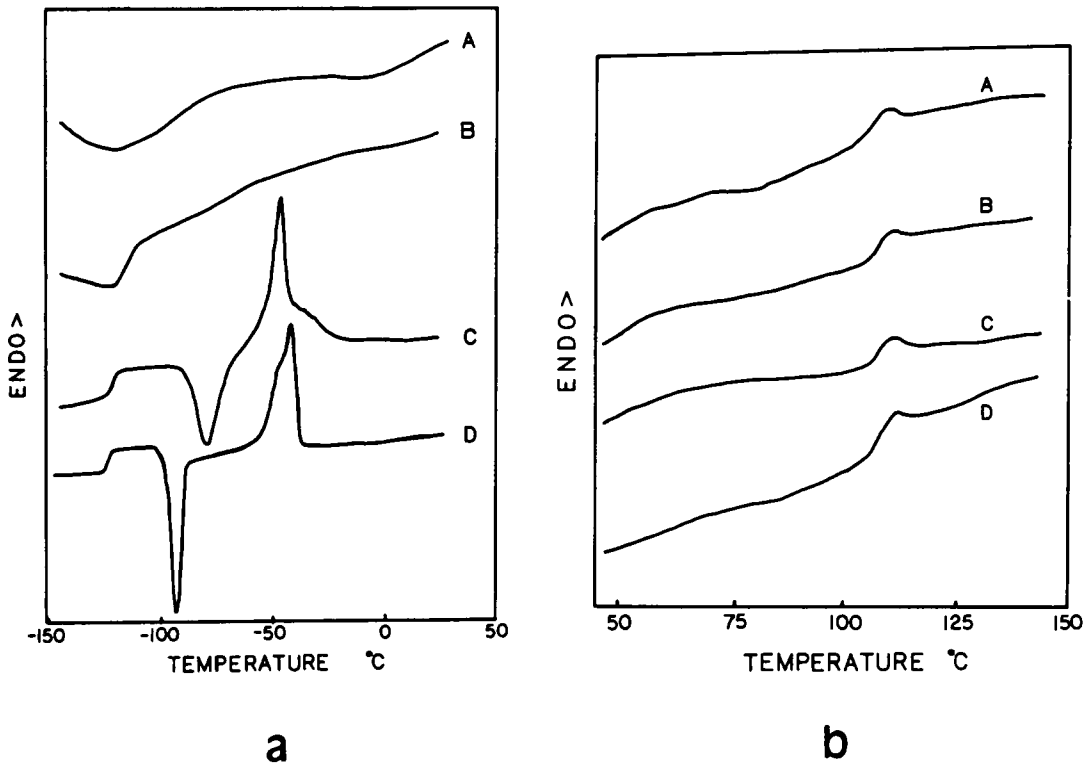

Figure 15. DSC thermograms of high conversion free radical synthesized PDMS-PS block polymers.: (a). Low temperature range. (b). High temperature range. Curves: A. S14-95-M, B. S45-95-M, C. S99-95-M, D. S193-95-M.

Table 3. Glass transition and melting point of the free radical PDMS-PS block polymers.

Sample	PDMS Block			PS Block
	T_g °C	T_c °C	T_m °C	T_g °C
S14-95-M	-100			104
S26-91-M				103
S45-95-M	-116			104
S89-34-M	-125	-82	-51	101
S99-95-M	-123	-81	-49	107
S193-95-M	-125	-94	-43	107

PDMS block length. As expected, the melting temperature of the PDMS blocks is lower than that of pure PDMS homopolymer.

The DSC results also indicate that the glass transition temperatures of the PS blocks for all of these high conversion level polymers is around 105°C (Table 3 on page 65), although there are some differences in the breadth of the T_g dispersion. The T_g values recorded here are higher than the values reported earlier by Crivello et. al.[14]. The lower T_g values presented earlier were caused by the presence of residual solvent in the samples[91]. The polystyrene T_g values (greater than 100°C) for these polymers suggest that a reasonably high molecular weight (greater than 10,000) PS block is formed during the free radical polymerization. The greater breadth of the T_g may result from a broadened molecular weight distribution of the PS block. A more detailed discussion on the molecular weight and the molecular weight distribution of the PS blocks will be given in later sections. The DSC results also show that the T_g of the PS phase is not altered with varied PDMS block lengths for these high conversion samples. However, the T_g of the PS phase does change with low levels of styrene conversion. For example, sample S89-34-M displays a distinctly lower T_g for the PS phase and is indeed a real effect which will be a topic of discussion in later sections where styrene conversion level is considered.

5.1.2.2 Dynamic Mechanical and Thermal Mechanical Behavior of the PDMS-PS Block Polymers

The dynamic mechanical data also clearly confirm that phase separation occurs in these materials. Figure 16 on page 68 shows the dynamic mechanical spectra for the high conversion PDMS-PS block polymers. For all samples, two or more transition states are displayed. Two of these transition states correspond to the glass transitions of the two components PDMS and PS respectively. A distinct plateau in the behavior of E′ also exists between these two transition states but its width is distinctly dependent upon the initial length of the PDMS block. For the polymers containing long PDMS blocks such as S99-95-M and S193-95-M, a small peak also appears at

-50°C in the tanδ spectra. This peak corresponds to the crystalline melting region of the PDMS blocks - see Figure 16 on page 68.

The dynamic mechanical results indicate that the PDMS block length has a strong influence on phase mixing. When the block length of the PDMS decreases, the behavior of tanδ of the PDMS T_g transition is distinctly broadened and shifted to higher temperatures. This shift is believed to be caused by phase mixing of the shorter PS blocks in the PDMS regions. Strong indirect support for this latter statement extends from the work of Hashimoto, et al.[92] who simulated the dynamic mechanical response of tapered PS-polyisoprene block polymers using a composite model. In particular, their calculations considered the relative effects of two component mixing within domains (domain mixing) and the effects of two components mixing in the boundary regions (interphase mixing) on the dynamic mechanical response. Some of the pertinent results of their simulation are shown in Figure 17 on page 69 and distinctly support the author's own experimental observations. As their results indicate, the E″ peak correlated with T_g of the soft segment is shifted to a higher temperature as the degree of phase mixing of two block components increases (Figure 17 on page 69), while the E″ peak of the hard block is only slightly shifted to lower temperatures. Comparing data of Figure 16 on page 68 with Figure 17 on page 69, one notes that these results are very similar except that the tanδ data have been utilized here instead of E″ - this change in variable will result in a somewhat higher transition peak but the general response is the same. This upward shift of the PDMS T_g shown in Figure 16 is strongly believed to arise from phase mixing of the shorter styrene blocks within the PDMS regions. Note that when the PDMS block is greater than 4,500, only a small shift of T_g is observed - recall Figure 16 on page 68. It is necessary to point out that the simulation results of Hashimoto et. al. are based on a composite model in which the different phase layers are perpendicular to the stretch direction. If the morphology of the polymer changes, the result would be expected to somewhat different.

It is interestingly to note that the position of the tanδ peak of the styrene phase is only slightly affected by the PDMS block length. This difference is an important clue and is believed to arise principally from the formation of the more prevalent high molecular weight PS blocks and hence there is at best little mixing of PDMS occurring within the rich PS phase. In Figure 16 on page

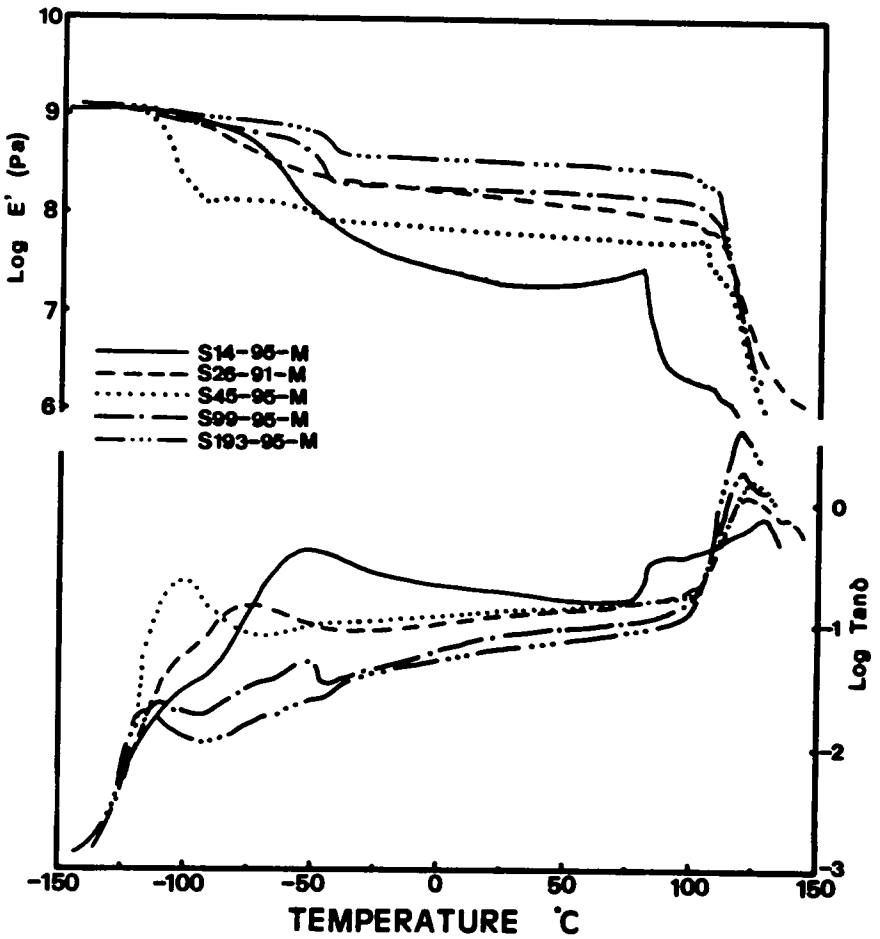

Figure 16. Dynamic mechanical behavior of the high conversion PDMS-PS block polymers.

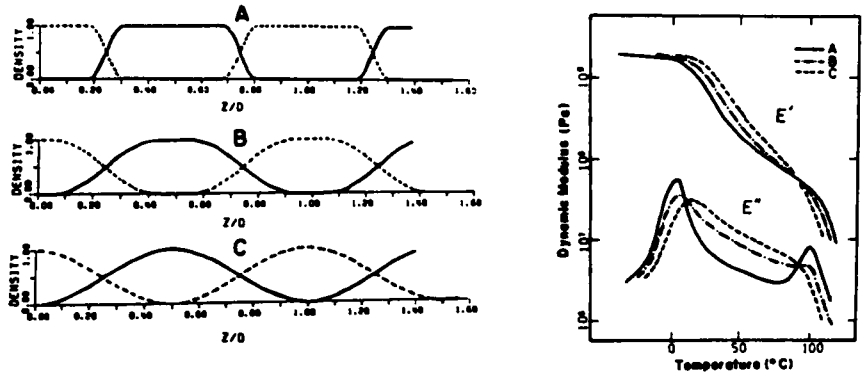

a

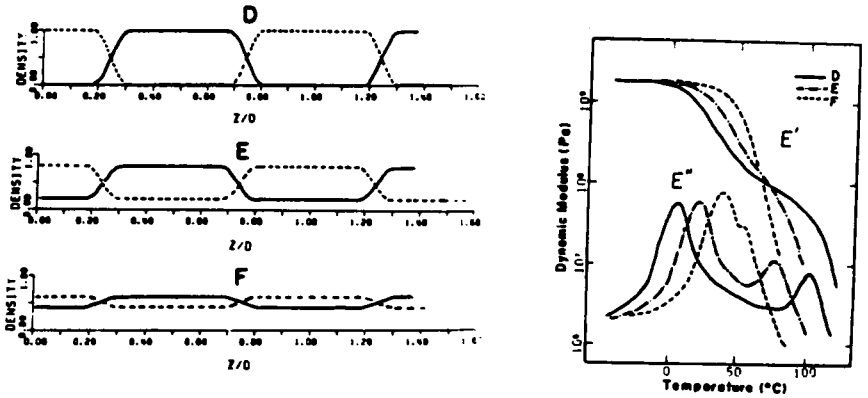

b

Figure 17. Spatial concentration distribution of PS-BD tapered block polymers and computer simulated dynamic mechanical responses: (a). The interphase mixing increases in the order from A to C, (b). The domain mixing increases from D to E. The frequency of computer simulated dynamic mechanical responses is 10 Hz. (From Ref.92)

68, the E′ behavior of S14-95-M shows an increase with temperature from 25°C to the T_g of the PS blocks. In this specific sample, the PDMS phase is a continuous phase. The increasing modulus with temperature is therefore believed to be caused by the rubber elasticity effect of the PDMS matrix. Another unusual feature of these PDMS-PS polymers is a small but reproducible two-step drop of the storage modulus, E′, for the PS glass transition region for most high conversion samples (Figure 16 on page 68). These two step transitions are highly frequency dependent and they possibly may be caused by the incompatibility between the large and the small molecular weight PS blocks which may result from the free radical copolymerization - see later discussion.

The TMA results are also in good agreement with the dynamic mechanical results. As Figure 18a shows, these systems each display two distinct glass transition regions. The T_g of the PDMS phase is shifted to higher temperatures as the PDMS block length decreases. For S193-95-M, the disappearance of the PDMS T_g is caused by the high degree of crystallization of the long PDMS blocks. At temperature higher than 50°C, a thermal expansion is observed which may be caused by some large PS blocks in this sample. The degree of penetration within the rubbery region (between the two T_g′s) also decreases with an increase of the PDMS block length. For all samples, there is a shoulder on the PS softening peak as noted from the derivative curves (Figure 18b). These shoulders indicate that the PS glass transition undergoes what appears to be a two step process in these materials. These results are consistent with the results from dynamic mechanical analysis. The changes in the penetration and the step transition in these materials are speculated from the changes in the block length and the molecular weight distribution of the PS blocks resulting from the changes in the PDMS block length. As a result, the morphological texture of these materials would be changed. TEM data that will be presented shortly will support this speculation.

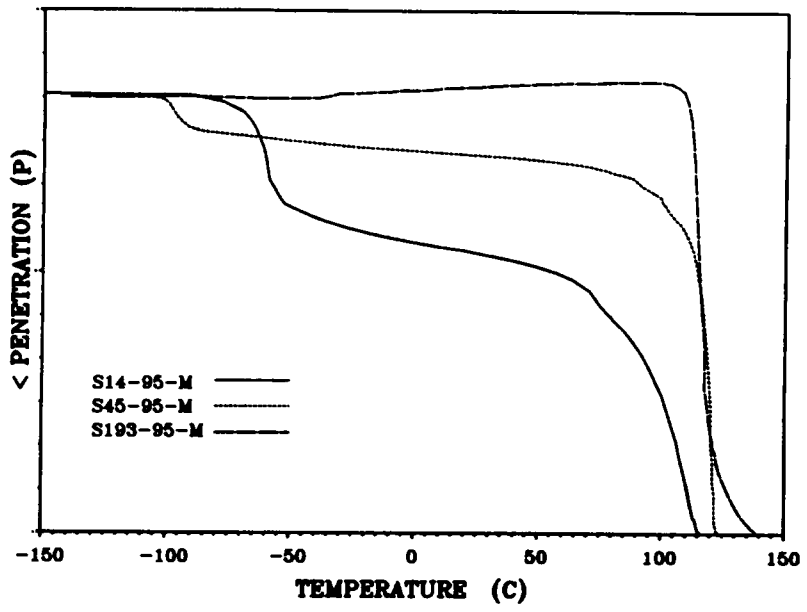

a

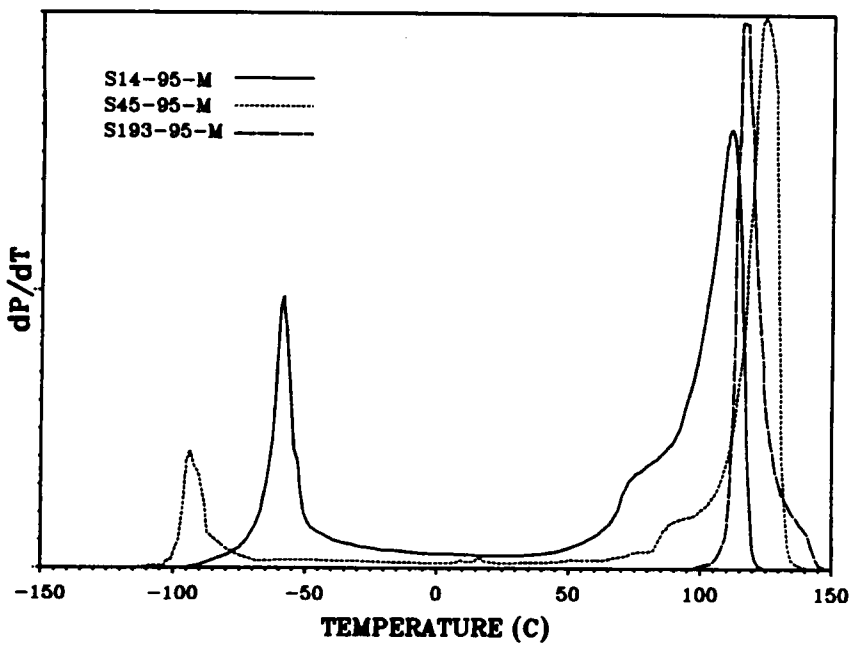

b

Figure 18. Thermal mechanical responses of high conversion PDMS-PS block polymers: (a). Penetration curves, (b). Derivative curves

5.1.3 Summary

As discussed above, these free radical synthesized PDMS-PS block polymers do show the characteristics of microphase separation such as two T_gs. The DSC and dynamic mechanical results indicate that the degree of phase separation in these materials changes with the PDMS block length, the conversion level of styrene monomers, and the type of styrene monomers. As will be shown in latter sections, the type of film casting solvent also strongly affect the phase separation and morphology of these materials.

5.2 EFFECT OF PDMS BLOCK LENGTH

5.2.1 Effect of the PDMS Block Length on the Degree of Phase Mixing

5.2.1.1 Estimating the Level of Phase Mixing and Its Dependence on PDMS Block Length

As is well known that at a given temperature, the level of microphase separation of nonpolar or low polarity block and segmented polymers is dependent on the square of the difference in the solubility parameters of the two components[24,30,37]. However, the block length of each component also affects the degree of phase mixing as does the general nature of certain architectural features such as the number of blocks or junction points per molecule[24,90]. While at times it is difficult to apply the general solubility parameter law in view of more complex interactions caused by polarity or ionic interactions, in the case at hand, the solubility parameter concept seems applicable. In fact, on this basis alone, since PDMS has a solubility parameter of about 7.3 and polystyrene about 9.4 $(cal/cc)^{1/2}$, one would anticipate very good phase separation because generally a difference in solubility parameters of nearly one unit promotes relatively sharp boundary regions at least for higher

molecular weight blocks[34]. A means of estimating the nature of phase mixing in a quantitative fashion can be estimated by scattering methods[45] but can also be determined by using calorimetry and in particular, the measurement of the change in heat capacity over the glass transition region. The latter of these methods will be applied here and in particular to the polystyrene glass transition.

Earlier studies[70,86,93,94] on the block polymer with the PS as the hard segments indicate that the T_g of the PS phase seems to principally depend on the block length of the PS blocks only. In these studies, the soft segments were either isoprene, butadiene, or PDMS. While the T_g of the PS blocks does not seem to change with the chemical nature of the soft segment except when phase separation is lost. However, the change in the heat capacity over the PS glass transition region (ΔC_p) and the breadth of the T_g have been noted to change with the nature of the soft segment. In block polymers, the ΔC_p of the styrene phase tends to provide lower values than the ΔC_p value of homopolymer styrene. Morese-Sequela et al.[93] have reported that the ΔC_p for the polystyrene block in an isoprene-styrene diblock polymer was below that observed for the corresponding styrene homopolymer. In their samples, the PS block molecular weight varied from 1400-4600. Cowie et al.[95] have also reported similar results on the value of ΔC_p for PS blocks of an isoprene-styrene triblock polymer. Krause et al.[86] have made related studies of PDMS-PS diblock polymers prepared by anionic synthesis. In their systems, the PS content ranged from 24 - 88 weight percent. The PS block molecular weight ranged from 1400-31,800 and the molecular weight of the PDMS block varied from 2400-23000. Again, they reported that the ΔC_p of the styrene block was equal or only slightly lower than that of the styrene homopolymer when the block length exceeded 8200. However, when the PS block length was less than this value, the ΔC_p of the PS block was either higher or lower than the homopolymer. The lower ΔC_p value was believed to be caused by mixing of some of the lower molecular weight PS into the PDMS phase. In contrast, a rise in ΔC_p can only be accounted for on the basis of a mixing of the soft block into the PS phase thereby promoting a greater rise in ΔC_p at the time the styrene transition occurs - this latter case assumes that no PS material has mixed in the PDMS phase. This mixing of the PDMS phase in the hard block however, would only be expected to occur when the polystyrene block length is low which would help promote a greater solubility of the two components[86].

Inspecting the DSC data of the free radical synthesized PDMS-PS block polymers - recall Figure 15 on page 64 - which indicates that the ΔC_p associated with the PS glass transition gradually increases with an increase of the PDMS block length. Since the T_g of the PS block is around 105°C for all high conversion samples (Table 3 on page 65) this indicates that the block length of the PS blocks may be well over 10,000 in molecular weight so that partial mixing of PDMS within the styrene phase would have negligible effects on the ΔC_p of the PS component. Hence, any change in ΔC_p of the styrene phase would in turn be indicative of the amount of polystyrene mixed within the PDMS phase. Indeed, one might expect a decrease in the ΔC_p of the PS phase which could then help account for the rise of the PDMS glass transition temperature noted in the shorter PDMS block length containing systems as was observed in the earlier dynamic mechanical spectra as well as the DSC data. Hence, by monitoring the ΔC_p change of each phase, one may be able to estimate the degree of phase mixing quantitatively. In the case of free radical PDMS-PS block polymers, the ΔC_p of the PDMS phase is difficult to utilize since as the PDMS block length increases, crystallization can also influence the results thereby making it difficult to separate the effects of phase mixing from that promoted by crystallization. Therefore, only the changes of ΔC_p of the PS glass transition temperature were utilized accordingly since this parameter is not convoluted with any other phenomena such as crystallization.

The ΔC_p method similar to that described by Pascault and Camberlin[96-98] has been employed to determine or estimate the phase mixing in these PDMS-PS block polymers. Figure 19a provides an illustration of the expected results and helps provide definition concerning the parameters utilized to estimate the degree of phase mixing (DPM) which will be defined as follows

$$\mathrm{DPM} = [1 - (\frac{\Delta C_p''}{w''})/\Delta C_p'] \times 100\% \qquad (10)$$

In Eq.(10), $\Delta C_p'$ is the normalized value for homopolymer styrene, $\Delta C_p''$ is the normalized ΔC_p for the block polymers, and w'' is the weight fraction of polystyrene in the block polymer. The value of $\Delta C_p'$ must be obtained from homopolymer polystyrene having comparable molecular weight of the PS blocks in a given block polymer. However, the ΔC_p of homopolymer styrene is almost

constant as well as the T_g value when the molecular weight (M_n) is greater than 10,000[86,99]. Since the T_g of the PS blocks in these free radical synthesized PDMS-PS block polymers is around 105°C which indicates the molecular weight of the PS blocks is reasonable high (> 10,000, refer to section 5.1.2.1.). Therefore, the ΔC_p values of homopolymer styrene with molecular weight of 19,000, which has a T_g of 104°C, has been chosen for the ΔC_p value. Utilizing this approach outlined above, ΔC_p data provided the results plotted in Figure 19b. The results show that the degree of phase mixing (DPM) decreases almost linearly with an increase in PDMS block length. The fact that there is a dependence for the shorter molecular weight PDMS is not surprising but the fact that it extends through the complete series where the PDMS block length is nearly 20,000 is somewhat unexpected. Certainly as the molecular weight of the PDMS blocks increase, their incompatibility with PS would also increase thereby enhancing phase separation which certainly the DSC results reinforce. It is somewhat surprising to see that the level of phase mixing suggested by these data is as high as calculated. But it should be kept in mind that the ΔC_p values would not be influenced to provide an over estimation if PDMS had mixed with the PS phase, i.e., indeed, the results would be the opposite!

Overall, these results are certainly supportive of the earlier observed dynamic mechanical and DSC results - the latter referring to the PDMS transition. That is, it is recalled that the PDMS glass transition observed by either method is shifted upward and broadened as was discussed in terms of the Hashimoto model. In view of the fact that the degree of phase mixing is in the range of 16 - 50%, therefore, broadening and shifting of the PDMS glass transition response in the dynamic mechanical result is not unreasonable. However, it is important to state again that the cause for this phase mixing within the PDMS component is believed principally due to the shorter styrene blocks - the presence of which will be further confirmed shortly. Interestingly, it is recalled that the upper glass transition for the PS phase shows it to be almost independent of the PDMS block length for both the dynamic mechanical and DSC results. In the case of the dynamic mechanical data, the intensity of this tanδ peak does indeed, however, depend on the PDMS block length. As the PDMS block length increases, the intensity of the PS tanδ peak also rises. This increase clearly suggests an enhancement of the degree of phase separation of the PS component, i.e. a lower

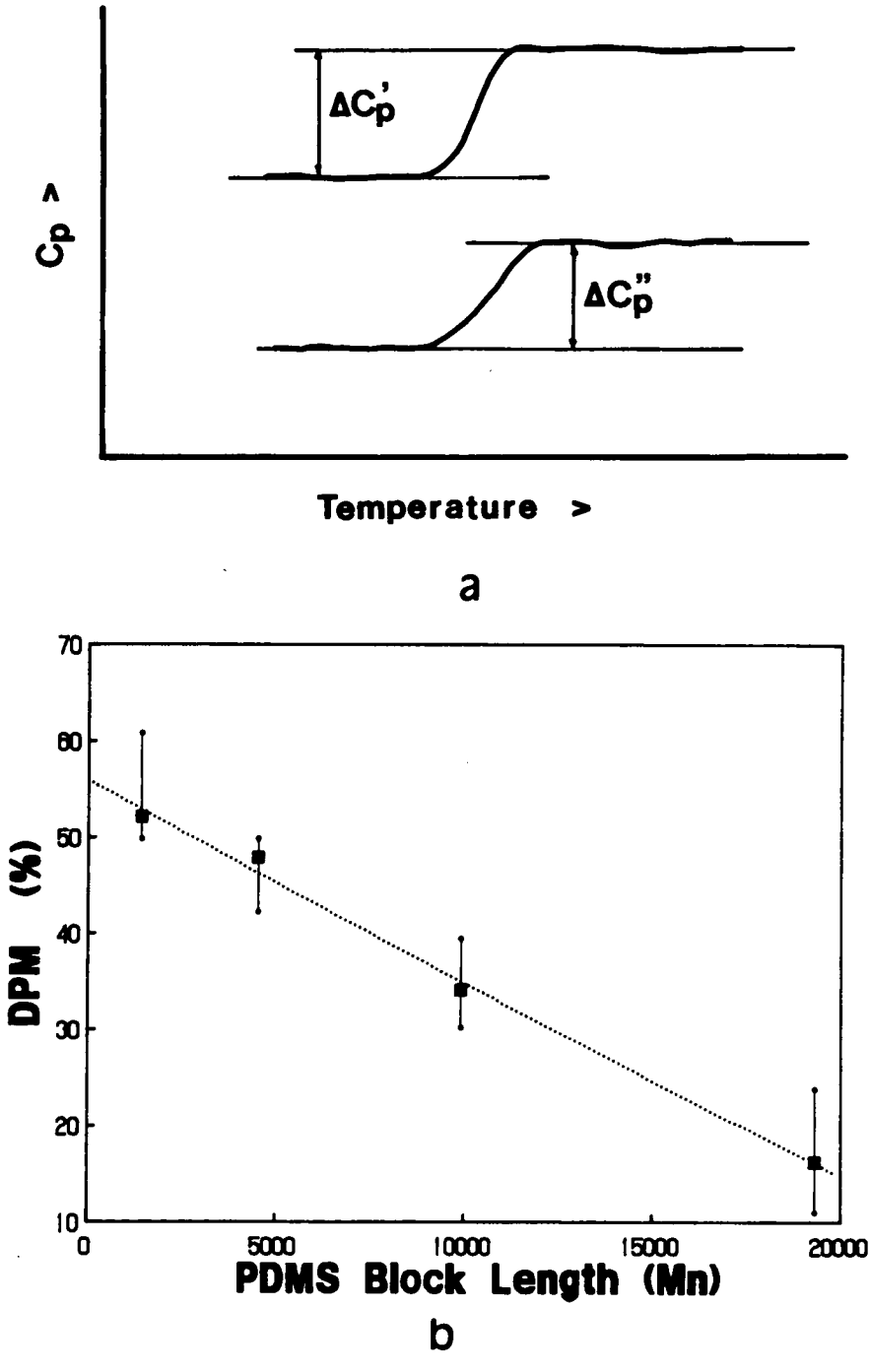

Figure 19. **Effect of the PDMS block length on the degree of phase mixing (DPM):** (a). Illustration of the ΔC_p method. (b). Effect of the PDMS block length on the degree of phase mixing in the PDMS-PS block polymers.

degree of phase mixing which is in line with the estimation of phase mixing from the DSC ΔC_p analysis.

5.2.2 Effect of the PDMS Block Length on Morphological Textures of the PDMS-PS Block Polymers

5.2.2.1 TEM Investigations

The results of the indirect methods such as DSC and dynamic mechanical analysis have clearly shown that these PDMS-PS block polymers display phase separation behavior although the nature of phase mixing varies within the two phases. In order to obtain a better understanding of these implications and the morphological character in general, small angle x-ray scattering studies were initially applied. However, it was immediately found that SAXS did not provide a scattering "peak" or "shoulder" indicative of microphase behavior for all of the higher conversion samples. This lack of a SAXS "interdomain distance" or correlation peak suggested that the domain structure may be too large to be detected within the resolution limits utilized. Hence, transmission electron microscopy (TEM) investigations were carried out on ultra-thin cryomicrotomed sections of the solvent cast films of these polymers (Note - these films were the same as those used for DSC, dynamic mechanical and other characterization studies).

TEM micrographs of these films as cast from methylene chloride (M) are shown in Figure 20 on page 79. The dark regions represent the PDMS phase and the whiter or lighter regions correspond to the PS phase. As mentioned previously, no staining procedures have been utilized nor were necessary to enhance the contrast between the two components. The TEM micrographs clearly show that a rather large styrene domain structure is formed in these block polymers irrelevant of the initial PDMS oligomer molecular weight. Specifically, the average styrene domain size in S14-95-M is about 40nm and the PS lamellar thickness of sample S193-95-M is about 80 nm - see Figure 20 (a and e). The large PS domain structures exceed the resolution

limits initially investigated by SAXS and clarify why a smaller interdomain spacing was not detected. A number of interesting features of these micrographs become readily apparent. The first is that the PDMS component is, in general, the continuous matrix phase for those systems displaying none lamellar morphologies, yet, the PDMS phase seems much lower in volume content than that of the PS component - see Table 2 on page 60. While certainly it is known that the choice of casting solvent can influence the morphology of PDMS-PS block systems[3,68,69,71,100], it is somewhat surprising that the lower volume fraction component can be clearly promoted to provide the continuous phase which, as will be illustrated later, distinctly controls the resulting mechanical properties. From these micrographs there is also the observation that rather sharp boundaries are observed between the two phases which might suggest that good phase separation has occurred in these block systems. Recall, the ΔC_p analysis and other related data that suggests that some polystyrene is distinctly mixed within the PDMS phase. This point will be addressed shortly. It might also be surprising that the degree of "black" PDMS phase appears to be of considerably lower volume content than the "white" PS phase in view of the fact that the PDMS should occupy the order of 45% by volume (this value will change slightly in view of density differences). However, in the case of where the more sphere-like domain structure exists such as in S14-95-M, one should recall that if a sphere-like morphology exists, the thickness of the outer encapsulating layer will appear much less than the radius, R, of the PS domains, since the volume scales with R^3 while the surface area scales with R^2. A simple calculation shows that the width of the PDMS region should be equal to one ninth of the diameter of the PS domain on a two dimensional projection for sample S14-95-M. The TEM results are close to this estimation. Caution must be given, however, to attempting to visualize what volume fraction of each phase should exist in view of composition due to domain boundary overlap and other microscopy considerations.

In considering the effect of the PDMS block length on the morphological textures observed, it is recalled that the PDMS block length is predetermined by the cationic synthesis of the macroinitiator. Therefore the PDMS block molecular weight distribution is predetermined from the equilibration reaction in generating the species used for the cationic polymerization. This distribution should be of the order of 2.0. In contrast, the PS blocks in these same polymers are produced

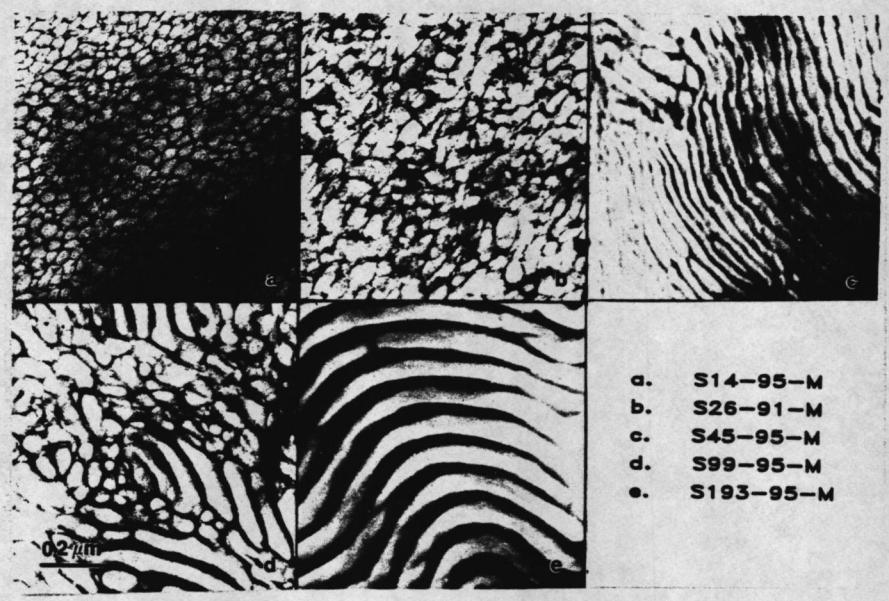

Figure 20. TEM micrographs of high conversion PDMS-PS block polymers : As the PDMS block length increases from a to e, the morphology of these polymers changes from spherical-like to lamellar structure.

by the free radical process and hence its molecular weight and molecular weight distribution may vary depending upon conversion level, size of macroinitiator and other variables - some of these points of which will be considered here. Clearly there is a correlation indeed in view of the PDMS block length and the type of morphology induced as observed in Figure 20. Specifically, as the PDMS block length increases, it is noted that the morphological textures for these methylene chloride cast systems changes from sphere-like styrene regions encapsulated within a PDMS matrix to that of the more expected lamella textures showing continuity of both phases. Observation that the domain structure changes with block length has been also observed by Saam et al.[3,69,71] in PDMS - PS diblock polymers prepared by anionic synthesis. In their polymers, the PDMS content was kept constant at 30 weight percent. By varying the Mn of the polymers, the PDMS block length was varied from 1700 to 17,900. As the PDMS block length decreased, the morphological structure changed from spaghetti like lamella to ill defined spherical textures. They suggested that 1700 was the lower block molecular weight limit of PDMS for phase separation to be induced[3]. Another interesting point was the fact that the PDMS phase was always noted to be the continuous phase even though it was the lower volume fraction component. Bajaj and Varshney[100] have also observed spherical PDMS domains in a styrene matrix for PDMS-PS-PDMS triblock polymers having 50 wt% PDMS where the block length of the PDMS was 23,400. When the PDMS block length and content was changed to 4700 and 34 weight percent respectively, the rodlike or cylindrical domain structure of styrene was formed. In both samples the PDMS was the center block with length 17000 in the former polymer and 11700 in the latter. But for the PDMS-PS multiblock polymers, the morphological texture does not change with the composition and the block length of the polymer[P123]. These additional observations of others provide some indication that the morphological features were not as predicted as usually implied based on composition ratio. However, there still is a need to account for the dependence upon PDMS block length and the size of the domains observed in these free radical synthesized PDMS-PS systems relative to the usual block systems where domain sizes are often considerably less if one were to assume that the block lengths of the two components being polymerized were comparable.

As discussed in earlier literature review sections (section 2.1.1.3), the domain size of a block polymer can be calculated by the 2/3 power law which relates the domain size with the molecular weight of the domain forming blocks or relates the interdomain spacing ("d" spacing) with the molecular weight of the polymer. This scaling law has been supported by both theoretical and experimental work[30,42,43]. It is necessary to point out that the experimental support have been based on di- or tri-block polymers in which the molecular weight of each blocks is well controlled with narrow molecular weight distribution. The author has, however, applied this 2/3 power law to the free radical synthesized PDMS-PS block polymers. In Figure 21 on page 82, the interdomain spacing measured from TEM micrographs have been plotted versus the molecular weight of the polymers. A linear regression has been applied, and the slope of the regression line is 0.7 which is close to the 2/3. However, there is a large divergence between the regression line and the data points. In fact, the regression coefficient is only 0.56! This large divergence may indicate that the application of this scaling relationship in the free radical synthesized PDMS-vinyl block polymers is limited due to the dispersity of block molecular weights particularly in the polystyrene region.

The domain size of a given block polymer especially for the polymer containing PDMS blocks can also be estimated from considerations of the unperturbed mean square end to end distance of a given chain. This value of the root mean square end to end distance (RMS) can be estimated by Eq.(8) shown in the section 2.1.3.1. as follows:

$$RMS = (CNL^2)^{1/2} \tag{8}$$

where **C** is the characteristic ratio and is 6.3 for PDMS and 10 for polystyrene. Within Eq.(8), **N** equals the number of bonds per block. In the case of PDMS, it represents the number of Si-O bonds whereas in the PS block it represents the number of C-C bonds per block. The value of **L** is the bond length and is equal to 0.164 nm for PDMS and 0.154 nm for PS respectively. It should be realized that in applying Eq.(8), unperturbed gaussian behavior is assumed. While this might be questioned in view of the short block lengths for the PDMS component in particular, this gaussian approximation has worked quite well in the case of PDMS-urea segmented polymers[45,88] in which the PDMS block length varies from 900 to 3,600. This gaussian approximation has also

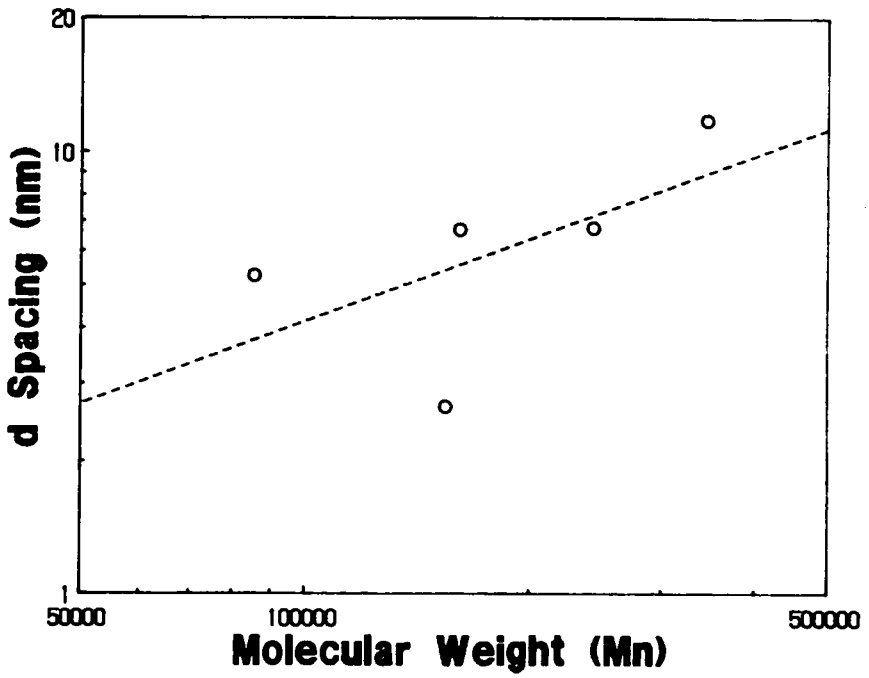

Figure 21. Relationship between "d" spacing and Mn of the PDMS-PS block polymers: The straight line is obtained by linear regulation, the slope is 0.7, and the regression coefficient is 0.563.

been used to interpret TEM results on PS-PI-PDMS triblock polymers of recent work from Malhotra et al.[101]. Their triblock polymers were prepared by an anionic method such that a well controlled molecular weight and narrow molecular weight distribution of each block was obtained. In their case, the PS, PI and PDMS blocks had molecular weights (Mn) of 12,400, 11,600 and 18,700 respectively and a lamellar structure was observed. The lamellar thickness measured from TEM micrographs was 10±2nm, and 8±1.5nm for the PS and the PDMS blocks. In applying Eq.(8) to the directly measured the PS and the PDMS lamella spacings, each result was in very close agreement to gaussian behavior, the calculated values being 7.4nm for the PS block and 9.3nm for the PDMS block.

Using the TEM micrographs, care was taken to determine the distance across the sharpest block boundary regions (PDMS phase) as well as the white regions (PS phase) and an average value determined accordingly. This was done for the various PDMS block length materials. In addition, Eq.(8) was utilized to estimate the expected RMS values. The results of the experimentally determined values with their standard deviation (σ) as well as those calculated from Eq.(8) are provided in Table 4 on page 85. It is noted that for the shorter PDMS block lengths, the measured value is only somewhat greater than that obtained from Eq.(8). Because the ends of the PDMS segments in the block polymers are somewhat restricted by polystyrene segments and the fact that some degree of mixing of PS is believed to occur in the PDMS phase, it is not surprising that the PDMS RMS value is somewhat enhanced. In addition, the PDMS chains might be expected to be indeed perturbed from their RMS value caused by the restrictions of the PS blocks. One might expect, however, as the PDMS block length increases, the chain would become more flexible and less perturbed as well as the fact that their would be less mixing with the PS component as discerned from the earlier DSC ΔC_p analysis. Hence, a closer approximation of the gaussian result might occur. The results show just the opposite. For the longer PDMS block containing samples, the block determined length is over twice as long as that obtained from the gaussian calculation from Eq.(8). Also the standard derivation (σ) increases with the PDMS segment length. Since the error in the measurements is not so great as to cause this large a discrepancy (Table 4 on page 85). Therefore, these results suggest that exceedingly large PDMS blocks may have been formed during

the free radical copolymerization by coupling of two or more of the original PDMS blocks with only a few styrene units, i.e. the observed thicker PDMS lamella are a result of the polymerization scheme. It should also be noted that based on the size of the styrene regions, lamella or sphere-like regions, suggests that the average styrene block length may be considerably large and therefore explain the observed high T_g of this component. At the same time, it also accounts for why the SAXS technique did not provide an interdomain spacing as would have been expected if the PS block lengths were comparable to those of the corresponding PDMS block in the same polymer.

As stated above, the calculated lamella thickness of the PDMS block is considerably greater than its gaussian value as determined from Eq.(8) - at least in those systems with the higher PDMS block lengths. This much higher measured value of the lamella thickness is believed to be explained by the formation of longer PDMS blocks promoted during the free radical process thereby leading essentially to much longer PDMS block lengths. The PS domain size from TEM results and from the gaussian calculations utilizing Eq.(8) as based on the calculated average block length initially proposed by Crivello[14] are also listed in Table 4 on page 85. The results indicate that much larger PS blocks clearly have been formed during the free radical polymerization than that based on the calculated block length utilizing composition ratio etc. Clearly, larger average PS block length would certainly account for the much larger PS domains or lamella as directly observed in Figure 20 on page 79 (It is recalled that the same weight ratio of PDMS macroinitiator to styrene was used in each polymerization[14]). Therefore the formation of larger PDMS blocks might well be expected to lead to the formation of larger PS blocks and hence the number of blocks per chain in the final polymer would be reduced accordingly. This of course assumes that the average molecular weight of the final product of all materials is essentially the same. Indeed, the speculation for the formation of large PS blocks is highly supported by the DSC and dynamic mechanical data -recall Figure 15 on page 64 and Figure 16 on page 68. It indicated that the T_g of the styrene block for these high conversion samples is *ca.* 105°C.

Table 4. Domain size or lamellae thickness of the PDMS and PS blocks.

	PDMS Domain Size (nm)			
Sample	TEM*	σ**	RMS***	TEM/RMS
S14-95-M	4.6	1.2	3.6	1.3
S26-91-M	6.6	1.7	4.9	1.4
S45-95-M	7.5	1.8	6.4	1.2
S99-95-M	14.1	4.6	9.5	1.5
S193-95-M	31.8	5.4	13.3	2.4

*Domain size measured from the TEM micrographs.
**σ is the standard deviation
***Root mean square end-to-end distance calculated by Eq.(8)

	PS Domain Size (nm)			
Sample	TEM	σ	RMS*	TEM/RMS
S14-95-M	47.6	10.7	2.8	17.0
S26-95-M	59.9	18.7	4.3	4.4
S45-95-M	18.8	5.8	4.5	4.2
S99-95-M	52.4	25.9	7.7	3.4
S193-95-M	85.1	9.7	9.6	8.9

*Based on the calculated values of Mn for the PS blocks (from Ref. 14)

5.2.3 Molecular Weight and Molecular Weight Distribution of the PS Blocks in the PDMS-PS Block Polymers

In view of the DSC, dynamic mechanical analysis, TMA and TEM studies, the results suggest that this system may have a fairly broad molecular weight distribution of the PS blocks due to the nature of free radical synthesis. As shown in Figure 20 on page 79, the size of the PS domains does clearly vary. The samples, S45-95-M and S99-95-M, also have a mixed morphology of sphere-like domains and lamella. The variation in the domain size and the mixed morphological structure could be a result of a broad molecular weight distribution. However, this was not observed directly by DSC likely due to the general breadth of the distribution. Although, it was strongly suggested on the dynamic mechanical results as well as on the TMA results in the glass transition region of the PS blocks. In view of this, a more direct proof has been sought to indicate the existence of high PS block molecular weights by applying GPC analysis to the by-products of a trifluoroacidic acid degradation of some of the high conversion samples. This degradation successfully causes selective chain scission at the linking unit (pinacolate unit) connecting the PDMS and PS blocks but causes no further degradation. This latter point is proven by the analysis of the resulting PDMS block lengths of the degraded samples which are directly in line with the hydride difunctional PDMS (di-H-PDMS) precursors utilized prior to the preparation of the macroinitiator (Table 5 on page 88). In carrying out the analysis, the UV detector was again set at 254nm to detect the aromatic groups of the polystyrene and the IR detector was placed at 9.2μm for determining the Si-O bond in the PDMS component. The degradation results were compared with the results of the ^{29}Si NMR and the original GPC data on the silicon hydride difunctional PDMS precursors. The results are given in Table 5 on page 88 and Figure 22 and indicate that complete degradation of these block polymers has been achieved for the molecular weight of the PDMS degraded material is the same as the PDMS precursor systems (Figure 22a). With this data establishing the "cleanness" of the selected degradation, it is then noted that the PS results illustrate very high molecular weight PS blocks and that the PS molecular weight distribution varies with initial PDMS block length - see Figure 22b. Here it is noted that in the S45-95 material, there is a distinct bimodal character

to the PS blocks in the final polymer, one region of which illustrates very high molecular weights and another of which is of the order of 10,000 or more. For S99-95 polymer, a trimodal distribution is observed. In this sample, the high molecular weight portion is dominate. There is also a fair amount of lower molecular weight blocks (around 10,000) and a small amount of the lowest molecular weight (Mn < 1,000) blocks. In the case of S193-95, the bimodal distribution is obtained again. As Figure 22b shows, the high molecular weight blocks are dominant. The lower molecular weight (around 10,000) blocks are much less as compared to the former systems. The lowest molecular weight portion seems relatively absent. It is noted, however, that there is a distribution of low molecular weight styrene blocks that could be mixed mixed with the PDMS phase which would account for the rise in PDMS T_g as discussed earlier. Similarly, the presence of the shortest PS block lengths could easily account for the fact that these would serve to couple PDMS chains thereby promoting a much longer PDMS apparent block length which would account for the rise in the lamella thickness of this particular phase based on calculations utilizing the TEM micrographs.

The bimodal molecular weight distribution of the PS blocks in these PDMS-PS systems can be explained by a hypothesis (a dynamic model) proposed by Crivello[14] shown in Figure 23 on page 91. During thermolysis, the intermediate polymer (shown at the top of the scheme) undergoes cleavage at the strained C-C bond to generate two radical fragments, A and B. Radical species A can either couple with another identical species to form a dead chain D or can add additional styrene monomer units to form species C which can couple with the similar species either A or C to give a dead chain D. The species B which bears the ketyl radical could couple with itself, however, this is a strongly unfavorable process because the temperature is well above the threshold for the dissociation of this bond. Therefore, most of these species will react with styrene monomer units to form species A and eventually form the dead chain. The length of the PS chain formed will depend upon the concentration of both monomer and the radical chain ends present. If the concentration of radicals is high during the polymerization, the PS chain can only grow very little before irreversible termination occurs. If the concentration of monomer is low and the concentration of radicals is high at the early stage of the polymerization, a great deal of PDMS segments

Table 5. Results of the selective degradation studies.

Polymer	di-H-PDMS Mn*		PDMS Block Mn
	^{29}Si	GPC	GPC (After Degr.)
S45-95	4,520	5,380	5,970
S99-95	9,890	9,940	10,180
S193-95	19,300	22,500	13,300

*di-H-PDMS are the difunctional hydride PDMS precursors which are used to prepare the PDMS macroinitiators.

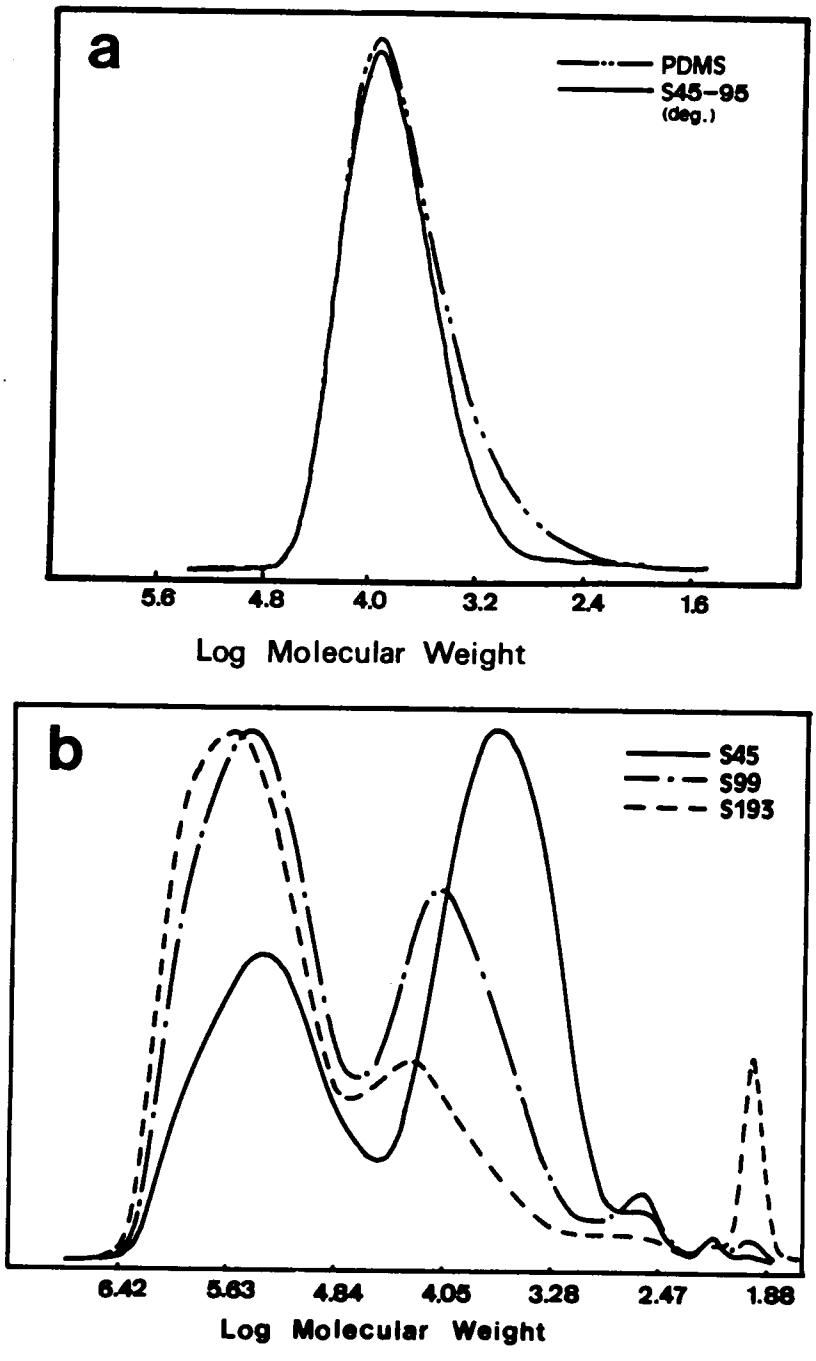

Figure 22. GPC results from the selective degradation studies of high conversion PDMS-PS block polymers: (a). GPC results of silicon hydride difunctional PDMS precursors and the PDMS blocks of S45-95 polymer after degradation. (b). GPC results of the PS blocks after degradation.

will link together by very short PS chains due to the permanent termination by coupling. As the polymerization proceeds, the concentration of radicals will drop rapidly as they are consumed by the coupling process. In the later stages of the polymerization, the length of the incorporated PS chains will increase dramatically as the probability of coupling decreases. Hence, the PS blocks in the final polymer will have a very unequal molecular weight distribution.

According to the dynamic model, if the concentration of the radicals is high, there will be more chance for the PDMS segments to be linked together by very short PS units due to the coupling process. In high conversion samples, the same weight ratio of macroinitiator to styrene monomer has been used for polymerization, therefore, the concentration of radicals should be higher in the sample which contains shorter PDMS segments than in those samples containing longer PDMS blocks. During the polymerization, the same weight ratio of monomer to macroinitiator is used and the amount of monomer is the same for all samples. Therefore, the monomer concentration concentration should be lower in the sample with shorter PDMS blocks than in the sample with long PDMS blocks. Hence, the polymer with shorter PDMS blocks should have more PDMS segments linked together by very short PS chains, and the PS blocks of these polymers should show a more distinct bimodality than those polymers with longer PDMS blocks. If this is true, the TEM results would indicate that the PDMS domain size in the polymers with shorter PDMS blocks should be larger than that calculated from the gaussian coil approximation (RMS). The ratio of the domain size measured by TEM to RMS would increase as the PDMS block decreases. Since the results (Table 4) indicates the opposite, the ratio increases as the PDMS block length increases, there should be a dominating factor other than the concentration effect.

One possible cause of the multimodal molecular weight distribution of the PS blocks is the Trommsdorff-Norrish (T-N) effect. It has been know as autoacceleration in free radical polymerizations observed by many researchers on methyl methacrylate, styrene and other monomers[102–108]. This has also been observed in free radical copolymerization of styrene and methyl methacrylate with peroxide initiators[8] The autoacceleration effect is a result of diffusion controlled termination. As the conversion level increases, the chain length and the viscosity of the reacting materials increases. The chain entanglement also increases with the chain length. There-

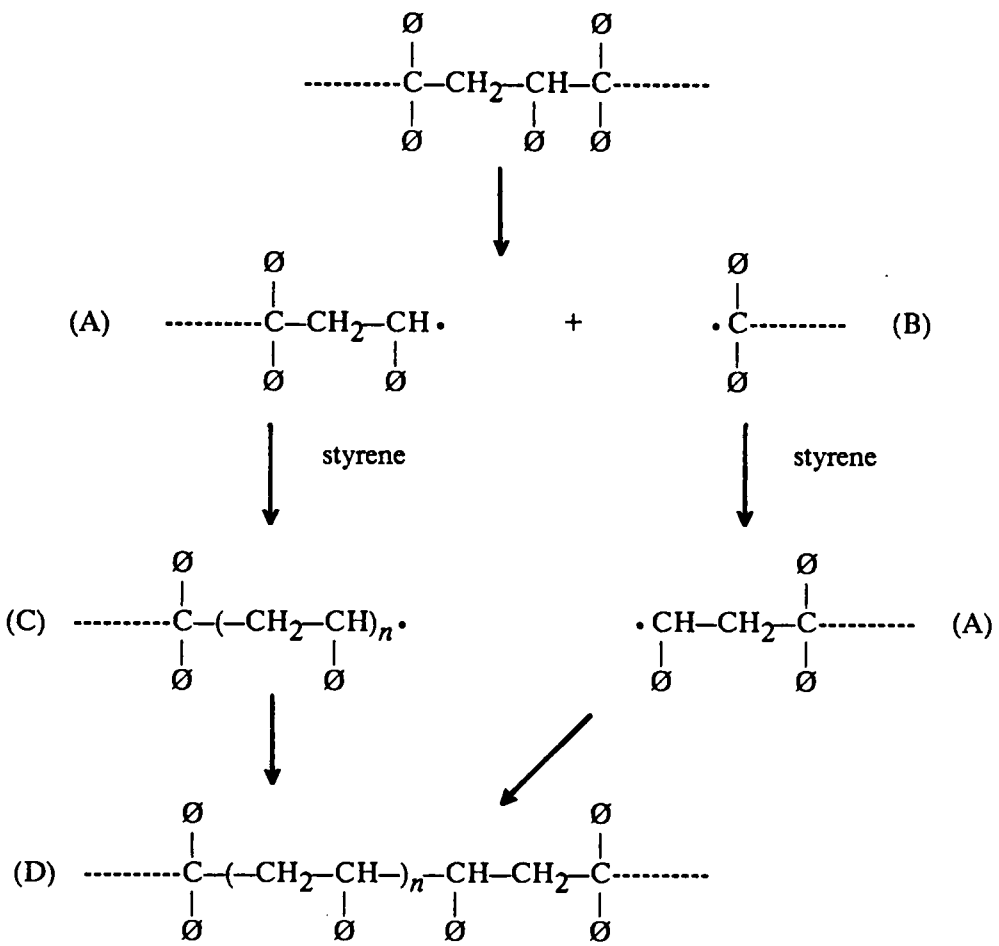

Figure 23. Schematic speculation of the formation of a bimodal MWD of the PS blocks.

fore, the growing chain ends become immobilized, and the termination rate is reduced and the conversion rate increases.

In the case of the free radical synthesized PDMS-PS block polymers, the macroinitiator gives rise to PDMS diradical species which can grow from both ends. The macroinitiators having longer PDMS blocks may more rapidly reach the T-N conditions where the termination by coupling is suppressed more than for the corresponding shorter PDMS diradicals. Therefore, the block polymer which starts with macroinitiators containing long PDMS blocks will have a higher probability to form long PS blocks due to the T-N effect. In the early stages of the polymerization, the intermediate polymers are thermolysized to generate diradicals. These diradicals react with styrene monomers and couple with other diradicals to form long chains. When the polymerization reaches the T-N condition, the chain ends become immobilized and the coupling process is suppressed. Therefore, the chains can only grow by adding the styrene monomers at both ends and the long PS blocks will be formed. As the result, the multimodal molecular weight distribution of the PS block occurs. Since the macroinitiators having longer PDMS blocks can reach the T-N condition more quickly than the macroinitiators with shorter PDMS blocks. Thus the multimodal molecular weight distribution is more distinct and the PS blocks are longer in the polymers with longer PDMS blocks than those with shorter PDMS blocks.

It is necessary to point out that the above discussion of the T-N effect is a pure speculation. This speculation fits the TEM and degradation GPC results very well. However, it lacks direct support from the reaction data. As will be discussed in the section 5.3, the polymerization data show no sign of autoacceleration at least in four hours of polymerization and the conversion of the polymer increases linearly with the time of polymerization up to four hours[14]. Hence, the T-N effect seems not to apply in view of polymerization data. As a reminder, the polymerization time of high conversion samples is 12 hours.

Another possible cause of multimodal behavior is the heterogeneous polymerization conditions. The free radical PDMS-PS block polymers have been synthesized by bulk polymerization. As the polymerization proceeds, the viscosity of the polymerizing materials should increases as the MW of the polymer increases. Crivello has noticed that the reacting materials become so viscous

and starts to pull away from sides of the reaction container and to climb up to the stirring rod after only 60 minutes of polymerization[91]. As the viscosity of the reacting materials increases, it is more difficult for styrene monomers to diffuse into the center of the reacting materials to react with the radicals inside the reacting materials. The temperature gradient inside the reacting materials may also play an important role. Since the polymer mixture is a poor thermoconductor, there must be a temperature gradient inside the reacting materials. Therefore, the temperature in the inner reacting materials should be lower than that in the outer reacting materials because the reacting materials is heated from outside. The temperature gradient should increase as the viscosity of the reacting materials increases. Also, the probability of thermolysis and coupling processes is lower in the center of the reacting materials than the outer layer. In the early stage of the polymerization, the viscosity of the reacting materials is low, so that the thermolysis and coupling processes occur evenly in both inner and outer parts of the reacting mass. There are many PDMS segments linked together by short PS segments and forms high molecular weigh intermediate polymers. As the molecular weight increases, the viscosity of the reacting materials increases, more and more chains become immobilized. The temperature gradient inside the reacting mass increases and the styrene monomer is getting more and more difficult to diffuse into the reacting materials. As a result, the thermolysis and the coupling processes can only take place on the outer layers of the reacting mass to form very large PS blocks. Thus, the PS blocks in the final polymers have a very uneven MWD. For macroinitiators containing long PDMS segments, the molecular weight of the intermediate polymer should increase very quickly in the early stages of the polymerization. The bimodality of the PS blocks in these polymers should be more distinct than that of the polymer with shorter PDMS blocks due to the heterogeneous bulk polymerization condition. If this is the case, the ratio of the measured PDMS domain size to the RMS should increase as the PDMS block length increases. As the TEM results show, this heterogeneous assumption also fits very well with the experimental data.

To simulate the occurrence of a mixture of both low and high molecular weight styrene block lengths, a direct blend of two diblock polymers each containing the same PDMS block length (10K was utilized) but where the PS block length varied was used. The diblock materials which were

obtained through the courtesy of Dr. S. Smith and Dr. J. E. McGrath (VPI & SU) were diblocks of PS(10K)-PDMS(10K) as well as a corresponding diblock where the PS was of 100K molecular weight. These systems had been prepared anionically and were well characterized systems[109]. They were solvent cast as blend from methylene chloride in the weight ration of 80/20 100K/10K to that of 10K/10K respectively. The corresponding film of this blend was then analyzed by dynamic mechanical analysis and the TMA. The dynamic mechanical results were shown in Figure 24 on page 95. It is very clear that the dynamic mechanical and the TMA response is exactly analogous to the S99-95-M free radically polymerized block polymer discussed earlier, i.e. a two step transition or softening behavior is observed which is due to the occurrence of two styrene domain regions. Similar to the result for S99-95-M, the DSC result of this blend did not show two transition peaks, but the breadth of the transition was broad. TEM studies carried out on this blend showed very good phase separation behavior but no distinct signs from the microscopy that allowed one to judge where the relative blocks of each of the species are located - see Figure 24 on page 95.

5.2.4. Stress Strain Results in Correlation with Morphology

The earlier electron micrographs clearly showed that the morphology for the methylene chloride cast samples changes in a systematic way as the PDMS block length increases. In particular, it is recalled from Figure 20 on page 79 that the S14-95-M sample illustrated polystyrene domains encapsulated within a rubbery siloxane matrix. While at the other extreme, sample S193-95-M, indicated connectivity of both phases as promoted through a lamella texture. Hence, while the composition ratio of all of these materials shown in Figure 20 on page 79 are very nearly equivalent, the mechanical response with loading would be expected to be quite different. Indeed, as shown in Figure 25 on page 97, the results are exactly in line with the electron micrographs. In particular, sample S14-95-M (the encapsulated polystyrene domain system) illustrates a low modulus as does S26-91-M which also has larger but still encapsulated PS domains. In contrast, the three samples S45, S99 and S193-95-M materials which possess a greater extent of lamellar

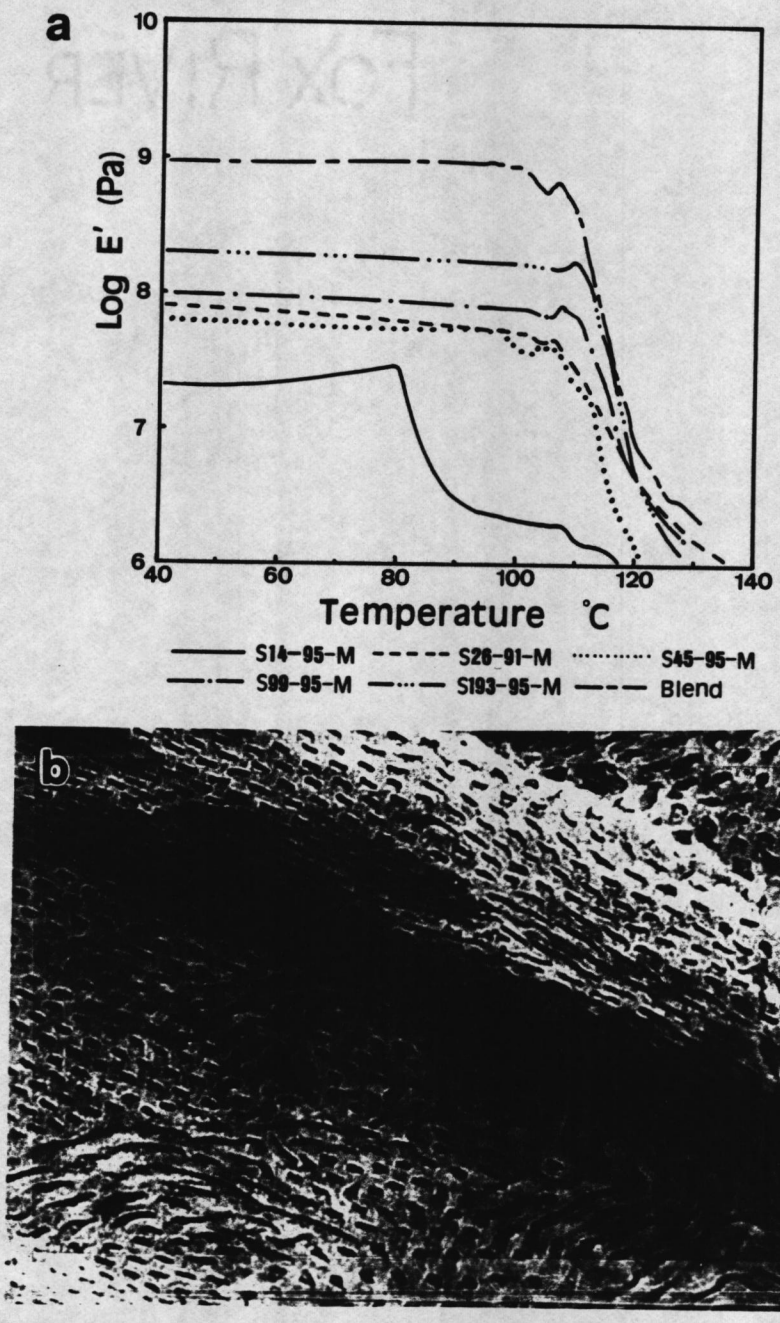

Figure 24. Dynamic mechanical spectrum and morphology of PDMS-PS block polymers and a polymer blend: (a). Dynamic mechanical response of free radical PDMS-PS block polymers and the 10k/10k-10k/100k PDMS-PS diblock polymer blend near the PS glass transition range. (b). morphological structure of the 10k/10k-10k/100k PDMS-PS diblock polymer blend cast from methylene chloride.

texture as the PDMS block length increases clearly shows a systematic rise in modulus due to the higher connectivity of the polystyrene glassy phase. While there is a much higher elongation to break for the S99 material (based on several tests), this may arise from the effects of the hard segment size and the number of blocks per chain, **n**. Earlier studies by Saam et al.[3,69,71] did find that the ultimate properties of the PDMS-PS multiblock polymers were strongly dependent on the size of the PS block and **n**. The polymer with larger size PS blocks had higher ultimate stress. They also found that the ultimate properties were increased greatly as **n** increased when **n** was less than 8[69]. When **n** was greater than 8, only a small improvement was obtained. In case of the free radical synthesized PDMS-PS block polymers, the same weight ratio of PDMS macroinitiator to styrene monomer was used. Therefore, **n** will increase as the PDMS block length decreases. Based on the ^{1}H NMR and GPC data, Crivello et. al.[14] calculated the values of **n** which were in a range from 8.7 to 21.9 depending on the PDMS block length. These values are average number of block per chain. However, the equivalent number of blocks per chain, $\mathbf{n}_e$, might be much less, If the PS blocks have a multimodal molecular weight distribution as confirmed by the experimental results, For example, if two long PDMS blocks are linked together by a very short PS block as illustrated at top of Figure 25b, the polymer chain will act more like a single large block. In this case, $\mathbf{n}_e$ equals one even if **n** is really 3. This speculation is supported by the GPC results of selective degradation study.

The GPC results of sample S193-95 shown in Figure 26 on page 98, one would notice that some of the PS blocks (dot-dash line) have a very large large molecular weight which are close to the molecular weight of the whole polymer (solid line)! There are also some very short PS blocks formed (recall Figure 22b). If there are many PDMS blocks linked together by some very short and long PS blocks as shown in the bottom of Figure 25b, in this case, the multiblock system would act as a triblock polymer, and the ultimate properties will decrease. Also, a very large size of both PDMS and PS domains would be observed as shown in Figure 20 on page 79 and Table 4 on page 85.

For S45-95-M, S99-95-M, and S193-95-M, the overall molecular weight is in the range from 162,000 to 345,000. Sample S193-95-M, however, has a much larger PS block size than the other

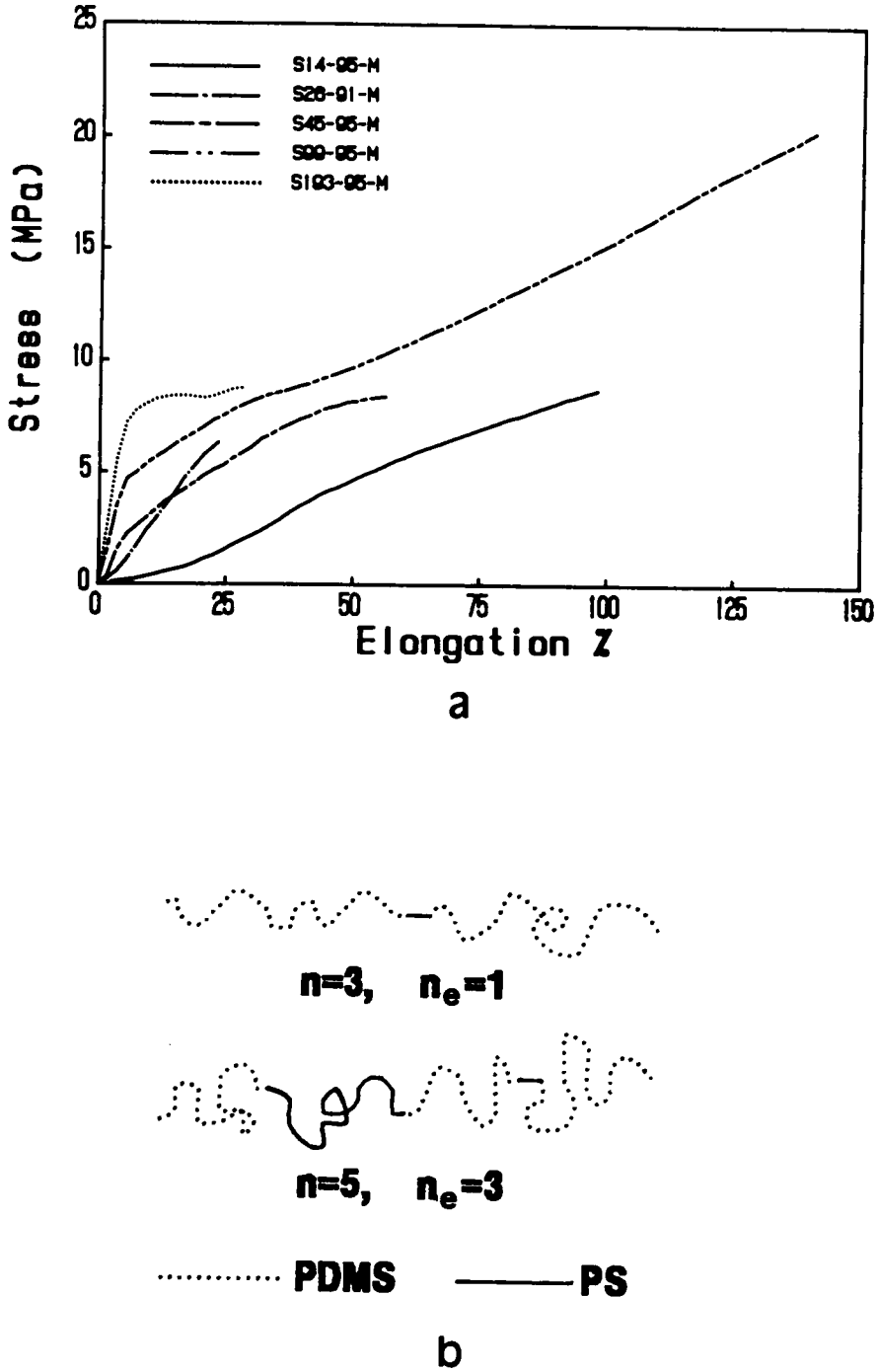

Figure 25. **The stress-strain behavior of high conversion PDMS-PS block polymers:** (a). Stress-strain behavior of high conversion PDMS-PS block polymers. (b). Illustration of equivalent number of blocks per chain.

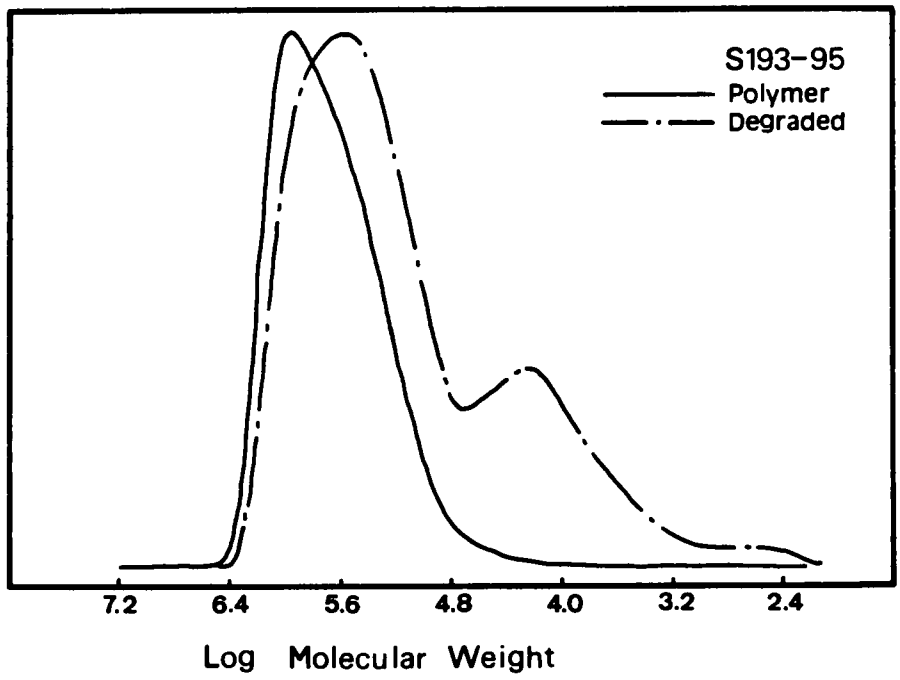

Figure 26. GPC results of S193-95 polymer and the PS blocks of this sample after selective degradation : Solid line is the result of the whole polymer and dot-dash line is the result of the PS blocks.

two (recall Table 4 on page 85, Figure 20 on page 79 and Figure 22 on page 89). Therefore, fewer blocks per chain for S193-95-M are expected. The bimodal molecular weight distribution of the PS blocks leads to even a much lower value of n_e for this sample. The shortest break elongation of this sample might result from a small value of n_e and the continuous PS lamella. On the other hand, the PS block size in S45-95-M is much smaller than the other two and the multimodal molecular weight distribution of the PS blocks in this sample, therefore, the ultimate stress for this sample might be expected to be the lowest among these three samples as shown inFigure 25 on page 97. Sample S99-95-M has the highest ultimate properties among these three samples, which could be due to the continuous PS blocks and the higher value of n_e. The important point is that the general modulus characteristics are indeed reflective of whether or not the PDMS component is the continuous phase or whether the polystyrene material also displays connectivity thereby strongly enhancing the modulus due to its glass like behavior at ambient.

5.2.5 Summary

In summary, the results presented here further confirm the existence of only block polymers produced by this interesting free radical polymerization scheme. In addition, however, the author has demonstrated that the resulting chain structure is much more complex than initially thought. Changes in final polystyrene block lengths depend greatly on initial PDMS block length as well as likely upon the reaction conditions or phase separation may be promoted more rapidly due to higher molecular weight PDMS block components - recall iridescence was observed by Crivello in the stages of styrene polymerization for these higher PDMS containing systems. The ΔC_p analysis can provide an insight into at least an estimate of the degree of phase mixing that occurs but it is principally a mixing of low molecular weight styrene block with the PDMS component - a result that is not only dependent upon the initial chain structure involved but the choice of casting solvent - the latter point of which will be further confirmed in a later sections. The use of selective degradation of the final polymer into its respective blocks has proven of great assistance in accounting

Table 6. Mechanical properties of high conversion PDMS-PS block polymers.

Sample	Modulus (MPa)	Tensile Strength σ_B(MPa)	Ultimate Elongation ε_B(%)
S14-95-M	0.05	4.24	105
S26-91-M	0.10	3.50	115
S45-95-M	0.40	5.40	60
S99-95-M	0.82	8.35	138
S193-95-M	1.34	6.88	31

for many of the observations made. Some of these observations have been further confirmed by the use of blending two well defined molecular weight diblock PS-PDMS species together to promote a similar thermal mechanical response. Finally, based on electron microscopy, the anticipated mechanical response in terms of stress-strain behavior - at least at lower elongations, was verified by carrying out mechanical testing accordingly.

5.3 EFFECT OF STYRENE CONVERSION LEVEL

Previous discussions suggest that the molecular weight distribution of the PS blocks play a very important role on the morphology and the bulk properties of these free radical PDMS-PS materials. In the free radical polymerization, the molecular weight distribution is a very complicated matter because the free radical polymerization involves various terminations mechanisms such as disproportionation, coupling, various transfer reactions, and autoacceleration. Therefore, the molecular weight of the PS blocks and the molecular weight of the polymer produced at any instant varies with the styrene conversion level dependent on changes in the monomer conditions, the propagation and the termination rate. Due to the mechanism of the free radical polymerization, the PS block size in these free radical PDMS-PS block polymers will be smaller at a low conversion level than at a high conversion level, and the molecular weight distribution of the PS blocks will also be narrower. Consequently, the bulk properties and the morphology of these materials will be expected to vary with the conversion level of styrene monomer. In the following sections, the effect of conversion on the bulk properties and the morphology of free radical synthesized PDMS-PS block polymers will be discussed.

5.3.1. Effect of Conversion on the Morphology and the Bulk Property of the S45 Series

In order to study the conversion effects on these free radical PDMS-PS block polymers, the polymer having a PDMS block length of 4500 mol/gm (S45 series) was chosen for a model study. Several samples, S45-15′, S45-25′, S45-35′, S45-45′, and S45-60′, were sampled during a polymerization at reaction times of 15, 25, 35, 45, and 60 minutes respectively. The conversion of these samples were within the range from 2% to 8%. Another sample with 45% conversion was prepared separately. All of the polymers were prepared by Dr. Crivello in GE. The ^{1}H NMR results indicated that the composition of these samples was about 50-60 wt% of PDMS except S45-15′ and S45-60′ (refer to Table 2 on page 60).

5.3.1.1 Molecular Weight and Molecular Weight Distribution of the S45 Series

Figure 27a shows the relationship of molecular weight of the polymer and the reaction time of very low conversion samples. At very low conversion (< 10%), the molecular weight increases linearly as the reaction time increases. This result is in good agreement with the results from an earlier study which showed that the molecular weight of the polymer increases continuously up to 4 hours of polymerization[14]. It is necessary to point out that the reaction time for the high conversion sample (> 95%) is 12 hours.

As expected, the molecular weight distribution (MWD) of these materials also changes with the conversion. Figure 27b show a definite trend to bimodality as the conversion or polymerization time increases. The very low conversion sample, S45-25′, has a unimodal MWD. As the conversion or polymerization time increases, a shoulder begins to develop on the GPC curve of S45-45′. When polymerization time is over 60 minutes, the shoulder becomes very distinct. These shoulders are believed to be caused by the bimodal MWD of the PS blocks.

The formation of bimodal MWD of the PS blocks in high conversion samples with various PDMS block length has been discussed in section 5.2.3. using Dr. Crivello's dynamic model. In

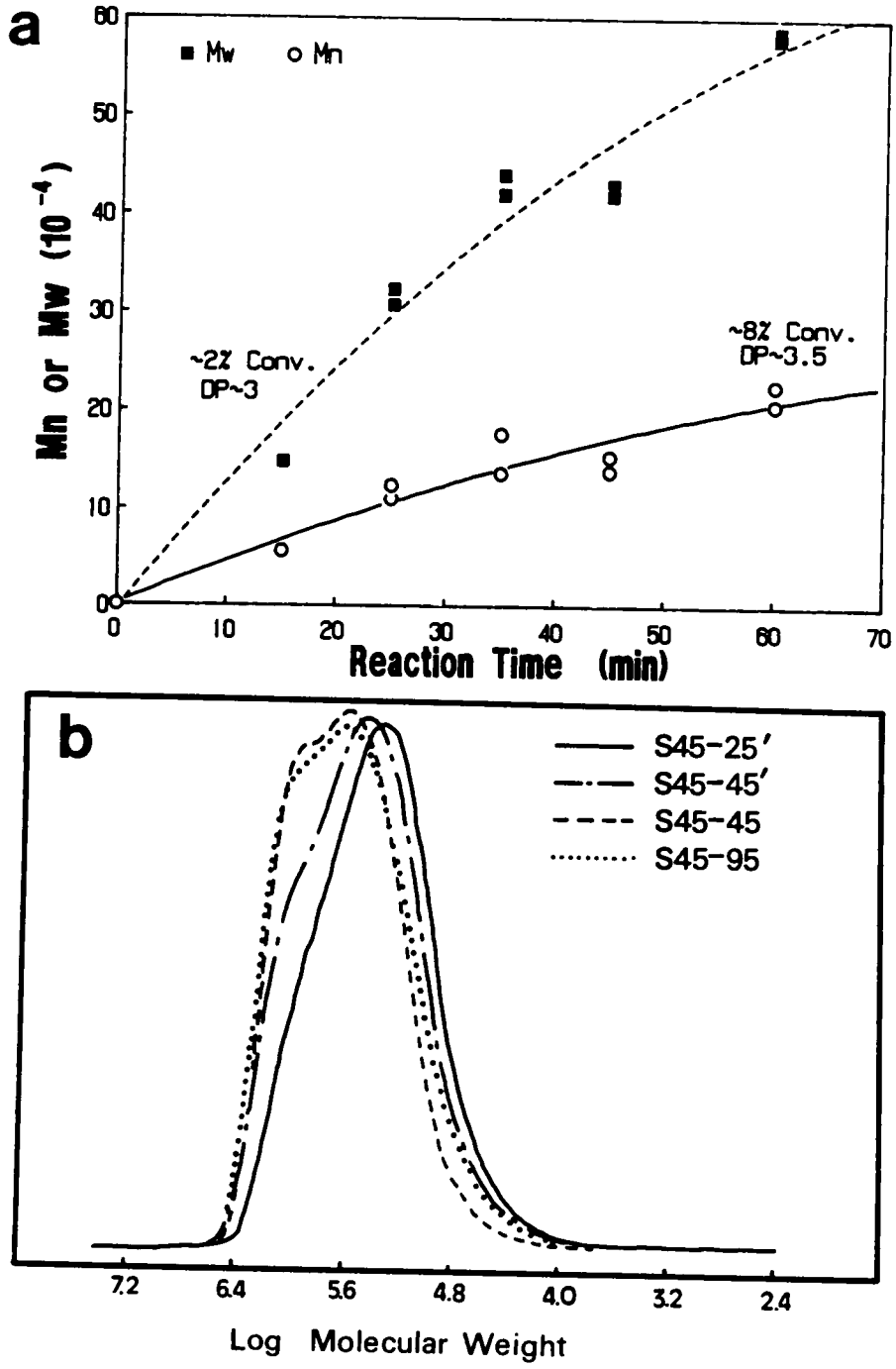

Figure 27. The relation of molecular weight and the reaction time of the S45 polymers: (a). The relation of MW and the reaction time of S45 polymers. (b).GPC results of the S45 polymers using RI detector.

that model, the uneven MWD of the PS blocks is a result of both thermolysis of macroinitiators or intermediate polymers, which generate diradicals, and the coupling termination. Therefore, the formation of the multimodal MWD of the PS blocks is governed by the concentration of both radicals and monomer. If the concentration of monomer is low and the concentration of the radicals is high at an early stage of the polymerization, the coupling termination will be the most probable process and the majority of PDMS segments will link together by short PS blocks. As the polymerization proceeds, the concentration of radicals will drop rapidly as they are consumed by the coupling process, the length of the incorporated PS blocks will increase as the probability of coupling decreases. Therefore, a very unequal MWD of the PS blocks is formed.

In the S45 series, the PDMS block length is the same for all different conversion samples. In order to keep the same composition of the final polymers, the amount of styrene monomer should be higher for the low conversion samples than that for the high conversion samples when the same amount of macroinitiators is used. Therefore, the monomer concentration in the early stages of polymerization should be lower for the high conversion samples than for the low conversion samples. According to the dynamic model, the high conversion samples should contain more PS blocks with very unequal MWD. This model well fits samples S45-45 and S45-95 because they are prepared separately with different initial concentration of monomer and initiator. For samples S45-15′, S45-25′, S45-35′, S45-45′ and S45-60′, the situation is different. These samples are extracted at different reaction times in the same polymerization, and the starting concentrations were the same for all samples. Therefore, the bimodality shown on S45-45′ and S45-60′ samples can not be explained by the dynamic model only. The other possible causes of the bimodal MWD left are the T-N effect and the heterogeneous polymerization conditions as described in section 5.2.3.

As discussed in section 5.2.3, the speculation of the the T-N effect lacks of supports from the experimental data. Figure 28 shows that the conversion increases linearly with the reaction time up to four hours. In general, if the T-N effect occurs, there should be a sudden rapid increase of the conversion on the conversion time curve[102]. Since the bimodal MWD starts to develop after

45 minutes of the polymerization, and there is no a such sudden changes in the conversion level shown in Figure 28. The possibility of T-N effect on the bimodal MWD can be ruled out.

Of course, the heterogeneous reaction condition must also contribute to the broadening of the MWD of the PS blocks. As the conversion level increases, the molecular weight of the polymer as well as the viscosity of the polymerizing materials increases. Therefore, the MWD of the PS blocks becomes more uneven with increasing conversion level. Based on experimental data, the bimodal MWD of the PS blocks in these low conversion samples is therefore believed to be caused by the combination of heterogeneous polymerization condition and the concentrations of both monomers and radicals.

5.3.1.2 Morphological Texture of the S45 Series

The effect of the conversion on the morphological texture of the S45 polymers has been shown on Figure 29 on page 107. The low conversion samples, S45-25′-M, S45-45′-M, and S45-45-M, have morphologies of spherical PS domains in a continuous PDMS matrix. The PS domain size increases with conversion level. For the very low conversion samples, S45-25′-M and S45-45′-M, the size of the PS domains is fairly uniform. For S45-45-M, the PS domain size is much larger than that of the low conversion samples, and the size distribution of the PS domains becomes very broad(Figure 29c). The high conversion sample, S45-95-M, has a morphology of mixed PS spherical and rod-like domains. The changes in the type of the morphology of these polymers is directly related to the change in the MWD of the PS blocks.

Besides the change in the morphology, the degree of microphase separation in these materials should also be expected to change with conversion. One should notice that the contrast on the TEM micrograph of S45-25′-M (Figure 29a) is much weaker than the others. As the conversion increases, the contrast of the TEM micrographs becomes sharper. This may indicate that the degree of phase mixing decreases with increasing of conversion in these samples. However, the contrast

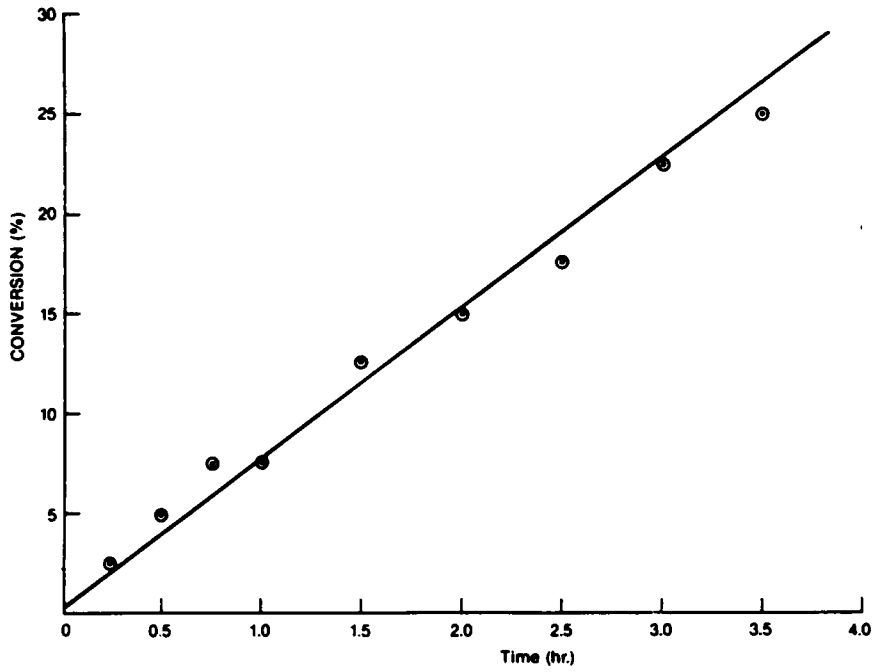

Figure 28. Molecular weight as a function of polymerization time: The bulk polymerization of styrene at 100°C using 0.1M bis(trimethylsilyl)benzopinacolate. (From Ref.14)

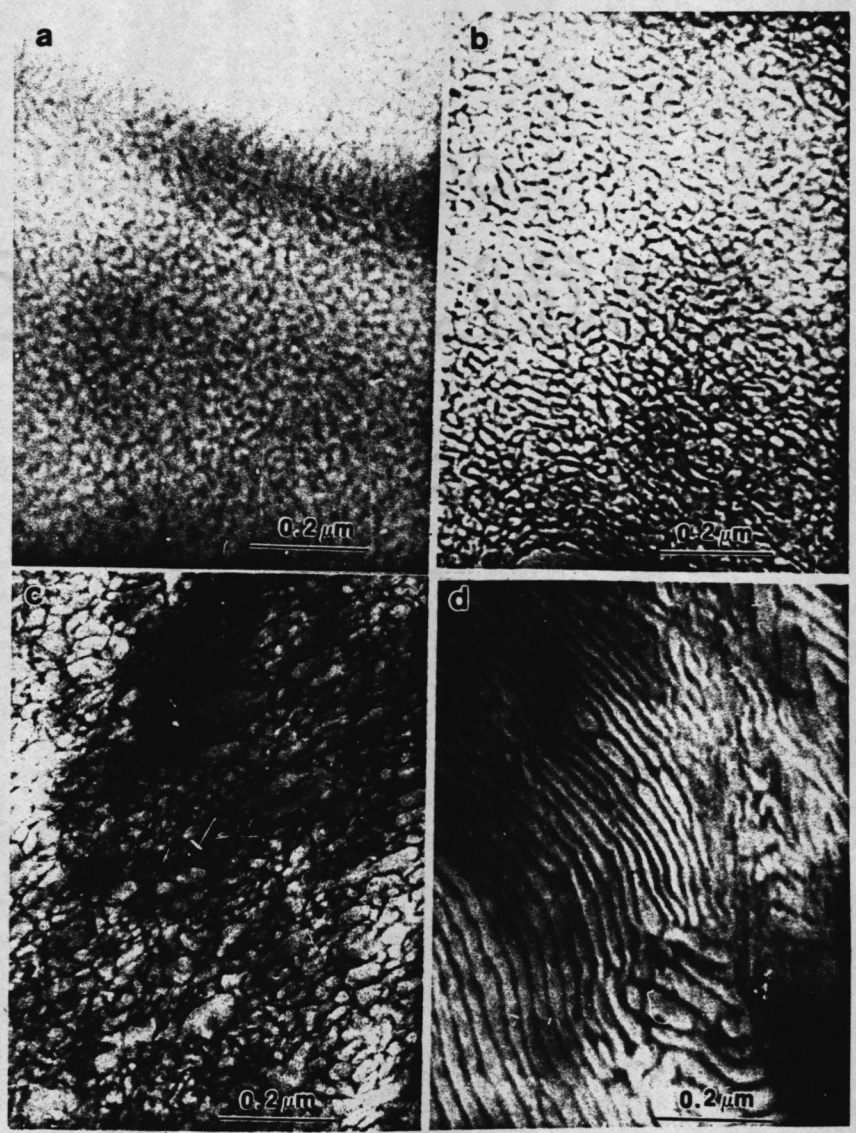

Figure 29. Morphological textures of the S45 polymers: a. S45-25′-M, b. S45-35′-M, c. S45-45-M, and d. S45-95-M.

of sample S45-95-M which has the highest conversion level in the S45 series becomes weaker again. This may be due to a higher degree of phase mixing.

5.3.1.3 Thermal Properties of the S45 Series

Figure 30 on page 109 shows the DSC thermograms from the series of S45 polymers. For the low conversion samples, S45-25'-M, and S45-35'M, a small transition occurs around 70°C (pointed by an arrow). This transition begins to disappear as the conversion increases. At a temperature around 105°C, there is another transition except for the S45-25'-M sample. As the conversion increases, this transition becomes more distinct. Both transitions are believed to be the glass transition of the PS blocks. The changes in T_g are due to the changes in the PS block length. It is well-known that the T_g of the PS blocks are strongly dependent on the PS block length and the degree of phase mixing[70,86,93,94]. For the low conversion samples, the PS blocks are mostly short, therefore, the T_g of these samples are low. As the conversion increases, the block length of the PS blocks increases, the T_g of the PS phase shifts up to a higher temperature and the lower T_g transition temperature gradually disappears depending on the proportion of the short PS blocks. The high conversion samples contain mostly long PS blocks, therefore, the T_g transition is only observed at the higher temperature and it is also very distinct. The magnitude of ΔC_p at the T_g transition also increases with conversion.

The ΔC_p method has also been applied to the S45 series. The results are shown in Figure 30b. As expected, the degree of phase mixing (DPM) decreases as the reaction time increases or the conversion increases. When the conversion increases, the block length of the PS blocks increases and the incompatibility between the two components, PDMS and PS, increases. Therefore, the microphase separation is enhanced and the DPM is reduced. One would note that the DPM of the high conversion sample, S45-95-M, is slightly higher than that of S45-45-M. The slightly increases in DPM may be due to a very uneven MWD of the PS blocks in this sample (recall Figure 22 on page 89). In this case, the polymer contains some very short PS blocks which

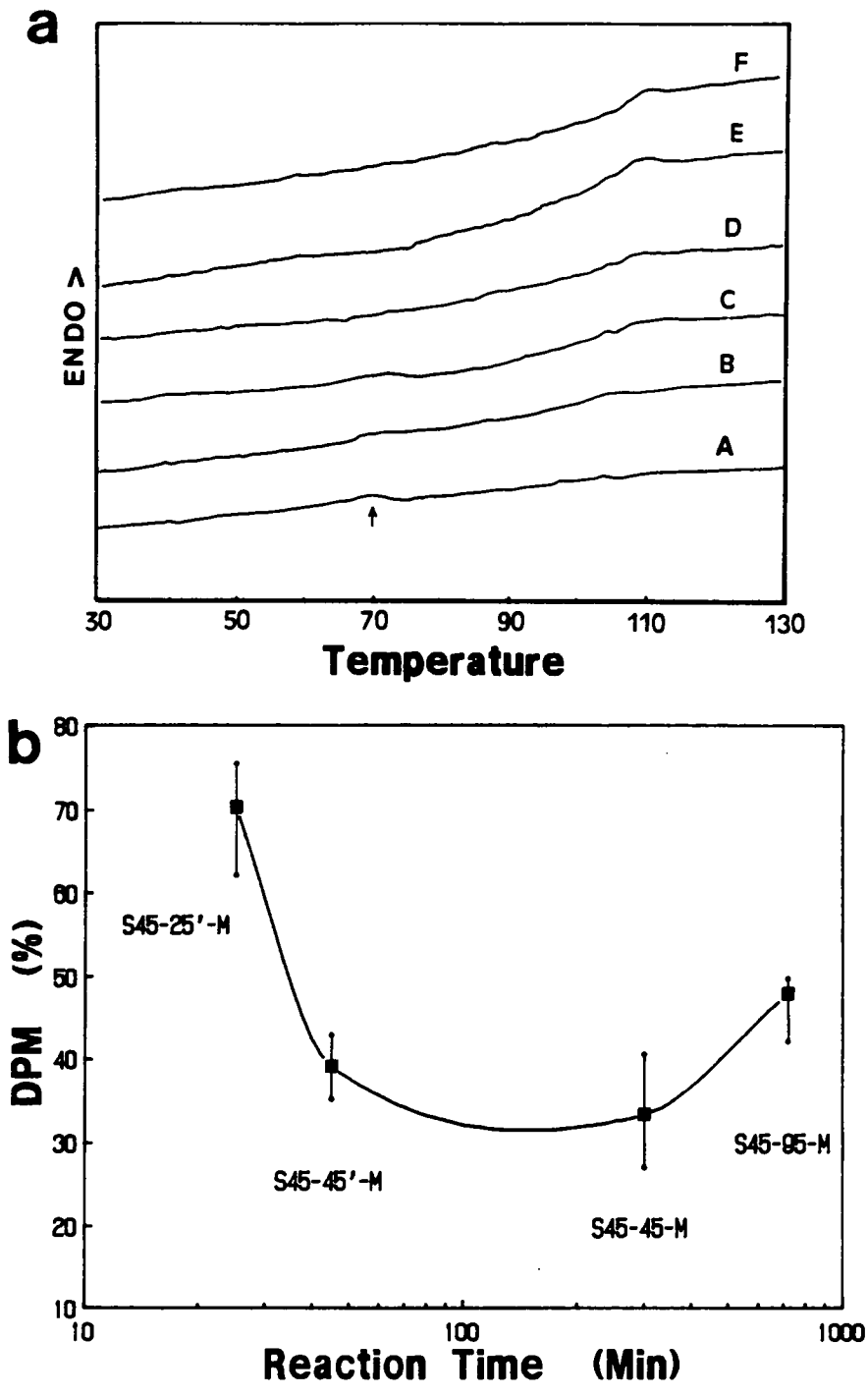

Figure 30. DSC thermograms of the S45 PDMS-PS block polymers: (a). DSC scans of the S45 polymers, A. S45-25′-M, B. S45-35′-M, C. S45-45′-M, D. S45-60′-M, E. S45-45-M, and F. S45-95-M. (b).Effect of conversion in the degree of phase mixing in the S45 polymers determined by ΔC_p method.

can be trapped in the PDMS phase, which will increase the domain mixing. The DSC ΔC_p results directly support the apparent observations of the change in contrast in the TEM micrographs.

5.3.1.4. Dynamic Mechanical Behavior of S45 Series

Dynamic mechanical spectra of the S45 Series are shown in Figure 31 on page 111. Two distinct transitions at -100°C and 105°C are observed which are the T_g's of the PDMS and the PS phases. At -50°C, there is a small loss peak shown on the tanδ spectra. This peak is due to the melting of the PDMS crystallinity.

As shown on the tanδ spectra, the T_g of the PDMS phase of the lowest conversion sample, S45-25'-M, is about -109°C. As the conversion increases, the PDMS T_g shifts down to lower temperature. S45-45-M has the lowest T_g of the PDMS phase (-120°C) among these samples, then the PDMS T_g slightly shifts back to a higher temperature as the conversion further increases. S45-95-M has the highest PDMS T_g (-100°C) among all the S45 polymers. The level of tanδ within the rubbery region which is the region between the T_gs of the PDMS and the PS phases also decreases with an increase of conversion and it reaches the lowest level at 45% conversion. Again, S45-95-M has the highest level of tanδ within the rubbery region. The changes in the T_g and the tanδ level indicate the changes in the degree of phase mixing in these samples. As discussed earlier (Section 5.2.1.1), the T_g shifting is believed mainly due to the domain mixing while the interphase mixing mainly affects the level of tanδ within the rubbery region. At very low conversion, the size of the PS blocks is small and the incompatibility between the two components is low. Therefore, both the domain mixing and the interphase mixing are high. As the result, the degree of phase mixing is high. When the conversion level increases, the incompatibility between the two components increases with the increase in the PS block length and the microphase separation is enhanced therefore reducing both the domain mixing and the interphase mixing. The overall degree of phase mixing (DPM) measured by DSC decreases accordingly. For the high conversion sample, S45-95-M, the molecular weight of the PS blocks become very uneven. It is believed there are some

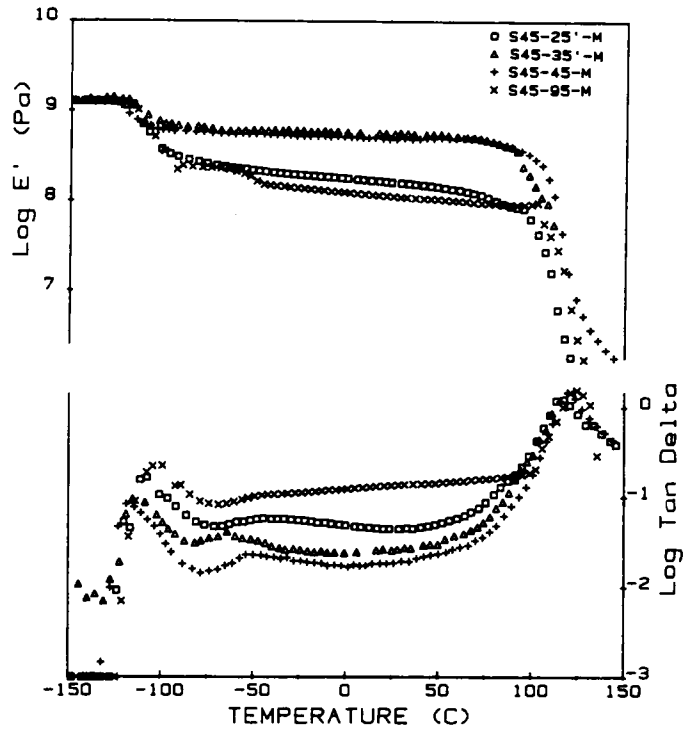

Figure 31. Dynamic mechanical responses of the S45 polymers.

very short PS blocks formed. These short PS blocks may be trapped within the PDMS matrix and results in a higher degree of domain mixing. Thus, the T_g of the PDMS blocks shifts toward a high temperature and the DPM rises due to the higher level of the domain mixing. Meanwhile, the volume of the boundary region in the high conversion sample also increases due to these large PS blocks. Therefore, the interphase mixing could also increase and the level of tanδ within the rubbery region rises.

As shown on Figure 31 on page 111, the T_g of the PS blocks also shifts toward higher temperatures as the conversion increases. This is caused by the increase in the PS block length with conversion. The E′ spectra indicate that the moduli of these materials within the rubbery region also change with the conversion. As the conversion increases, the modulus rises and reaches the maximum at the middle range of conversion. Then the modulus drops down as the conversion increases further. The changes in the modulus are related to the changes in the degree of phase separation, the morphological textures, and the number of blocks per chain in these polymers. More detail discussion in mechanical properties of these materials with their molecular structure is given in the next section.

5.3.1.5 Mechanical Properties of the S45 Series

The stress-strain behavior of S45 polymers is shown in Figure 32 on page 113 and some mechanical properties of the polymers are listed in Table 7 on page 114. The stress level as well as the ultimate elongation increases with conversion. S45-35′-M displays the highest stress level, modulus and tensile strength. As the conversion increases further, the stress level, modulus and the tensile strength fall down. S45-95-M which has the highest conversion has the lowest modulus and the ultimate properties. The changes in the mechanical properties of S45 polymers may be explained by the filler effect and the equivalent number of blocks per chain, $\mathbf{n_e}$.

Small particles such as carbon black are commonly used as reinforcing fillers in rubber to improve the mechanical properties of the rubber as has been well documented. Indeed, the effect of

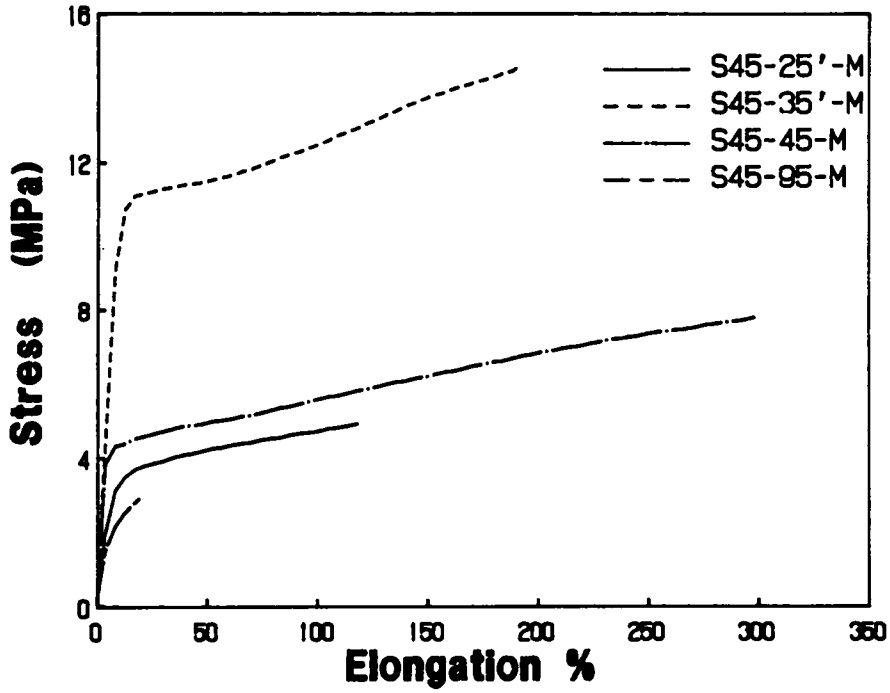

Figure 32. The stress-strain behavior of the S45 polymers.

Table 7. Some mechanical properties of the S45 polymers obtained at 25°C.

Sample	Modulus (MPa)	σ_B (MPa)	ε_B (MPa)
S45-25'-M	36.0	4.9	118
S45-35'-M	100.0	14.5	190
S45-45-M	74.1	7.8	298
S45-95-M	29.1	3.0	20

fillers in polymers has also been well studied[112,113]. Alter[112] investigated the effect of filler size on mechanical properties of polyethylene, styrene-butadiene, and natural rubber with various types of fillers. The size of the fillers was in a range from 0.05 μm to 0.2 μm. He found that the relative properties (properties of a sample with fillers to the original sample without filler) such as modulus, tensile strength (σ_B), and ultimate elongation (ε_B), were linear functions of the reciprocal filler size and were independent of the nature of the fillers. Recently, Otterstedt et. al.[113] used fine colloidal silica as reinforcing fillers in elastomeric polyurethane polymers. The tensile stress of these systems was strongly depending on the size of particle size. The particle size in their study was in a range of 1.5nm to 15nm. The relative tensile stress of these polyurethanes increased as the particle size increased, and went through a maximum at particle size between 1.5 to 2.5nm for a polyether based polyurethane (Estane 5714) and between 4 to 5nm for a polyester based polyurethane (Estane 5710 F1). As the size of particles further increased, the tensile properties decreased.

In the case of PDMS-PS block polymers, the PS hard domains act somewhat as reinforcing fillers in the PDMS matrix besides just a "physical crosslink". As shown in the TEM results of S45 series (Figure 29 on page 107), the PS domain size increases with conversion. As the domain size increases, the ultimate properties and modulus of the S45 series increase and reach their maximum values. Then the modulus and the tensile strength decrease as the PS domain size further increases. This behavior, which is similar to the behavior of polyurethane-silica system[113], suggests that the changes in mechanical properties of the S45 series may be caused by the filler effect. Besides the filler effect, the degree of phase separation also plays an important role on the mechanical properties of these materials. S45-25'-M has the smallest size of the PS domain and the highest degree of phase mixing. The lower mechanical properties of this sample may due to the high degree of phase mixing.

As mentioned before, the number of blocks per chain (**n**) or equivalent number of blocks per chain ($\mathbf{n}_e$) will strongly influence the mechanical properties of a block polymer[1,69]. In the free radical PDMS-PS block polymers, **n** is directly related to the termination process. If the polymerization is terminated by a coupling or combination process, the multiblock polymer is formed. If termination occurs by disproportionation, a triblock polymer would be formed[14]. In

general, the coupling process would be dominated if the blocks are short. If the blocks are long, the disproportionation process will be the major termination process. Since the low conversion samples contain mostly short PS blocks, the coupling termination would be expected. Thus the final polymers are mainly multiblock polymers and the ultimate properties of these samples are high. For the high conversion samples, the disproportionation mechanism may be the main termination process because most PS blocks are large blocks, the final polymers are expected to contain many more triblock polymers. Therefore, their ultimate properties are lower than that of the lower conversion samples.

Besides the termination process, the molecular weight distribution of the PS blocks can also influence the mechanical properties. For a butadiene-styrene-butadiene block polymer system, the polymer with the PS center block having a narrow molecular weight distribution has a higher tensile strength than the polymer in which the center styrene block has a broad molecular weight distribution[112]. In the S45 series, the multimodal MWD of the PS blocks occurs after 45 minutes of polymerization. Due to the multimodal MWD of the PS blocks, the value of $\mathbf{n}_e$ becomes smaller as discussed in section 5.2.4. Hence, the mechanical properties, especially the tensile strength of the S45 series, decreases with further increase of conversion. Therefore, sample S45-95-M has much lower mechanical properties than other low conversion samples believed due to the combination of the filler effect and the broad MWD of the PS blocks.

5.3.2. Effect of Conversion on the PDMS-PS Block polymers with Different PDMS Block Length

5.3.2.1. Effect of Molecular Weight and the Molecular Weight Distribution

As discussed before (sections 5.2.3), the molecular weight (MW) and the molecular weight distribution (MWD) of the PS blocks vary with the macroinitiator PDMS block length. In order to study the combination effects of conversion and the PDMS block length, four polymers,

S26-58-M, S26-91-M, S89-34-M and S99-95-M, have been chosen. Figure 33 on page 118 shows the GPC results of these polymers. Figure 33a shows GPC curves of the S26 polymers by using a RI detector. There is a single asymmetrical peak on both GPC curves. The peak is shifted toward higher molecular weight as the conversion level increases. The asymmetrical peaks suggest that there are some bimodality in molecular weight distribution of these materials. The bimodal MWD of the PS blocks in these materials has been directly confirmed by the degradation studies. Figure 33b shows that there is a bimodal MWD of the PS blocks for all samples with different conversion levels. The high conversion sample, S99-95, has two peaks in its GPC curve, and the low conversion samples, S26-58 and S89-34, have shoulders shown on their GPC peaks. The shoulder on S89-34 GPC curve is also more distinct than that of S26-58. Since the conversion level of S89- 34 is much lower than S26-58 (34% vs. 58%), and the PDMS block length of S89-34 is much longer than S26-58 (8900 vs. 2600), the GPC results suggest that the PDMS block length has more influence on the MWD of the PS blocks than the conversion level. These results also provide direct support for that the heterogeneous polymerization condition is the cause for the multimodal MWD of the PS blocks rather than a T-N effect.

5.3.2.2. Effects of Conversion and the PDMS Block Length on Morphology

As the MW and the MWD of the PS block changes, the morphological texture of these PDMS-PS block polymers are changed. Figure 34 on page 120 shows the morphological texture of S26-58-M, S26-91-M, S89-34-M, and S99-95-M polymers. All low conversion polymers have smaller PS domains than the high conversion samples with similar PDMS blocks, because the MW of the PS blocks is smaller in low conversion samples than in high conversion samples, (recall Figure 33b). The size distribution of the PS domains is determined by the MWD of the PS blocks in these materials. The low conversion samples have more uniform PS domains because the MWD of the PS blocks in these materials is relatively narrow compared with that of the high conversion

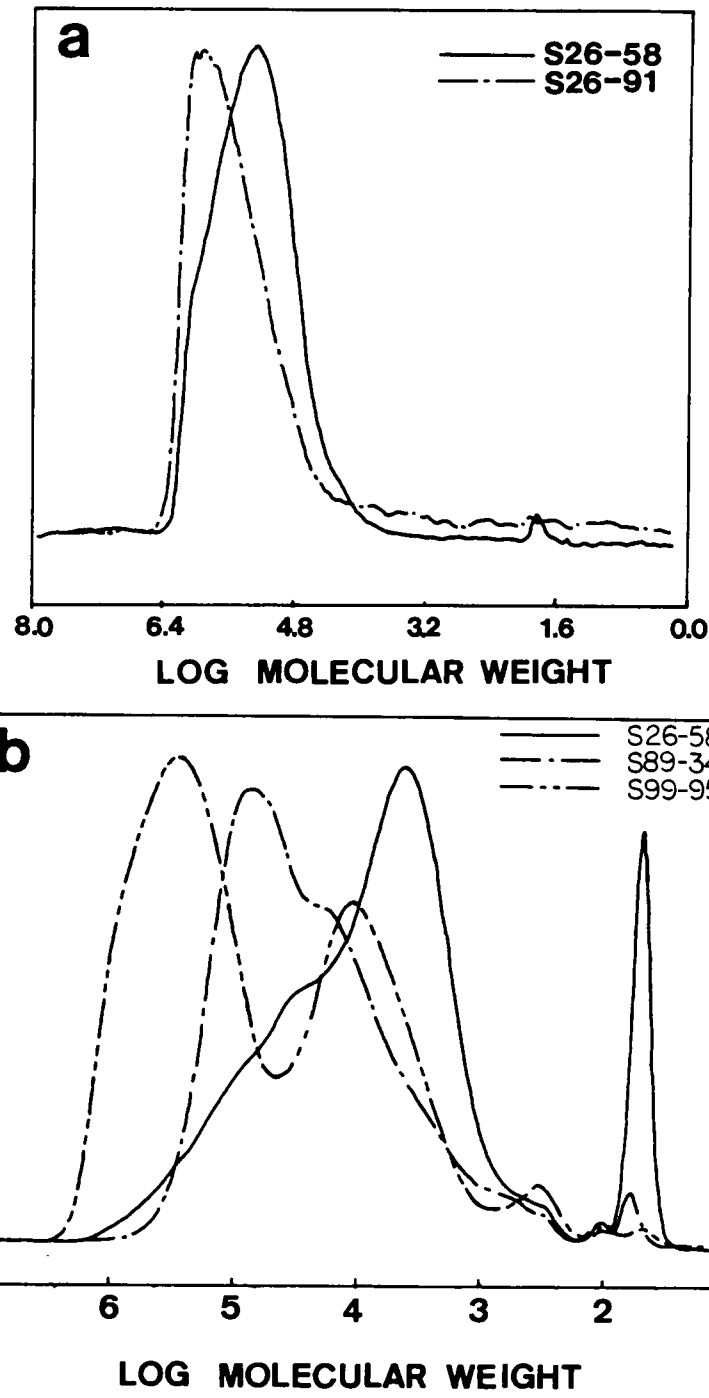

Figure 33. GPC curves of PDMS-PS block polymer with different conversion and the PDMS block length: (a). GPC curves of S26 polymers using a RI detector. (b). GPC results from the selective degradation studies.

samples. The size distribution of the PS domains in high conversion samples are very broad which is due to the very broad MWD of the PS blocks.

The type of morphological texture is mainly governed by the PDMS block length. For S26 polymers which contain short PDMS blocks, spherical PS domains are formed. For the polymers containing longer PDMS blocks such as S89-34 and S99-95, the rod-like and lamellar PS domains are formed.

5.3.2.3. Effect of Conversion and the PDMS Block Length on the Thermal Properties

Due to the changes in the MW and the MWD of the PS blocks in these PDMS-PS block polymers which are caused by the conversion level and the PDMS block length, the thermal properties of these materials are changed accordingly. Figure 35 on page 121 shows the DSC thermograms of these four polymers. The PS T_g's of low conversion samples, S26-58-M and S89-34-M, are lower and the T_g transitions of these two polymers are much less pronounced than that of the high conversion samples. This is due to the smaller PS blocks and a higher degree of phase mixing in these low conversion polymers. The ΔC_p analysis indicates the DPM for the high conversion samples is always lower than for the low conversion samples with similar size of PDMS blocks (Table 8 on page 122). The DPM of S26 polymers are lower than the DPM of both S89-34-m and S99-95-M. This is caused by the MWD of the PS blocks. As a reminder, the ΔC_p method measures the overall degree of phase mixing. In S89-34-M and S99-95-M, there should be a lot of very short PS blocks trapped in the PDMS phases because the bimodal MWD of the PS blocks in these polymers. Therefore, the domain mixing in these polymers is high, which results in a higher DPM. The DPM results indeed give direct support to the heterogeneous polymerization hypothesis. If the broader MWD is due to a heterogeneous polymerizations, the polymer with longer PDMS blocks should have a higher DPM.

The dynamic mechanical behavior of these materials also reflects the changes in the MW and MWD of the PS blocks in these materials. Figure 36 on page 124 shows the dynamic mechanical

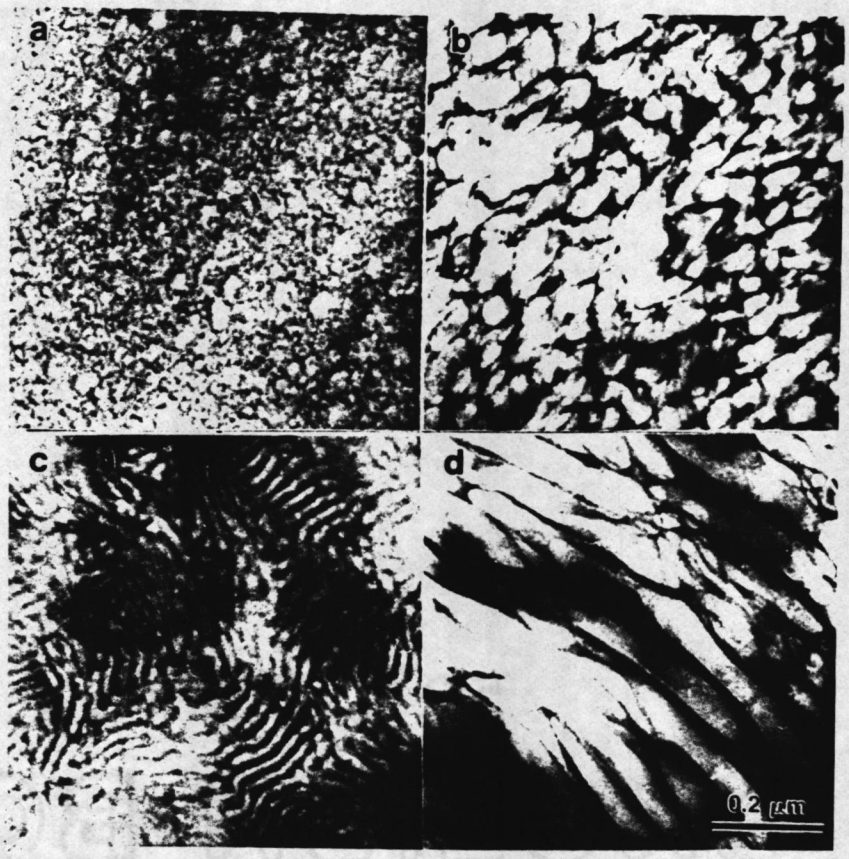

Figure 34. Effects of conversion and the PDMS block length on morphology: (a). S26-58-M, (b). S26-91-M, (c). S89-34-M, and (d). S99-95-M.

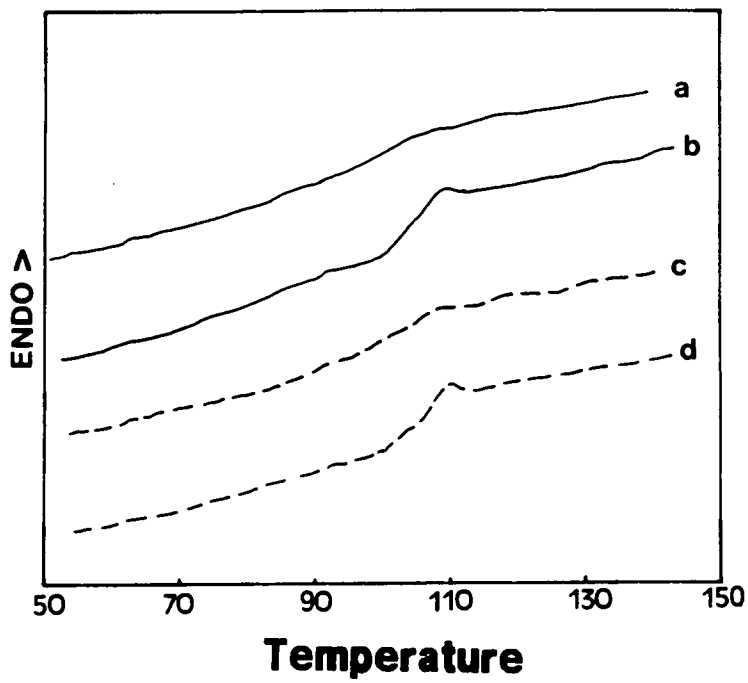

Figure 35. DSC thermograms of PDMS-PS block polymers with various conversion and the PDMS block length : a. S26-58-M, b. S26-91-M, c. S89-34-M, and d. S99-95-M.

Table 8. Degree of phase mixing of PDMS-PS block polymers with various conversion and PDMS block length.

Sample	T_g °C	DPM (%) average	DPM Up Limit	DPM Lower Limit
S26-58-M	97	33.1	34.8	31.3
S26-91-M	102	21.4	25.4	16.5
S89-34-M	99	40.8	43.6	38.3
S99-95-M	105	34.1	39.4	30.1

spectra of these polymers. For S26 samples, the low conversion sample, S26-58-M, has a higher E′ and a lower tanδ level within the rubbery region than that of the high conversion sample S26-91-M. Both the PDMS and PS T_g for S26-58-M are lower than those of S26-91-M. The lower PS T_g of S26-58-M is a result of a lower MW of the PS blocks in S26-58-M. The higher PDMS T_g and the tanδ level within the rubbery region of S26-91-M is caused by a broader MWD of the PS blocks in this sample. In S26-91, there are some very short PS blocks formed, and these short PS blocks are easily trapped within the PDMS phase resulting in an increase in the domain mixing, therefore, the PDMS T_g is shifted to a higher temperature. On other hand, the large PS domains would cause an increase in volume of the interphase region and raise the interphase mixing which results in a high level of tanδ at rubbery region. A similar situation has been observed for S89-34-M and S99-95-M. In this case, the T_g shifts are very small because of the large block sizes of both PDMS and PS blocks. But the low conversion sample, S89-34- M, has a lower tanδ level within the rubbery region than its high conversion counterpart, S99-95-M. Also, sample S89-34-M has a flatter rubbery plateau and higher storage modulus than that of S99-95-M. This may due to the better phase separation in the interphase regions and a higher value of n_e for S89-34-M than S99-95-M.

5.3.2.4. Effects of Conversion and PDMS Block Length on Mechanical Behavior

The stress-strain behavior of these polymers is also altered with both conversion and PDMS block length(Figure 37 on page 126). In general, the low conversion samples, S26-58-M and S89-34-M, have higher modulus and elongation than the high conversion samples, S26-91-M and S99-95-M. For the S26 series, the higher modulus and ultimate properties of the low conversion sample may result from more blocks per chain and smaller PS domains. For the polymer with longer PDMS blocks, the situation is different. Both stress strain curves of S89-34-M and S99-95-M have a well pronounced yield point which is the result of continuous rod-like or lamellar PS domains in these polymers. The tensile strength of both polymers are similar.

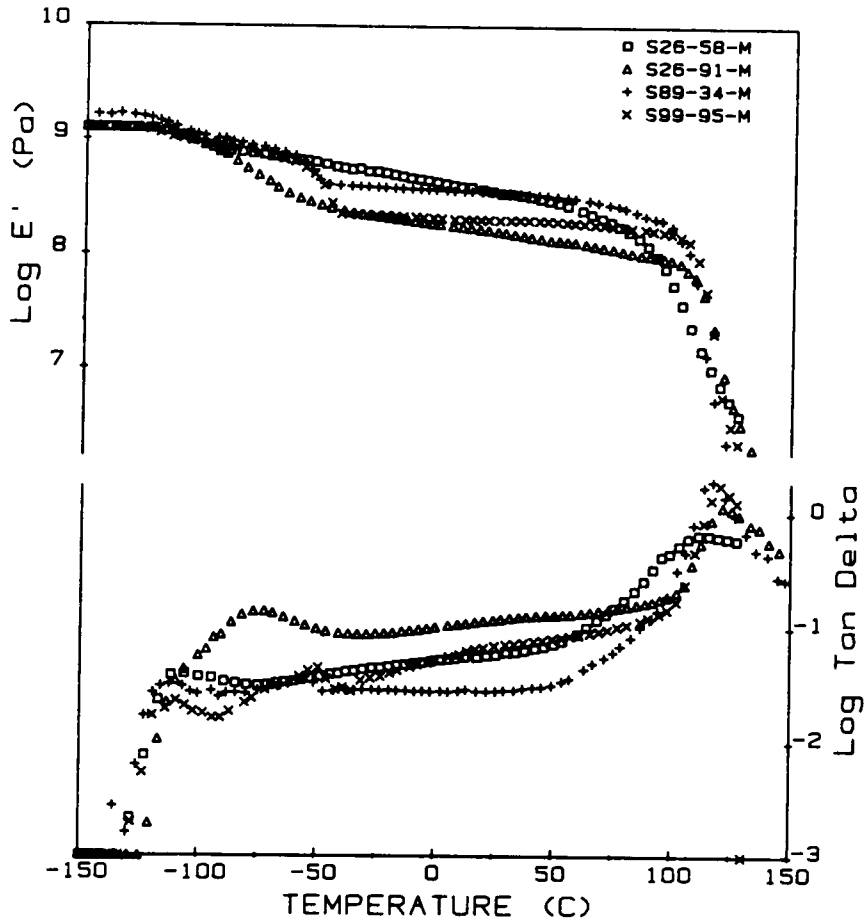

Figure 36. Effects of conversion and PDMS block length on dynamic mechanical behaviors of PDMS-PS block polymers.

S89-34-M has a higher modulus and elongation than that of S99-95-M. The higher modulus and elongation of S89-34-M is believed due to a better phase separation and more regular lamellar structures. Compared to S26-26-58-M, the ultimate properties of both S89-34-M and S99-95-M are much lower. This suggests that S89-34 and S99-95 have fewer equivalent blocks per chain than S26-58-M.

5.3.3. Summary

The styrene conversion level of these free radical PDMS-PS block polymers controls the MW and the MWD of the PS blocks in these materials. As the conversion increases, the MW of the PS blocks increases and the MWD of the PS blocks is broadened. These changes result from the changes in both radical and monomer concentration during the polymerization and the heterogeneous polymerization conditions. Based on the experimental data, the possibility of T-N effect has been ruled out.

Both the conversion and the PDMS block length affect the morphological texture of these PDMS-PS block polymers. The conversion mainly affects the domain size. When the conversion increases, the domain size increases because of the increase of the PS block length (MW). The size distribution of PS domains also becomes broader with the conversion due to the broadened MWD of the PS blocks. The type of the morphology is mainly dependent on the PDMS block length. As the PDMS block length increases, the morphology of these polymers is changed from spherical PS domains to rod-like or lamellar PS domains. The degree of phase separation also depends on the conversion. Since the MW and the MWD of the PS blocks vary with the conversion, the DPM is altered.

Mechanical properties of these polymers are dependent on the morphological texture and the number of blocks per chain in these polymers. The low conversion samples have higher modulus and ultimate properties than that of the high conversion samples, because the low conversion samples have smaller, more uniform PS domains, and more blocks per chains.

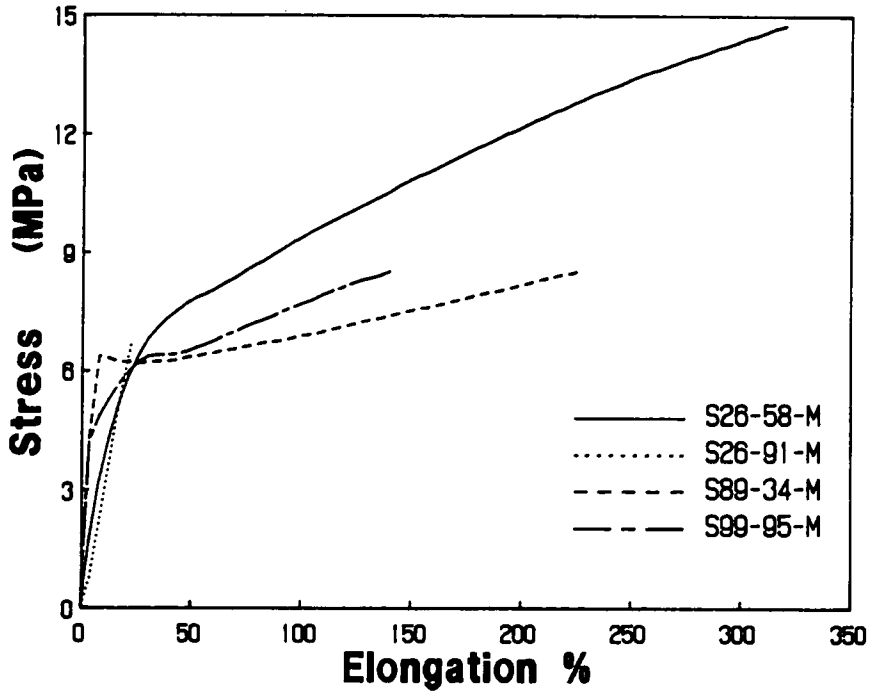

Figure 37. Mechanical behavior of S26, S89-34, and S99-95 polymer films cast from methylene chloride.

5.4. EFFECT OF FILM PREPARATION METHODS

It is well known that the bulk properties and morphology of block polymers are strongly influenced by the film preparation methods[3,68,69,100,113–116]. In general, there are two type interactions, block - block interaction (A-B interaction) and polymer - solvent interactions (P-S interactions), occurring during the film preparation process. The A-B interaction is repulsive interaction between two different components of the block polymer. This interaction arises from the thermodynamic incompatibility between the two components. As the difference between the solubility parameters of each component and the degree of polymerization increases, or the number of blocks per chain decreases, the incompatibility increases as well as the A-B interaction. In the thermal process, the A-B interaction is the dominate factor which governs the final solid state properties of the polymer.

In the solution casting process, the polymer chains interact with the solvent molecules by the polymer - solvent (P-S) interactions which involve the A block - solvent (A-S) and the B block - solvent (B-S) interactions. The strength of the P-S interactions depend on the solubility parameters of the solvent and the polymer. In solution casting, the A-B interaction and the P-S interactions contribute to the final state of microphase separation and the conformation of polymer chains. The changes in the degree of phase separation and the chain conformation will alter the final morphology and the properties of the polymer.

In the case of PDMS-PS block polymers, the solubility parameters of the two components are constants. Therefore, the final properties of the polymer films are dependent upon the molecular weight (MW) and the molecular weight distribution (MWD) of each block and the type of casting solvent. Since the MW and the MWD of the PS blocks are related to the conversion level, the discussion on the effect of film preparation method will be given in two parts. The first part deals with the high conversion samples, followed by a discussion of the low conversion samples.

5.4.1. Effect of Film Preparation Method on High Conversion PDMS-PS Polymers

5.4.1.1 Thermal Processibility of Higher Conversion PDMS-PS Polymers

The PDMS-PS block polymers were prepared either by compression molding and solution casting. In compression molding, the polymers were pressed at 150°C for 30 minutes. All high conversion samples as well as the low conversion sample with long PDMS blocks could not be thermally processed because of the large solubility parameter difference between the two components. Such films were not uniform and hence mechanical properties could not be accessibly measured.

5.4.1.2. Bulk Properties of Solution Cast PDMS-PS Polymer Films

The solution casting method did yield uniform polymer films. Depending on the type of casting solvent, and the PDMS block length, the physical appearance of the polymer films were different. For the systems containing short PDMS blocks such as S14-95, the films cast from different solvents were almost equal in terms of clarity and elastomeric behavior. For the polymers with large PDMS blocks, the films cast from methylene chloride and toluene are opaque but uniform films. These films display a typical plastic behavior: high modulus, distinct yield point, high tensile strength and low elongation to break (recall Figure 25 on page 97). Scanning electron microscopy (SEM) has been carried out on the cryo-fractured cross section of sample S193-95-M. Some signs of lamellar texture are also seen in the SEM micrographs which is in consistent with the TEM micrographs shown in Figure 20 on page 79. In contrast, films of these same system cast from cyclohexane are clear, transparent and soft films. These films have elastomeric behavior with low modulus, low tensile strength, and high elongation. Also, changes in the PDMS block length have a much lower effect on the mechanical properties of cyclohexane cast films relative to those cast by methylene chloride.

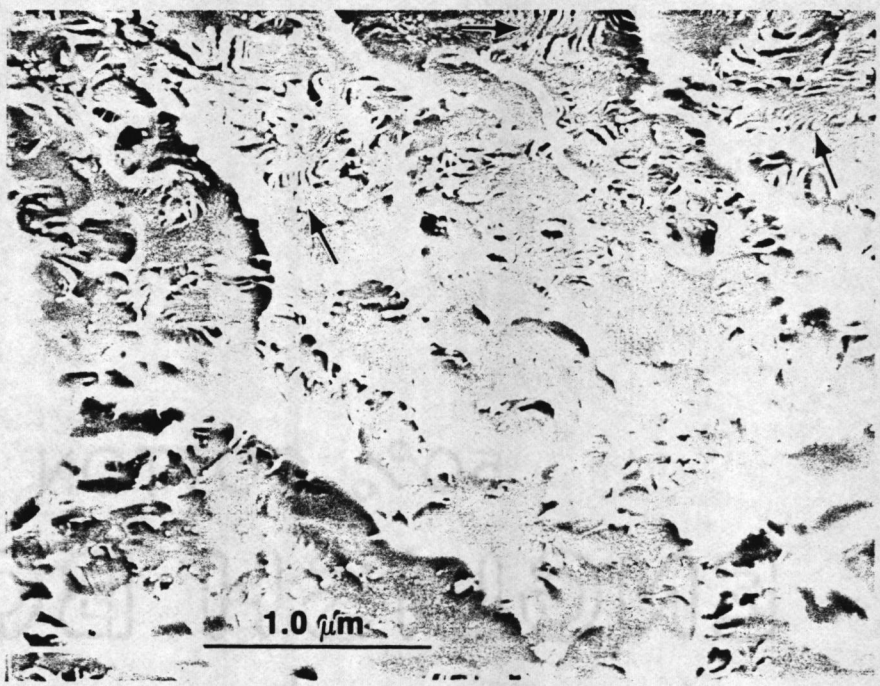

Figure 38. SEM micrograph of a fractured cross section of sample S193-95-M: Some lamellar structures can been seen in the area pointed by arrows.

As mentioned in Section 5.2.4, the dependence of the stress strain behavior with the PDMS block length is caused by changes in the morphological texture of the polymers. The changes in mechanical properties caused by different casting solvents may also reflect changes in the morphology and the degree of phase mixing in these materials.

5.4.1.2 Effect of Casting Solvent on Morphology

The morphology of high conversion PDMS-PS block polymers cast from different solvents are shown in Figure 39 on page 131. Figure 39a, b, and c show the morphological textures of the S14-95 polymers. Both films cast from methylene chloride and cyclohexane have a similar morphology: spherical PS domains dispersed in a PDMS matrix. But the toluene cast film has a lamellar structure (Figure 39b). As the PDMS block length increases, the molecular weight and the molecular weight distribution of the PS blocks greatly changes, hence, the resulting morphology is changed. When the PDMS block length is larger than 4,500, the morphology of methylene chloride and toluene cast films are alike, while the morphological texture of cyclohexane cast films are very different. As shown in Figure 39d, e, and f, S45-95-M and S45-95-T have a mixture of spherical and rod-like PS domains in a PDMS matrix. However, S45-95-C has pure spherical PS domains dispersed in a PDMS matrix. Similar results were obtained on samples S99-95 and S193-95 (Figure 39 g to k). Indeed, both S99-95-M and S99-95-T display similar rod-like structures and S193-95-M has a lamellar structure, and both S99-95-C and S193-95-C have a morphology of very large PS spherical domains encapsulated by PDMS layers. One also notes that the toluene cast films always have the most defined structure or the highest contrast in the TEM micrographs. These well defined structures may result from a higher degree of phase separation as indicated by the DSC ΔC_p analysis. Further discussion on this subject will be given in the following sections.

Changes in the morphology of the PDMS-PS block polymers with the type of casting solvents have been reported before[3,5,68,69,105,100]. Saam et. al[3,68,69] studied the morphology of PDMS-PS,

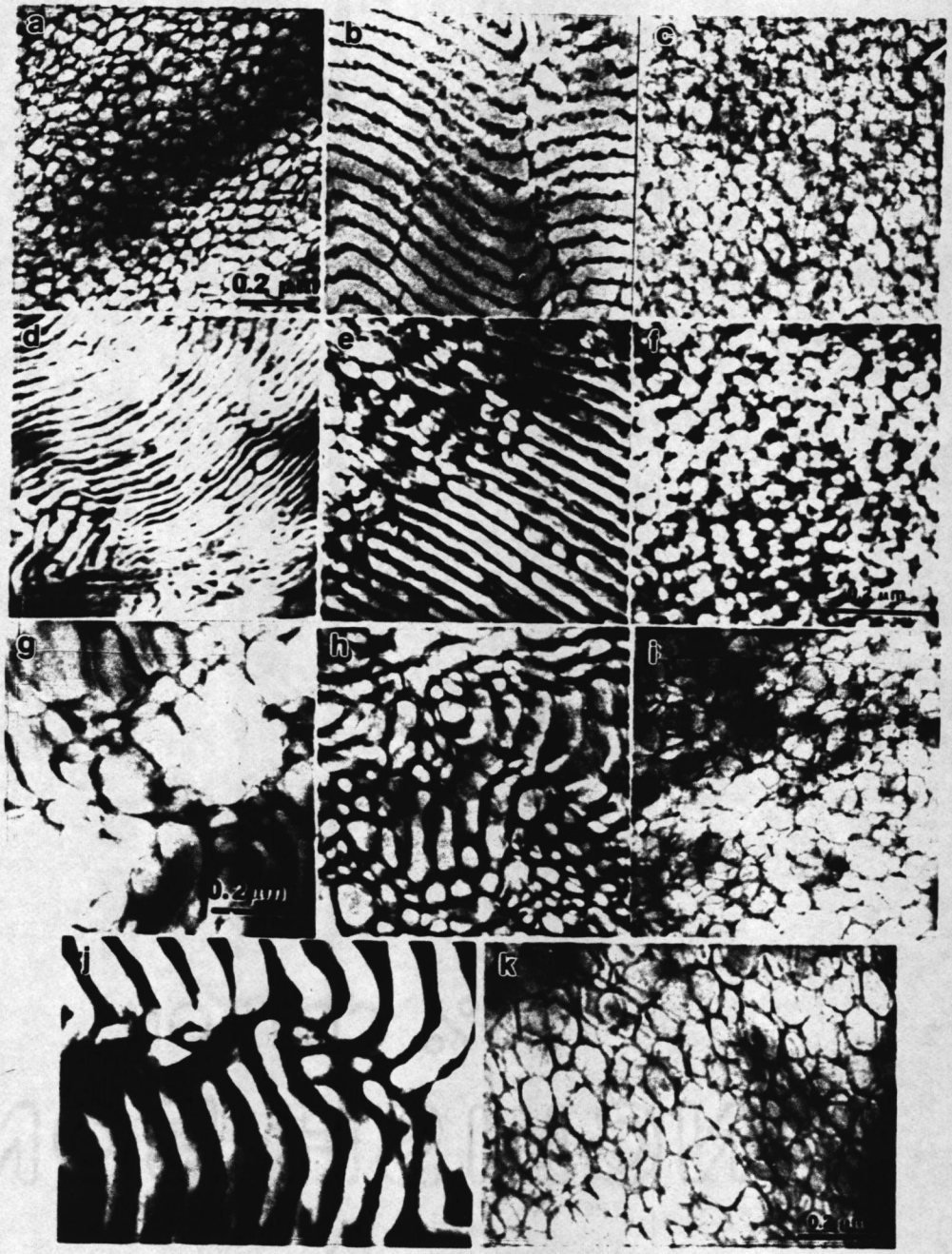

Figure 39. Morphological Textures of PDMS-PS films cast from different solvents: a. S14-95-M, b. S14-95-T, c. S14-95-C, d. S45-95-M, e. S45-95-T, f. S45-95-C, g. S99-95-M, h. S99-95-T, i. S99-95-C, j. S193-95-M, and k. S193-95-C.

PDMS-PS-PDMS, and -(PDMS-PS-PDMS)$_n$- block polymers. They found that the changes in the morphology of the block polymers mainly depended on the solubility parameter, δ, of the solvent. For example, the morphology of a PDMS-PS diblock polymer with 33 mol% of PS was the observation of PDMS domains in a PS matrix when bromobenzene was used for film casting. Bromobenzene has value of δ of 10.7 and it is a good solvent for the PS phase. When cyclohexane ($\delta = 8.2$) was used as casting solvent for the same polymer, the morphology became PS domains dispersed in a PDMS matrix. When the film was cast by toluene ($\delta = 8.9$) the morphology of the polymer was a "high contrast spaghetti-like" structure.

Similar results on PDMS-PS-PDMS triblock polymer have also been obtained by Varshney and Bajaj[5,100]. Their polymer contained 50 wt% of PDMS and the casting solvents were methyl ethyl ketone (MEK), toluene, and cyclohexane with δ values of 9.3, 8.9 and 8.2 respectively. The morphology of the MEK cast film showed spherical PDMS domains in a PS matrix, whereas cyclohexane gave a reversed structure, and toluene induced a distinct lamellar structure.

However, the situation was different for -(PDMS-PS-PDMS)$_n$- multiblock polymers. The dependence of morphology on the casting solvent also changed with the repeat sequence **n**. Bajaj and Varshney[5] found that the changes in morphology of a PDMS-PS multiblock with 55 mol% of PDMS were similar to that of a PDMS-PS-PDMS triblock polymer discussed in the previous section. Their polymer had a value of **n** of 2.4. When **n** was greater than 6, Saam et. al.[69] found no gross changes in the morphology when the polymer was cast from different solvents. In this case, the polymer contained 50 wt% of PDMS and the casting solvents were bromobenzene, toluene, or a decane-benzene mixture.

Several important things need to be pointed out relative to the previous studies discussed above. The first is that all the polymers studied before were synthesized by the anionic method giving a narrow molecular weight distribution of each block. In those studies, the thin cast films were used for the morphology studies. The morphology of thin cast films could differ from that of thick cast films because of possible changes in thermal dynamic equilibrium during the casting process. However, Wilkes et. al.[114,115] have found that the morphology of SBS block polymers does systematically vary with the type of casting solvents for thicker films and correlate well to observed

mechanical behavior. Finally, all the above morphological studies on the PDMS-PS block polymers showed that the toluene cast PDMS-PS block polymer films have the highest contrast and the most defined structure than other solvent cast films.

The solvent dependence of PDMS-PS block polymers may be related to their solution properties. Intrinsic viscosity measurements of PDMS-PS-PDMS triblock polymers have been carried out in different solvents having a solubility parameter, δ, ranging from 7.8 to 10[5004]. The results show that the intrinsic viscosity, $[\eta]$, increases with δ and reaches a maximum in toluene which has a δ value of 8.3 close to the "average value" of δ of the PDMS-PS block polymer. As δ of the solvent further increases, $[\eta]$ decreases. For cyclohexane and MEK which are near θ solvents at ambient for the PDMS and PS blocks respectively, lower values of $[\eta]$ are observed relative to toluene. These results suggest that the changes in the δ of solvents causes changes in the amount of the A-B and the P-S interactions. The relative contribution of the A-B interactions may be estimated from the intrinsic viscosity data. By initially considering a block polymer as a binary mixture of homopolymers, the intrinsic viscosity can be estimated by the mole fractions and the Mark-Houwink constants of each component. The values of $[\eta]$ for PDMS-PS block polymers have been calculated by Davis and Jones[6] and Bajaj and Varshney[100]. They found that the experimental values were always greater than the calculated values. In toluene, $\Delta[\eta]$, the difference between the experimental and the calculated values, is only about 4-14% of the calculated value and it is also independent on the molecular weight and the composition of the polymer. In cyclohexane which is the θ solvent for the PS segments, $\Delta[\eta]$ is also small; about 1.5-18% of the calculated value. But in MEK, the θ solvent of the PDMS segments, the $\Delta[\eta]$ values are up to 50% greater than those calculated and are proportional to the mole fraction of the PS blocks. These results suggest that the PDMS-PS block polymer chains are the most expanded in a good solvent such as toluene which has the value of δ close to the "average δ value" of the polymer. Therefore, $[\eta]$ has the highest value. The expansion of the chains is mainly due to the P-S interactions, and the A-B interaction is minimized[6,100]. Whereas in a θ solvent for one of the blocks, the A-B interaction may contribute towards coil expansion considerably depending on the solvent used. If the solvent is cyclohexane, agglomeration of precipitated PS blocks takes place

and results in a lower viscosity. In this case, the A-B interaction do contribute to the agglomeration of the PS blocks but the contribution is relatively small. Vice versa, the lower viscosity in MEK is a result of aggregation of the PDMS blocks. In this case, the contribution of A-B interactions is much greater than that in cyclohexane, and the chains become more expanded than in cyclohexane. Therefore, $[\eta]$ is higher in MEK than in cyclohexane. The morphological textures of these polymers directly reflect the change of the aggregation states of the polymer in solution. Both MEK and cyclohexane cast films have a spherical morphology while the toluene cast films have a lamellar structure[100].

In the case of free radical synthesized PDMS-PS block polymers, the morphology depends on both the type of casting solvent and the PDMS block length. For the short PDMS block sample, S14-95, the morphology of both methylene chloride and cyclohexane cast films are PS spherical domains surrounded by a PDMS matrix. In contrast, the film cast from toluene has a lamellar structure (Figure 39a, b, and c). In toluene, the polymer chains are mostly extended because of the P-S interactions, therefore, a lamellar structure is formed. In the other two solvents, methylene chloride and cyclohexane, one of the component (PS) is precipitated and aggregated to form the spherical domains due to the combination of both A-B and P-S interactions. It is necessary to point out that a phase inversion has occurred in the methylene chloride cast films. In this study, the thick film casting method has been used, therefore the thermodynamic equilibrium condition may differ somewhat from that of the thin film casting which has been used in the previous studies. In fact, phase inversion did occur for all of the methylene chloride cast films of this study (Figure 20 on page 79).

For the polymers containing longer PDMS blocks (greater than 4500), the situation is different. As shown in Figure 39g to k, the morphology of the methylene chloride cast films are similar to that formed in toluene cast films: a mixed morphology of spherical and rod-like PS domains, while a cyclohexane cast film has purer PS spherical domains. These may be caused by the large molecular weight and the multimodal molecular weight distribution of the PS blocks in these materials. When the molecular weight of both PDMS and PS blocks increases, the A-B interaction between two components will be increased, thus, the contribution of A-B interaction to the

chain expansion increases. The contribution of the A-B interaction also depends on the type of solvent. In these free radical synthesized PDMS-PS block polymers, the molecular weight of the PS blocks increases with the PDMS block length. The strength of the A-B interactions increases as well. When the polymers are cast from methylene chloride, the polymer coils are more expanded because of the stronger A-B interaction. Therefore, the resulting morphology is more like those of toluene cast films. In cyclohexane, the contribution of A-B interaction is much less than in methylene chloride, therefore the PS segments can agglomerate easier and spherical PS domains are formed.

5.4.1.3. Effect of Casting Solvents on the Degree of Phase Mixing

The type of casting solvent not only affects the morphology, but also strongly affects the degree of phase mixing (DPM) in these free radical synthesized PDMS-PS block polymers. Figure 40 on page 136 shows the effects of casting solvents on the DPM of these materials. For methylene chloride and cyclohexane cast films, the DPM decreases as the PDMS block length increases because the strength of A-B interaction increases with the molecular weight of both PDMS and PS blocks. The DPM of cyclohexane cast films is just slightly greater than that of methylene chloride cast films. However, the DPM of toluene cast films is much lower than that of the other two solvents and it is almost independent of PDMS block length. The ΔC_p results indicate that the DPM of S14-95-M and S14-95-C is around 55%. But the DPM of S14-95-T is only about 30% (Figure 40) This is due to more extended polymer chains which are caused by the stronger P-S interactions in toluene. The higher degree of chain expansion in toluene explains why toluene cast films have lower DPM, lamellar or rod-like morphology, and the higher contrast in the TEM micrographs.

Figure 41 on page 138 shows the dynamic mechanical spectra of the S14-95 and S99-95 samples. In the tanδ spectra of S14-95 samples (Figure 41a), there are two major transition peaks at -50°C and around 100°C. These transitions correspond to the glass transitions of the PDMS

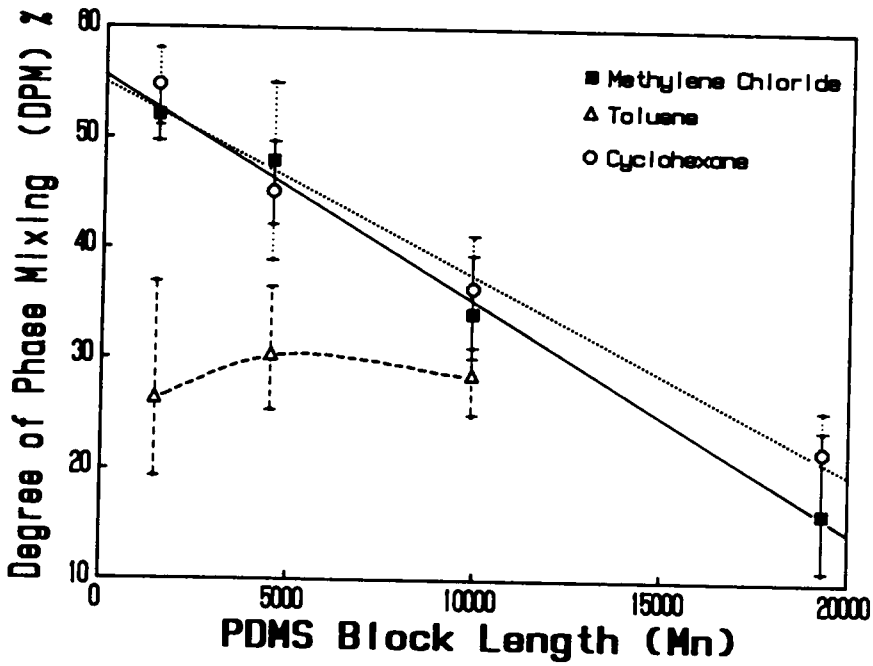

Figure 40. Effect of casting solvent on degree of phase mixing on PDMS-PS block polymers.

and the PS blocks respectively. For the S14-95 samples, both the PDMS and PS blocks are expected to be shorter, therefore, the A-B interactions between the two blocks may be less. Consequently, the degree of phase mixing is high. The upward shifting of the PDMS T_g (-50°C vs. -120°C of homopolymer PDMS) of this material indeed indicates a considerable PS mixing into the PDMS phase. During solution casting by methylene chloride and cyclohexane, the P-S interactions make smaller contribution to the chain expansion and phase separation. Therefore, there are some short PS blocks trapped in the PDMS phase and a high value of DPM results. For methylene chloride and cyclohexane cast films, S14-95-M and S14-95-C, the tanδ and E′ spectra are very similar except for the T_g of the PS phase. The PS T_g of S14-95-C is around 70°C while the PS T_g of S14-95-M is around 90°C. The lower PS T_g of S14-95-C indicates that some PDMS segments have mixed into the PS phase, thus, the T_g of the PS phase is suppressed. However, the toluene cast film, S14-95-T, has a different behavior. The PDMS T_g of S14-95-T is about 10°C lower than that of other two, while the PS T_g of this film is about 30°C higher than the PS T_g of S14-95- M. Also the T_gs of S14-95-T are more distinct than those of S14-95-M and S14-95-C. These results indicate that there is much less phase mixing in the toluene cast film than in methylene chloride and cyclohexane cast films. The dynamic mechanical results directly support these ΔC_p results.

In the rubbery region, the storage modulus (E′) of S14-95-T is higher than S14-95-M and S14-95-C. The higher modulus clearly results from the continuous PS phase of the lamellar structure of S14-95-T (Figure 39 on page 131). There is another weak transition shown in the tanδ spectra near -100°C. This transition may be the T_g of some very large and relatively pure PDMS blocks which are formed by several short PDMS blocks linked with just a few styrene units.

For S99-95, the results are different from that of S14-95 because of change in both molecular weight and the molecular weight distribution of the PS blocks (recall Figure 22 on page 89). The DSC results show that the DPM for the toluene cast film is only a little lower than that when the other two casting solvents are used (Figure 40 on page 136). The dynamic mechanical spectra (Figure 41b) show that the location of T_g peaks does not shift with the type of casting solvent used. Since S99-95 polymer contains mostly large blocks of both PDMS and

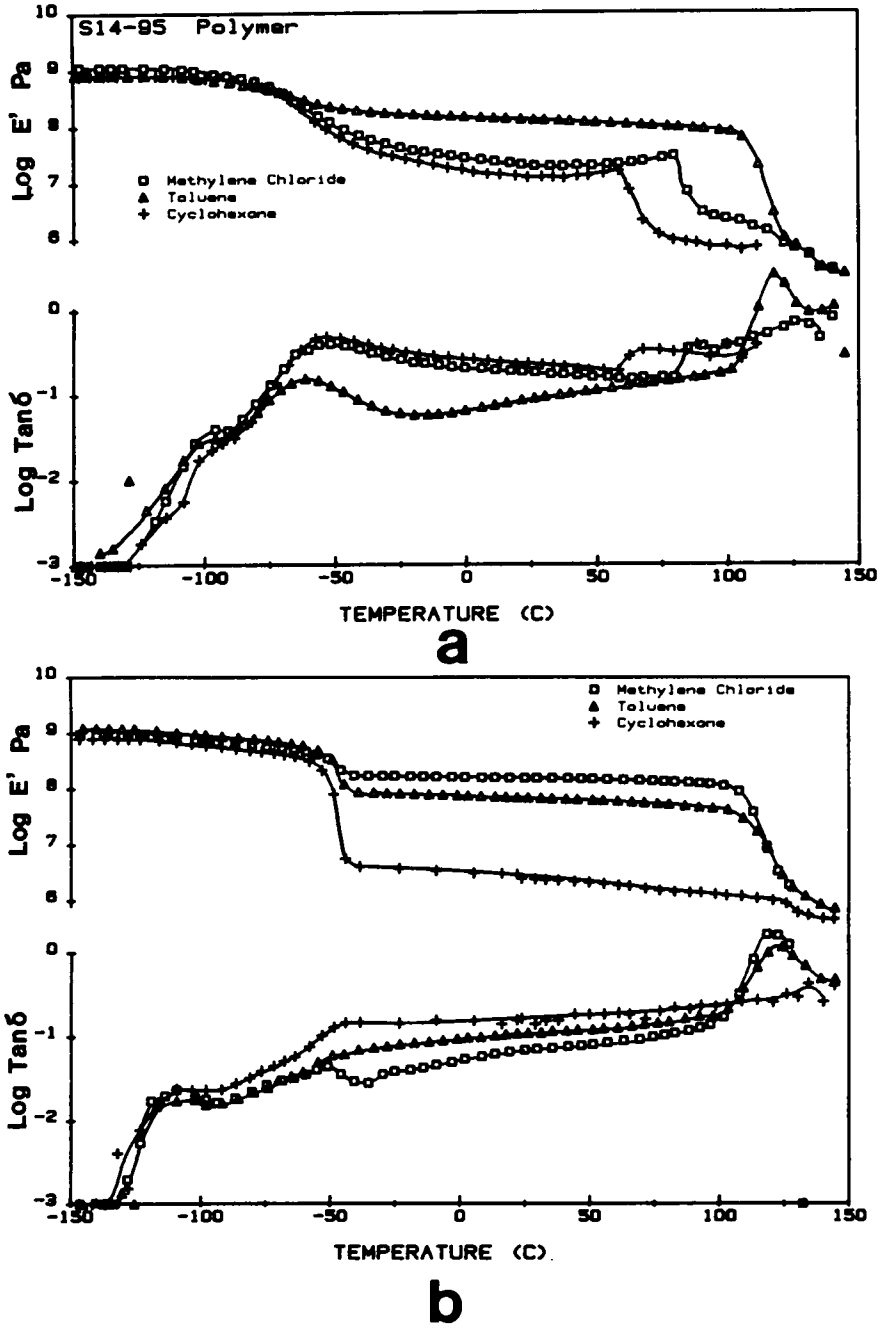

Figure 41. **Effect of casting solvent on dynamic mechanical behavior of the PDMS-PS block polymers:** (a). Dynamic mechanical behavior of S14-95 polymer. (b). Dynamic mechanical behavior of S99-95 polymer.

PS, the A-B interactions in this polymer should be larger than that for S14-95. During solution casting from cyclohexane, the large PS blocks are more easily precipitated out of the PDMS phase, and much less PS blocks are trapped in the PDMS phase compared to S14-95 which contains mostly short PS blocks. Therefore, the DPM is lower for S99-95. A similar situation occurs when S99-95 is cast by methylene chloride. In this case, the A-B interactions contribute more to the chain expansion and phase separation. Thus the DPM is lower, the PS coils expand more when cast from toluene (Figure 39 on page 131).

By using different casting solvents, an additional insight on the nature of the phase mixing have been identified. As discussed in section 5.1.2.2, there are two type of phase mixing; domain mixing and interphase mixing. In the former, some short PS (PDMS) blocks are trapped into the PDMS (PS) phase. And in the latter, the mixing only occurs in the interfacial region between two different domains (refer to Figure 42 on page 140).

For the PDMS-PS block polymers, the chain mobility of the PDMS blocks and the PS blocks is different at room temperature. At this temperature, the PDMS blocks have higher mobility than the PS blocks because the PS blocks are in the glassy state while the PDMS blocks are in the liquid state. When in a good solvent such as toluene, both the PDMS and the PS blocks can be dissolved, the mobilities of both PDMS and PS blocks increase. Due to the strong P-S interactions, the chains also become more expanded. Therefore, both PS and PDMS blocks can much more easily precipitate from each other and aggregate with themselves and both the domain mixing and the interphase mixing are reduced greatly. When methylene chloride is the casting solvent, the mobility of the PS blocks increases. The PDMS blocks mixed in the PS phase, especially in the interphase region, will be removed from the PS phase more easily and interphase mixing reduced. However, the mobility of the PDMS blocks have not changed much in this case. Thus, those short PS blocks which are trapped in the PDMS phase might not be able to escape, and the domain mixing may remain unchanged. When cyclohexane is used to cast films, the mobility of the PS blocks remains unchanged, but the mobility of the PDMS blocks increase. Therefore, the level of the interphase mixing will not change because the PS blocks are still "locked" in place. Domain mixing, however, could decrease because the trapped PS blocks may be able to escape due to the

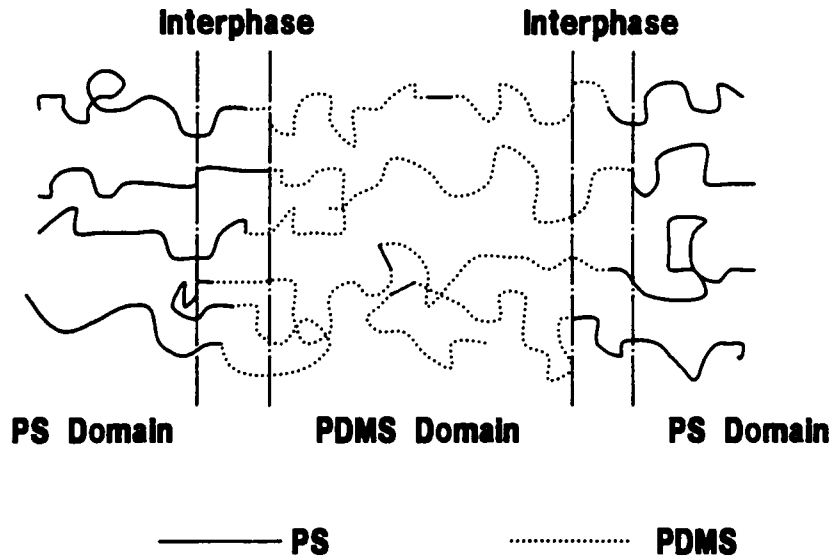

Figure 42. Illustration of domain mixing and interphase mixing.

higher mobility of the PDMS blocks and the DPM may drop down. However, if the phase mixing is caused by the PDMS blocks trapped in the PS phase, then the level of the phase mixing may not be able to be reduced by using cyclohexane as the casting solvent. However, for this case, the DPM will be reduced if methylene chloride is the casting solvent.

The above discussions combined with DMA and DSC data leads to the following conclusions (refer to Table 9). The DPM value of the toluene cast films should be the lowest in either domain mixing or interphase mixing. However, the DPM of cyclohexane cast film should be the highest one if interphase mixing occurs. If domain mixing occurs, the DPM of cyclohexane cast film would be lower than the DPM of methylene chloride cast film if the PS blocks mix in the PDMS domains as shown in Figure 42. Vice versa, if the PDMS blocks mix in the PS domain, the DPM of methylene chloride cast film should be lower than cyclohexane cast film. If the situation is as the drawing in Figure 42, both interphase mixing and domain mixing with PS blocks in the PDMS domains occur, hence, the DPM of both cyclohexane and methylene chloride cast films would be very close.

As mentioned in section 5.1.2.2, the dynamic mechanical spectra of the block polymers also reflect the changes in the type of phase mixing, i.e. the shift of T_g results from domain mixing and the changes in the tanδ level within rubbery region relates to the degree of interphase mixing. Therefore, by combining the DSC (DPM values from the ΔC_p measurements) and DMA results, the type of phase mixing in these free radical PDMS-PS block polymers should be identifiable.

For sample S14-95, the DPM of its toluene cast film is the lowest, while the methylene chloride and cyclohexane cast films give almost the same values of the DPM (Figure 40 on page 136). There are significant shifts of T_gs for both the PDMS and the PS phases shown in the tanδ spectra (Figure 41a). The tanδ spectrum of S14-95-T has the lowest level within the rubbery region and the other two are at nearly the same level. These results suggest that phase mixing occurs in both domains and interphase region. The mixing is mainly caused by domain mixing. The shifts of the T_g's indicate that there is a considerable amount of PDMS and PS blocks mixed with each other. For S99-95, its cyclohexane cast film has the highest value of the DPM, while its toluene cast film has the lowest. The cyclohexane cast film also has the highest tanδ level in the

Table 9. Relationship between the type of phase mixing with DSC and DMA results.

DSC	Domain Mixing		Interphase Mixing
	PS in PDMS	PDMS in PS	
Methylene Chloride	H*	M	M
Toluene	L	L	L
Cyclohexane	M	H	H
T_g Shifts	Y	Y	N
tanδ level	N	N	Y

* indicates the relative value of DPM; H = high, M = medium, and L = low.

rubbery region, while the methylene cast film has the lowest level. There are no significant T_g shifts in the tanδ spectra (Figure 41b). The results suggest, phase mixing in this sample is mainly in the interphase region.

It must be pointed out that the above discussion is based on an assumption of that the domain mixing in these polymers are mainly due to the PS blocks mixed into the PDMS phase. Most experimental evidence presented here support this assumption. In most cases, the T_g of the PS blocks does not change when the T_g of the PDMS blocks is shifted toward a higher temperature which indicates that mixing of the PS blocks into the PDMS phases except for the case of sample S14-95. In sample S14-95, however, the mixing of the PDMS blocks into the PS phase does occur, and the T_g of the PS phase does decrease.

5.4.1.5 Solvent Dependence of Mechanical Properties.

The stress strain behavior of samples S14-95 and S99-95 cast from different solvents is shown in Figure 43 on page 145. For S14-95, the films cast from methylene chloride and cyclohexane have similar elastomeric behavior. This is due to the continuous PDMS rubbery phase as has been shown in Figure 39 on page 131. The somewhat lower stress level of cyclohexane cast film may be due to a higher degree of phase mixing than that within the methylene chloride cast film. In contrast, S14-95-T behaves total differently than its counterparts. It has a much higher modulus, lower elongation, and a distinct yield point is also observed. This behavior is caused by the continuous phase of the PS lamella (recall-Figure 39b).

The polymers with longer PDMS blocks behave total differently than for S14-95. For example, S99-95-M and S99-95-T behave more like a plastic: low elongation, high modulus and tensile strength, and a distinct yield point (Figure 43b). However, S99-95-C has a more elastomeric behavior: high elongation, low modulus and tensile strength. The different stress-strain behavior is therefore clearly caused by the different morphological textures of these samples (recall Figure 39 on page 131). Both S99-95-M and S99-95-T have a cylindrical-like and some lamellar

PS domains while S99-95-C has spherical PS domains in a continuous PDMS matrix. The plastic behavior of S99-95-M and S99-95-T is due to some continuity of the PS phases. Finally, the rubbery behavior of S99-95-C is clearly due to the continuous PDMS matrix.

5.4.2. Effect of Film Preparation Methods on Low Conversion PDMS-PS Polymers

5.4.2.1. Thermal Processibility of Low Conversion Samples

Two low conversion polymers, S26-58 and S89-34, have been used to study the effect of film preparation methods. For sample S26-58, all films prepared either by solution casting or thermal molding are clear transparent and tough films. For sample S89-34, solution cast films are also clear transparent films. However, the films cast from methylene chloride is a tough film while cyclohexane provides a soft one. Thermal molding of sample S89-34, however, results in a non-uniform film with very poor mechanical properties.

5.4.2.2. Effect of Preparation Methods on Mechanical Properties of low Conversion Samples

Figure 44 on page 147 shows the stress-strain behavior of low conversion polymer films prepared by different methods. For sample S26-58, there are only small differences in the stress-strain behavior between different preparation methods and the type of casting solvents. While some differences exists, the stress-strain behavior of all these films is nearly the same which indicates that the morphology of these materials may be the same. Although the changes in the ultimate properties may be due to the changes in degree of phase separation of these materials. The situation for sample S89-34 is totally different. S89-34-M, the methylene cast film, displays a distinct yield point and high modulus, and S89-34-C has a typical elastomeric behavior (Figure 44b). This results again from a different morphology in these two films as will be presented in the next section.

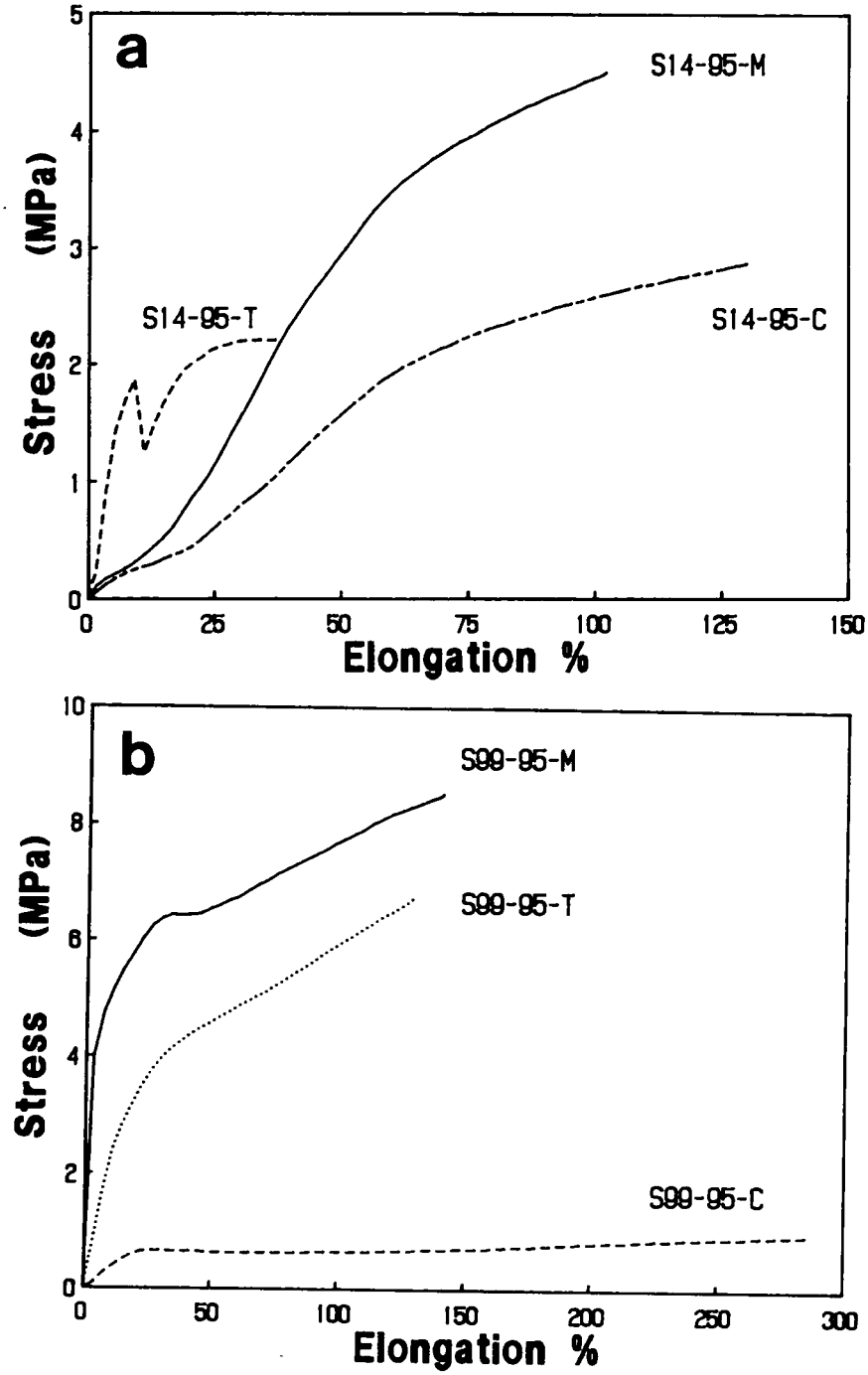

Figure 43. **Effects of casting solvents on the stress-strain behavior of PDMS-PS block polymers:** (a). Stress-strain behavior of S14-95 polymers. (b). Stress-strain strain behavior of S99-95 polymers.

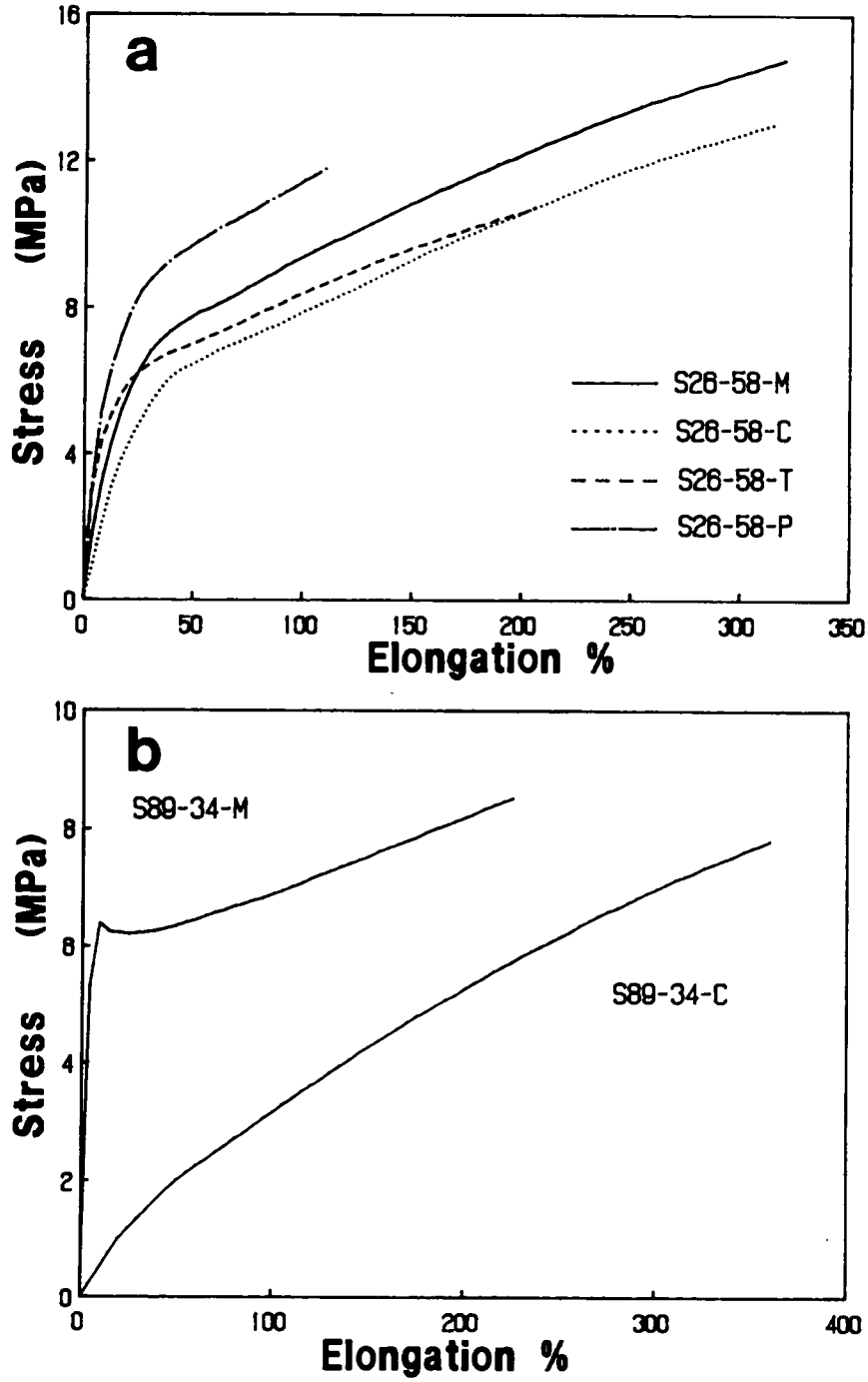

Figure 44. **Effect of film preparation methods on the mechanical behaviors of S26-58 and S89-34 polymers:** (a). Stress-strain behavior of S26-58 polymer, and (b). Stress-strain behavior of S89-34 polymer.

5.4.2.3. Morphology of Low Conversion Polymer films Prepared by Different Methods

The TEM micrographs shown in Figure 45 on page 148 and Figure 46 on page 149 are the morphological textures of sample S26-58 and S89-34. For sample S26-58, all polymer films prepared by the different methods have really the same morphology: spherical PS domains in the PDMS matrix. This is why all of these films have the similar stress-strain behavior, since there are no gross changes in morphology in the S26-58 films. also, the domain size is very regular in these films. This suggest that the equivalent number of blocks per chain (n_e) in S26- 58 polymer is higher than other free radical PDMS-PS block polymers. This is also consistent with early observations on anionic synthesized PDMS-PS blocks polymers reported by Saam et. al.[69]. They reported that there was no gross morphological changes caused by different casting solvents on PDMS-PS multiblock polymers when the number of block per chain greater than 6. The higher value of n_e in S26-58 is believed to result from the short PDMS blocks and low conversion which promotes a narrower MWD of the PS blocks. Therefore, there is no gross changes in morphology caused by different casting solvents in S26-58 polymer films and they have much higher ultimate properties than other samples (recall Figure 37 on page 126).

For sample S89-34, the morphology does change with the type of casting solvent. As shown in Figure 46 on page 149, S89-34-M has a lamellar structure with both the PS and PDMS phases being continuous. The plastic stress-strain behavior of S89-34-M is caused by a continuous PS phase. Meanwhile, the cyclohexane cast film of S89-34 has a morphology of spherical PS domains in a PDMS matrix. This is why S89-34-C displays elastomeric behavior because of the continuous PDMS matrix. The solvent dependence of the morphology of S89-34 indicates that the value of n_e is small in this polymer, because the ultimate properties of PDMS-PS block polymers are correlated to n - the number of blocks per chain[69]. Since sample S89-34 has similar ultimate properties and solvent dependent morphology as the high conversion sample S99-95. Therefore, the value of n_e for S89-34 is expected to be as small as the value for S99-95 even thought the domain size in S89-34 is much smaller than in the S99-95.

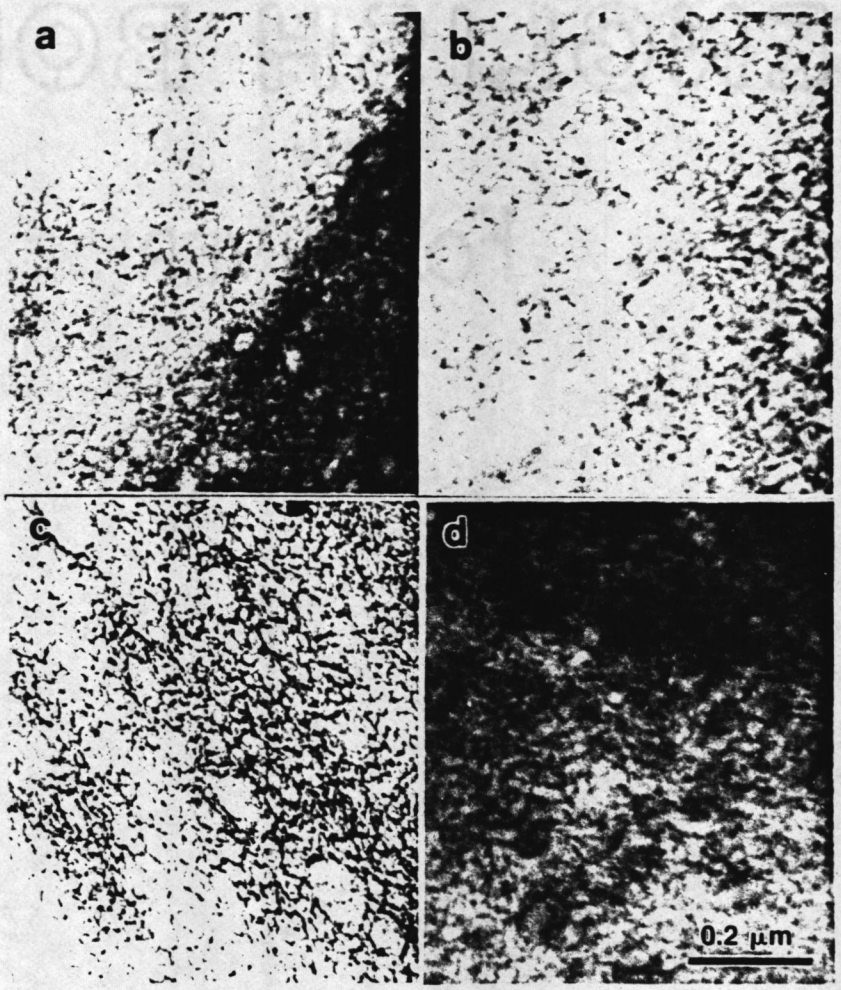

Figure 45. Morphological texture of S26-58 polymers: (a). S26-58-M, (b). S26-58-T, (c). S26-58-C, and (d). S26-58-P.

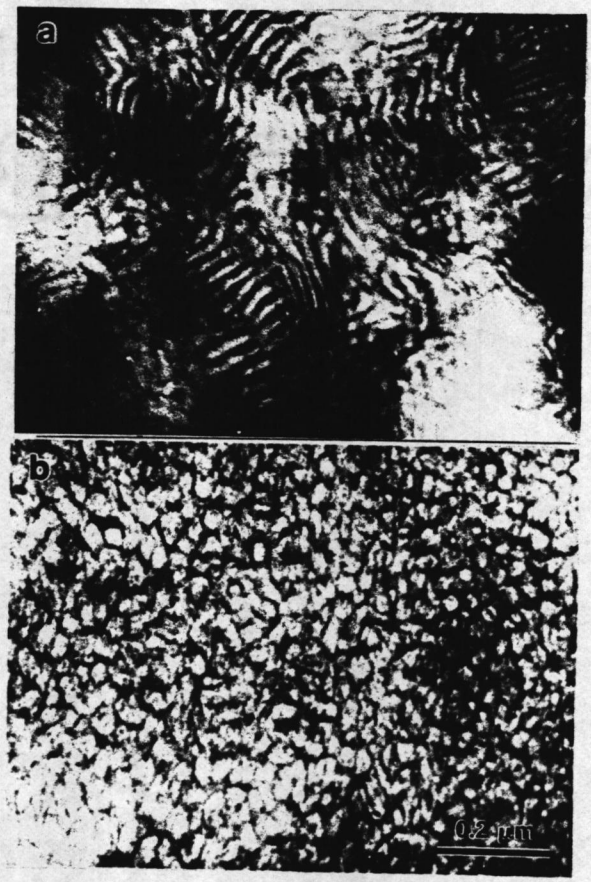

Figure 46. Morphological texture of sample S89-34: (a). S89-34-M, and (b). S89-34-C.

5.4.2.4. Effect of Film Preparation Methods on the Degree of Phase Separation

At the low conversion level, the PS blocks in S26-58 and S89-34 are small with a narrow MWD, thus the degree of phase mixing (DPM) in these materials should be relatively independent of the type of casting solvent and the film preparation method. In Table 10, the DPM of samples S26-58 and S89-34 measured by DSC are listed. Indeed this is the case although there are some small differences of the value of DPM between different film preparation methods and the type of casting solvents. In these low conversion materials, the molecular weight distribution of the PS blocks is narrow, and there are not many very short PS blocks that exist as in high conversion materials (recall Figure 33 on page 118). Therefore, the domain mixing is reduced. Since the block length of the PS blocks in these low conversion samples is not as large as in the high conversion samples either, the interphase mixing may be the major type of microphase mixing. This assumption has been directly supported by the dynamic mechanical data.

Dynamic mechanical spectra of S26-58 polymer films prepared from different methods and casting solvents are shown in Figure 47 on page 153. There are no T_g shifts due to neither the type of casting solvents nor the film preparation methods. This indicates that there is no major phase mixing in domains. However, the level of tanδ within the rubbery region does change with the type of casting solvents. S26-58-P has the highest tanδ level while S26-58-M has the lowest. The difference is due to the contribution of the A-B interaction and the P-S interactions. In the thermal molding process, only the A-B interaction contribute to the phase separation. However, the P-S and the A-B interactions contribute to the phase separation in solution casting. When the solubility parameter, δ, of the solvent is close to the value of δ of the PS phase, the contribution of A-B interaction increases more rapidly. Due to the strong P-S and A-B interactions, the polymer chains become more expanded. As a result, interphase mixing will be reduced. Thus, the degree of phase mixing and the level of tanδ within the rubbery region of solution cast films are lower than for the thermal molding film because of the combination of the A-B and the P-S interactions.

Table 10. Degree of phase mixing of low conversion PDMS-PS block polymers.

Sample	T_g °C	DPM (%) average	DPM Up Limit	DPM Lower Limit
S26-58-M	97	33.1	34.8	31.3
S26-58-T	100	43.4	44.4	42.5
S26-58-C	96	41.2	41.8	40.5
S26-58-P	99	36.9	38.2	35.3
S89-34-M	99	40.8	43.6	38.3
S89-34-C	101	35.5	36.7	34.4

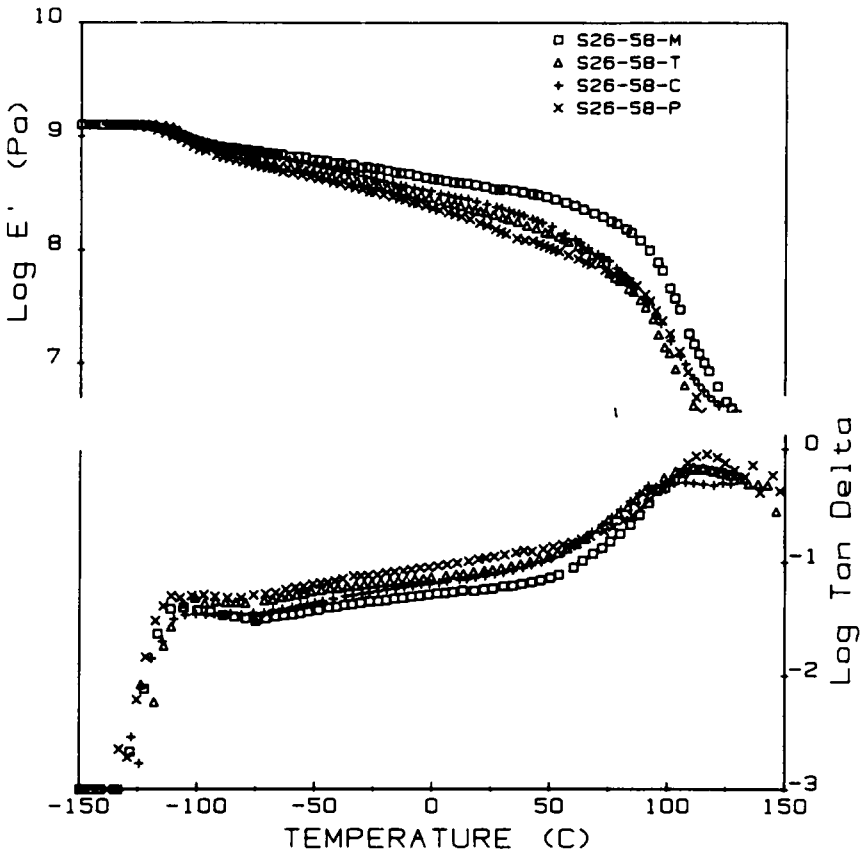

Figure 47. Dynamic mechanical behavior of sample S26-58.

5.4.2.5. Summary

For the high conversion samples, because there exists a high degree of incompatibility between the PDMS and the PS phases which is caused by the large molecular weight of the PS blocks and their respective solubility parameters, thermal molding can not be undertaken to prepare uniform polymer films. However, the solution casting of these same high conversion samples does produce uniform polymer films. The bulk properties and their respective morphological textures, and the degree of phase mixing is dependent on the type of casting solvents because of the influence of the molecular weight and the molecular weight distribution of the PS blocks in the high conversion samples.

The low conversion sample containing short PDMS blocks can be easily thermally processed. But the low conversion sample with large PDMS blocks can not be thermal molded into a uniform film. For the low conversion sample with short PDMS blocks, there is no gross morphological changes with casting solvent. It is to be believed that is due to the larger number of blocks per chain in this particular sample. The morphology of S89-34 does change, however, with the type of casting solvent because of fewer blocks per chain.

By using different type of casting solvent, an insight to the nature of microphase separation has been identified. By monitoring the ΔC_p of the PDMS-PS block polymers on DSC on DSC and dynamic mechanical measurements, the type of phase mixing may be identified.

5.5. EFFECTS OF DERIVATIVE STYRENE MONOMERS

Several other PDMS-vinyl block polymers were also prepared using various derivative styrene monomers. These monomers were chosen because their primary mode of termination was by coupling (like styrene) to form multiblock systems[14]. One interest is the T_g of the corresponding homopolymers, i.e. 4-t-butylstyrene has a T_g of 130°C. Thereby providing a potential greater ser-

vice window than the styrene system if equivalent phase separation could be obtained. Since these monomers have different solubility parameters than styrene (Table 1 on page 48), the degree of phase separation and the morphology of these polymers may differ form that of the PDMS-PS block polymers. In order to compare the properties of the PDMS-Poly(derivative styrene) block systems with the PDMS-PS systems, the constant PDMS block length of 9,900 mol/gm was used in these PDMS-vinyl systems, the PDMS content of these system was also the same as the corresponding PDMS-PS system. The conversion level of all these PDMS-vinyl system was above 95% (refer to Table 2 on page 60). Based on the type of vinyl monomer, these polymers have been designed as B99-95, M99-95, or O99-95 when the vinyl monomer is 4-t-butylstyrene, 4-methylstyrene, or 4-methoxystyrene respectively.

In this study, films of these polymers were prepared by solution casting from methylene chloride and cyclohexane. However, it was found that the PDMS-methoxystyrene block polymer could not be dissolved by cyclohexane.

Before proceeding, it is important to point out that much less detailed studies have carried out these systems, so that limited information is available.

5.5.1. Thermal Properties of the PDMS-vinyl Block Polymers.

Figure 48 on page 156 shows the DSC scans of these PDMS-vinyl block polymers and the T_g values of these polymers are listed in Table 11 on page 157. There are four transitions observed in the DSC thermograms. The one at ca. -120°C corresponds to the T_g of the PDMS soft segments. The exothermic peak in the DSC thermograms is due to the crystallization of the PDMS blocks, and the endothermic peak at ca. -50°C results from the melting of the PDMS crystallites. The transition occurs at a temperature above 100°C and it varies with the type of styrene derivative monomer. This transition is clearly due to the glass transition of the styrene derivative hard blocks. As the DSC results show, both T_g of the PDMS soft block and the styrene derivative hard blocks are very close to the values of the corresponding homopolymers which is a strong sign of a high

degree of microphase separation in these block polymers. Since the T_g of the PDMS blocks does not change with the type of vinyl monomers, this suggests that the type of vinyl monomer has a little influence on domain mixing in these systems. The crystallization behavior of the PDMS blocks, however, does vary with the type of styrene derivative. The crystallization temperature upon heating, T_c, of samples B99-95-M and M99-95-M is higher than the T_c of samples S99-95-M and O99-95-M. However, the melting behavior of the PDMS blocks is only affected slightly by the type of styrene derivative monomers. Due to the lack of corresponding styrene derivative homopolymers, no ΔC_p analysis has been carried out on these systems.

The dynamic mechanical behavior of these polymers is shown in Figure 49 on page 159. The DMA spectra also confirm the occurrence of the microphase separation in these materials. Three transitions are shown on the spectra. Again, the one at -120°C correspond to the T_g of the PDMS blocks, and the second transition at -50°C is due to the melting of the PDMS crystallites in these polymers. The third transition occurs at a temperature above 100°C and it is the T_g transition of the styrene derivative blocks. As shown in Figure 49, the intensity of the PDMS T_g peaks increases in the order of S99-95-M, O99-95-M, M99-95-M and B99-95-M. Since the loss peak intensity is direct related to the amount of amorphous PDMS blocks, the low intensity of the PDMS T_g peak of sample S99-95-M is due to the higher crystallinity of the PDMS blocks which form during the cooling process. During the DMA experiments, the cooling time period was essentially the same for all these materials, thus, the amount of the PDMS crystallinity appears to be related to different rates of crystallization. As suggested by the dynamic mechanical data, the crystallization rate of the PDMS blocks in these materials is affected by the type of styrene derivative, which is consistent with the DSC results. The tanδ level within the rubbery region of B99-95-M and M99-95-M is much higher than that of S99-95-M and O99-95-M, which suggests that the interphase mixing level in the former is possible higher than that in the latter. The higher degree of mixing may also affects the storage moduli of these materials. As shown in the E′ spectra (Figure 49), the value of E′ within rubbery region decreases in the order of S99-95-M, O99-95-M, B99-95-M to M99-95-M which is the same order of the decrease in tanδ in the same region. Of course, the morphological texture of these systems also influences the modulus. As will be pre-

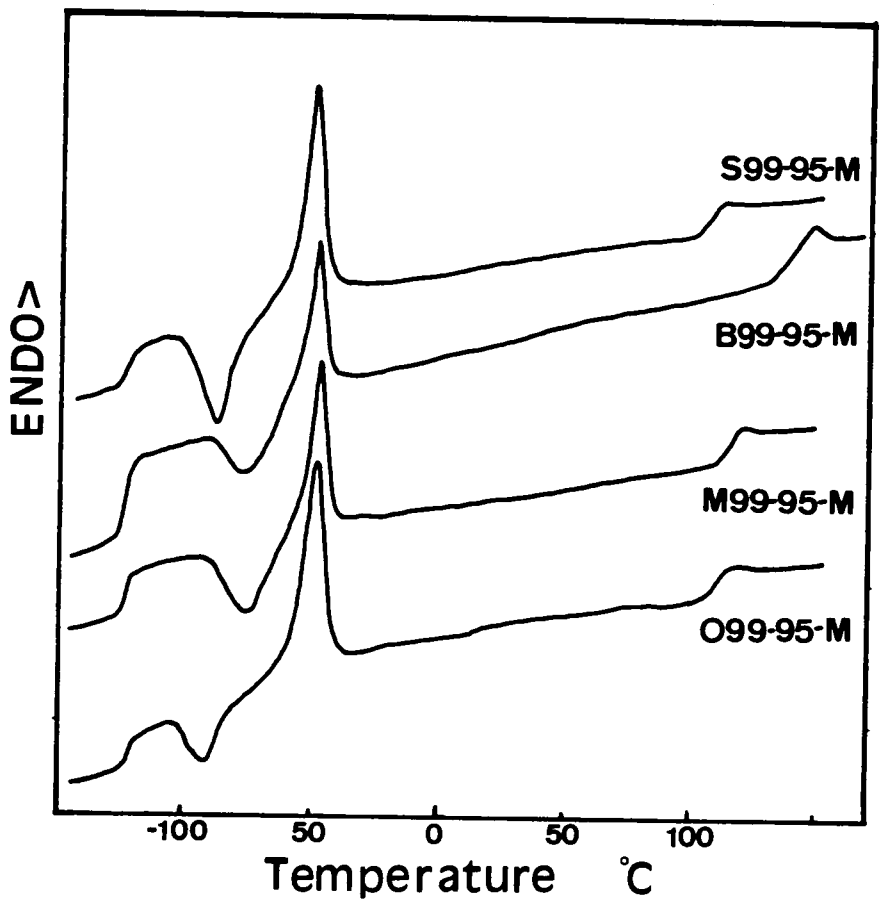

Figure 48. DSC thermograms of the PDMS-vinyl block polymers.

Table 11. Glass transition and melting point of the free radical PDMS-vinyl block polymers.

Sample	PDMS Block			vinyl Block
	T_g °C	T_c °C	T_m °C	T_g °C
S99-95-M	-122	-99	-58	106
B99-95-M	-122	-86	-53	139
M99-95-M	-123	-87	-47	113
O99-95-M	-123	-102	-58	109

sented in the next section, the morphology of S99-95-M is different from B99-95-M and M99-95-M, thus, a difference in E′ of this sample would be expected.

5.5.2. Morphology of the PDMS-vinyl Block Polymers

Figure 50 on page 160 shows the morphological texture of these PDMS-vinyl polymers. All samples show a clear two phase morphology except O99-95-M. It is believed that the contrast between the two phases of this sample is too low to be distinct by TEM without selective staining. Clearly, the morphology of these materials is affected by the type of vinyl monomer used. Sample S99-95-M has a mixed morphology of spherical and rod-like PS domains. The morphology of sample B99-95-M shows only partially elongated spherical hard domains, while the majority of hard domains in sample M99-95-M are short rod-like structures. The size of the hard domains in these systems also varies. The hard domains of samples B99-95-M and M99-95-M are smaller and more regular than the vinyl domains in sample S99-95-M. This suggests that the vinyl blocks in samples B99-95 and M99-95 have a shorter length and a narrower MWD than the PS blocks in S99-95 sample. If the MWD of the PS blocks in S99-95-M is broader than the other two samples, the formation of some continuous PS domains in S99-95-M is possible, thus, the mechanical properties of S99-95-M might be different than the others.

5.5.3. Mechanical Properties of the PDMS-vinyl Block Polymers

The stress-strain behavior of these PDMS-vinyl block polymers is shown in Figure 51 on page 162. The stress-strain behavior of methylene chloride cast films of all of these block polymers is rather similar. Among the methylene chloride cast films of these materials, S99-95-M has the highest modulus and ultimate properties. The higher modulus of S99-95-M may result from larger hard domains with some degree of continuity which results in a distinct yield point. The

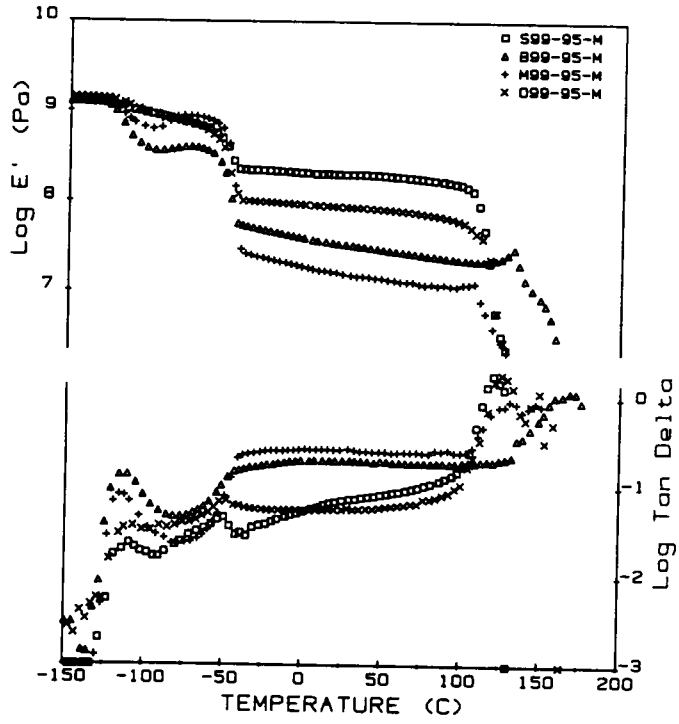

Figure 49. Dynamic mechanic behavior of the PDMS-vinyl block polymers.

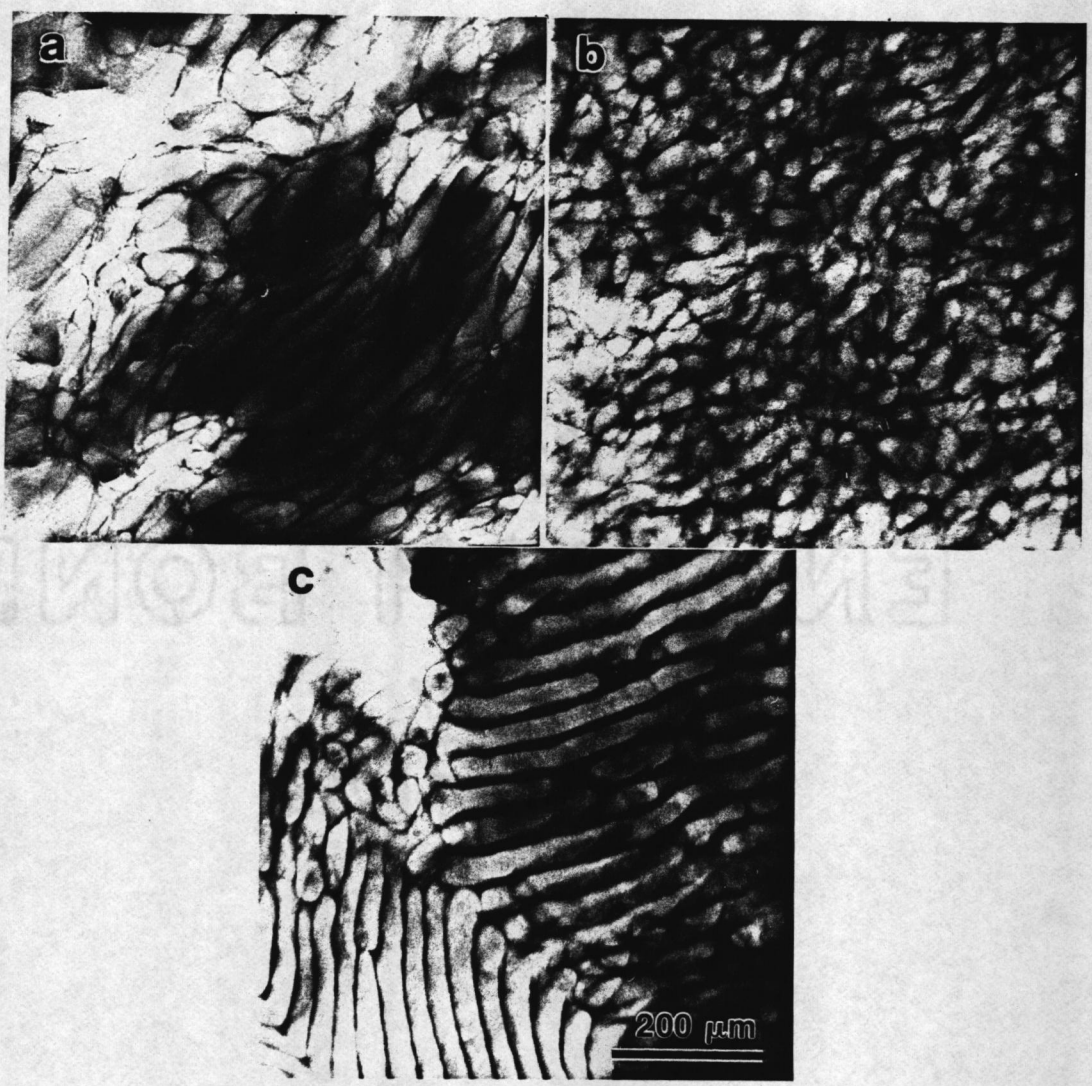

Figure 50. TEM micrographs of the PDMS-vinyl block polymers: (a). S99-95-M, (b). B99-95-M, and (c). M99-95-M.

higher ultimate properties of S99-95-M may be due to a higher equivalent number of blocks per chain (n_e). Based on the ^1H NMR and GPC results, the number of repeat sequences (n) for these systems has been calculated by Dr. Crivello[14]. The value of n is 13.0 for S99-95, 12.3 for B99-95, 8.3 for M99-95, 10.9 for O99-95. It is noted that S99-95 indeed has the highest number of repeat sequences among these polymers but as must be recognized, this is only an average value. As discussed earlier, these calculated values are believed to be too high because of the very uneven molecular weight distribution of the vinyl blocks. However, these calculated values still reflect the effect of the different vinyl monomers on the number of repeat sequences. The great difference in the ultimate properties between S99-95-M and the other these samples suggests that the value of n_e in the PDMS-styrene derivative block polymers may will be smaller than for the PDMS-PS system. The difference in the ultimate properties may reflect the difference in the polymerization mechanism, especially in the termination process, between the PDMS-PS and PDMS-styrene derivative block polymers.

For cyclohexane cast films, both S99-95-C and M99-95-C behave differently than the methylene chloride cast films, but B99-95-C has a similar behavior to B99-95-M. The changes in the stress-strain behavior by the casting solvent should be related to changes in the solubility parameter of the monomers as discussed earlier.

5.5.4. Summary

The type of vinyl monomer has a strong influence on the morphology and the bulk properties of the free radical synthesized PDMS-vinyl block polymers. Depending on the glass transition temperature of the styrene derivative, the width of the rubbery region of the PDMS-vinyl block polymers (the region between two T_gs) is changed as expected. The crystallization behavior of the PDMS blocks and the degree of phase separation in these block polymers are also changed likely due to the chemical nature of the different hard blocks. According to the DMA results, the type

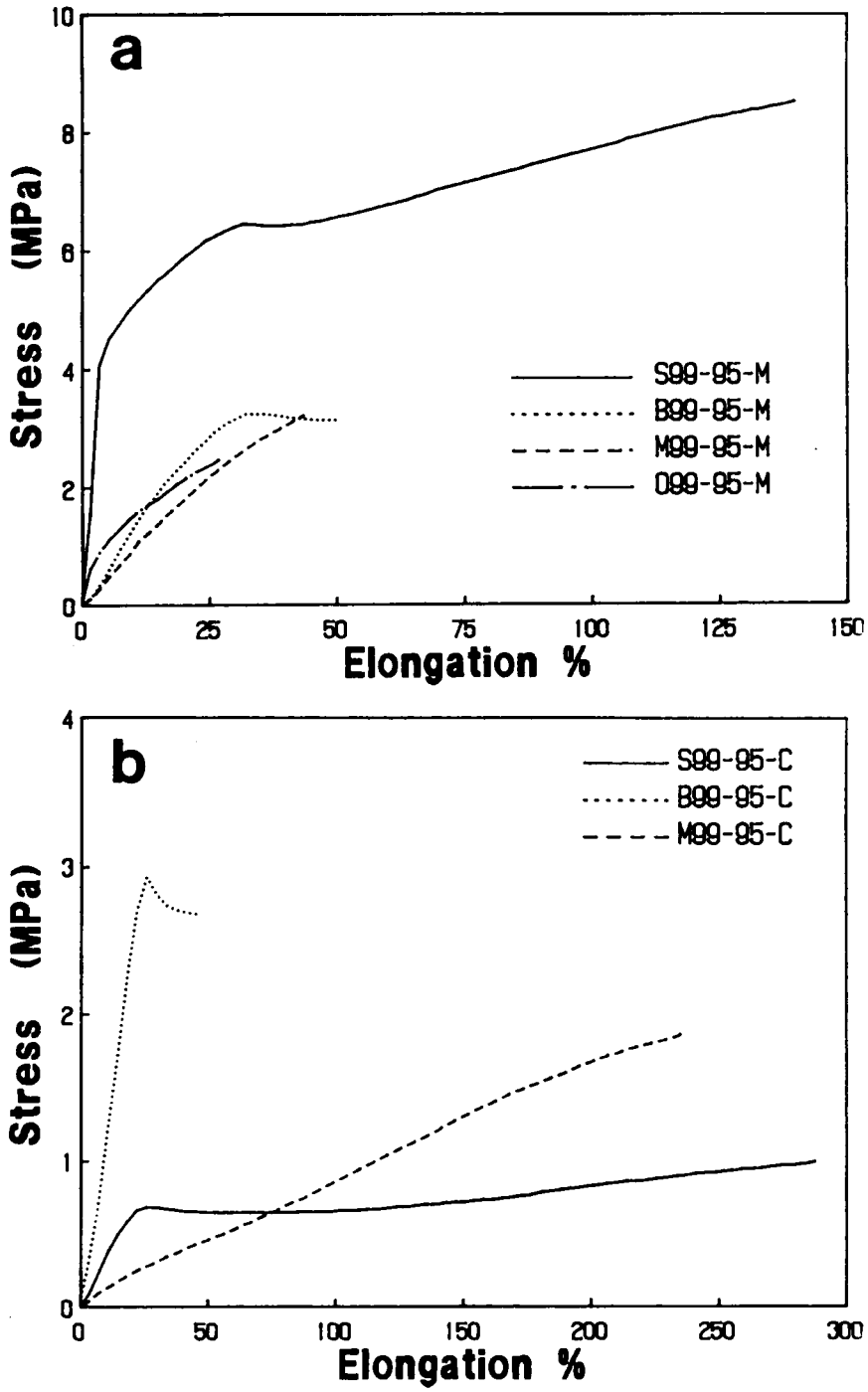

Figure 51. Stress-strain behavior of the PDMS-vinyl block polymers: (a). Methylene chloride cast films, and (b). cyclohexane cast films.

of monomer has only a small effect on domain mixing, however, interphase mixing does appear to be affected depending on the styrene derivative monomer used.

The morphological texture of these materials is also changed with the type of hard block. For samples B99-95-M and M99-95-M, the hard domain size is smaller and more uniform than in the S99-95-M. This suggests but does not conform that the hard block in the B99-95-M and M99-95-M has a smaller MW and narrower MWD than the PS blocks in the S99-95-M.

As the morphology and the degree of phase mixing changes, the mechanical properties of these materials are altered. Also, the much lower ultimate properties of PDMS-styrene derivative block polymer compared with the PDMS-PS block polymer may indicate the difference in the polymerization process of these materials which is caused by the type of monomer.

5.6. CONCLUSIONS AND RECOMMENDATIONS

5.6.1. Conclusions

The results of this study indicate that the PDMS-vinyl block polymers have been formed by this unique free radical synthesis route. There is no experimental evidence which indicates the formation of vinyl homopolymers during the free radical polymerization.

The morphological texture, the degree of phase separation, and the bulk properties of these free radical synthesized PDMS-PS block polymers are strongly governed by the block molecular weight (block length) and the molecular weight distribution of both the PDMS and the PS blocks. The PDMS block length is predetermined by the PDMS segments in the macroinitiators. The molecular weight and the molecular weight distribution of the PS blocks are dependent on the PDMS block length and the conversion level.

At a constant conversion level, as the PDMS block length is increased, the PS block length increases and the molecular weight distribution becomes broader. Consequently, the domain size

increases as well as the degree of phase separation. The type of morphological domains is also changed from spherical PS domains to lamellar PS domains as the PDMS block length increases and the number of blocks per polymer chain decreases. The mechanical properties of these materials is altered accordingly.

The PS block length and the molecular weight distribution is also governed by the conversion level. The PS block length increases with the conversion level, and the molecular weight distribution becomes broader. As the PS block length increases, the number of blocks per chain will decrease and the morphology is altered. In general, the low conversion samples have a much more uniform morphological texture than the high conversion samples having similar PDMS block length. The ultimate properties of the low conversion samples are better than the high conversion samples. Experimental evidence also indicates that the block length of each block in the low conversion samples are more uniform than in the high conversion samples, which suggests that the equivalent number of blocks per chain in the low conversion samples is higher than in the high conversion samples. This may help to explain the better ultimate properties of the low conversion samples.

Like other block polymers, the morphology and the bulk properties of these free radical PDMS-vinyl polymers are altered with the type of casting solvent. Depending on the block length and the molecular weight distribution of both the PDMS and the vinyl blocks, the effect of casting solvent can be very pronounced. For the low conversion samples with short PDMS blocks, the type of casting solvent has only a small effect on the morphology and the bulk properties of the polymer. For the polymers with both large PDMS and PS blocks, the morphology and properties of the polymers changes drastically dependent on the solubility parameter of the casting solvent used. Also, the polymers having large PDMS and PS blocks can not be thermally processed.

The type of vinyl monomers also changes the properties of these free radical PDMS-vinyl polymers. Depending on the nature of the vinyl monomer, the final morphological textures and bulk properties (both mechanical and thermal properties) of the block polymers are altered. However, the tensile strength and the ultimate elongation of the PDMS-styrene derivative block polymers are much lower than for the PDMS-PS block polymers other factors being constant.

The lower ultimate properties may result from a smaller number of blocks per chain in these PDMS-styrene derivative block polymers compared with the PDMS-PS block polymer.

5.6.2. Recommendations

In these PDMS-PS block polymers, very large domains have been formed. Hence, the scattering peak caused by the interdomain scattering will be shown at a very small angle region. Due to the resolution limits of the SAXS instrument in our laboratory, the scattering profile at very small angle region could not be obtained. Without this information, no SAXS analysis could be done. Therefore, no SAXS study was carried out on these free radical synthesized PDMS-PS and PDMS-styrene derivative block polymers, and the degree of phase separation was not be determined by this approach. The results of the degree of phase separation on these materials based on the DSC and dynamic mechanical techniques are more qualitative and they are in need of some further confirmation although the trends are strongly believed to be correct. In the future scattering study, the experiments should be carried out on a SAXS camera which has a very long sample to detector distance which will improve the resolution of the low angle region greatly. Thus, entire scattering profiles of these PDMS-PS systems could be obtained. By analyzing the scattering profile, the interdomain spacing, the interphase thickness, and the type of phase mixing could be obtained.

Another unclear question is the equivalent number of blocks per chain. This property is believed critical to the mechanical properties of these materials, and it is also related to the polymerization mechanism of this free radical synthesis. The SAXS, NMR, GPC and the selective degradation techniques could be used to study this problem. SAXS could monitor the domain size and the interdomain spacing more accurately than the TEM. The SAXS results could be used to calculate the block molecular weight for the domain forming blocks. While GPC could be used to determine the molecular weight of the whole polymer and the block molecular weight after the selective degraded system. And NMR could determined the average molecular weight of each block.

Combining results form SAXS, GPC and NMR, the number of block per chain could be determined.

A very interesting problem is the crystallization of the PDMS blocks in these block polymers. The crystallization of the soft blocks could cause a drastic change in the low temperature properties of these materials. To day, there are no studies of this type on PDMS contained block systems. Therefore, a crystallization study of the PDMS blocks in these systems could be of interest. The results of the present study strongly suggested that the crystallization of the PDMS blocks was also affected by the type of vinyl monomer used. Thus, a crystallization study of the PDMS blocks must also provide further understanding of the polymerization mechanism of this free radical synthesis method. The proposed crystallization study could be carried out by DSC method.

CHAPTER VI

STRUCTURE-PROPERTY BEHAVIOR OF POLY(TETRAMETHYLENE OXIDE) BASED SEGMENTED IONENE ELASTOMERS

The ionene elastomers are newly developed ionomers which have some potential as a TPE as well as for other potential applications. However, no systematic studies of the structure-property behavior of these materials has been conducted before this study. In order to have a better understanding of these novel ionene elastomers for future development and applications, a full structure-property study on the segmented PTMO ionene elastomers was conducted. The results will be discussed in four parts. The first part will be concentrated on the general structure-property behavior of ionene elastomers. The second part will focus on the morphological structure of the PTMO-dihalide ionene elastomers. In the third part, the structure-property behavior of PTMO-dipyridinium ionene elastomers will be discussed. Finally, some of the unusual properties of ionene elastomers will be discussed.

Based on the molecular weight of the PTMO soft segments and the types of counter ion and ionene hard segments, the ionene elastomers used in this study will be designated as follows:

IB - NS - 14
| | |
| | **PTMO segment Mn/100**
| |
| **Type of hard segment**
| NS = dihalide xylene, S = dibenzyl halide butane,
| BP = bipyridinium, and BPE = bipyridinium ethane.
|
Type of counter ion
B = Bromide, C = Chloride, I = Iodide, and S = triflic acid anion.

The chemical structures of these ionenes are shown in Figure 52 on page 169. The composition and inherent viscosity (I.V.) of these materials are listed in Table 12 on page 170.

6.1. GENERAL STRUCTURE-PROPERTY BEHAVIOR OF SEGMENTED PTMO-DIHALIDE IONENE ELASTOMERS

6.1.1. Structure-Property Behavior of the IB-NS Ionene Elastomers

6.1.1.1. Mechanical Properties of the IB-NS Ionene Elastomers

Figure 53 on page 172 illustrates the stress-strain behavior of the IB-NS ionene elastomers (IB-NS series). In general, these materials display significant elongation at break (ca. 1000%). Also, the tensile strength is of the order of 40MPa which is quite significant for elastomeric materials. It is also observed that there is a distinct upturn in the stress when elongations of the order of 400 to 600% are exceeded. This behavior is primarily due to the strain induced crystallinity of the PTMO soft segments which has been confirmed by a wide angle X-ray scattering studies.

It has been noted that the modulus and stress level at a given elongation increases as the PTMO soft segment molecular weight (segment length) decreases (Figure 53 and Table 13). Since the ion content increases with the decrease of PTMO segment molecular weight, these enhance the

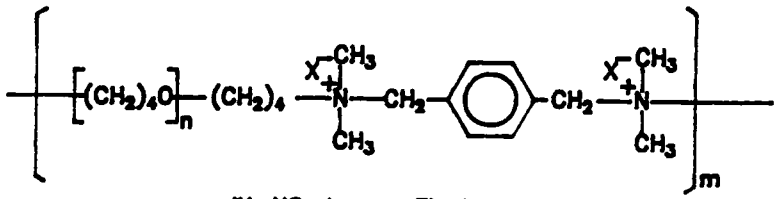

IX–NS Ionene Elastomer

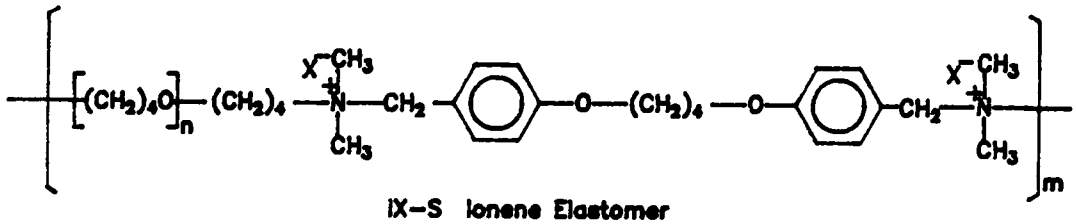

IX–S Ionene Elastomer

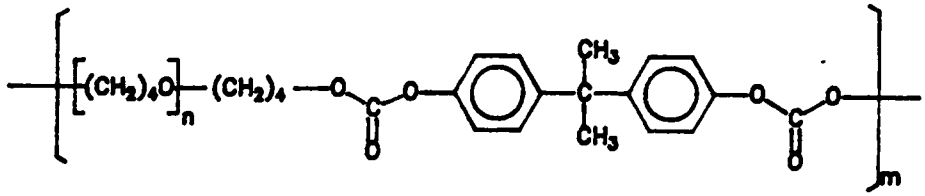

IB–NC none–ionene polymer

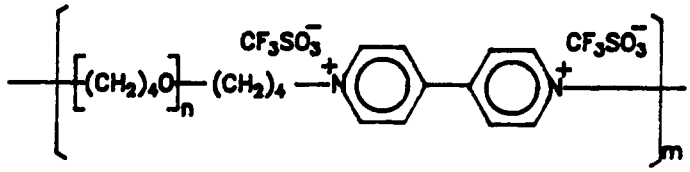

IS–BP Ionene Elastomer

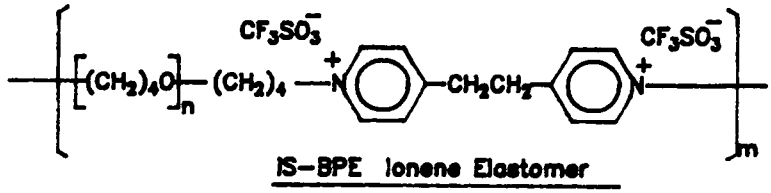

IS–BPE Ionene Elastomer

Figure 52. Chemical structure of the ionene elastomers used in this study.

Table 12. Composition and inherent viscosities (I.V.) of ionene elastomers.

Sample	PTMO Segment Mn	Ion Content # ion/PTMO unit	Hard Segm. (vol%)	I.V. 0.4 dl/gm
IB-NS-14	1400	0.10	8.3	0.43
IB-NS-18	1800	0.081	6.6	0.75
IB-NS-26	2600	0.055	4.7	1.17
IB-NS-34	3400	0.042	3.6	1.31
IB-NS-66	6600	0.022	1.9	2.13
IB-NS-100	10000	0.014	1.3	2.23
IB-S-34	3400	0.042	7.5*	1.57
IB-S-66	6600	0.022	4.0*	2.77
IB-S-100	10000	0.014	2.7*	2.62
IC-NS-21	2100	0.069	5.4	0.69
IC-NS-34	3400	0.042	3.4	2.40
IC-NS-66	6600	0.022	1.8	2.52
IC-NS-100	10000	0.014	1.2	3.20
IC-S-66	6600	0.022	4.8**	2.35
IC-S-100	10000	0.014	3.2**	2.48
II-NS-15	1500	0.096	8.8	0.70
II-NS-72	7200	0.020	2.0	1.0
IS-BP-6	550	0.262	20.7	N/A
IS-BP-8	750	0.192	16.1	N/A
IS-BP-13	1350	0.107	9.6	N/A
IS-BP-17	1700	0.085	7.5	N/A
IS-BP-25	2550	0.056	5.3	N/A
IS-BPE-13	1350	0.107	9.6	N/A
IS-BPE-18	1800	0.080	7.4	N/A
IS-BPE-25	2500	0.056	6.5	N/A

* Estimated by assuming density = 1.5 gm/cc
** Estimated by assuming density = 1.0 gm/cc

coulombic interactions and provide stronger association[120]. The higher modulus as well as the stress level may result from the stronger ionic association. Besides the coulombic interactions, the molecular weight of these polymers also influence the mechanical properties. In general, the higher the molecular weight is, the higher the stress level will be at a given set of draw conditions[117,118]. As shown in Figure 53, IB-NS-14 displays a lower stress level than IB-NS-18 and IB-NS-26, even though the ion content of IB-NS-14 is the highest. This is believed due to the lower molecular weight of IB-NS-14. As shown in Table 12 on page 170, the value of the inherent viscosity (I.V.), which is directly related to the molecular weight of the polymers, is the lowest for IB-NS-14 among the IB-NS ionene elastomers.

The mechanical hysteresis data from the IB-NS ionene elastomers are shown in Figure 54a. The hysteresis of these ionene elastomers indicates formation of a stable physical network. The behavior is distinctly dependent on the PTMO segment length. For the ionene elastomers with short PTMO segments such as IB-NS-14 and IB-NS-18, the level of hysteresis increases rapidly at low elongation (< 100%), and it flattens as the the elongation further increases. Interesting, the level of hysteresis for IB-NS-66, which has a much longer PTMO segment, increases gradually with elongation to about 300% and then it also flattens as the elongation further increases. The changes in the hysteresis behavior may result from changes in the morphological structures of these materials. As will be discussed in the section 6.4, the morphology of IB-NS-18 is a rod-like hard segment domain structure, while, the morphological texture of IB-NS-66 is believed to be more spherical ionic domains in a PTMO matrix.

The general network or microphase separation character of these ionene elastomers is demonstrated by investigating the stress-relaxation and the creep behavior of IB-NS-100 in Figure 54b). The time period of the tests was about 10 days at 23°C. Both types of transient response clearly illustrate that this ionene elastomer displays a strong pseudo network behavior since there is only the order of a 50% decrease in stress and doubling of the creep compliance over this ten day period.

Figure 55 on page 176 shows the effect of the PTMO soft segment molecular weight (segment length) on the creep behavior of the IB-NS ionene elastomers. The data clearly indicate that a

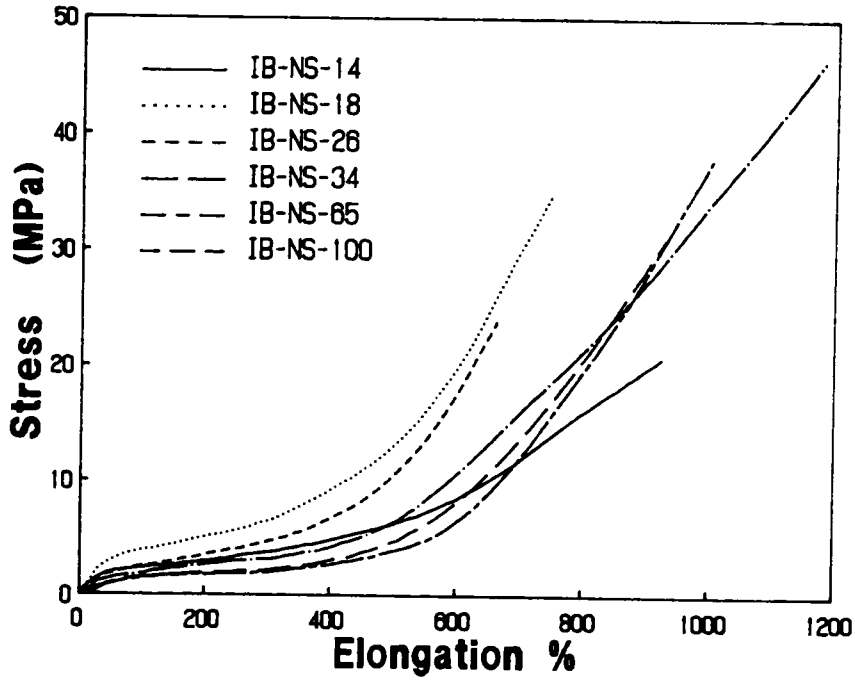

Figure 53. Stress-strain behavior of the IB-NS series.

Table 13. Young's modulus of IB-NS ionene elastomers at ambient temperature

Sample	Young's Modulus (MPa)	
	Fresh*	Aged
IB-NS-14	12.8	N/A
IB-NS-18	17.8	20.1
IB-NS-26	6.1	6.3
IB-NS-34	4.1	4.3
IB-NS-66	2.3	35.3
IB-NS-100	2.2	62.7

* The values of fresh samples are obtained after holding the sample at 60°C for 1 hour and quenching to ambient. The aged values are obtained after the sample had been aged at ambient for at least one month.

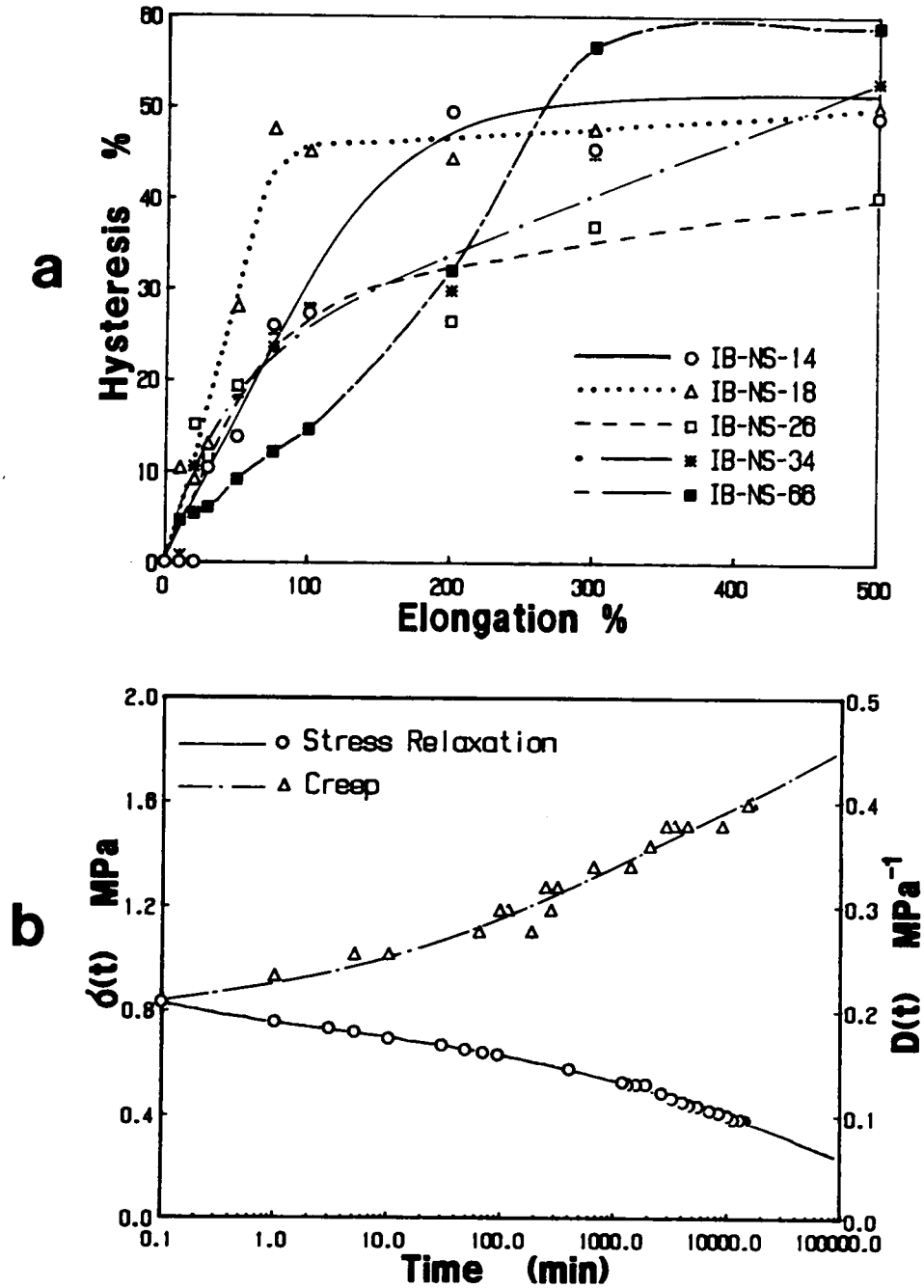

Figure 54. Mechanical behavior of the IB-NS ionene elastomers: (a). Hysteresis behavior of the IB-NS ionene elastomers. (b). Stress-relaxation and creep behavior of the IB-NS-100.

physical network is present by ion clustering and potentially some chain entanglements as well may also contribute. Therefore, the strength and the stability of the network depends on the both the ionic content and the molecular weight of the ionene systems. As the creep data in Figure 55a illustrates, the compliance level decreases as the ion content increases or the PTMO segment length decreases. This suggests that the compliance level may mainly depend on ionic interactions. However, the total network stability may depend on both ionic association and chain entanglements. For example, sample IB-NS-18 has a higher ion content than the others, therefore, it has the lowest short term compliance level. However, IB-NS-18 gives a faster decay than the others (Figure 55b). Because the molecular weight of IB-NS-18 is lower than the others (except for IB-NS-14) according to the I.V. data in Table 12 on page 170, the network in IB-NS-18 may mainly depend on the ionic association rather than chain entanglements. If the network stability depended on the ion content only, sample IB-NS-18 should display a slower decay than the others because of its higher ion content. Therefore, the faster decay of IB-NS-18 suggests that the network stability of these ionene systems also depends on the chain entanglements.

In fact, the network stability of these ionene systems is greatly improved when the molecular weight of the IB-NS ionene increases. Samples IB-NS-66 and IB-NS-100 have a much higher molecular weight than IB-NS-14 and IB-NS-18 according to the I.V. data. The normalized creep results indicate that the networks of these two samples decay much slower than the others. Since the ion content in these two samples is very low, the higher network stability may partially arise from chain entanglements. Another possible factor is the crystallization of the long PTMO segments in IB-NS-66 and IB-NS-100. If the PTMO segments do under go any crystallization, the network stability would also be improved. However, the DSC and WAXS results indicated that there was no detectable crystallization occurred during the test period.

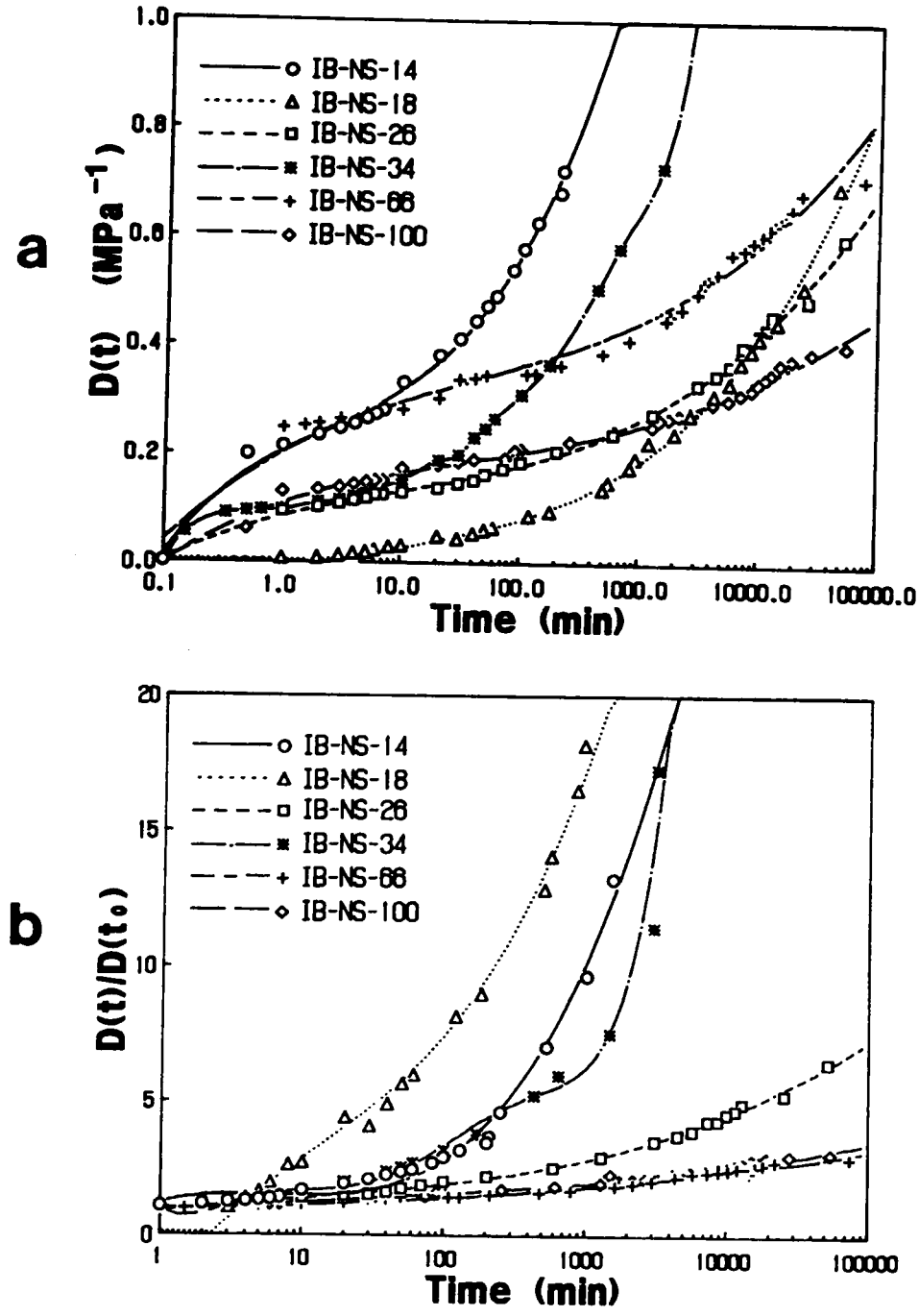

Figure 55. Creep behavior of the IB-NS series: (a). Creep behavior of the IB-NS series. (b). Normalized creep behavior of the IB-NS series (the creeping data at t = 1min was chosen as $D(t_0)$).

6.1.1.2. Thermal Properties of the IB-NS Ionene Elastomers

TGA spectra of the IB-NS ionene elastomers are shown in Figure 56 on page 178. As the PTMO segment length increases, the temperature, T_{d1}, at which the initial weight lost occurs, increases. This initial weight loss may be related to the depolymerization of the ionene elastomers because of the reversible quaternary polymerization mechanism[20]. However, the value of T_{d2}, at which a drastic weight lost occurs, decreases with an increase of the PTMO segment length (see Table 14 on page 181). This weight lost is clearly related to the decomposition of the ionene materials. In these polymers, the PTMO segments are connected to the ionene hard segment, therefore, the thermal stability of the PTMO segments is affected by the ionene hard segments (chain end effect). As the PTMO segment length increases, the influence of ionic hard segments should decrease, which may reduce the thermal stability of the PTMO segments as illustrated by the TGA results. As will be discussed later in section 6.3.1.1, when the dihalide hard segment is replaced by bipyridinium or bipyridinium ethane hard segments, the thermal stability of the ionene polymers also varies. This supports the chain end effect mentioned above.

Figure 57 on page 180 shows the DSC thermograms of the IB-NS ionene elastomers. The transition at ca.-80°C is due to the glass transition of the PTMO segments. The T_g of the PTMO segments in the ionene elastomers is very close to the T_g of homopolymer PTMO which therefore suggests a very good phase separation occurring in these systems. For a PTMO segment molecular weight less than 2600 mol/gm, there is no crystallization or melting behavior. A crystal melting peak of the PTMO segment is observed when the PTMO segment molecular weight (segment length) is greater than 3400 mol/gm. Also, the melting point increases with an increase of PTMO segment length. This behavior clearly relates to the anchoring effects of the soft PTMO segment by end group restrictions. As the PTMO segment length between two ionic hard segments (anchoring points) increases, the PTMO segments become more mobile and the end groups have less restrictions on the PTMO segments. Therefore, longer PTMO segments should be easier to crystallize than shorter ones as is supported by the DSC thermograms. Since the melting point of the PTMO segments in IB-NS-34 is much lower than ambient temperature, IB-NS-34 can not

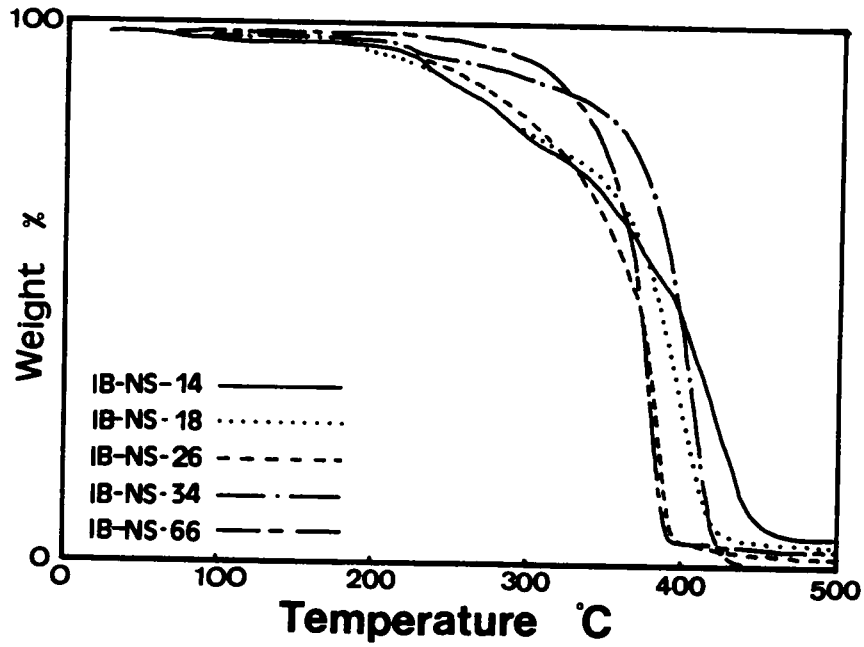

Figure 56. Thermogravimetric behavior of the IB-NS series.

be crystallized at ambient temperature. As the PTMO segment length increases, the melting point increases. Hence, the PTMO segments in IB-NS-100 can crystallize at ambient temperature at a slow rate because of a higher T_m (ca. 14.5°C onset point).

6.1.1.3. Crystallization Behavior of the IB-NS Ionene Elastomers as Studied by WAXS

The crystallization behavior of the PTMO segments in the ionene elastomers has been confirmed by WAXS. Figure 58 on page 182shows the WAXS patterns of a pure PTMO oligomer, a undeformed sample of IB-NS-100, a deformed (at 400% elongation) sample of IB-NS-100, and an aged undeformed sample of IB-NS-100. For the PTMO oligomer, two sharp rings are observed in the WAXS pattern (Figure 58a), which results form PTMO crystallites. For the undeformed IB-NS-100, there is a diffuse amorphous halo in the WAXS pattern (Figure 58b). When the sample has been stretched to 400% elongation, the presence of oriented PTMO crystallites is readily apparent (Figure 58c). The observed reflections match with those of oriented semicrystalline homopolymer PTMO and hence these WAXS results clearly support the earlier comments relating the enhancement of the tensile strength caused by strain induced crystallization of the PTMO soft segments. When the PTMO segment length exceeded 6,600, the PTMO segment can crystallize at ambient over a long period of time (over 15 days). Figure 58d clearly shows this in the WAXS pattern of an aged sample of IB-NS-100 which has been conditioned at ambient for 30 days. It has been found that the ambient crystallization of PTMO segments in undeformed IB-NS-100 is very slow, and it takes at least 15 days to develop some detectable crystallinity.

6.1.1.4. Dynamic Mechanical Behavior of IB-NS Ionene Elastomers

Figure 59 on page 184 provides the dynamic mechanical spectra of the IB-NS ionene elastomers. There are three principal transitions observed for all samples. The γ transition at -120°C is strongly believed to arise from the methylene sequencing in the PTMO segments and is

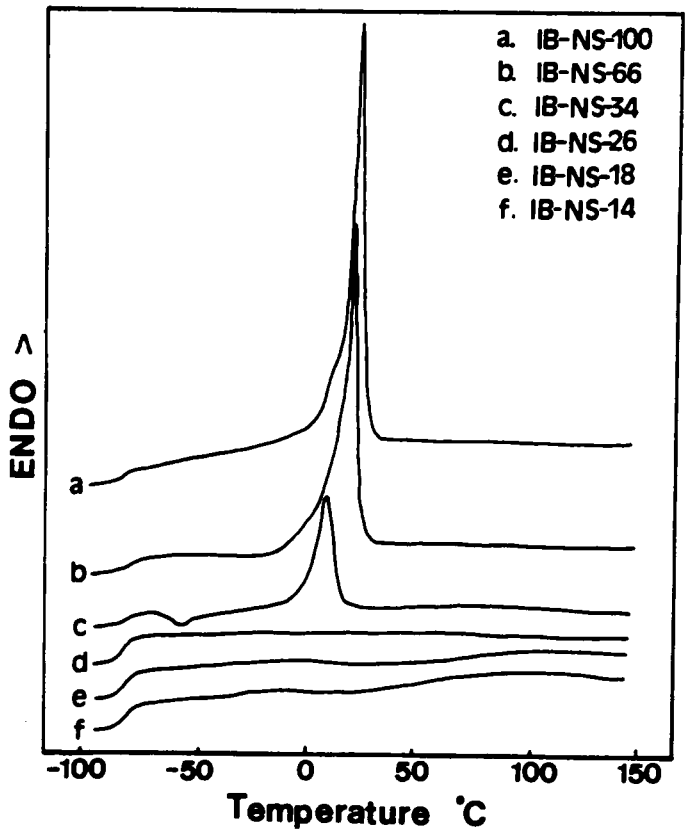

Figure 57. DSC thermograms of the IB-NS series.

Table 14. Thermal character of the IB-NS ionene elastomers.

Sample	T_g (C)	T_c (C)	T_m (C)	T_{d1}(C)	T_{d2}(C)
IB-NS-14	-82.4			215.9	443.1
IB-NS-18	-82.4			198.3	421.3
IB-NS-26	-83.0			216.1	399.6
IB-NS-34	-84.0	-57.6	0.7	202.1	428.4
IB-NS-66	-77.6		7.8	338.0	391.8
IB-NS-100	-82.3		14.9		

* T_{d1} is the onset point at which the weight starts to be lost.
T_{d2} is the onset point at which a significant weight loss occurred.

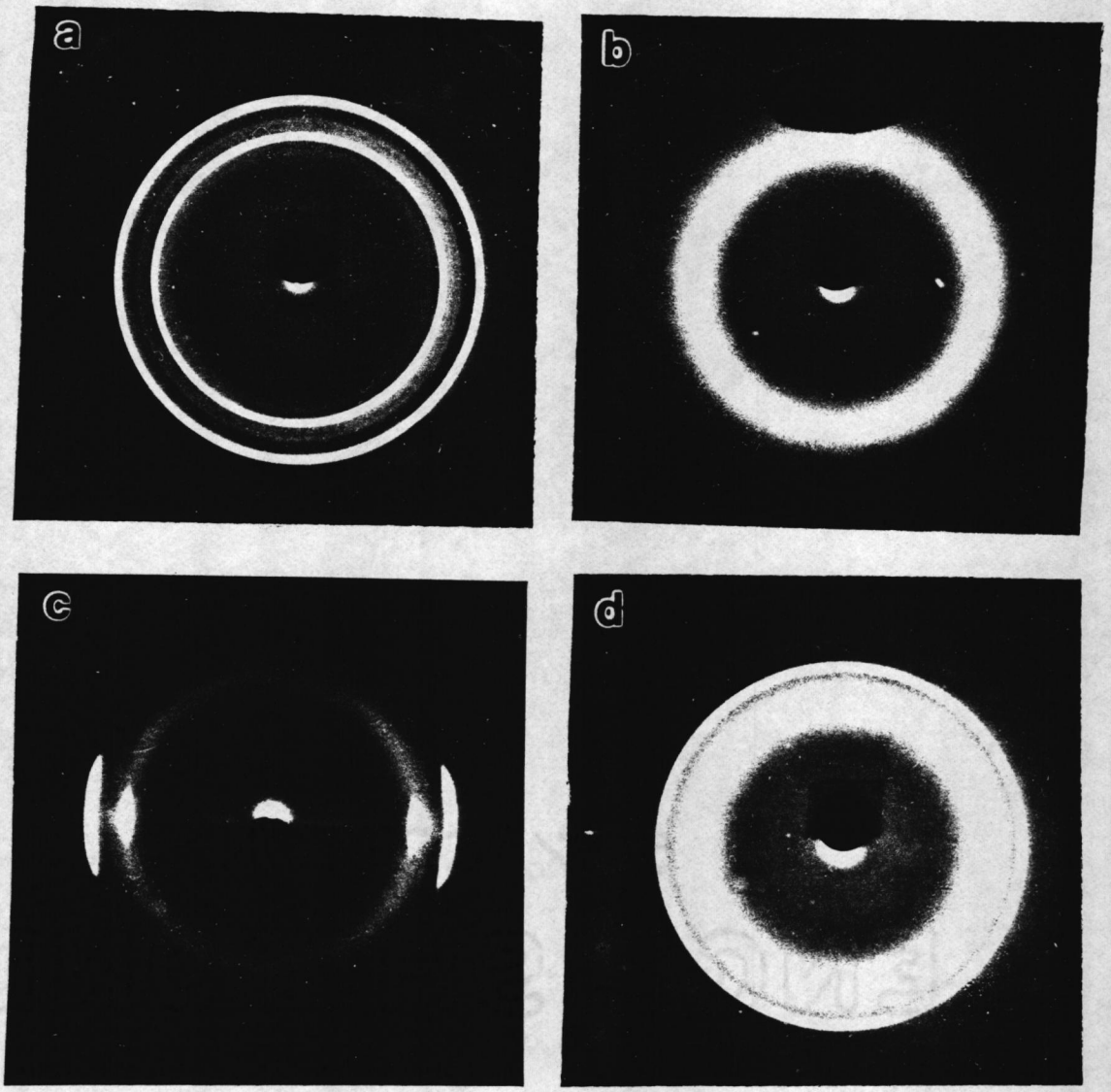

Figure 58. WAXS patterns of sample IB-NS-100: (a). PTMO oligomer. (b). undeformed IB-NS-100. (c). deformed IB-NS-100 (elongation is about 400%). (d). aged IB-NS-100 (undeformed).

in excellent agreement with the reported values for this same transition observed in polymers possessing sequences in the backbone of methylene units[119]. The observation of this transition indirectly suggest that the degree of phase separation of the soft segment from the ionene moieties may be very high.

The α transition at ca. -80°C results from the glass transition of the PTMO segments. Since the value for pure PTMO is also in this range, this response also strongly suggests that there is little mixing of the PTMO segments with the dihalide ionene hard segments. This observation is in line with the earlier suggestion based on the γ transition. Due to the T_g transition, the value of E′ decreases at this temperature. The magnitude of the decrease in E′ is directly related to the PTMO segment length. The ionene system with shorter PTMO segments has a greater decrease in E′. While this at first seems strange, it is caused by the crystallization of the PTMO segment. The longer PTMO segments can undergo crystallization easier during the cooling period, and therefore, they have higher crystallinity. The high values of E′ following the T_g region of samples IB-NS-66 and IB-NS-100 results form the higher crystallinity of the PTMO segments.

The third transition, β_1, is related to the crystallization and melting behavior of the PTMO soft segments. The location of β_1 varies with the PTMO segment length and the intensity of β_1 increases as the PTMO segment length decreases which suggests that shorter PTMO chains appear to undergo less crystallization. The rapid drop in the E′ spectra at ca. 20°C directly corresponds to the melting of the PTMO crystallinity. It should be noted that the α and β_1 transitions are directly in line with the DSC data discussed in the earlier section.

There is actually a forth transition, β_2, at ca. 70°C but which is not well pronounced in the tanδ spectra and it has been only observed in samples IB-NS-14 and IB-NS-18. At this transition temperature, the E′ spectra of IB-NS-14 and IB-NS-18 exhibit a unusual modulus "jump". The magnitude of the "jump" increases with the decrease of PTMO segment length. Also the "jump" is highly reversible. No such phenomenon has ever been reported on these ion containing polymers before. For a PTMO segment length greater than 2600 mol/gm, there is no modulus "jump" observed. Except for the DMA results, there is no other evidence related for this transition

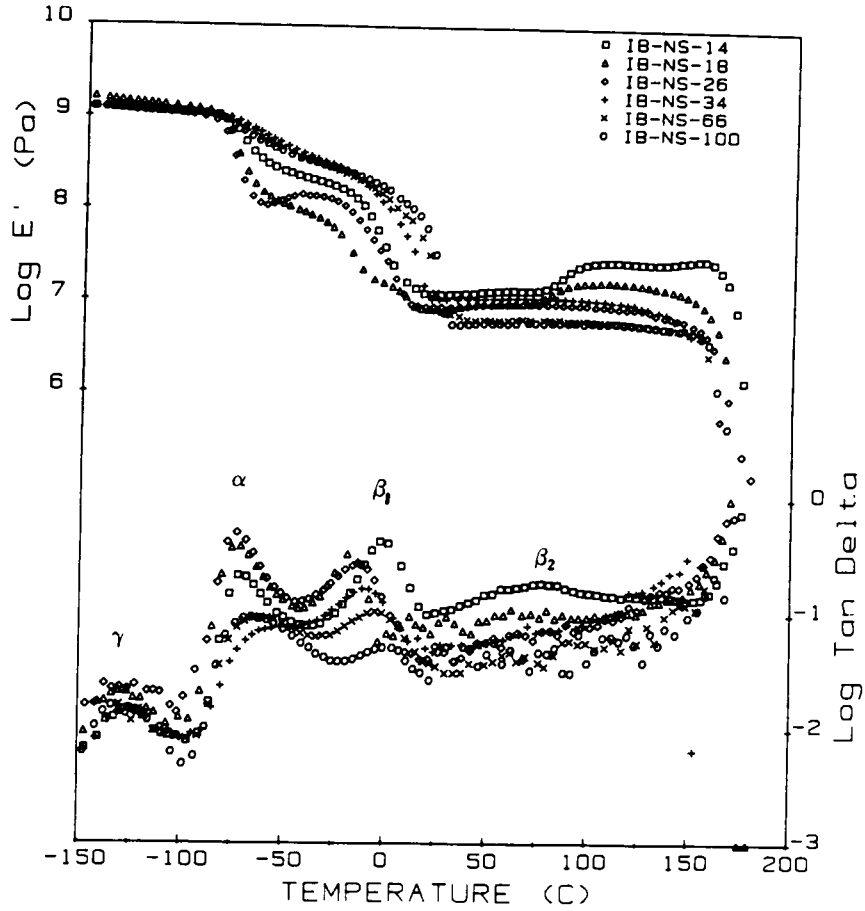

Figure 59. Dynamic mechanical spectra of the IB-NS series.

by either TMA or DSC. It is also found that the "jump" is related to the ion content of the ionene, the type of hard segments, and the type of counter ions as will be discussed in section 6.4.

The last transition shown in the DMA spectra is at ca. 160 - 170°C, but it is not completed within the tanδ results due to the loss of sensitivity of the instrument in this range. This is the region where the ionene elastomers display significant softening. The softening temperature decreases as the ionic content decreases (or in the PTMO segment length increases). This transition is believed due to the loss of association of the ionene moieties. In fact, it is likely correlated to some decrease in the overall molecular weight due to reversion to the initial reactants - the dimethylamino terminated PTMO and the dihalide compound (reverse Menschutkin reaction)[20].

It is also noted that the value of E′ within the rubbery plateau region (ca. 20 - 80 °C) increases with decreasing PTMO segment length. This behavior is consistent with the stress-strain results and it is expected since the shorter PTMO segment length leads to a higher volume fraction of hard segment "reinforcing component". More importantly, the shorter PTMO segment length leads to a higher ion content which provides a stronger ionic association thereby enhancing modulus.

These ionene materials display many of the characteristics common to the segmented and block polymer elastomers. However, the elastomeric behavior of these ionene elastomers is mainly due to the ionic clustering or domain formation in these materials. As the PTMO segment length decreases, the ionic content increases which results in increased ionic interactions and the mechanical properties of these materials are enhanced. The changes in the ionic content may also change the morphological structure of these ionene elastomers. A detailed discussion on the morphology of these ionene materials will be given in Section 6.2.

6.1.2. Effect of the type of Counter Ions and Architecture of Hard Segment

As discussed in the previous section, the excellent elastomeric behavior of ionene elastomers suggest that strong ionic interactions may arise from the ionene groups in the polymer backbone. Therefore, the bulk properties of these materials are altered with ion content. It might be expected

that by changing the type of counter ion or the architecture of the hard segment, the strength of the ionic interaction may change and thus influence the bulk properties. In this section, the effect of type of counter ion and hard segment architecture will be discussed.

6.1.2.1. Thermal Processibility and Thermal Stability of IB-NS and IC-NS Ionene Elastomers

One main feature of the ionene elastomers is their potential for their reverse polymerization ability at elevated temperature. Earlier inherent viscosity studies on ionene structures indicated that the ionene linkages can sometimes undergo a depolymerization - repolymerization process[20]. However, these inherent viscosity (I.V.) studies had been carried out on several PTMO ionene elastomers which either are chloride ionenes or polymer blends containing mostly chloride ionenes. The same inherent viscosity measurements have been performed by the author on IB-NS-100. Upon holding a melt at 180°C for 5 minutes, its I.V. value in chloroform immediately drops to 1/3 of its original value and never increases even after 200 hours at 65°C which was the original polymerization temperature. These results indicates that the IB-NS ionene elastomers can not undergo the repolymerization process as was partially found for the chloride ionene elastomers. Furthermore, the earlier I.V. studies showed that the ionene containing chloride counter ions did recover a significant molecular weight in several hours[20]. However, the stress-strain behavior of a chloride ionene (IC-S-66) thermal pressed film shows that its mechanical properties do not recover its original values after thermal treatment (Figure 60a). This film was compression molded at 170°C and then kept in vacuo at 65°C for 48 hours. Dogbone specimens were cut just prior to testing. At 5 minute after cooling, the sample basically behaved as a pure viscous material. Five hours after compression, its mechanical properties had been partially regained. Finally, after 48 hours at 65°C, the mechanical properties of the film were found to be still very poor. This result indicates that the repolymerization process for the chloride ionene elastomers is either very slow in the solid state or the sample has been partially decomposed at the thermal molding process thereby limiting the repolymerization.

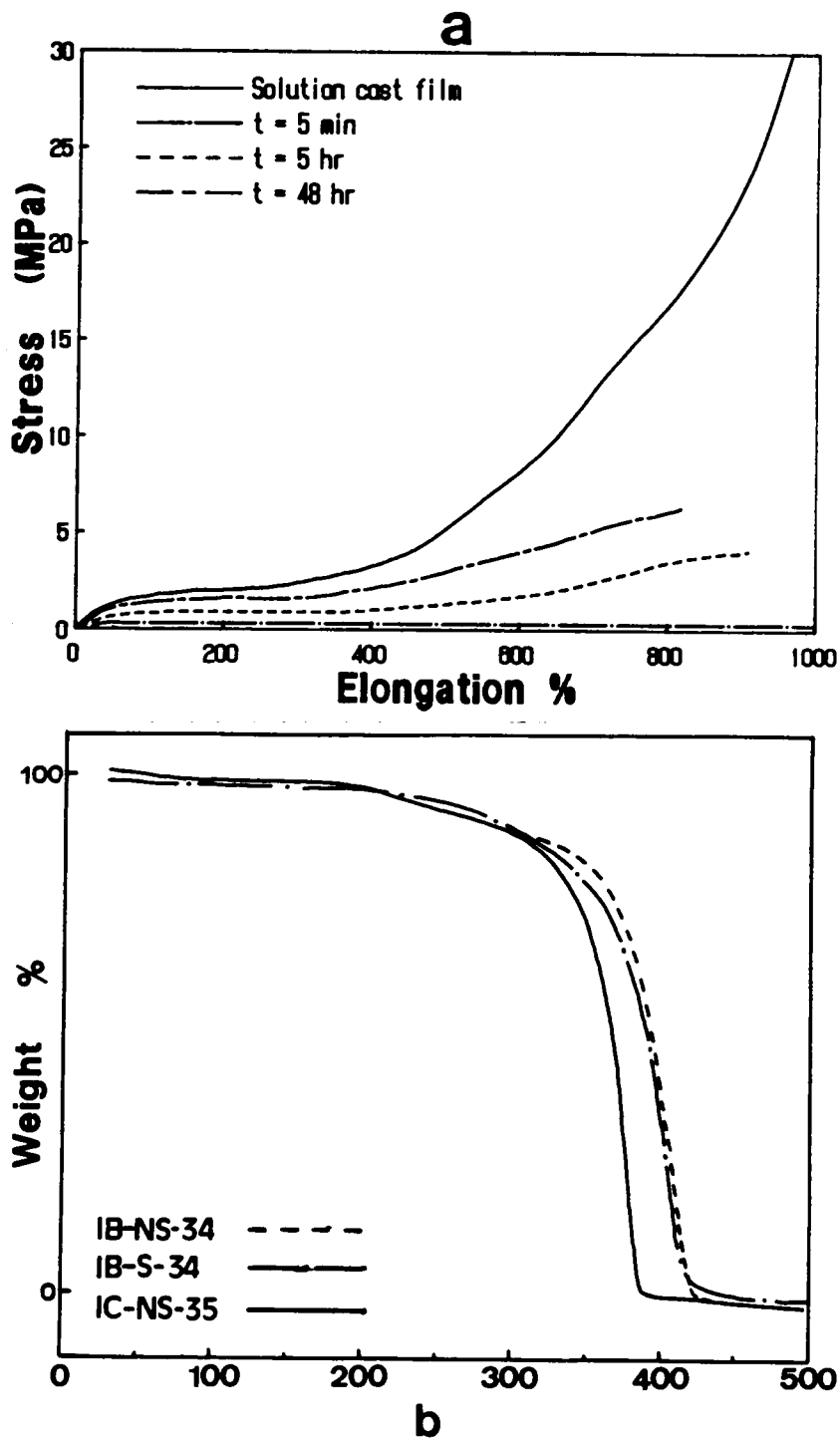

Figure 60. Thermal processibility and stability of the ionene elastomers: (a). Thermal processibility of sample IC-S-66. (b). TGA thermograms of the ionene elastomers with different type of counter ion or hard segments.

The TGA results of the 34 series of ionene elastomers are shown in Figure 60b. In this series, all the ionenes have similar PTMO segment length of 3,400 mol/gm but with different counter ions or hard segment architecture. The thermal stability of this series greatly depends on the type of counter ion. The decomposition temperature of IC-NS-35 is ca. 40°C lower than its bromide counterpart. There is a little difference between IB-NS-34 and IB-S-34 which suggests that the hard segment architecture has only a small influence on the thermal stability.

6.1.2.2. Mechanical Properties of Ionenes with Different Counter Ions or Hard Segment Architecture

Figure 61a shows the general stress-strain behavior of the 34 series. The general stress-strain behavior of this series is very similar. However, the system possessing the chloride counter ion consistently provides a somewhat higher stress value relative to those containing bromide counterions. This may well be due to the smaller and more electronegative chloride ion (3.2eV) in contrast to bromide ion (3.0eV) in the ionene linkage. Specifically, these differences may promote a better packing and stronger coulombic interactions with the positively charged ionene species thereby providing stronger association[120].

The effect of the spacer group in the hard segment is also illustrated by Figure 61a. The results show that when the aliphatic ether containing spacer group is present, other factors being constant, the material shows a lower stress at a given elongation than that in the absence of the spacer. This behavior was also typical for other ionene systems when analogous structures were compared with and without spacer groups. It is speculated that this arises due to the fact that there is a weaker association of the ionene moieties caused by the more aliphatic character and thereby possibly poorer phase separation occurs in the IB-S and IC-S materials. Indeed, the SAXS analysis indicates that the degree of interphase mixing increases slightly when the spacer group is present[121]. However, the increase is still quite small relative to the ionene elastomers with no spacer, and hence the main cause of the lower stress at a given elongation is more likely due to a

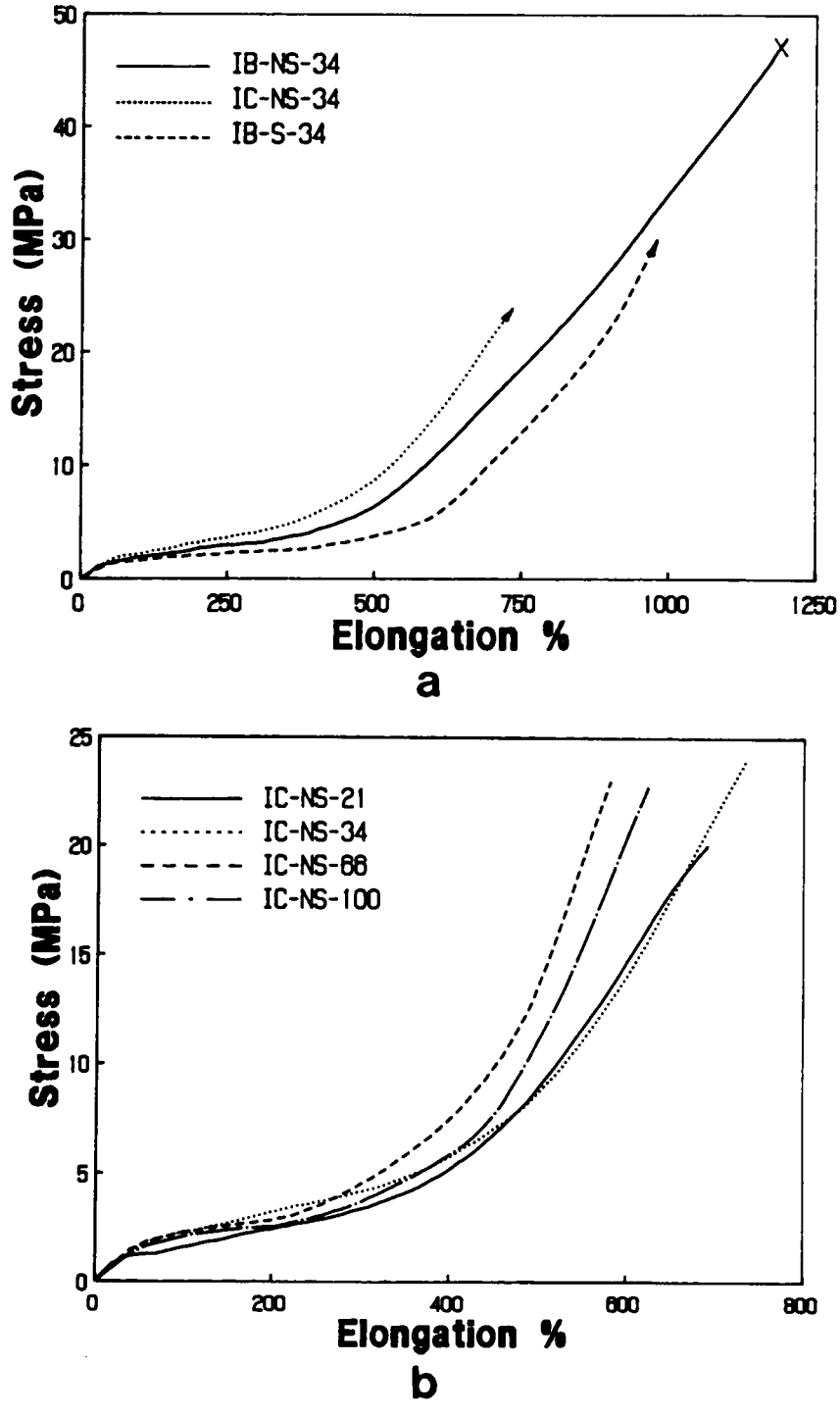

Figure 61. Mechanical behavior of the ionene elastomers with different counter ion or hard segment architecture: (a). Stress-strain behavior of the 34 series. (b). Stress-strain behavior of the IC-NS series.

weaker association rather than caused by the phase mixing. There is also a third possible explanation that may be relevant. For those systems containing a spacer, a molecular space filling model of the over all hard segment has been constructed. It is found that the benzyl halide of one end of the hard segment can fold over and interact with the other benzyl halide on the other end due to the flexible ether linkage. This suggests that there may be some initial "kinks" placed into the chain when the spacer group is added in the hard segments. Therefore, the interchain interaction in these materials may be reduced and the lower stress at a given elongation would occur because these "kinks" may dissociate under load.

As shown earlier, the PTMO segment length does affect the mechanical properties. Figure 61b shows the effect of PTMO segment length on the IC-NS series. The stress-strain behavior of the IC-NS series varies with the PTMO segment length in a very similar manner as occurred in the IB-NS series (recall Figure 53 on page 172). In fact, the changes in bulk properties and the morphological features of the IC-NS series with the PTMO segment length are also similar to the IB-NS series.

The creep behavior of the two series ionene elastomers, the 34 series and the 66 series, is presented in Figure 62 on page 191. In these two series, the PTMO segment length of the ionenes is either ca. 3,400 for the 34 series or ca. 6,600 gm/mol for the 66 series, while the counter ion or the hard segment architecture is different. As expected, the IC-NS samples always have the lowest compliance level and the most stable network because of the strong ionic association. Other factors being the same, the network character of the iodide ionene is the weakest which is believed due to the bulky iodide counter ion which provides less ionic association than the Br^- or the Cl^- counter ions. When a spacer group is added into the ionene linkage, the compliance level increases and the network stability is reduced because of a weaker coulombic association and interchain interactions. When other factors are the same, the ionene with longer PTMO segments has a more stable network.

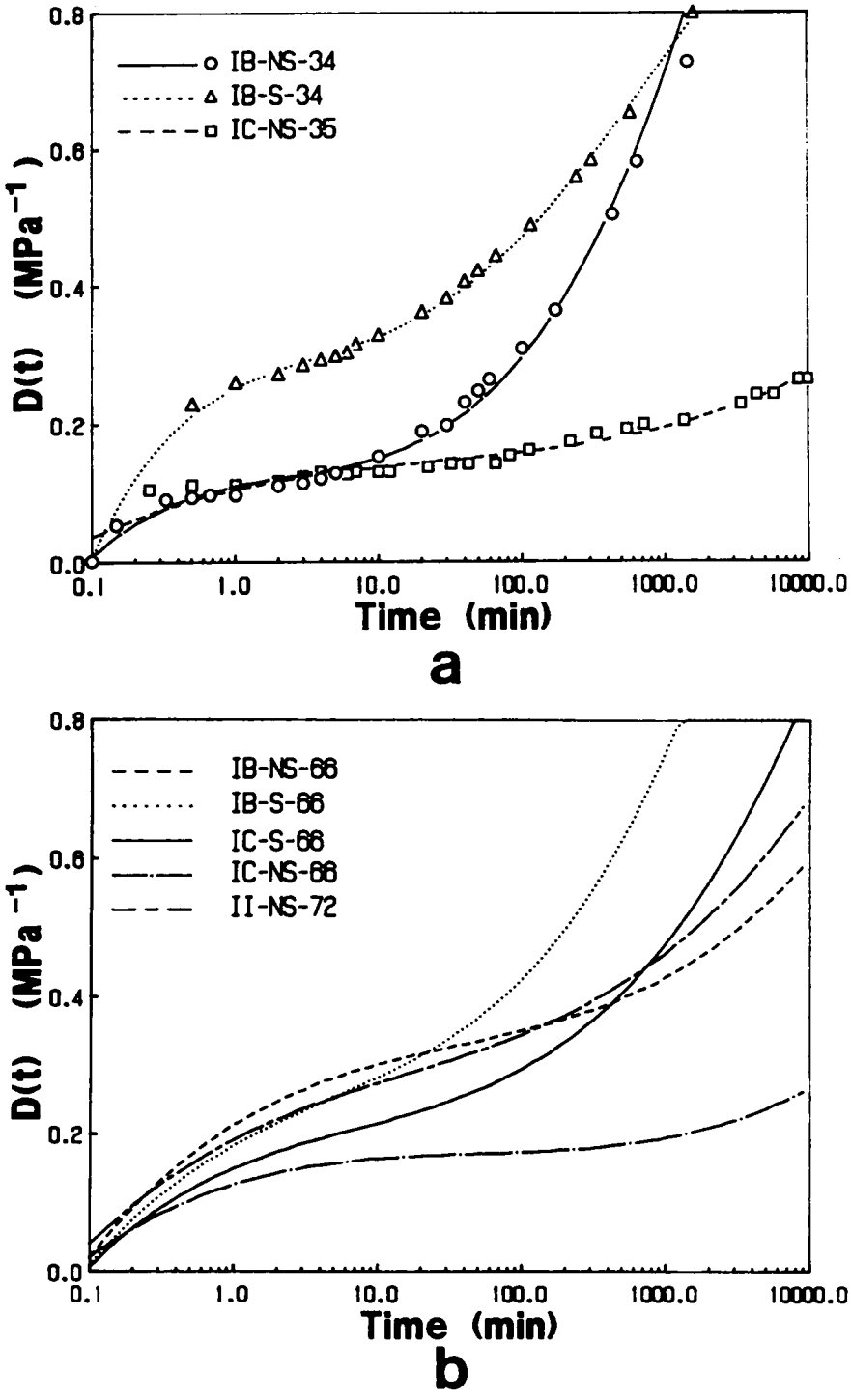

Figure 62. Creep behavior of the ionene elastomers: (a). Creep behavior of the 34 series. (b). Creep behavior of the 66 series.

6.1.2.3. Thermal and Dynamic Mechanical Properties

Figure 63 on page 193 shows the DSC thermograms of the 34 series. The data indicate that the PTMO glass transition (-80°C) has not been affected by either the type of counter ion nor the hard segment architecture as might be expected. However, since there is only ca. 4 vol% of hard segment in this series, even if there were some mixing in the PTMO phase, the T_g of the PTMO segments should not be greatly influenced. The crystallization behavior of the PTMO segments is affected by the type of counter ion. As illustrated in Figure 63, the crystallization peak of sample IC-NS-34 is ca. 20°C lower than for samples IB-NS-34 and IB-S-34, and both the crystallization and the melting peaks of IC-NS-34 are much sharper than for others. There is no distinct difference on the crystallization behavior between samples of IB-NS-34 and IB-S-34. The difference in the crystallization behavior of chloride and bromide ionenes may be due to more chain end restriction of the PTMO segments in the bromide ionene polymers because of the bulky Br ions and less compact hard domains.

The dynamic mechanical behavior of all three members of the 34 series is very similar. The γ transition is observed for all samples which indicates that the spacer group has only a small effect if any on phase separation. As the tanδ spectra show, the T_g of the PTMO segments is the same for all samples. However, the melting peak of IC-NS-34 is about 10°C lower than the others, and the softening temperature of IC-NS-34 is the highest among the three samples. Also, IC-NS-34 has the most flattened E′ behavior in its rubbery region. The softening temperature of IB-S-34 is the lowest and IB-S-34 has the greatest decline of E′ within the rubbery region. This is believed to be caused by a weaker ionic association within IB-S-34.

As stated earlier, when the PTMO segment length increases, the ion content decreases. Thus, the overall influence of the counter ion or the hard segment architecture should be reduced accordingly. Figure 65 on page 196 shows the dynamic mechanical spectra of the 66 series. These spectra are essentially the same expect for the softening temperature. The ionenes with spacer groups in their hard segments have a lower softening temperature than those without spacer groups.

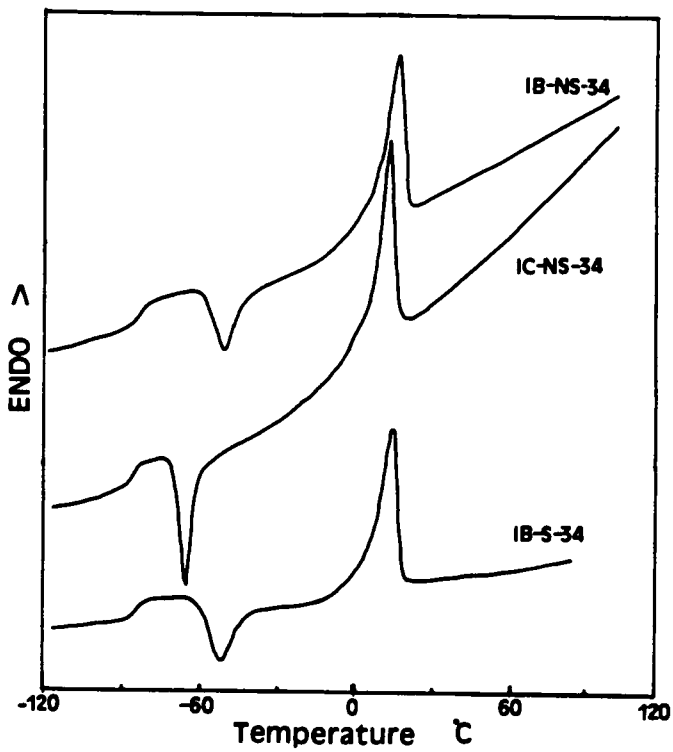

Figure 63. DSC thermograms of the 34 series.

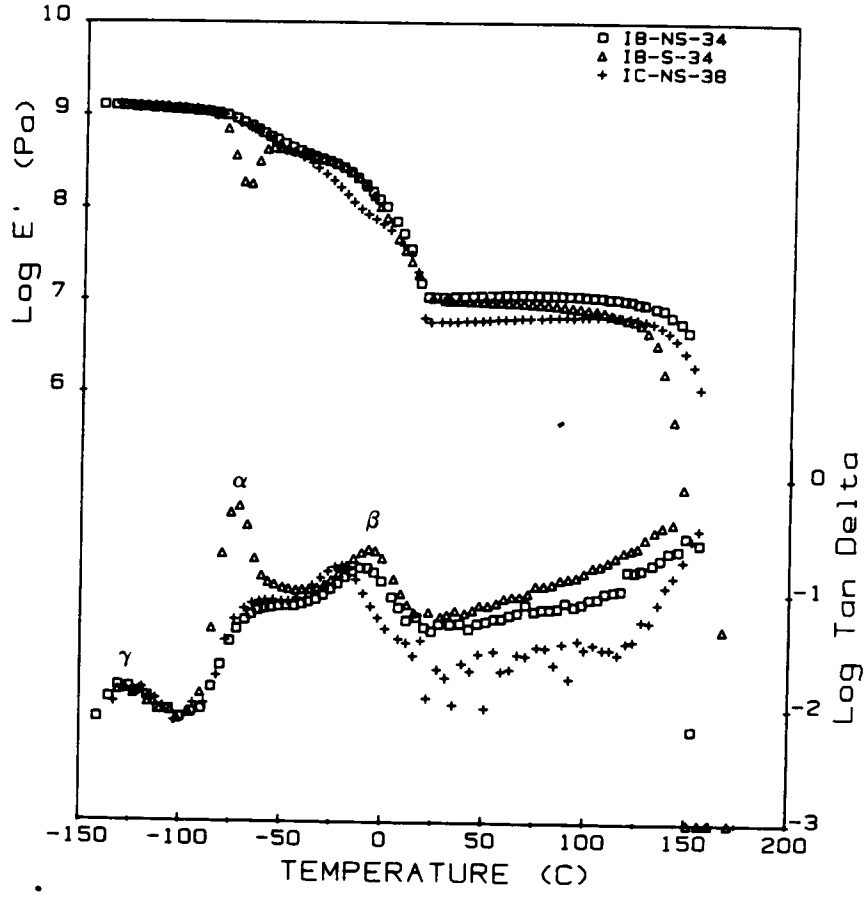

Figure 64. Dynamic mechanical spectra of the 34 series.

The difference is also greater for the ionene with Cl^- counter ions than for the ionene with Br^- counter ions.

The DSC and DMA results indicate that neither type of counter ion nor the hard segment architecture has a strong influence on the glass transition of the PTMO segments in the 34 series. The type of counter ion also strongly affects the crystallization behavior of the PTMO segments. The main effect of the type of counter ion or the hard segment architecture is on the level of ionic association in these materials. By replacing the Br counter ion with Cl, the ionic association increases. Thus, the softening temperature of the ionene increases and the slope of the E′ spectrum in the rubbery region becomes flattened. When a spacer group is introduced into the hard segments, crystallization of the PTMO segments is hardly affected, but the ionic association in the ionene is reduced because of the spacer group. As a result, the softening temperature decreases and E′ decreases as temperature increases in the rubbery region.

6.1.2. Origin of Microphase Separation in Segmented PTMO ionene elastomers

As discussed in the previous sections, these ionene elastomers display some excellent mechanical properties; high tensile strength and high elongation. Despite their low ionic content, the elastomeric behavior of these materials may be due to the phase separation caused by chemically incompatibility of the hard and soft segments, ionic association, or a combination of both. To address this latter point, a non-ionene segmented polymer consisting of PTMO soft segments and brominated aromatic hard segments was prepared by Dr. C. M. Leir[20] as a model system. The non-ionene segmented polymer is designated as IB-NC-20 (refer to Figure 52 on page 169). This material has a somewhat similar chemical structure as the PTMO-dihalide ionene but without ionic associations. Also, the difference of solubility parameters ($\Delta\delta$) between the two segments in IB-NC-20, as estimated by the group contribution method, is 8.1 $(cal/cc)^{1/2}$. The $\Delta\delta$ value of a ionene system estimated from the solubility parameters of its two components is 8.4 $(cal/cc)^{1/2}$. Therefore, if the elastomeric behavior of the ionene systems results from the phase separation of

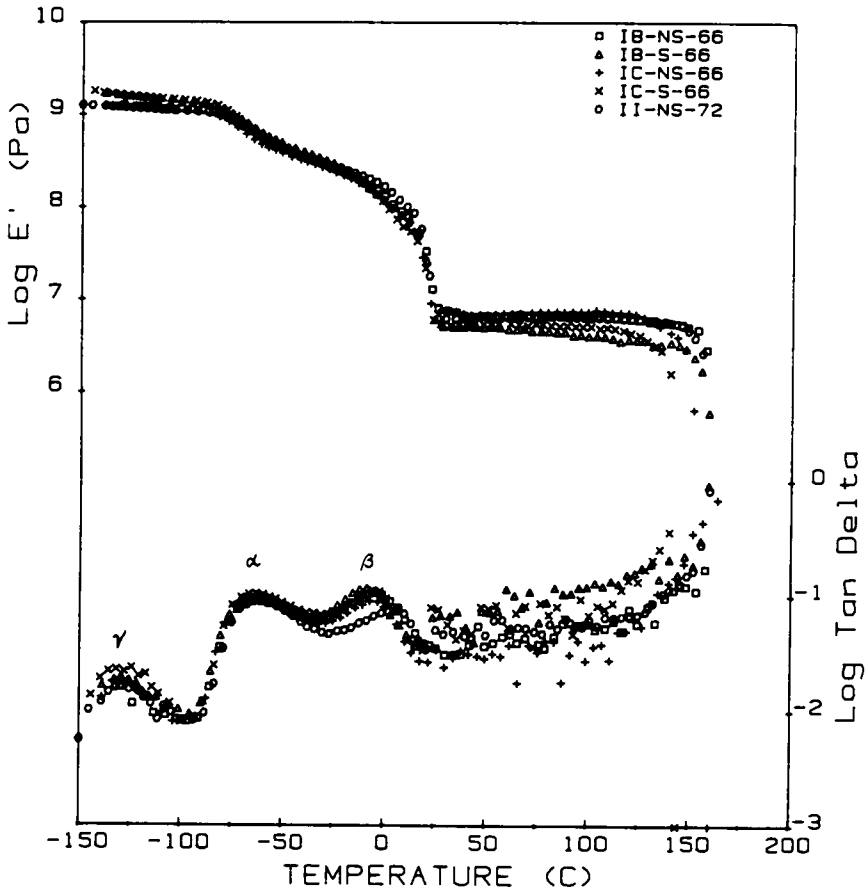

Figure 65. Dynamic mechanical spectra of the 66 series.

hard and soft segments on the basis of chemical incompatibility as in the non-ionic segmented polymers (eg. segmented polyurethanes), the mechanical behavior of IB-NC-20 would be similar to the ionene system because of the similar value of $\Delta\delta$.

Figure 66 on page 198 shows the thermal mechanical behavior and SAXS profiles of both samples IB-NS-18 and IB-NC-20 each of which have a similar PTMO segment length. Figure 66a shows the TMA spectra of these systems. At temperatures below 30°C, they have similar behavior. The first transition on the penetration curves is due to the T_g transition of the PTMO segment. The second transition is due to the melting of the PTMO crystallites. However, the non-ionene polymer IB-NC-20 is distinctly softened at ca. 40°C, while the ionene sample IB-NS-18 does not soften until 150°C. At ambient temperature (ca. 25°C), IB-NS-18 displays excellent elastomeric properties, while IB-NC-20 exhibits a tacky non-elastomeric behavior. The differences in mechanical properties of these two systems indicate that IB-NC-20 may not have an effective network of physical crosslinks caused by phase separation. In other words, there is no microdomain formation in IB-NC-20 which indeed was confirmed by the SAXS results shown in Figure 66b. The SAXS profile of IB-NS-18 has two very distinct scattering peaks which result from a well phase separated microstructure and will be discussed more in detail later. However, there is no scattering peak observed in the SAXS profile of IB-NC-20, This clearly suggests that there is no microphase structure in IB-NC-20 even though it has a similar value of $\Delta\delta$ between its hard and soft segments as in IB-NS-18. This proves that the phase separation and the elastomeric behavior of ionene elastomers are due to the ionic clustering in these materials which are essential for the attainment of effective physical crosslinks and the microphase separated domain structure in these materials.

6.1.3. Summary

The excellent elastomeric properties of PTMO-dihalide ionene elastomers arise from the ion clustering and the good microphase separation in these materials which is promoted by the ionic

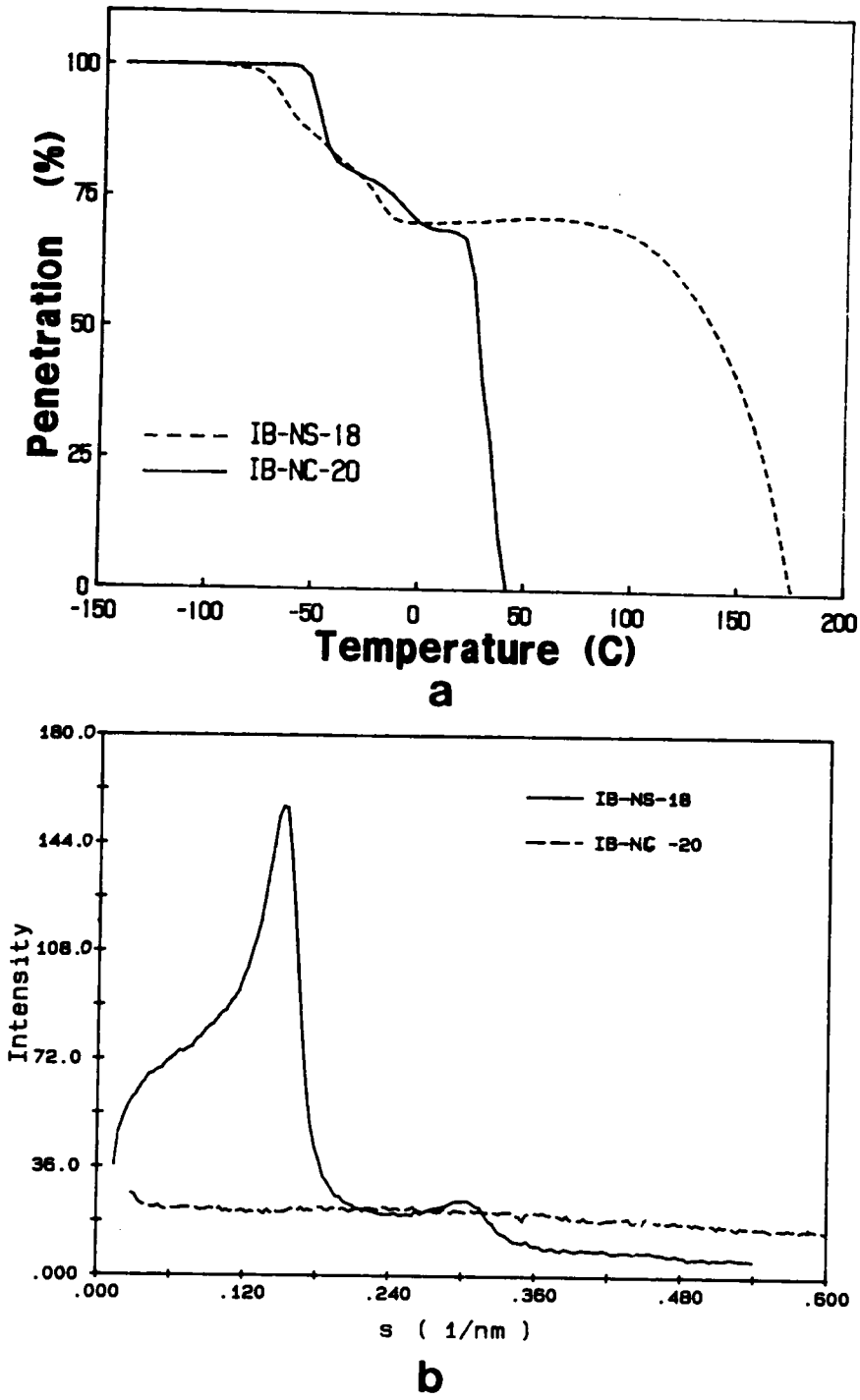

Figure 66. **TMA and SAXS behavior of an ionene elastomer and the non-ionene polymer:** (a).TMA spectra of the non-ionene polymer (IB-NC-20) and a ionene elastomer (IB-NS-18). (b).SAXS profiles of polymer IB-NS-18 and IB-NC-20.

interaction. When the PTMO segment length is changed, the ionic content changes as well. Consequently, the overall strength of the ionic network is altered. As a result, the physical properties of these materials are changed.

By varying the type of counter ion or the hard segment architecture, the ionic association also changes as well as the bulk properties. However, when the PTMO segment length (or molecular weight) is in excess of 6,600 mol/gm, the effect of counter ion or the hard segment architecture is limited because of the small ion content.

Since the microphase separation in these ionene polymers is promoted by ionic association, the change in ionic content or the type of counter ion should have a strong influence on the morphological texture of these materials. In the next section, the morphology of these ionene polymers will be discussed in detail.

6.2. MORPHOLOGY OF THE SEGMENTED PTMO-DIHALIDE IONENE ELASTOMERS

In this section, the morphology of the PTMO-dihalide segmented ionene polymers will be considered in view of studies carried out using both SAXS and TEM techniques. As discussed in the literature review section, the past TEM investigations on ionomers have yielded various results. Those results have fit neither the scattering data nor any existing models. This may be caused by the very small size of ionic domains and their somewhat random arrangement (short range order only) in these ionomers in conjunction with the resolution limitations of an electron microscope. Therefore, a brief review on the theory of TEM image formation is considered necessary in view of the SAXS and TEM results of this study that will be presented. In the author's TEM study of the ionenes, a JEOL 2000EX high resolution transmission electron microscope has been used.

6.2.1. Theory of TEM Image Formation

Two types of contrast can arise in TEM images: amplitude contrast and phase contrast. Amplitude contrast is due to the elastic scattering of electrons and it arises from fluctuations in density, atomic number, or thickness of a specimen. Both mass-thickness and diffraction contrast contribute to amplitude contrast. Also, the level of amplitude contrast is strongly dependent on the accelerating voltage and the atomic number of the scattering atoms. This form of contrast can be directly interpreted at medium resolution which is typically taken to mean specimen detail on a scale greater than 1 nm or 10 Å. In general, amplitude contrast is dominant for large structures while phase contrast is dominant for small structures and becomes the principle or sole source of contrast for very small object points of low atomic number components [122].

Phase contrast which is produced by interference of the unscattered electron wave and the scattered electron wave is only slightly dependent on the accelerating voltage and the atomic number of the scattering atoms. An object which does not significantly alter the amplitude of the transmitted electron waves is called a weak phase object. Most unstained polymer specimens are weak phase objects. The image of such an object must be interpreted by utilizing transfer theory which has been developed in detail in many texts [125-125]. A simplified form of transfer theory has been provided by Thomas et. al.[64,65,126-128] and applied to polymers. The pertinent transfer theory will be briefly reviewed here for it greatly relates to our results and their interpretation.

The microscope object function, denoted as $\psi(\mathbf{r})$, is directly related to the mean inner potential $\phi(\mathbf{r})$ as

$$\psi(\mathbf{r}) = \frac{\pi}{\lambda V_o} t\bar{\phi}(\mathbf{r}) \tag{11}$$

where λ is the wave length, V_0 is the accelerating voltage, t is sample thickness, and $\mathbf{r}$ is a position vector between two scattering points. For polymer solids, the mean inner potential may be estimated by[65]

$$\overline{\phi}(\mathbf{r}) = 69\frac{\rho}{\mathrm{M}}\sum \mathrm{n}_i \mathrm{f}_i \tag{12}$$

where ρ is the density (gm/cc) of the polymer, M is the molecular weight of the repeat unit, f_i is the electron scattering factor at zero angle of the ith type atom, and n_i is the number of the ith type atom in the repeat unit. For a phase separated segmented polymer in which the two segments are formed by repeat units 1 & 2, the mean inner potential difference between them can be calculated by

$$\Delta\overline{\phi}(\mathbf{r}) = 69\{\frac{\rho 1}{\mathrm{M}_1}\sum \mathrm{n}_i \mathrm{f}_i^{(1)} - \frac{\rho 2}{\mathrm{M}_2}\sum \mathrm{n}_j \mathrm{f}_j^{(2)}\} \tag{13}$$

and the relative phase shift between domains, $\Delta\psi(\mathbf{r})$, is simply:

$$\Delta\psi(\mathbf{r}) = \frac{\pi}{\lambda \mathrm{V}_o} t\Delta\overline{\phi}(\mathbf{r}) \tag{14}$$

For a weak phase object, $\psi(\mathbf{r})$ can be described by a phase term: $\exp[i\psi_{ph}(\mathbf{r})]$. According to the first Born approximation[123], the object function becomes

$$\psi(\mathbf{r}) = \exp[i\psi_{\mathrm{ph}}(\mathbf{r})] \simeq 1 + i\psi_{\mathrm{ph}}(\mathbf{r}) \tag{15}$$

For the bright field axial image, the image intensity $\mathbf{I}(\mathbf{r})$ is just the inverse Fourier transform ($\mathbf{F}^{-1}$) of a δ function and a term involving the Fourier transform of the object function, $\mathbf{F}[\psi(\mathbf{r})]$, modulated by the transfer function $\mathrm{T}(\mathbf{K})$ of the microscope:

$$\mathbf{I}(\mathbf{r}) = \mathbf{F}^{-1}\{\delta(\mathbf{K}) - 2\mathrm{T}(\mathbf{K})\mathbf{F}[\psi(\mathbf{r})]\} \tag{16}$$

In Eq.(16), $\mathbf{K}$ is the scattering vector, $|\mathbf{K}| = (4\pi/\lambda)\sin\theta$, and θ is half of the radical scattering angle. The transfer function, $\mathrm{T}(\mathbf{K})$, is given by

$$\mathrm{T}(\mathbf{K}) = \mathrm{A}(\mathbf{K})\sin[-\chi(\mathbf{K})] \tag{17}$$

where, A(K) is the objective aperture function. The value of A(K) is unity inside the objective aperture and zero outside. The phase shift $\chi(\mathbf{K})$ is given by

$$\chi(\mathbf{K}) = \pi\lambda(\Delta f)\mathbf{K}^2 + \frac{\pi}{2} C_s \lambda^3 \mathbf{K}^4 \tag{18}$$

where, Δf is the defocus and C_s is the spherical aberration coefficient of the object lens of the microscope. In Eq.(18), the effects of incoherent and chromatic aberrations are neglected. Image contrast is then given by

$$\frac{\mathbf{I}(\mathbf{r}) - \mathbf{I}_{av}}{\mathbf{I}_{av}} = \mathbf{F}^{-1}\{2\mathrm{A}(\mathbf{K}) \sin \chi(\mathbf{K})\mathbf{F}[\psi(\mathbf{r})]\} \tag{19}$$

Equation (19) indicates that image contrast for a weak phase object is governed by the Fourier transform of the object function and the transfer function of the microscope. If $\sin\chi(\mathbf{K}) = 1$ for all K, the microscope would be a perfect phase contrast microscope and the image contrast would be interpreted intuitively. In practice, the value of $\sin\chi(\mathbf{K})$ is very sensitive to the state of defocus [64,65,123–128]. The effects of defocus on $\sin\chi(\mathbf{K})$ for the JEOL 2000EX microscope in which the C_s has a value of 1.4mm used in our study is plotted in Figure 67a. At zero defocus ($\Delta f = 0$), $\chi(\mathbf{K})$ is determined solely by the spherical aberration of the microscope which is significant only at higher spatial frequencies. For larger scale distances, i.e., $\mathbf{K} < 0.15$ Å^{-1}, $\sin\chi(\mathbf{K})$ is near zero. For the case of the JEOL 2000EX, the calculated optimum defocus value is around -674Å. In this case, $\sin\chi(\mathbf{K})$ is close to -1.0 in the range $0.16 < \mathbf{K} < 0.33$ Å^{-1}. Also in this region, image contrast is identical with the object transform. For a defocus of -2022Å, the peak of normal phase contrast is sharpened and moves to lower spatial frequencies. A periodic spacing between 50 Å to 25 Å ($0.02 < \mathbf{K} < 0.04$Å^{-1}) will then be imaged with enhanced phase contrast and artifacts will occur for resolution beyond 20Å or $\mathbf{K} > 0.1$Å^{-1}. Because of the sign change of $\sin\chi(\mathbf{K})$ at higher frequencies, a "salt and pepper" phase contrast structure will often be exhibited with the exact texture being dependent on the optical conditions of the microscope employed.

The first order expression for the image transform, Eq.(19), arises from the interference between the imaginary scattered wave and the unscattered or background wave. Therefore, the image

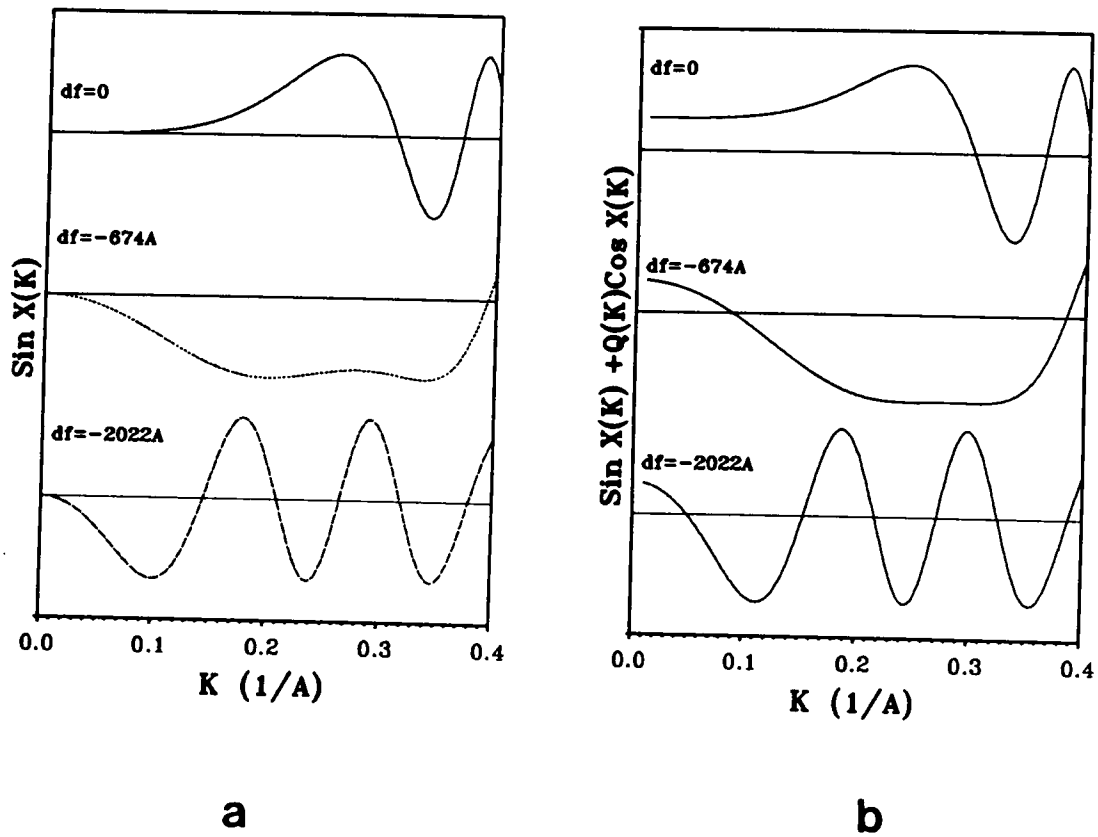

Figure 67. The effect of defocusing on the transfer function of JEOL 2000EX: The value of C_s is 1.4mm, and $\lambda = 0.0025$nm. Coherent illumination was assumed. (a). Without the effect of mass-thickness contrast (Q(K)=0). (b). With the mass-thickness contrast effect (Q(K)=0.4).

contrast arises from phase contrast and the image corresponds to the phase contrast image. However, the modification of the wave in the diffraction plane by the aperture function would account for the loss of electrons scattered outside the aperture and the effects of amplitude contrast should arise naturally.

To describe the effects of amplitude contrast, an extra amplitude term $\exp[\psi_{ampl}(\mathbf{r})]$ is introduced into Eq.(15), and $\psi(\mathbf{r})$ becomes

$$\psi(\mathbf{r}) = \exp[\psi_{\mathrm{ampl}}(\mathbf{r})]\exp[i\psi_{\mathrm{ph}}(\mathbf{r})] \tag{20}$$

By employing the first order approximation, the object function is estimated by equation 21.

$$\psi(\mathbf{r}) \simeq 1 + \psi_{ampl}(\mathbf{r}) + i\psi_{ph}(\mathbf{r}) \tag{21}$$

In this case both the ψ_{ph} and ψ_{ampl} terms must be smaller than unity for the first order approximation. The image contrast then becomes

$$\frac{\mathbf{I}(\mathbf{r}) - \mathbf{I}_{\mathrm{av}}}{\mathbf{I}_{\mathrm{av}}} = \mathbf{F}^{-1}\{\mathbf{F}[\psi(\mathbf{r})]2\mathrm{A}(\mathbf{K})[\sin\chi(\mathbf{K}) + \mathrm{Q}(\mathbf{K})\cos\chi(\mathbf{K})]\} \tag{22}$$

In Eq.(22), the maximum possible contribution from amplitude contrast relative to that from phase contrast is given by the factor Q(**K**) having a form of

$$\mathrm{Q}(\mathbf{K}) = \frac{\mathrm{S}_t\mathrm{A}}{2\lambda\mathrm{N}\mathrm{f}} \tag{23}$$

where, f is the electron scattering factor, S_t is the total cross section per gram of matter for scattering outside a given object aperture, A is the atomic number and N is Avogadro's number. Experimental results from Burge and Smith[129] have shown the value of $S_t = 1.2\mathrm{X}10^5\ \mathrm{cm}^2\mathrm{gm}^{-1}$ which was correct for all elements at 75kV. By employing this estimated S_t value, the value of Q(**K**) is estimated as 0.12 for carbon, 0.26 for bromine, and 0.4 for uranium at 75 kV. These values may be lower if a larger aperture or higher accelerating voltage is used. Because of the theoretical uncertainties, the most direct approach to determining Q(**K**) is to obtain it experimentally. Exper-

imental results[130] indicate that the Q(**K**) is about 0.4 at **K** less than 0.02 $Å^{-1}$, and it decreases to less than 0.1 for **K** > 0.05 $Å^{-1}$ for uranium. These results are consistent with the value predicted above, but show that amplitude contrast is most important at low resolution.

By employing a value of 0.4 for Q(**K**) into Eq.(22), the function of $[\sin\chi(\mathbf{K}) + Q(\mathbf{K})\cos\chi(\mathbf{K})]$ vs. **K** was plotted in Figure 67b. At zero defocusing, the result indicates that for $\mathbf{K} < 0.1Å^{-1}$, there is no sign change. In other words, the image contrast obtained for $\mathbf{K} < 1Å^{-1}$ arises from amplitude contrast.

In the case of our PTMO ionene polymer, the difference in the inner potential $\phi(\mathbf{r})$ of two components, PTMO and dibromine-xylene, is about 2.23V as estimated by Eq.[13] with values of zero angle scattering factor [131] , which is quite high (e.g. compare this with the value of 1.65V a for a segmented polyurethane consisting of hard segment of 4,4′-diphenylmethane diisocyanate (MDI) and 1,4 butene diol with soft segment of MDI and polypropylene oxide diol[127]). If the phase shift $\Delta\psi(\mathbf{r})$ is limited to less than 0.5 radian for a weak phase object, the thickness of the ionene specimen which one could wish to investigate should be less than 30 nm as estimated by Eq.[14]. In practice, the cryo-microtomed sections which have been utilized in this work have a thickness of the order of 50nm. Therefore, mass-thickness contrast should also contribute to the final image.

Besides the thickness effects, the geometry of the domain structure is also a key factor. The TEM image is a two-dimensional projection of the three-dimensional specimen. Figure 68 on page 207 shows just three possible geometries of domain structures. If the domain thickness and the film thickness are similar (Figure 68a) or the domain thickness is much smaller than the film thickness but a long range ordered structure is presented (Figure 68b), the projected image is uncomplicated, and correct interpretation of the domain image is possible. In the latter case, Figure 68b, the diffraction contrast will also contribute to the image contrast. However, if the domain size is smaller than the film thickness and the domains are randomly distributed, the resulting projection will be almost indistinguishable from random noise (Figure 68c). In this case, a very thin specimen must be prepared to resolve this problem. In general, the thickness of a cryomicrotomed section is on the order of a few hundred to 1000Å. The domain or cluster structure of ionomers studied by others is believed to generally have a "spacing" or correlation length under 100Å as determined

by SAXS. Therefore, it is quite understandable that the previous TEM studies have produced a wide variation of the postulated "domain types" and "size" while the SAXS results were similar [53,62,64,132].

In the TEM and SAXS studies of ionene polymers, the TEM sections were microtomed in three different directions (a parallel and two perpendicular directions) to the film surface (refer to Figure 69 on page 208). Also, the incident X-ray beam in SAXS study has been imposed on the same three directions on Warhus camera. In this way, the three dimensional structure of the ionene polymer can be studied. With these materials as background, the details of TEM and SAXS studies on these ionene polymers will be discussed in the oncoming sections.

6.2.2. SAXS and TEM studies on the IB-NS Ionene Polymers

6.2.2.1. SAXS Results of the IB-NS series

The general characteristics of solution cast ionene films are that they display a high strength elastomeric behavior with good extensibility and recoverability[20]. As discussed in section 6.1, the PTMO segments in these ionene systems can crystallize under the right conditions. However, the undeformed samples have no sign of PTMO crystallization at ambient temperature for PTMO segment molecular weights less than 3400. For the samples containing higher molecular weight PTMO segments, IB-NS-66 and IB-NS-100, crystallization at ambient temperature does occur at a slow rate (over two weeks) to develop a detectable amount of crystallinity. In order to eliminate any possible effects of PTMO crystallinity on the SAXS pattern, all samples were heated at 60°C for two hours prior to any SAXS studies to remove any possible traces of crystallinity of the PTMO segments.

Earlier studies[20] indicate that the distinct elastomeric behavior of these materials is an indication of a very high degree of microphase separation. Figure 70 on page 210 shows the SAXS intensity profiles of IB-NS series obtained from the Kratky camera. As noted, there are very dis-

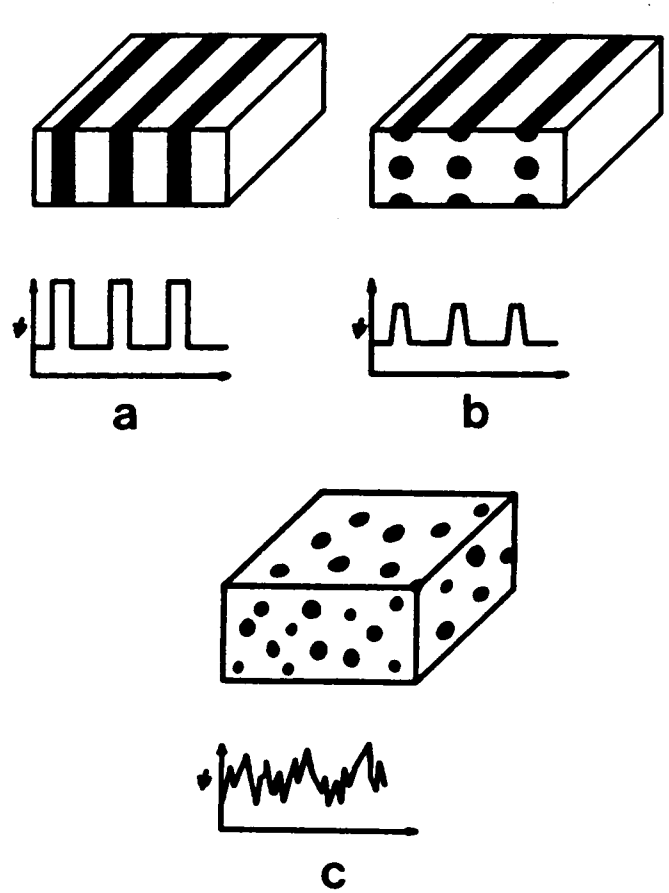

Figure 68. The effect of domain geometry on the TEM objective function.

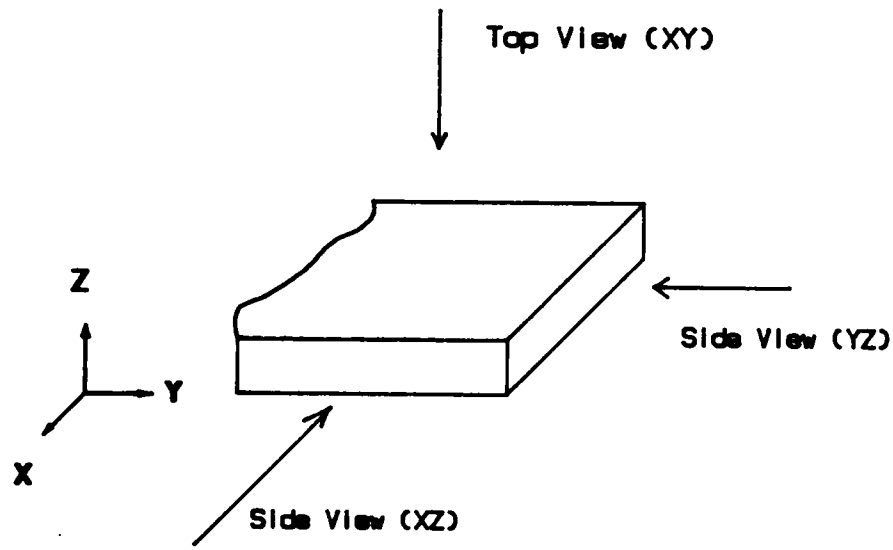

Figure 69. Illustration of directions of X-ray and electron beams.

tinct maxima shown in the SAXS profiles. In this figure, the angular dependent variable is expressed as "s" ($s=(2/\lambda)\sin\theta$, and θ equals 1/2 of the radical scattering angle). The SAXS results of the ionene with the longer PTMO segments, as IB-NS-66 and IB-NS-100, are rather similar to the SAXS profile of a telechelic ionomer which has been investigated in this laboratory and discussed elsewhere[117]. In fact the basic single "shoulder" in the SAXS profile is quite typical of most ionomers samples as studied by other laboratories[64,133]. For the case of the segmented ionene systems, the high scattered intensity near zero angle may arise from randomly placed ionene linkages and the stronger single peak intensity may similarly result from the scattering from ion clusters or domains[133]. For the ionene materials, the peak "bragg" or correlation distance may be interpreted as a interdomain or intercluster distance. This estimated "bragg" distance and the scattered intensity of the ionene elastomers are both strongly dependent upon the PTMO segment length as shown in Figure 70. One sees that the first peak spacing decreases as the PTMO segment length decreases. This of cause suggests that the spacing is directly related to an average interparticle or interdomain spacing between the ionene containing domains and is in line with earlier observations of Teyessie et. al. although their materials were telechelic in nature (not segmental) nor were they based on ionene chemistry[134].

The peak intensity of ionene elastomers (particularly those of higher ionene content) is high and the peaks of the ionene elastomers are also much more distinct than usually noted for ionomers or in fact for related segmented polymers that developed domain structure by segment incompatibility e.g. the segmented urethanes[45]. While the high intensity and the sharpness might also relate to the narrow molecular weight distribution of the PTMO segments, it is strongly believed that it is from induced long range order structure as discussed below.

Another and more noteworthy feature of the ionene elastomers is the multiple scattering peaks. The effect of the PTMO segment length on the morphological structure of the ionene elastomers has also been shown in Figure 70. As the PTMO segment length decreases or increases in ion content (Table 12 on page 170), the peak intensity increases and a second scattering peak develops. Also, a distinct downturn at low "s" is observed when compared to the intensity of the first maximum For sample IB-NS-18 which contains the shortest PTMO segments, a very weak

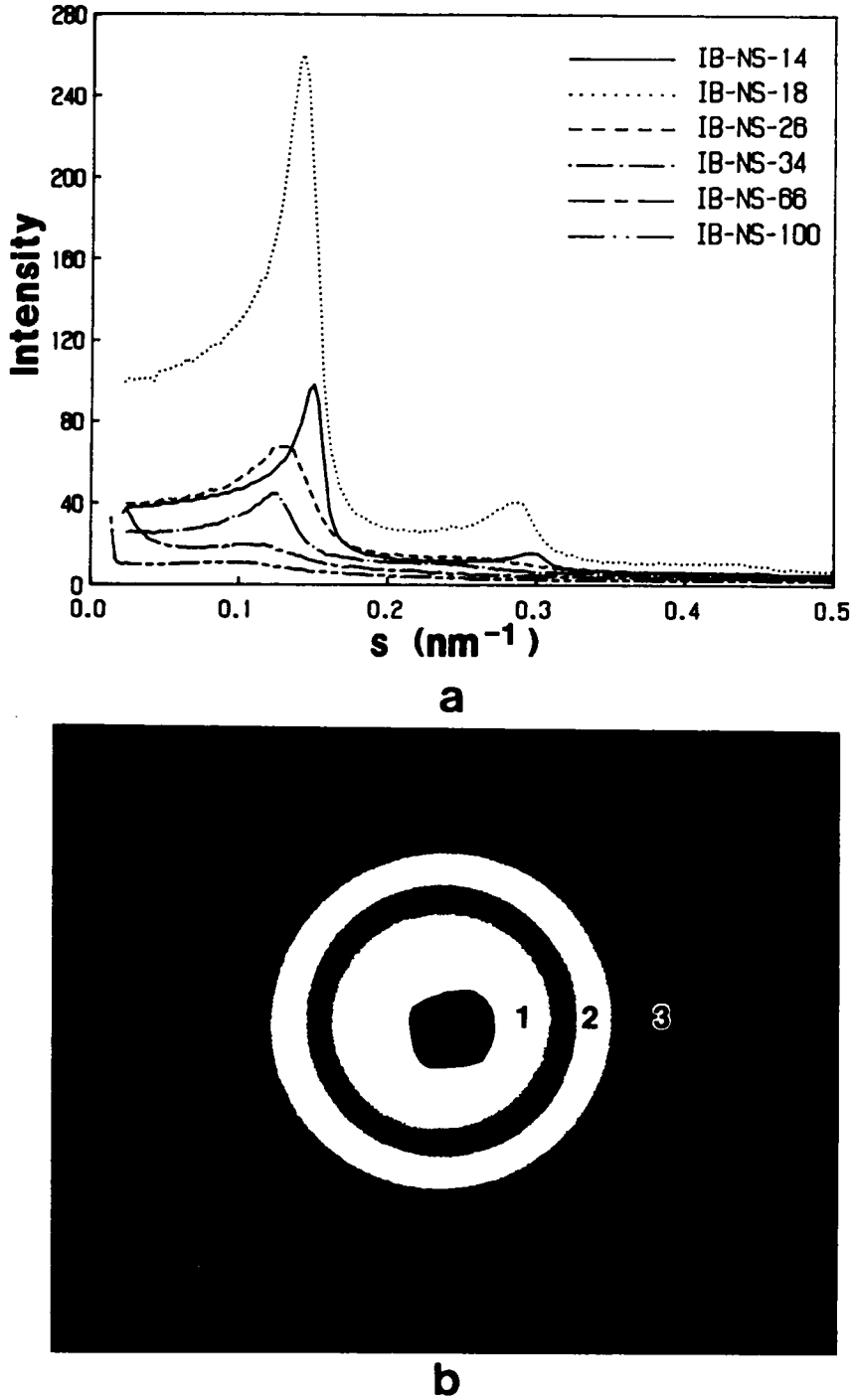

Figure 70. SAXS profiles and a SAXS pattern of the IB-NS ionene elastomers: (a). SAXS profiles of the IB-NS series obtained from Kratky camera. (b). SAXS pattern of the IB-NS-18 obtained from Warhus camera with x-ray beam parallel to the normal of the film.

third peak is observed even from the smeared SAXS profile (Figure 70a). It is noteworthy that this observation of three scattering peaks has never been observed in a segmented ionene material let alone any other ionomer materials at the time this SAXS data was obtained. The estimated "bragg" spacing calculated from the smeared SAXS profile of IB-NS-18 shows a close relationship of 1:2:3 for the first three peaks with the first order being 7.0nm (There is a question of whether the multiple SAXS peaks arise from increasing orders of scattering as will be discussed later). This general scattering behavior suggests a lamellar structure with considerable long range order similar to the scattering behavior that has been observed in certain of the styrene-isoprene and related block polymers[36]. Such a morphological structure is somewhat surprising because the volume percent of the hard segment is only ca. 6 vol% for the IB-NS-18 polymer. By utilizing the unsmeared pinhole collimation of a Warhus camera, the two dimensional scattering pattern for the IB-NS-18 ionene was also obtained and is shown in Figure 70b (with the beam parallel to the film normal). This result is in very good agreement with the earlier results from the slit collimated experiments. In fact, even a fourth maximum is observed with a long exposure time. The spacings from the multiple rings scale again nearly as 1:2:3:4 with the first being ca. 6.5nm which is consistent with the largest spacing calculated from the desmeared data from the Kratky camera[121]. As an important reminder, the SAXS results were obtained by passing the X-ray beam normal to the film surface (along the z-direction in Figure 69 on page 208) in Figure 70

As stated above, the high scattering intensity of ionene elastomers is undoubtedly caused by good phase separation of the high electron dense ionene containing units from that of the relatively low electron density PTMO segments. The Porod analysis of the high angular scattering intensity (the tail region of the SAXS profile) indicates that the thickness of the domain interface is on the order of 0.1-0.2 nm which is quite small thereby providing another good indication of a very high degree of phase separation.

6.2.2.2. TEM Results of Sample IB-NS-18

The extremely high degree of phase separation, long range order and small hard segment volume fraction of these materials, especially for IB-NS-18, tempted the author to investigate ultrathin cryo-microtomed sections from the same solvent cast films by transmission electron microscopy (TEM). In order to study the spatial microstructure of this ionene material, ultrathin sectioning was carried out so that the morphological features could be investigated for all three observation directions (recall Figure 69 on page 208).

The TEM studies were carried out on a JEOL 2000EX microscope. The astigmatism of the microscope was well adjusted. A 200kV accelerating voltage was used. The high voltage provides higher penetration power while reducing the radiation damage of the sample. Also the higher accelerating voltage improves resolution due to a shorter wave length as well as minimizes multiple scattering[122]. The TEM results showed that when a specimen was exposed to the electron beam over five minutes, there was no difference in the morphological texture of the specimen. This implied that there is no significant radiation damage on these ionene samples. A small objective aperture (20μm) was also used to minimize the artifacts of the microscope at higher spatial frequencies or smaller scale distances.

Figure 71 on page 214 shows the results of the TEM studies on sample IB-NS-18. The micrographs were taken at medium resolution (50,000X) and near focus. The dark regions in the micrographs contain the ionene units having the high electron density bromide ions. The brighter regions represent the PTMO containing regions. Figure 71a illustrates the view normal to the surface of the film (xy-plane in Figure 69 on page 208) which displays some phase separated structure, however, there is no distinct sheet-like or lamellar or even rod-like structure observed. In fact, this view seems like the rather common "salt and pepper" texture sometime seen at high magnification and, thereby, makes one initially suspect with regard of interpretation of this micrograph. However, in Figure 71b & c, the micrographs present the two "side views" of the same film (xz and yz planes in Figure 69 on page 208) and each shows a very distinct lamellar or rod-like structure with long range order. The periodic spacing of this structure is ca. 6.5nm which is in direct

agreement with the SAXS data. Of particular importance is the fact that this structure is preferentially oriented perpendicular to the surface of the film apparently as a result of the solution casting procedure.

This striking morphological structure was verified by defocusing procedures. Figure 72 on page 215 shows the defocusing pictures as viewed for the xz plane. As the focus was varied over the wide range from + 67.4nm to -1,011nm, the image remained almost unchanged. These through focusing pictures indicate that the image obtained mainly results from the mass-thickness contrast rather than phase contrast. As mentioned in the earlier sections on transfer theory, phase contrast mostly contributes to the high spatial frequency or small spacing region. The transfer function calculation indicates that "artifacts" having a spacing of 7.0nm could be introduced but at a defocusing of -10,000nm. Such a large defocusing is unrealistic in this case. At near focus, the value of $\sin\chi(\mathbf{r})$ is almost zero for $\mathbf{K} < 0.1\ \text{Å}^{-1}$, or a physical spacing > 1.0nm (10Å). Therefore, artifacts or an anomalous texture of this type should not be produced for the image having a spacing greater then 1.0nm.

Since the medium resolution bright field images exhibit dominantly amplitude contrast when operating near focus [135], the rod-like structure presented on Figure 71b and c is believed to arise from amplitude contrast. As Figure 67 on page 203shows, the function $\sin\chi(\mathbf{r}) + Q(\mathbf{r})\cos\chi(\mathbf{r})$ is about 0.4 in the region of $\mathbf{K} < 0.1\text{Å}^{-1}$ or a spacing > 1.0nm, and there is no sign change. Therefore, the image in this region arises principally from amplitude contrast. In other words, the image in Figure 71b and c truly represents the real morphological structure of the ionene mentioned.

Further proof of the structure was obtained by passing the X-ray beam through both surfaces and the sides of the film in the Warhus pinhole collimated camera (refer to Figure 69 on page 208). For the case where the beam is parallel to the film normal, the X-ray pattern shows no orientation effects (Figure 73a). But for the case where the beam is orthogonal to the film normal, the SAXS patterns of Figure 73b and c were obtained. These patterns clearly and conclusively verify the basic results of the TEM studies. That is there appears to be at least three orders of scattering but more noteworthy is the strong azimuthal dependence which is due to the orientation

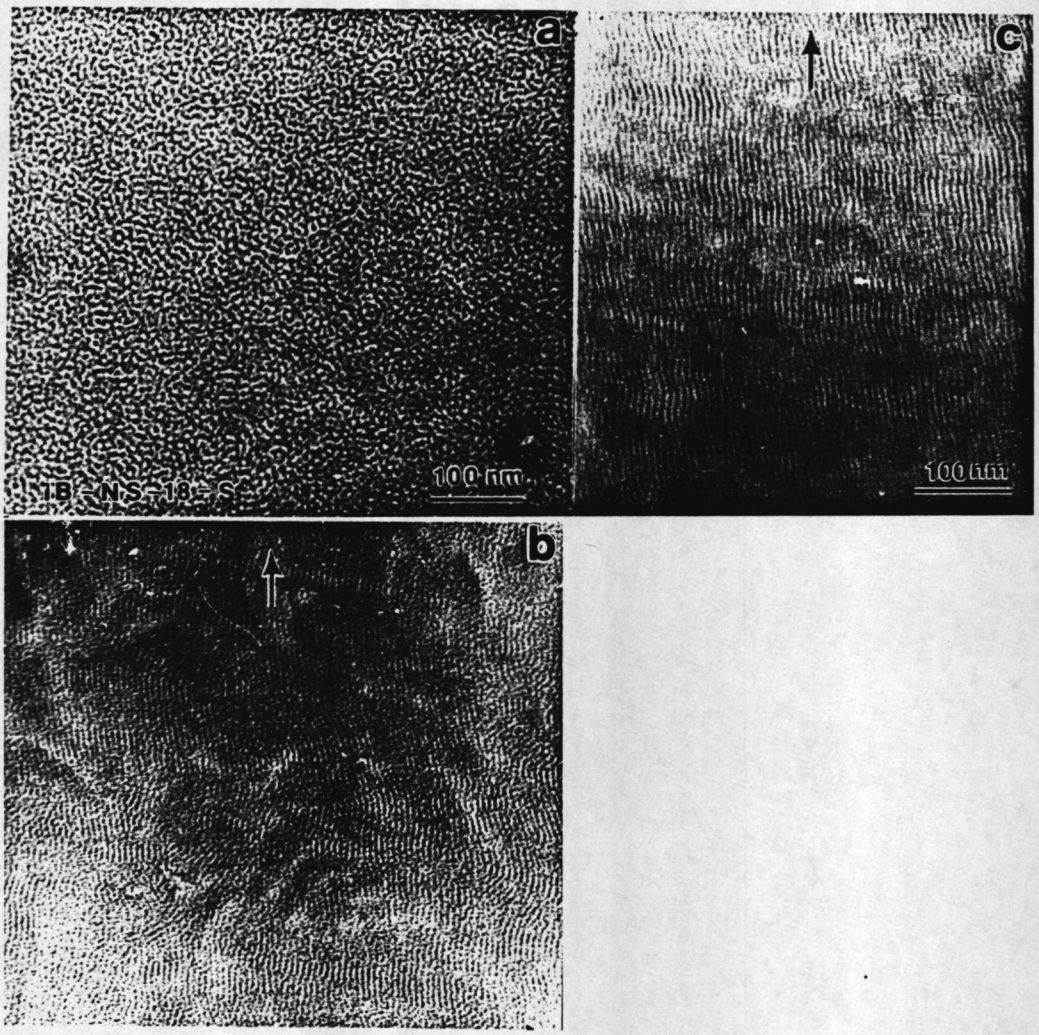

Figure 71. TEM micrographs of sample IB-NS-18: (a). The top view (xy-plane). (b). The side view (xz-plane). (c). The side view (yz-plane). Arrows indicate the normal of film surface.

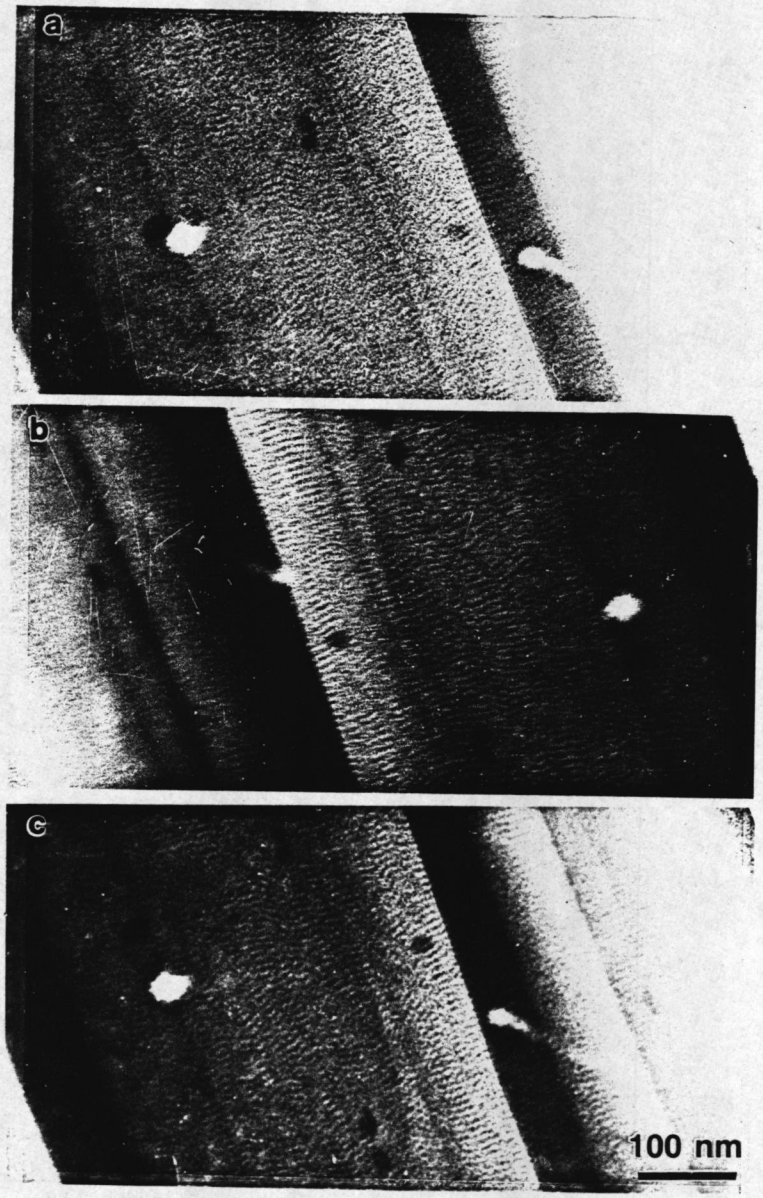

Figure 72. Side view (xy plane) defocusing, df, TEM micrographs of sample IB-NS-18: (a).df = 67.4nm, (b). df = 0nm, (c). df = -1,011nm.

of the morphological structure, i.e. "slit like" scattering. Assuming that the scattering represents four orders, the "bragg" spacing calculated from the edge shot patterns provides the same result that from the pattern in Figure 73a and again is in good direct agreement with the "side view" TEM experiments.

6.2.2.3. Domain Structure of Sample IB-NS-18

At this point, the SAXS results in conjunction with the side view TEM micrographs, strongly support the presence of a lamellar texture. There is, however, some question concerning this proposed structure if the TEM micrographs of the perpendicular view to the film surface is taken into account, i.e., a lamellar structure was not directly seen but rather the micrograph suggests a structure that could arise from rodlike units being viewed end on. Indeed, the salt and pepper pattern observed in this direction was believed real in view of the analysis of the microscopy procedures utilized, i.e., the defocusing analysis. Hence, there is some question as to whether the structure is truly a lamellar texture as based on the perceived four orders of scattering by the SAXS analysis or whether there may be more of a rodlike packing which would not be expected to lead to the same equivalent SAXS interpretation of the four scattering peaks having a Bragg spacing ratio of *ca.* 1 : 2 : 3 : 4. Therefore, it was attempted to further consider the system in view of possible line broadening effects that occur in the SAXS data (recall Figure 70 on page 210 and Figure 73 on page 217) and what the general spacing ratios are as determined from several samples. Utilizing both the desmeared Kratky data as well as several patterns collected from use of the Warhus camera, the average "d" spacing with associated error range are presented in Table 15.

By carefully examining Table 15, one notes that the ratios of the relative Bragg spacings are in a range of 0.9-1.1 : 1.69-2.27 : 2.56-3.7 : 3.56-4.28. While these data might again strongly support the general lamellar texture in that the four spacings do occur in a range of ratios 1:2:3:4, there is some question as to whether this interpretation is correct. For example, for oriented cylindrical particles packed in a hexagonally close packed array, the same spacing ratios are determined to be

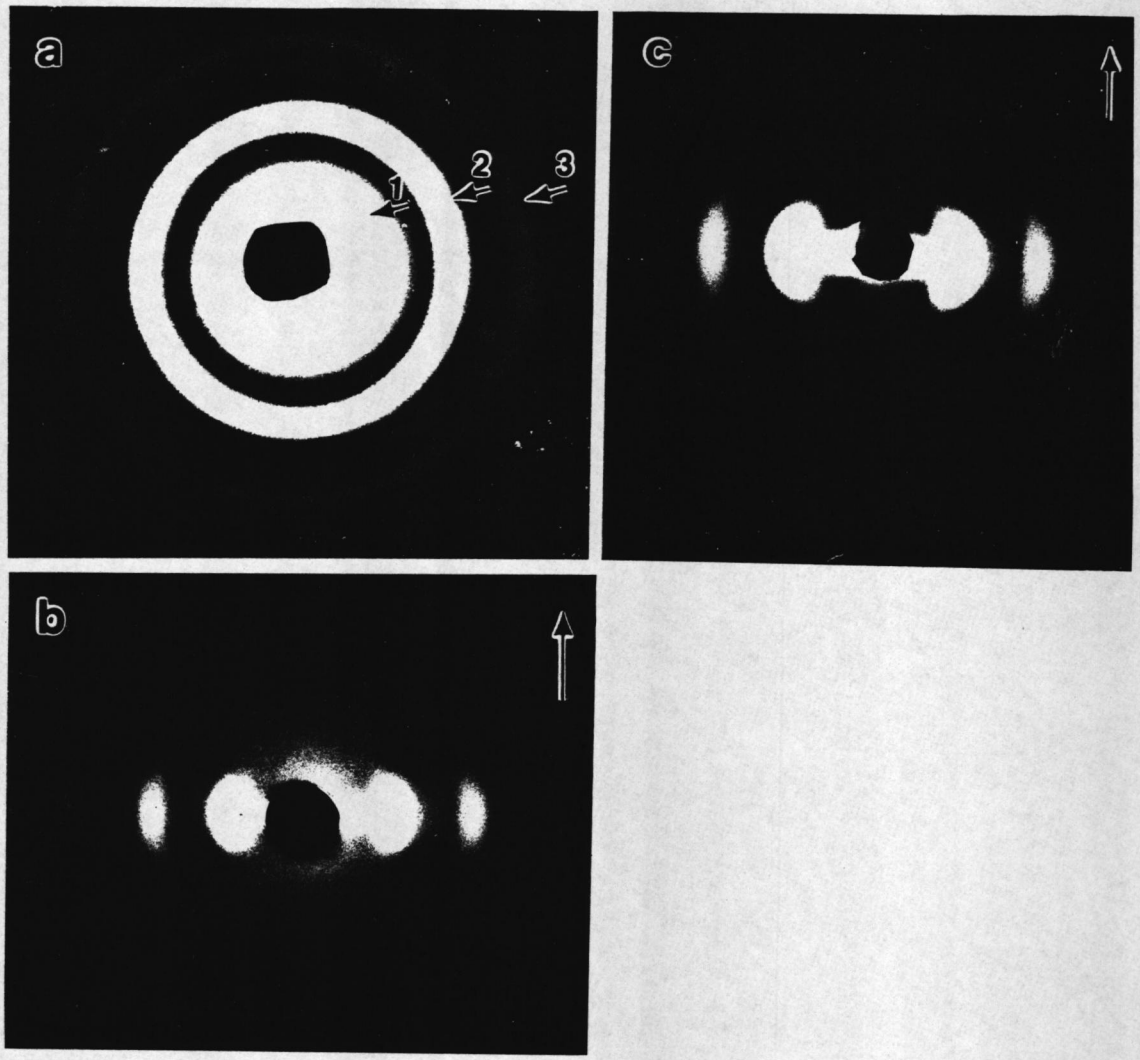

Figure 73. SAXS patterns of sample IB-NS-18 obtained from the Warhus camera: (a).The X-ray beam was parallel to the film normal (z-direction), (b).The X-ray beam was orthogonal to the film normal (x direction), (c).The X-ray beam was orthogonal to the film normal (y-direction).

Table 15. Values of "d" spacing of sample IB-NS-18 obtained from the Warhus camera.

"d" Spacing (nm)	d_1	d_2	d_3	d_4
Ave. d	6.51	3.31	2.21	1.66
relative spacing	1	1.97	2.95	3.92
Error Range$\pm 2\sigma$	6.51$\pm$0.6	3.31$\pm$0.18	2.21$\pm$0.1	1.66
Relative spacing	0.9-1.1	1.69-2.27	2.56-3.37	3.56-4.28
Measured d spacing	5.24-6.99	3.15-3.50	2.15-2.31	1.66
Relative Spacing		1.5-2.22	2.27-2.74	3.15-4.21

* σ is the standard deviation of the "d" spacing.

1 : 1.73 : 2:2.65 : 3:3.5 : 3.6:4. Since only four scattering peaks have been observed and they are broadened, it is possible that the ionene system might well also have the character of a cylindrically hexagonally packed array if the long range order is limited in the system thereby leading to line broadening and causing some of the expected peaks from a cylindrically packed array to be overlapped as has been observed and discussed for block copolymer systems by Hashimoto[92]. Hence, there is the possibility that having only four broad scattering peaks to work with from ionene material does not distinctly allow one to conclude that it is either lamellar or a hexagonally packed cylindrical domain texture although the earlier discussion strongly suggested a lamellar morphology based principally on the SAXS results from the side view TEM micrographs.

Extending the discussion of the possibility for a hexagonally packed system of rodlike domains, the volume fraction of the ionene domains that would occur for this morphological structure as well as for the case of a lamellar morphology has been estimated. Using an interdomain spacing of 6.5nm as based on the SAXS data and, assuming complete phase separation, i.e., sharp interfaces, a rough calculation of these volume fractions can be estimated. To carry out this calculation, an estimate of the domain width is needed and an upper and lower bound of 1.5 and 1.1 nm has been utilized in view of chemical bond lengths as well as including the large bromide counter ions. While indeed the ionene unit is not disk shaped, but it has been ignored in the calculation and considered its length as the diameter for the rod calculation as well as the width dimension for the lamellar structure. Using the upper and lower bounds for these diameters or widths, the calculations indicate that the minimum ionene domain volume fraction would be 5.3% for the hexagonal rod packed system versus 23.1 volume percent for the lamellar structure with the 1.5nm dimension. In the case of the 1.1nm dimension, the minimum ionene domain volume required would be 2.8 vol% for the hexagonally packed rod structure and 19.9 vol% for the lamellar texture. Further details of how the calculations were made are given within Appendix.

The estimates of the ionene volume content strongly suggest that it is unlikely to form a lamellar domain structure in the IB-NS-18 ionene sample. In fact, for this material the ionene segment volume is estimated to be 6.4 vol% based on chemical composition and some estimate of densities of the relative components. This number barely satisfies the minimum required hard

segment volume for the hexagonally packed structure but clearly is far below that expected for a lamellar texture. Hence, consideration of the ionene volume estimations above, the possibility of line broadening influencing the SAXS results and finally both the normal and perpendicular views of the ionene material by TEM, a tentative morphological structure has been proposed which may well be best described by a system of hexagonally packed rods with some degree of irregularity in contrast to a lamellar texture. The proposed domain structure and arrangement of the ionene moieties of IB-NS-18 is shown in Figure 74 on page 221. In this model, the ionene segments form rodlike domains which orient perpendicular to the surface of the solution cast film. Due to the wavy nature of these rodlike domains, their volume fraction shown in the TEM micrograph viewed normal to the surface would indeed be greater than expected as is in line with the observation made. This wavy nature also reduces the long range order of the structure which leads to some line broadening effect on the SAXS results.

6.2.3. Effect of PTMO Segment Length on Morphology

As illustrated by Figure 70 on page 210, the multi-peak scattering from the IB-NS series gradually disappears as the PTMO segment length increases. The long range ordered structure is no longer maintained as the volume fraction of the ionene component decreases. Figure 75 illustrates the dependence of the "d" spacing with the PTMO segment length. It clearly shows that there are two different regions. For IB-NS series, the "d" spacing increases much faster when the PTMO segment length is less than 3,400 mol/gm. When the PTMO segment length exceeds 3,400, the "d" spacing increases slightly with the PTMO segment length. The same behavior has also been observed for the IC-NS series. In this case, the difference between two regions is greater than in the IB-NS series.

The PTMO segment length dependence of the "d" spacing may result from changes in chain conformation of the PTMO soft segments. In these ionenes, the PTMO segments are connected with ionic hard segments. The repulsive coulombic forces between two ionic hard segments could

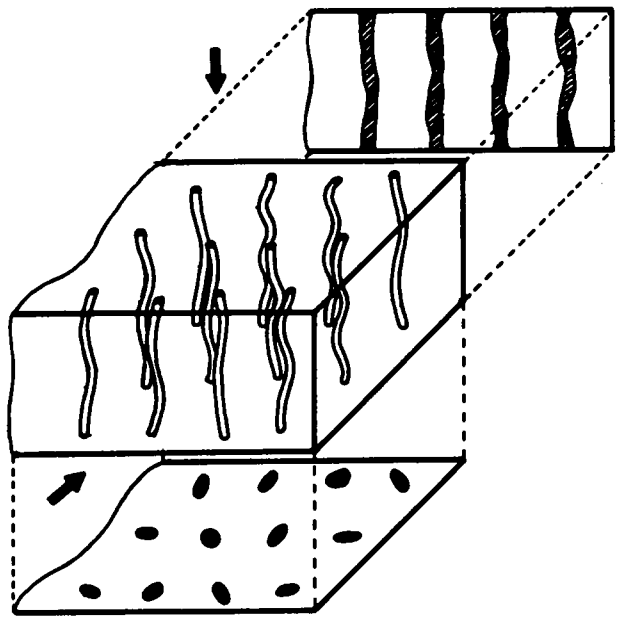

a

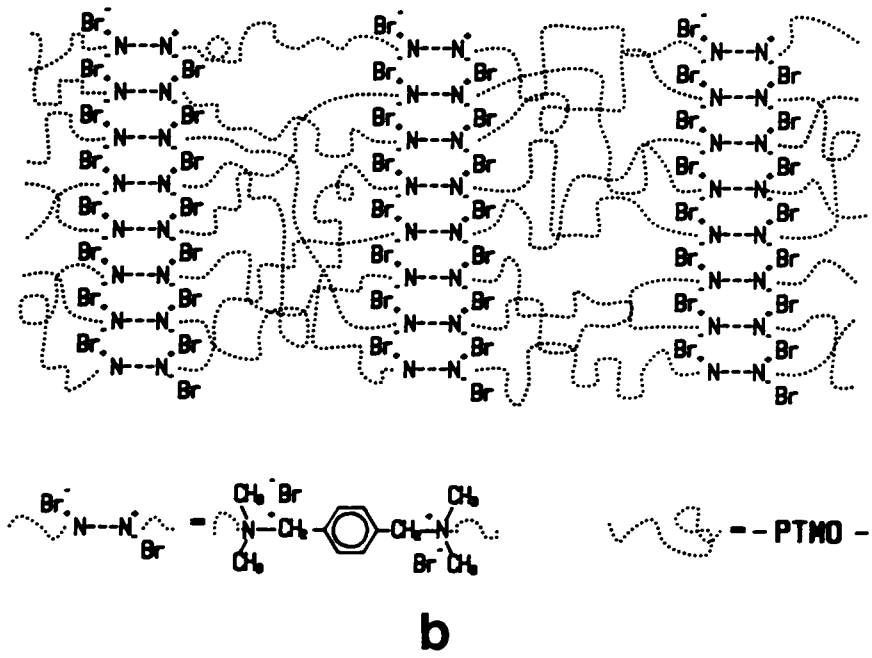

b

Figure 74. Proposed tentative domain structure of sample IB-NS-18: (a). Domain structure of IB-NS-18. (b). Arrangements of ionene moieties of sample IB-NS-18.

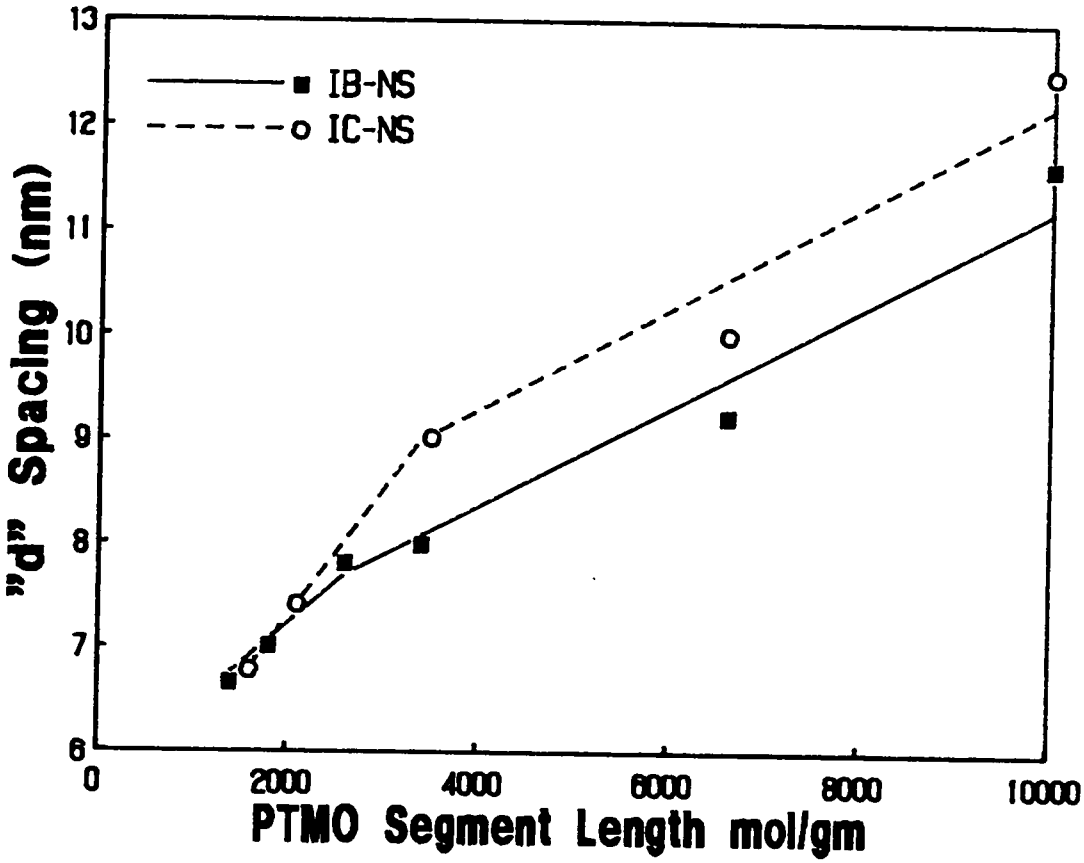

Figure 75. Relationship between the "d" spacing with the PTMO segment length.

stretch the interconnected PTMO soft segment in between. As the PTMO segment length decreases, the distance between two ionic hard segments decreases, and the strength of coulombic force increases thereby promoting this "stretching" effect. Since the hard segments in these ionenes are the single unit hard segments, the interdomain spacing of a fully stretched polymer chain ("ds") can be calculated by adding the length of hard segment to the length of a fully stretched PTMO soft segment. The values of "d" and "ds" of IB-NS and IC-NS series show that the ratio between the "ds" and "d" increases with an increase of the PTMO segment length as expected (Table 16). These results support that the PTMO segments between the two ionic hard segments may be somewhat stretched due to the coulombic forces between the ionic hard segments.

The conformation change of the PTMO segments in these ionene elastomers could also cause some changes in the morphological texture of these materials. Figure 76 on page 225 shows the SAXS patterns of the IB-NS series obtained by use of the pinhole Warhus camera. The X-ray beam was imposed on the x-direction illustrated as Figure 69 on page 208. As the PTMO segment length increase from 1,800 to 3,400, the azimuthal dependence disappears as well as the multi-order scattering. There is no azimuthal dependence observed on samples having PTMO segment length greater than 6,600. When the X-ray beam is perpendicular to the film surface (z-direction), similar ring patterns are obtained for all the IB-NS samples. Of course, the multi-scattering disappears with the increase of PTMO segment length in the same manner as shown in Figure 76 This behavior suggests that as the volume fraction of ionene hard segments decreases to a low percentage, the ionic domains are distributed more randomly, and there is no long range order maintained. The loss of the azimuthal dependence also indicates the possible change in the morphological texture from a rod-like structure to a spherical domain structure.

Figure 77 on page 227 shows the side view morphological texture of sample IB-NS-34. The domain structure is more like a spherical domain in a polymeric matrix rather than a pure rod-like structure as observed in sample IB-NS-18. Due to the loss of long range ordered structure, it is also difficult to interpret the morphological texture of this sample from TEM results because of the random distributed domains (recall section 6.2.1). For the samples having the

Table 16. Calculated and measured "d" spacing of IB-NS and IC-NS ionene elastomers.

Sample	"ds" nm	"d" nm	"ds"/"d"
IB-NS-14	12.97	6.64	1.95
IB-NS-18	16.43	7.00	2.35
IB-NS-26	23.34	7.81	2.99
IB-NS-34	30.26	7.98	3.79
IB-NS-66	57.93	9.22	6.28
IB-NS-100	87.32	11.61	7.52
IC-NS-21	19.02	7.40	2.57
IC-NS-35	31.13	9.00	3.46
IC-NS-66	57.93	10.00	5.79
IC-NS-100	87.32	12.50	6.99

* "d" is measured from smeared SAXS profiles obtained by Kratky camera.

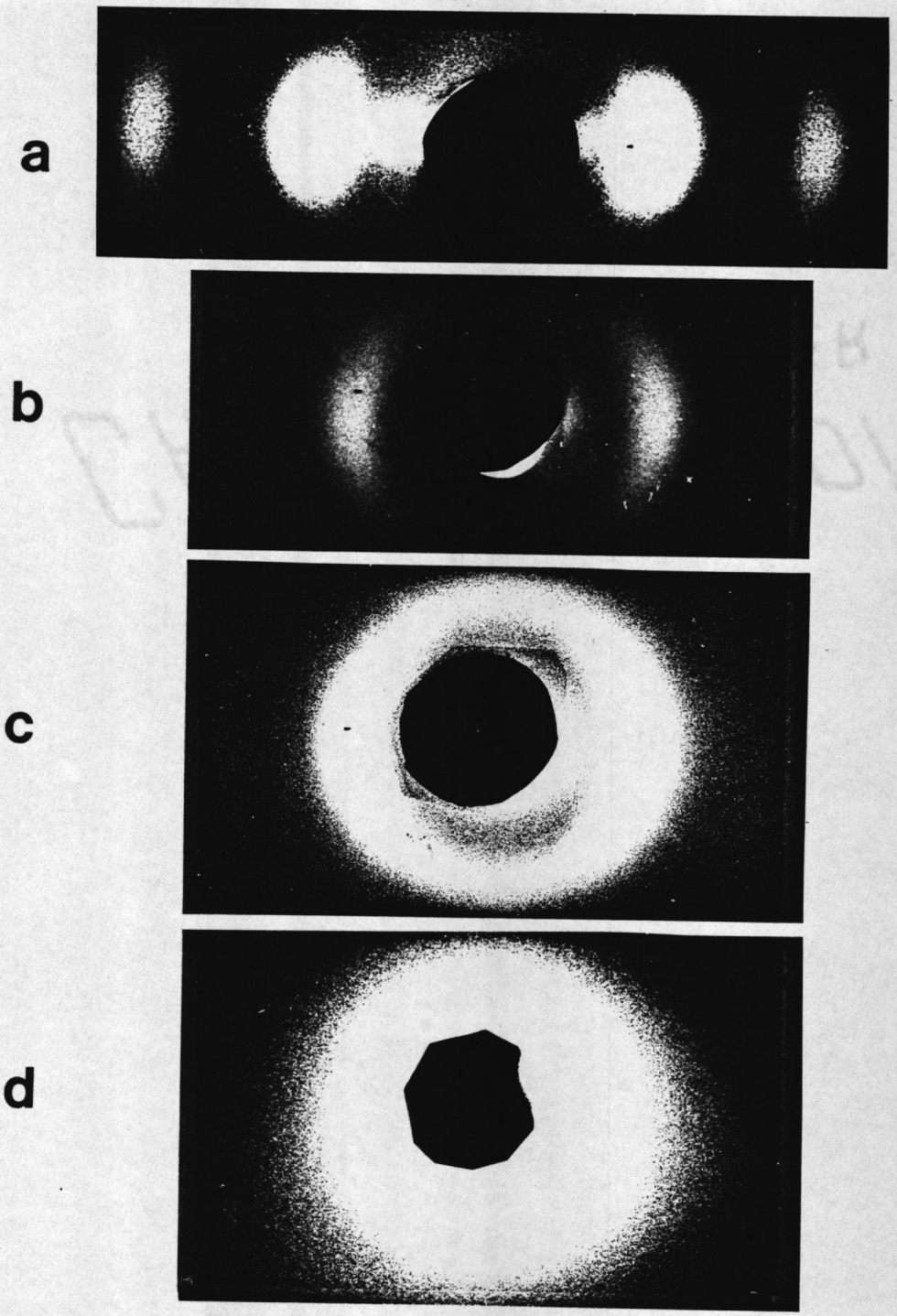

Figure 76. Side view SAXS patterns of the IB-NS ionene elastomers obtained from the Warhus camera: (a). IB-NS-18. (b). IB-NS-26. (c). IB-NS-34. (d). IB-NS-66.

PTMO segment length longer than 3,400, the TEM micrographs look like phase contrast pictures and no useful information can be obtained.

6.2.4. Effect of the Type of Counter Ion and Hard Segment Architecture

When the type of counter ion or the hard segment architecture changes, the ionic association in the ionene elastomers will be changed. Thus the morphology of the ionene polymers is expected to be altered. The effect of the counter ion or the hard segment architecture is shown in Figure 78a. The ionene elastomers with bromide ions have a much higher scattering intensity than the chloride ionene due to the higher electron density of the bromide ions thereby providing a higher contrast factor. The first order scattering peaks of samples with bromide ions are also much narrower than for the chloride ionene, which suggests the ionic domains in the IB ionene elastomers may well be distributed more regularly in the matrix than for IC-NS-34. As shown in Table 16 on page 224, the value of "ds"/"d" for sample IC-NS-34 is smaller than IB-NS-34. In fact the value of "ds"/"d" for all IC-NS samples are smaller than for the IB-NS samples with similar PTMO segment length. This suggests that the PTMO segments in IC-NS series are more stretched than in the IB-NS series due to stronger repulsive coulombic forces caused by the Cl^- counter ions. Figure 78a also shows that there is a second scattering peak shown in the SAXS profile of IB-NS-34, while there is no such peak within the profile of IB-S-34. This indicates that when a spacer group is added into the hard segments, and the ionic domains become more randomly distributed.

For the 66 series which has a PTMO segment length of 6,600 but with different counter ions or hard segments, the situation is slightly different. As shown in Figure 78b, the ionene elastomers with spacer groups in their hard segments have narrower scattering peaks than the samples without spacer groups. The ionene with iodide counter ions, II-NS-72, has the highest scattering intensity because of the high electron density of iodide ions.

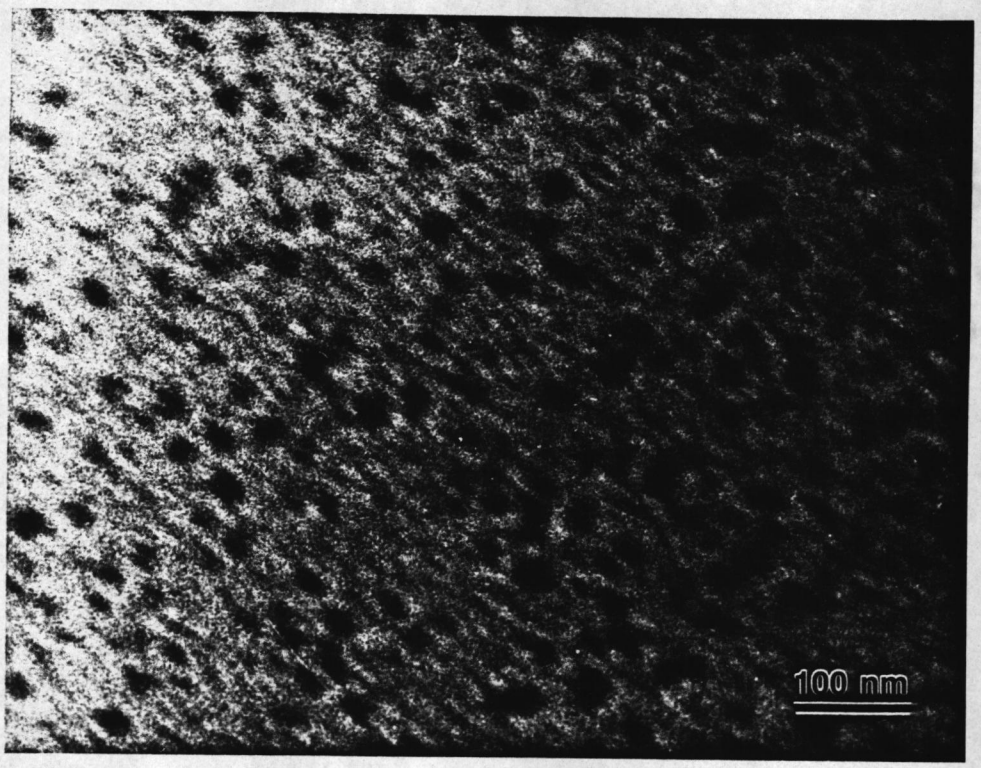

Figure 77. TEM micrograph of sample IB-NS-34.

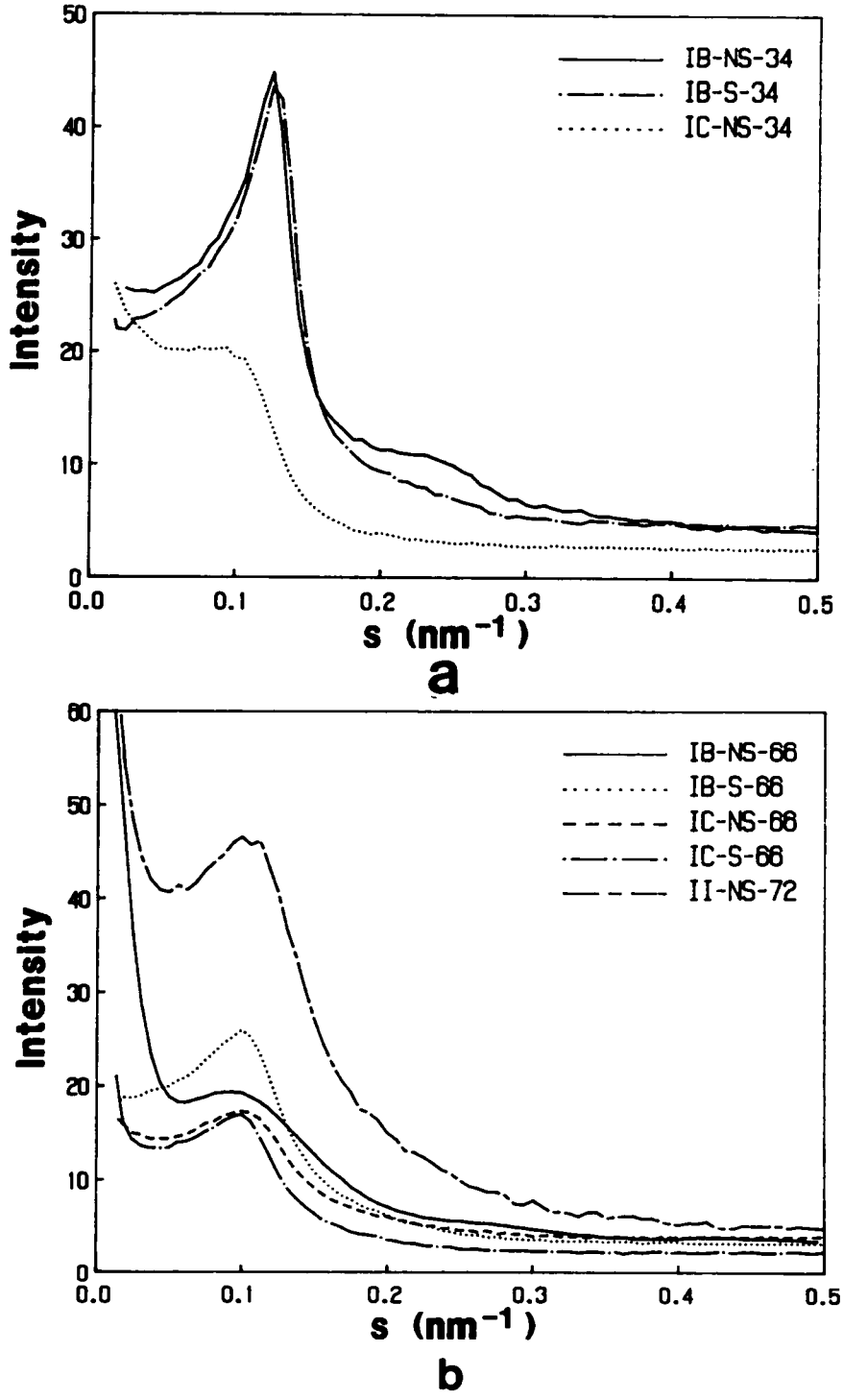

Figure 78. Effect of counter ion and hard segment architecture on the SAXS profiles of the ionene elastomers: (a). SAXS profiles of the 34 series. (b). SAXS profiles of the 66 series. The SAXS profiles are obtained from the Kratky camera.

6.2.5. Summary

It has been illustrated for the first time that direct observation of the microphase separation induced in such segmented ionene polymers can be obtained by using transmission electron microscopy. The microstructure observed by TEM is quite well in line with the interpretation of the SAXS results. Although, in view of potential line broadening features of the SAXS data, one is unable to unequivocally specify that the morphological texture is either lamellar versus that formed by a hexagonal array of cylindrical ionene domains. However, the latter model is favored for reasons that have been discussed.

It should be pointed out that the morphological texture observed in the ionene materials can be influenced by the solution casting procedure although this has not been discussed in great detail within this section. Specifically, as the PTMO segment length increases, which reduces the volume fraction of the ionene component, the distinct morphological texture can no longer be directly observed by TEM and the azimuthal dependence of the SAXS intensities for the side view profiles disappears systematically. This suggests that as the volume fraction of the ionene component decreases to very low percentages, there is no further long range order maintained but a more random distribution of the ionic domains occurs.

The type of counter ion and the hard segment architecture has some influence on the morphological texture of ionenes. In general, as the size of counter ion increases, the ionic domains distribute more uniformly in the matrix. Depending on the PTMO segment length, the effect of a spacer group is different. In the samples with shorter PTMO segments, the domains distribute more randomly for the sample with spacer groups in the hard segment as might be expected. For the samples with long PTMO segments, the samples with spacer groups seem to posses a narrower distribution of interdomain spacings (sharper SAXS peaks).

6.3. STRUCTURE-PROPERTY BEHAVIOR OF PTMO-DIPYRIDINIUM IONENE ELASTOMERS

Another type of PTMO based ionene elastomer investigated in this study was the PTMO-dipyridinium ionenes prepared by the coupling reaction of "living" polytetrahydrofuran dioxonium ions with either 4,4'-bipyridine or 1,2-bis(4- pyridinium) ethylene as shown in Figure 52 on page 169[22]. In this section, the details of the structure-property behavior of these PTMO-dipyridinium ionenes (IS ionenes) are discussed in detail.

6.3.1. Thermal and Mechanical Properties

6.3.1.1. Thermal Stability and Thermal Processibility

The thermal stability of these IS ionenes is illustrated by the TGA thermograms shown in Figure 79a. The initial decomposition temperatures of the IS-BP and the IS-BPE ionene elastomers all exceed 220°C and are clearly dependent on the ionic content[22]. At ca. 290°C, a primary catastrophic weight loss starts and this weight loss is due to the decomposition of the PTMO segments, and the secondary weight loss occurs at ca. 400°C which is the dissociation of the quaternary ammonium compounds[22]. Figure 79a also shows that there is no weight loss of the BPE based ionene until 300°C. The good thermal stability of the IS-BPE sample compared with the IS-BP sample is believed to be at least partially due to the charge separation of two single positive charges in the hard segment. The further apart of these charges are, the more stable the polymer will be[22]. For comparison, the TGA curve of sample IB-NS-18 has been plotted along with the IS ionene polymers. The initial weight loss of the IB-NS-18 at 200°C is believed due to the partial decomposition of the PTMO segments following depolymerization. However, the major weight loss of IB-NS-18 is about 100°C higher than for the IS samples.

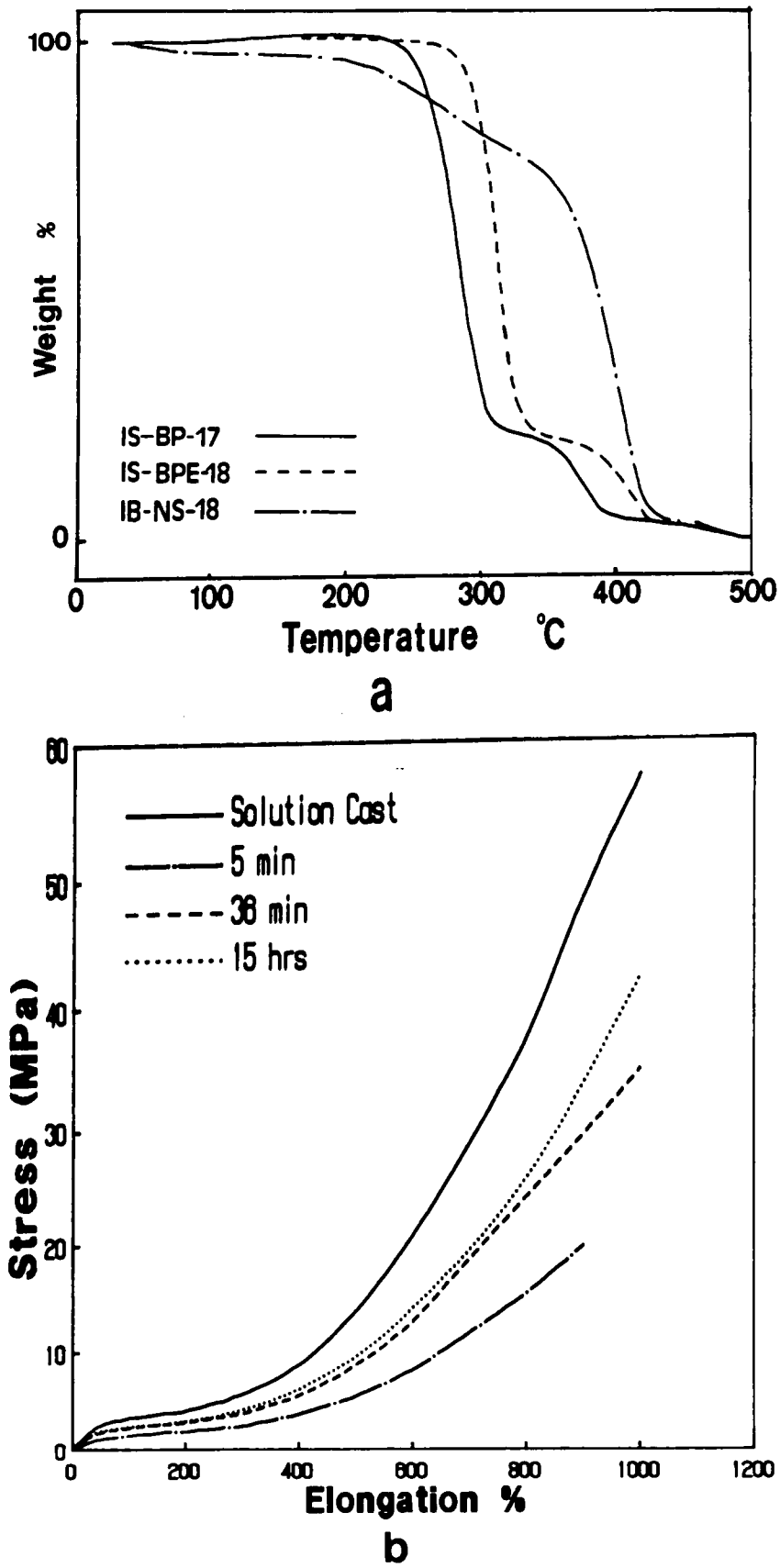

Figure 79. Thermal stability and processibility of the PTMO-dipyridinium ionene elastomers: (a). TGA thermograms of the PTMO-dipyridinium ionene elastomers. (b). Stress-strain behavior of thermally molded film of IS-BP-25.

Unlike the PTMO-dihalide ionenes, the PTMO-dipyridinium ionenes have a reasonably good thermal processibility which is demonstrated by Figure 79b. A film was thermally pressed at 220°C for 5 minutes, then the film was cooled down to 65°C and stored in a vacuum oven. The stress-strain results indicate that the film recovers some of its initial mechanical properties 5 minutes after molding. Thirty six minutes after molding, the tensile strength of the film was over half of the value of the solution cast film of the same sample. Fifteen hours after molding, the tensile strength of the molding film reaches about 3/4 of the tensile strength of the solution cast film. It is recalled that the PTMO-dihalide ionenes can not be thermally processed (see Figure 60 on page 187). The different behavior of the PTMO-dihalide ionenes and PTMO-dipyridinium ionenes may be due to their chemical structures. Another interesting feature is the time dependent recovery process of the IS ionene polymer. This might be caused either by a slow repolymerization process or a possible reforming of ionic domains from melt. Due to the limited amount of the material, no further investigation on the thermal recovery behavior of the IS materials has been done. However, this recover behavior is very critical for applications of these materials, further investigations are needed.

6.3.1.2. Mechanical Properties of the IS Ionene Elastomers

The stress-strain behavior of the solution cast IS ionene films is shown in Figure 80 on page 234. Similar to the PTMO-dihalide ionenes, these IS ionenes also exhibit excellent elastomeric properties except for samples IS-BP-6 and IS-BP-8. This good elastomeric behavior is, again, due to the strong ionic interactions in these materials. As the ion content increases, the modulus as well as the stress level at a given elongation increases. When the elongation exceeds 700%, the higher stress level at a given elongation is higher for the samples with longer PTMO segments which is due to the strain induced crystallization of the PTMO segments. The longer PTMO segments will have a higher degree of induced crystallinity which results in a higher stress level of the sample (recall the discussions in section 6.1.1.1 and 6.1.1.3). The poor mechanical properties of

IS-BP-6 and IS-BP-8 are believed due to the relatively low molecular weight of these polymers[22]. During the synthesis, the termination process is much more rapid for the ionene with shorter PTMO segments due to the higher concentration of ionic species. Therefore, the molecular weight of the final polymer is likely lower[22].

The network stability of these PTMO-dipyridinium ionenes has been demonstrated by the creep behavior of these materials. As shown in Figure 81a, the compliance level of these materials does change with the ionic content and the hard segment architecture. The very low network stability of IS-BP-13 may be due to the low molecular weight of this sample. This again indicates that the ionic clustering in these materials may not sustain a load for long times. For the samples with longer PTMO segments, the long term network stability has been improved drastically (Figure 81b). It is speculated to be due to the chain entanglements effects caused by higher molecular weight of theses sample (refer to Section 6.1.2.). Also, the BP series have a better network stability than the BPE series, which may be due to the stronger ionic associations in the BP series.

6.3.1.3. Thermal Properties of the IS Ionene Elastomers

Figure 82 on page 237 shows the DSC spectra of the IS-BP and the IS-BPE ionene polymers. Similar to the PTMO-dihalide ionene elastomers, three transitions are observed in these spectra: the T_g transition (ca. -80°C), the crystallization (ca. -50°C) and melting peaks (ca. 5°C) of the PTMO segments. For the IS-BP series, the T_g of the PTMO soft segment systematically decreases as the ionic content decreases. This may be due to the anchoring effects on the soft segment by end group restrictions[22]. As the soft segment length between two ionic domains (anchoring points) increases, the chains become more mobile and the T_g shifts to a lower temperature. Depending on the PTMO segment length, the crystallization temperature (T_c) of the PTMO segments increases greatly as the PTMO segment length decreases. The change in T_c could also be due to the PTMO chain mobility. As the PTMO segment length increases, the

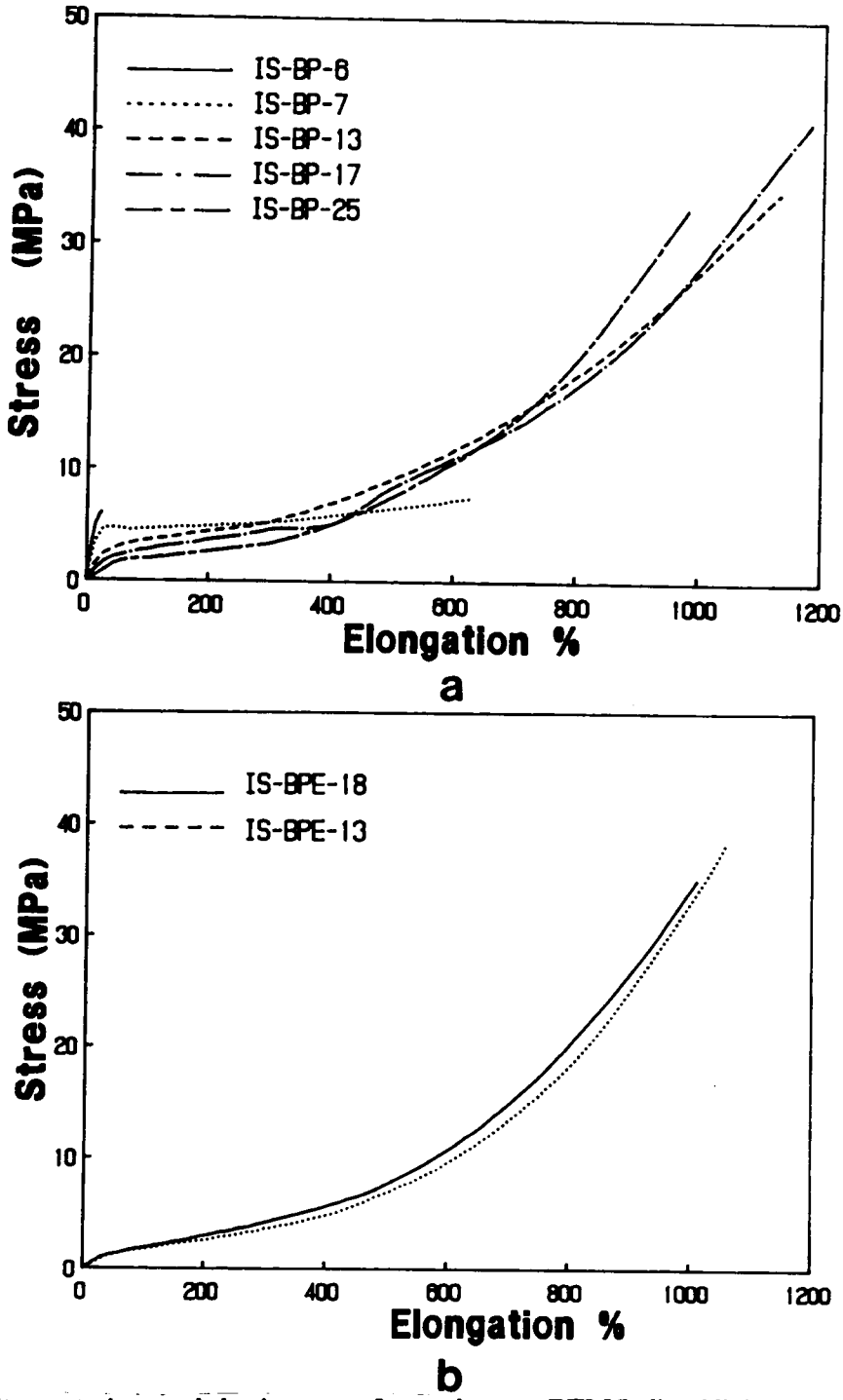

Figure 80. **Stress-strain behavior of the PTMO-dipyridinium ionene elastomers:** (a).Stress-strain behavior of the IS-BP series. (b). Stress-strain behavior of the IS-BPE series.

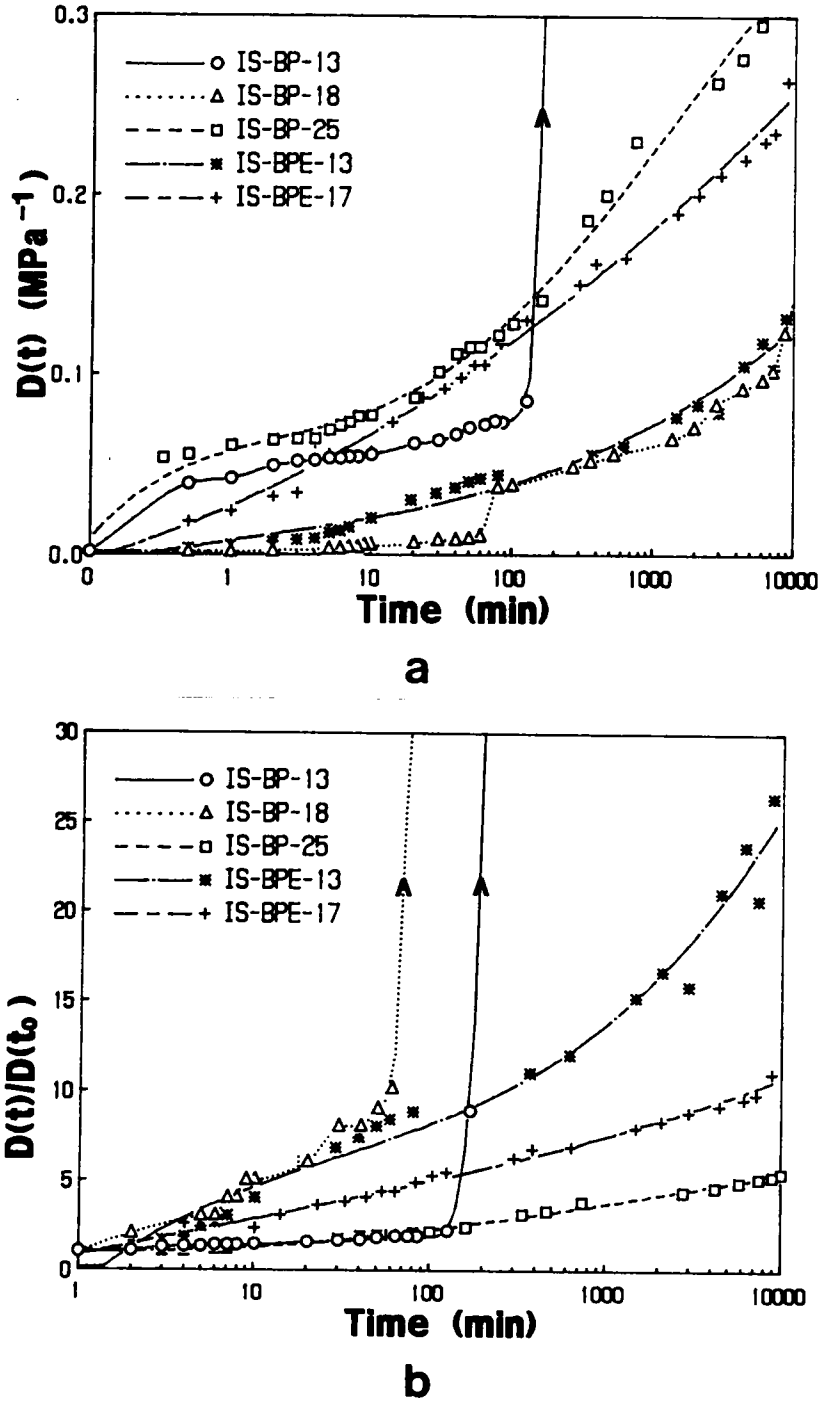

Figure 81. **Creep behavior of the PTMO-dipyridinium ionene elastomers:** (a).Creep behavior of the IS ionene elastomers. (b). Normalized creep behavior of the IS ionene elastomers.

PTMO segments become less restricted and could be crystallized at a lower temperature. Thus, the T_c shifts to a lower temperature. However, the melting temperature only decreases slightly as the PTMO segment length decreases. There is no crystallization - melting behavior observed for samples IS-BP-6 and IS-BP-8 because of their very short PTMO segments.

6.3.1.4. Dynamic Mechanical Behavior of the IS Ionene Elastomers

The dynamic mechanical spectra of the IS ionene elastomers are shown in Figure 83 on page 239. For the IS-BP series, the spectra are similar to those of the IB-NS series (recall Figure 59 on page 184). Four transitions, γ, α, β_1, and β_2, are observed. Again, the γ transition is due to the movements of coupled methylene units in the PTMO backbone which indirectly suggests a high degree of phase separation occurs in these materials. In fact, the SAXS analysis indicates the degree of phase separation in the IS-BP series is also even higher as in the IB-NS series based on the Porod analysis of the tail region of the SAXS profiles and the calculations of the interphase thickness[121]. As mentioned in section 6.2, the IB-NS systems already have a very high degree of phase separation based on the SAXS analysis. However, the IS-BP systems have a more flattened tail region and narrower interphase than the IB-NS systems which suggests a even higher degree of phase separation. The α transition is the glass transition of the PTMO segments, and β_1 is caused by the crystallization and melting of the PTMO crystallinity. The fourth transition, β_2, is again due to the mysterious modulus "jump". Similar to the IB-NS ionene elastomers, the amplitude of the "jump" increases as the ionic content increases. However, the "jump" temperature (T_j) of the IS-BP series is about 20°C lower than for the IB-NS series. Also, the T_j of the IS-BP series changes with the PTMO segment length. As the PTMO segment length increases, T_j is higher, but the amplitude of the "jump" is lower. By careful inspection of the DSC and DMA data, the author has noticed that the difference between the T_m and the T_j is ca. 34°C. This number has no physical significance, but it is a indication between the "jump" and the T_m. More details on the modulus "jump" will be given in section 6.4.

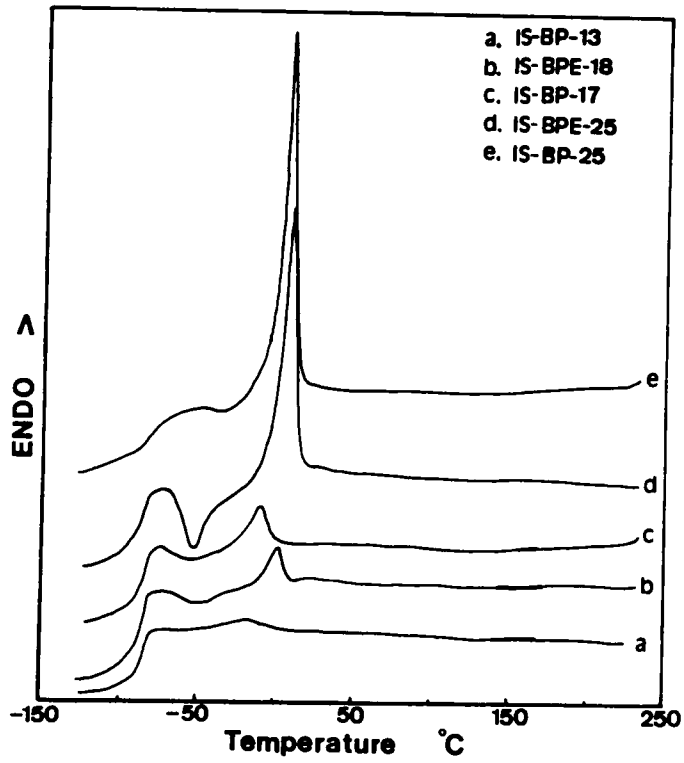

Figure 82. DSC thermograms of the PTMO-dipyridinium ionene elastomers.

As shown in Figure 83, the IS-BP ionene elastomers do not soften up to 200°C which is a much higher temperature then observed for the IB-NS ionene elastomers (ca. 170°C). Clearly, the higher softening temperature of the IS-BP materials suggests a broadened usage temperature range.

The DMA spectra of the IS-BPE series are similar to the IS-BP series at lower temperatures (< 0°C, see Figure 83b). However, there is almost no modulus "jump" observed for IS-BPE-18 and IS-BPE-25. Although, there is a sign of the "jump" for IS-BPE-13. The β_2 transition which relates to the "jump" is also recognizable within the tanδ spectrum of IS-BPE-13. Another major difference between the IS-BP and the IS-BPE ionene elastomers is the softening temperature. The softening temperature of the IS-BPE series is ca.125°C while the softening temperature of the IS-BP series is well in of excess 200°C. This apparently is due to the changes in the strength of the ionic association caused by the hard segment architecture. In the IS-BPE ionene elastomers, the ionic association could be weakened by introducing two methylene units in the hard segments, thus the interchain interaction will be weakened and the softening temperature reduced.

Figure 84 on page 240 shows the thermomechanical properties for IS-BP-17, IS-BPE-18, and IB-NS-18. Within the TMA spectra, the transition at -70°C is due to the glass transition of the PTMO segments. The transition at ca. 10°C is due to the melting of the PTMO crystallites which causes an expansion in volume. The last transition occurs within a temperature range from 130°C to 220°C. This is due to the softening of the ionene elastomers. It clearly shows that sample IS-BP has the highest softening temperature, while IS-BPE has the lowest. This is consistent with the DMA results. The TMA results also show that the IS-BP ionene has a much higher softening temperature than the IB-NS ionene even though the decomposition temperature of the latter is much higher than the former (recall Figure 79 on page 232).

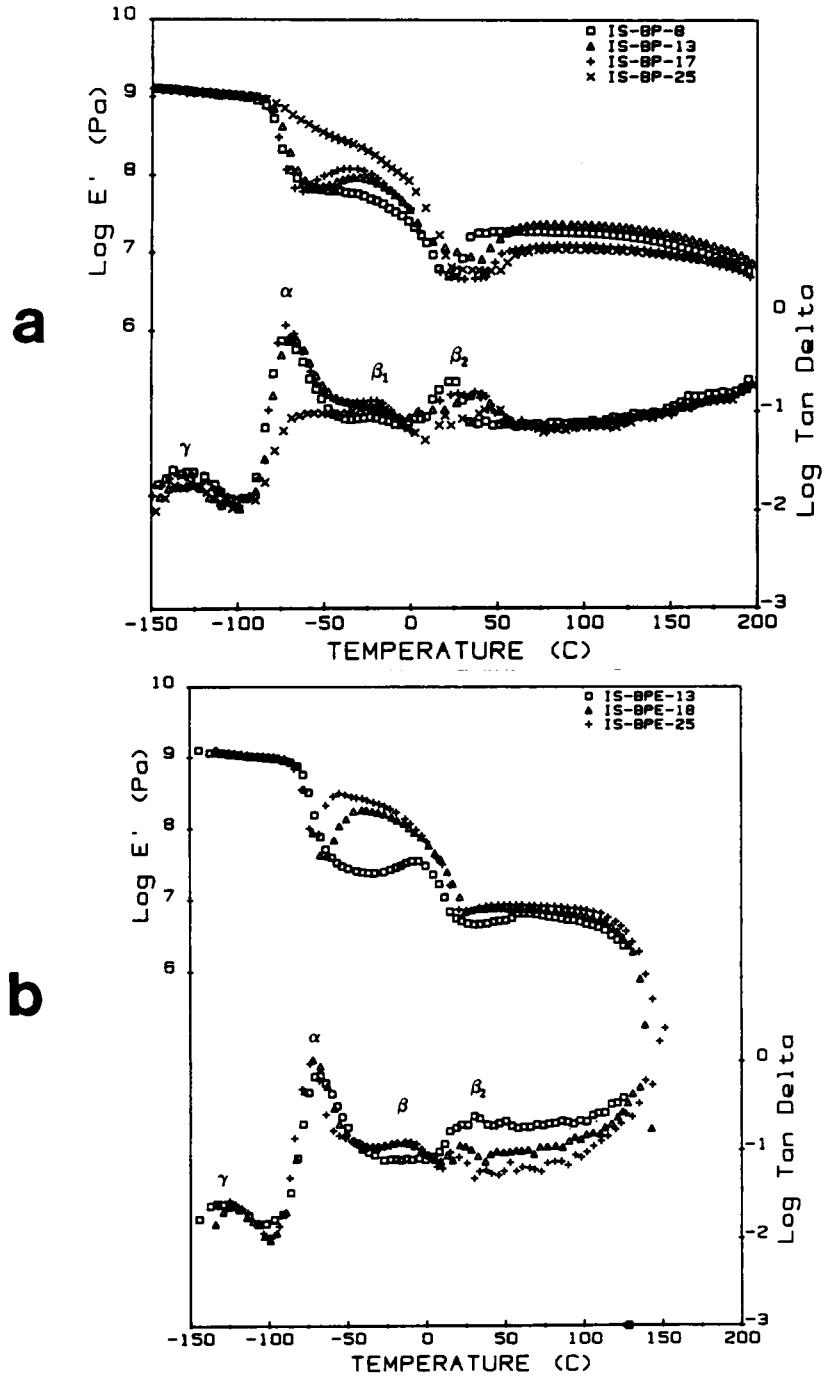

Figure 83. Dynamic mechanical spectra of the IS-BP ionene elastomers: (a). the IS-BP series. (b) the IS-BPE series.

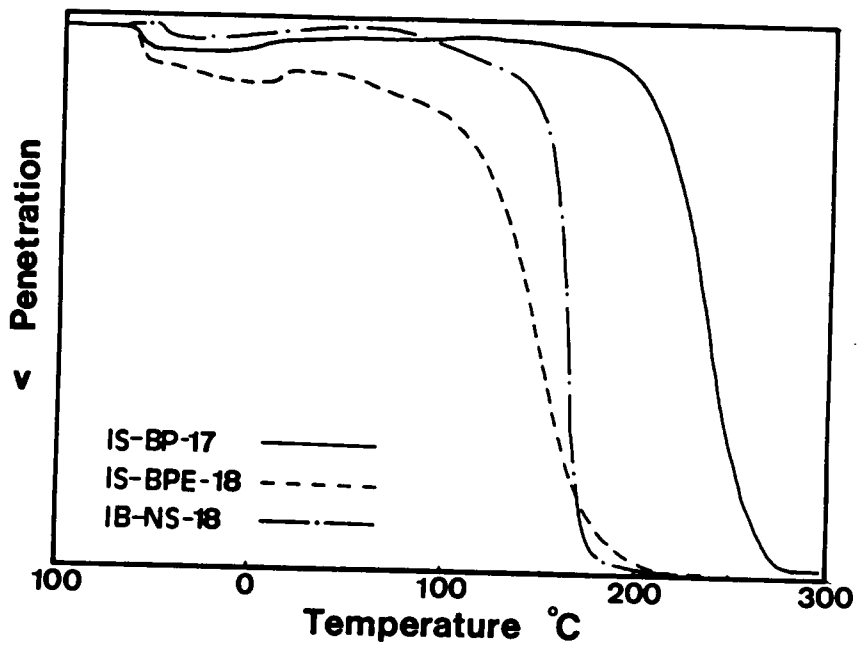

Figure 84. Thermomechanical behavior of the ionene elastomers.

6.3.3. Morphological Texture of the IS Ionene Polymers

6.3.3.1. SAXS Results of the IS Ionenes

Figure 85 on page 242 shows the SAXS profiles of the IS-BP ionene polymers. There is a broad scattering peak in the SAXS profile for all samples. The broadness of the peaks changes with PTMO segment length. Samples IS-BP-6 and IS-BP-8 have much narrower peaks than the other IS-BP ionene elastomers. The narrow scattering peaks of samples IS-BP-6 and IS-BP-8 may be due to the lower molecular weight of these polymers. Hashimoto et. al. [36] have reported that the scattering peak of a diblock polymer becomes narrower and more distinct when the molecular weight of the system decreases. The low molecular weight assumption is indirectly supported by the much poorer mechanical properties of these two samples. Another possible explanation is the molecular weight distribution of the PTMO soft segments. The broadness of the SAXS scattering peaks is also dependent on the PTMO segment molecular weight distribution which causes a distribution in the "d" spacing. As the PTMO segment molecular weight distribution increases, the "d" spacing distribution increases, thereby, the scattering peak becomes broader. The PTMO soft segments in samples IS-BP-6 and IS-BP-8 may have a narrower molecular weight distribution than in other samples, therefore, the scattering peaks of these two samples are narrower than the others.

Another interesting feature of the SAXS profiles of IS-BP series is that the "d" spacing increases as the PTMO segment length decreases for samples IS-BP-13, IS-BP-17, and IS-BP-25. This behavior seems very strange at the beginning because if the scattering peak was caused by the interdomain scattering, one would expect that the "d" spacing would decrease with the increase of the PTMO segments. One explanation for this behavior is chain extension.

It is well known that the solution behavior of polyelectrolytes and aliphatic ionenes influenced by chain extension features dictated by charge repulsion[77,81]. For example, in a non-polar solvent, the charges on the backbone of an aliphatic ionene can lead to a strong repulsion between segments which causes the polymer to extend resulting in a solution viscosity increase. When the concen-

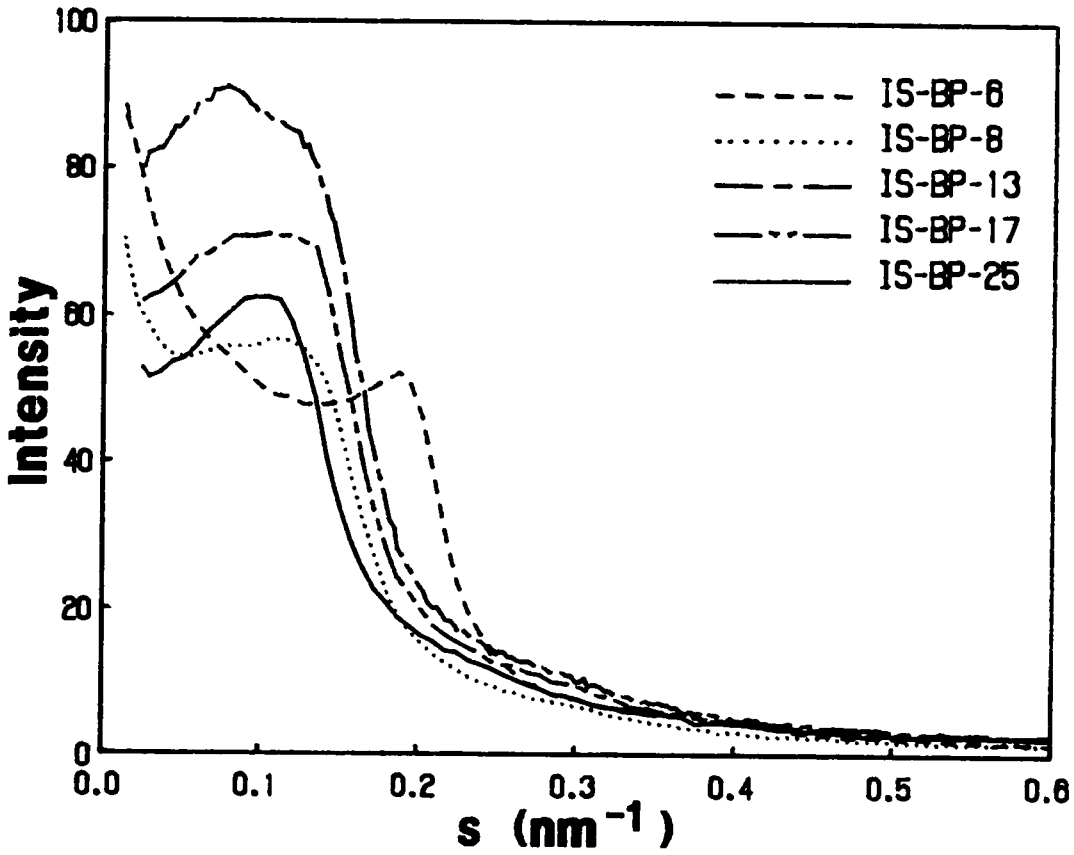

Figure 85. SAXS profiles of the IS-BP ionene elastomers.

tration of the polymer decreases, the positive charges in the ionene backbone became less shielded by the negative counter ions, thus, the chain becomes more extended. In the IS ionene elastomers, there are should be strong coulombic forces between ionic hard segments. Due to these coulombic forces, the ionic hard segments are attracted each other to form ionic domain, therefore, the PTMO segments between the hard segments could be stretched. If this is the case, when the PTMO segment length decreases, the ion content increases which results in more stronger coulombic forces. Therefore, PTMO segments may become more even stretched. By assuming the ionene moieties are linked by "fully stretched" PTMO segments, the "ds" of the IS-BP and the IS-BPE series has been calculated and listed along with the measured "d" from the SAXS profiles in Table 17 on page 244. Based on these data, it is suggested that the PTMO segments in these PTMO-dipyridinium ionenes are highly stretched, although the author finds this rather surprising. The SAXS results in Figure 86 on page 245 shows that the "d" spacings of the IS-BPE series is always greater then for the IS-BP series as expected. Because the hard segments in the IS-BPE series are longer than in the IS-BP series. The chain extension assumption not only can be used to support the increase of "d" spacing with PTMO segment length, but it also can help to explain the modulus "jump" as will be discussed in section 6.4.

The SAXS patterns of the IS-BP ionene polymers have also been obtained using the Warhus camera. Figure 87 on page 246 shows the SAXS patterns of sample IS-BP-25. These SAXS patterns are taken with the X-ray beam perpendicular and parallel to the film surface (x and z directions in Figure 69 on page 208). The "ring patterns" have been obtained on both directions. There is no second order scattering rings observed even with long exposure time nor is there any azimuthal dependence observed for the IS-BP ionene samples as was noted for the SAXS patterns of the IB-NS ionene polymers (recall Figure 76 on page 225). The lack of azimuthal dependence suggests that the morphological texture of these polymers is more likely dispersed domains rather than the long rod-like structures. Of course, the lack of long range ordered structure or random oriented rod-like structure would also eliminate the azimuthal dependence.

Table 17. Interdomain spacings of IS-BP and IS-BPE ionene polymers.

Sample	"ds" nm	"d" nm	"ds"/"d"
IS-BP-13	12.01	12.30	0.98
IS-BP-17	15.47	12.30	1.26
IS-BP-25	22.34	9.90	2.26
IS-BPE-13	12.22	14.30	0.85
IS-BPE-18	16.55	15.30	1.08
IS-BPE-25	21.61	12.30	1.76

* The hard segment length is estimated as 0.96nm for BP and 1.18nm for BPE.

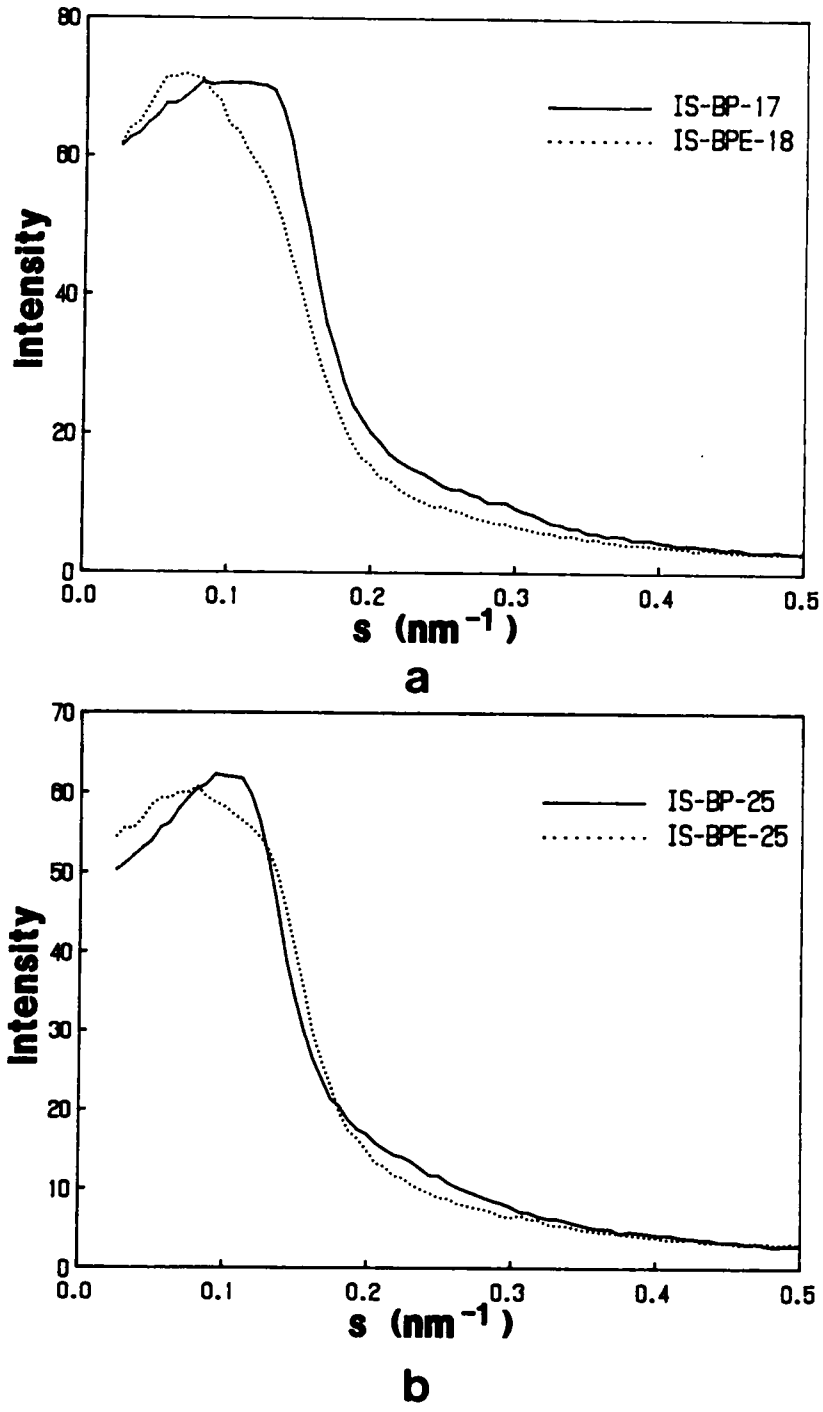

Figure 86. **SAXS profiles of the IS-BP and the IS-BPE ionene polymers:** (a). SAXS profiles of IS-BP-17 and IS-BPE-18. (b). SAXS profiles of IS-BP-25 and IS-BPE-25.

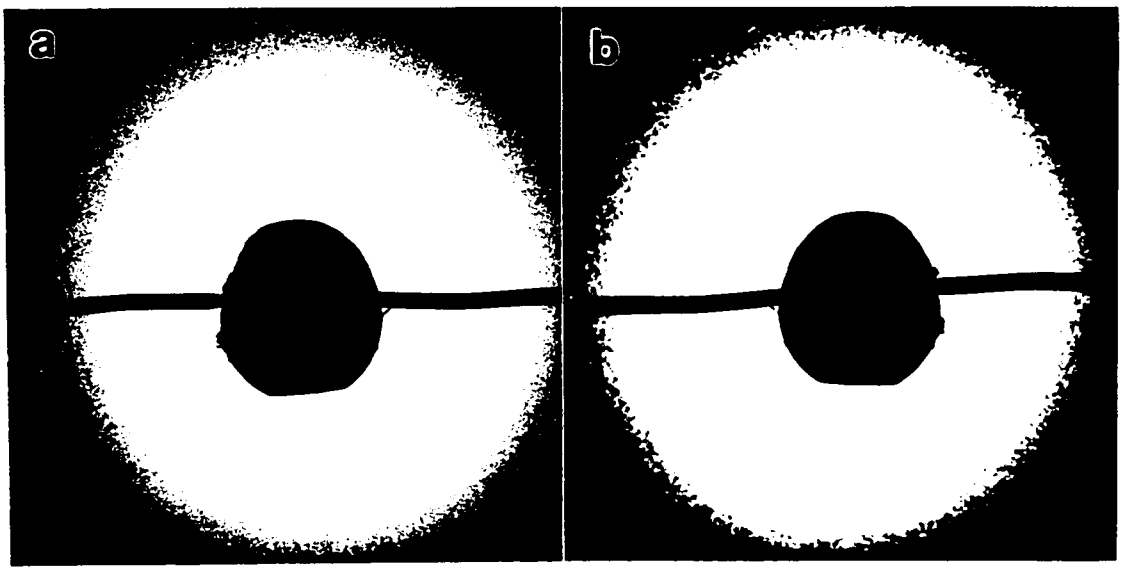

Figure 87. SAXS patterns of sample IS-BP-25: (a). X-ray beam is normal to the film surface. (b). X-ray beam is parallel to the film surface.

6.3.3.2. TEM results of the IS-BP-25

Some TEM studies have also been conducted on sample IS-BP-25 which had the sharpest SAXS scattering peak. Figure 88 on page 248 shows the side view micrograph of sample IS-BP-25. Only what may be spherical domains are observed. This micrograph appears somewhat like a phase contrast micrograph. However, the defocusing analysis indicates that the image is not produced by phase contrast. The top view and other side view micrographs are also similar to the micrograph shown in Figure 88, which again suggests dispersed domains rather than rod-like structures. The interdomain spacing measured from the micrograph is in the range of ca. 10nm which is in agreement with the SAXS results. The micrograph also shows that the domain size is not uniform and the domains are not ordered. This would support the observed broadness of the SAXS scattering peak.

6.3.3.5. Other properties

Several interesting features have been observed in the IS ionene elastomers. One of these is their photochromic property. When a methanol cast film of IS-BP polymer is exposed to light for a period of time (several weeks), the clear film will change to a brown color even though the film was stored in a vacuum desiccator during the exposition period. After recasting the film from methanol, the color will disappear, and the color will be regained if the film is exposed to light again. It also has been found that the modulus "jump" disappears for these colored ionene films. After recasting, the "jump" appears again. When the film is cast from acetone, the result is totally different. The photochromic effect disappears. Also the modulus "jump" remains unchanged. The photochromic behavior has been observed for the IS-BP ionene elastomers only!

The photochromic phenomenon was not a major focus of this study, therefore, no detailed study was undertaken. However, these properties are worth pointing out for possible interest as future investigations.

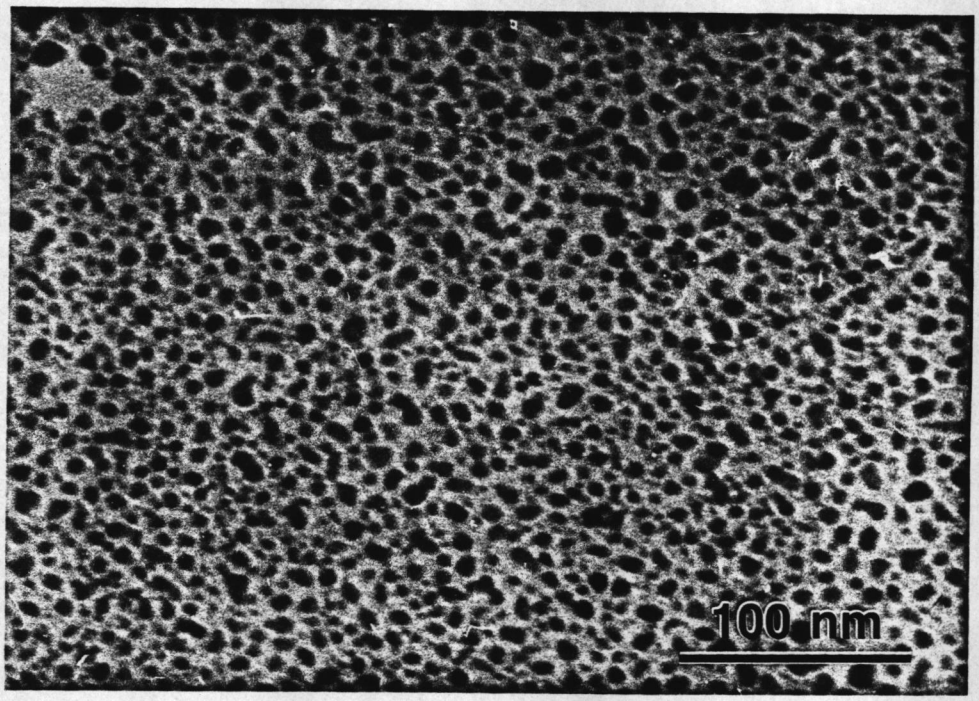

Figure 88. Side view TEM micrograph of sample IS-BP-25.

6.3.3. Summary

The general structure-property behavior of PTMO-dipyridinium ionene elastomers is very similar to the PTMO-dihalide ionene polymers. However, the IS-BP ionene polymers have a much higher softening temperature than the PTMO-dihalide ionene polymers. More importantly, the IS-BP ionene polymers can be thermally processed without total lost of properties. These may be due to a stronger ionic association existing in the IS ionenes than in the PTMO dihalide ionenes.

A reversible modulus "jump" is also observed for the IS-BP ionene polymers. The amplitude and the location of the "jump" varies with the ionic content. As the PTMO segment length increases or the ionic content decreases, the amplitude of the "jump" decreases, and the "jump" shifts to a higher temperature. Based on the DMA data of the IS-BP and the IS-BPE samples, the "jump" is also related to the hard segment architecture. When two methylene units are introduced into the hard segment, the "jump" almost disappears. This suggests that the "jump" may relate to a possible conformation change in the ionene segments.

The SAXS profiles of the IS ionene polymers contain a single broad scattering peak. No higher order scattering peaks have been observed nor any azimuthal dependence. This suggests that the ionic domains in these materials have varied spacing and have been more randomly distributed. Limited TEM results indicate that the domain structure in sample IS-BP-25 is of a dispersed spherical domain nature in a non-ionic matrix. No useful morphological information could be obtained from TEM studies on samples IS-BP-13 and IS-BP-25 because of the more randomly distributed domains which causes much broader X-ray scattering peaks in their SAXS profiles.

6.4. THE MYSTERIOUS MODULUS "JUMP" OBSERVED BY DYNAMIC MECHANICAL SPECTROSCOPY FOR THE IONENE ELASTOMERS

As discussed in previous sections, a very unusual reversible modulus "jump" (either E* or E') has been observed in the dynamic mechanical (DMA) spectra for both the PTMO-dipyridinium and the PTMO-dibromo xylene ionene elastomers. This modulus "jump" has been confirmed by stress-strain measurements at corresponding temperatures. To the author's knowledge, no such phenomenon has been reported in the literature. In this section, more experimental evidence will be presented, and a possible but highly speculative origin of this "jump" will be discussed. However, no definitive conclusion has yet been reached at this time. Further investigations are needed to achieve the solution and possible approaches will be considered.

6.4.1. Reversibility of the "Jump"

The modulus "jump" (referred hereafter as "jump" in the following discussion) was first observed in the DMA spectrum of sample IS-BP-25. In order to test the reversibility of the "jump", several DMA runs were carried out on a specimen of IS-BP-25 and the results are shown in Figure 89 on page 252. In the first run, the specimen was cooled to -150°C and then DMA measurements were made from -150°C to 150°C. After the first run, the specimen was cooled to 20°C inside the Rheovibron under a dry nitrogen flow over 4 hours. Then the specimen was further cooled down to 0°C and the second run was carried out from 0°C to 90°C.. After the second run, the specimen was taken immediately from the Rheovibron and stored in vacuo at 25°C for 24 hours. The same specimen was quickly loaded into the Rheovibron and tested again from -150°C to 90°C for the third time. After the third run, the sample was cooled to 25°C and held for 4 hours inside the Rheovibron under a nitrogen atmosphere, and then the fourth run was carried out form

25°C to 90°C. As Figure 89 shows, the results of these runs are almost identical which proves that the "jump" is highly reversible. Similar results have been also obtained for sample IB-NS-18.

6.4.2. Effect of Water Adsorption

At the beginning, the reversibility of the "jump" was considered to be from a water adsorption - desorption processes. In general, ionene polymers are hydrophilic and can adsorb moisture easily. Some ionene polymers with high ionic content such as IB-NS-14 and IS-BP-6 can even dissolve in water. The water molecules will act as a plasticizer in the ionene polymer and reduce the modulus. At elevated temperature, the water will be desorbed and the modulus will rise. A TGA moisture adsorption test was therefore carried out on sample IS-BP-25 and the results showed that the amount of water adsorbed is ca. 0.7 wt% over a period of 4 hours in the laboratory environment where the relative humidity was about 40-50% at 25°C. Therefore, it appears impossible for sample IS-BP-25 to adsorb a sufficient amount of moisture if the sample is in a bone dry nitrogen atmosphere for the same time period! Thus, the "jump" shown in the fourth run, at least, can not in anyway be caused by the moisture desorption.

A further test for water adsorption was carried out on sample IS-BP-13. In this test, a film of IS-BP-13 was immersed into water for 1 hour before the DMA measurement. The film was found to contain 10.3 wt% water and was designated as IS-BP-13-W. The DMA measurement was carried out from -150°C to 200°C without nitrogen flow to avoid drying in the low temperature range. The DMA results of the IS-BP-13-W are shown in Figure 90a along with the DMA results of IS-BP-13 and IS-BPE-13. These results show that the sample IS-BP-13-W has a lower softening temperature than IS-BP-13 which is believed due to the plasticizer effect of water molecules in the ionene. However, the "jump" in this sample still remained and, with a similar magnitude. If the "jump" was caused by the water, the "jump" magnitude of IS-BP-13-W would be expected to be much higher than IS-BP-13 because of the much higher water content. Also, if the water have been adsorbed by the ionene polymer, it would be very difficult to desorb due to the strong

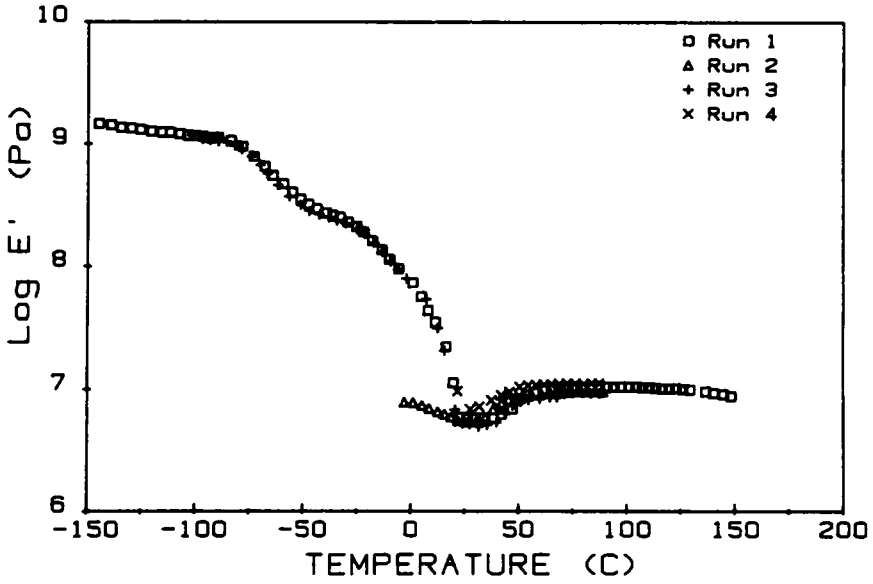

Figure 89. Reversibility of the modulus "jump".

interaction between the ionic species in the ionene polymer with polar water molecules. TGA experiments were also carried out the "wet" and "dry" samples of the IS-BP-13 at the same condition as the DMA measurements except for the temperature range. In this case, the "wet" sample was soaked in water for four hours, and then air dried at 25°C with the relative humidity of 35% for 24 hours. After drying, the water content of the "wet" sample was 11.2 wt% As Figure 90b shows, the weight of the "wet" sample was lost gradually from 25°C to 60°C, and the weight loss of the "wet" sample was only 1.0 wt%! There is no change in the sample weight from 60°C to 240°C until the polymer started to decompose. These results indicate that most of the adsorbed water can not be desorbed until the polymer decomposed. Due to the presence of water, the ionic association in the ionene elastomer would be expected to be lower which results in a lower softening temperature of IS-BP-13-W as shown in Figure 90a. If the water were removed, the softening point of IS-BP-13-W would be expected to be higher and close to the softening point of IS-BP-13. Yamashita et. al[18] reported that the modulus and tensile strength of a PTMO-dichloro xylene ionene was also drastically reduced when water was adsorbed. After drying, the tensile properties of the sample were partially recovered. The PTMO segment length in their ionene was 2,550 mol/gm. However, they did not specify the drying conditions in their paper. Therefore, both TGA and DMA results indicate that the water adsorbed by the ionene polymer can not be removed, at least, at a temperature below 150°C. Another interesting phenomenon is the change of the "jump" temperature, T_j. As the DMA data show, the T_j for the "dry" sample is ca. 50°C. However, the T_j of IS-BP-13-W is only ca. 20°C! Clearly, it is not likely that desorption water will occur at 20°C. Therefore, the "jump" can not be a result of water desorption.

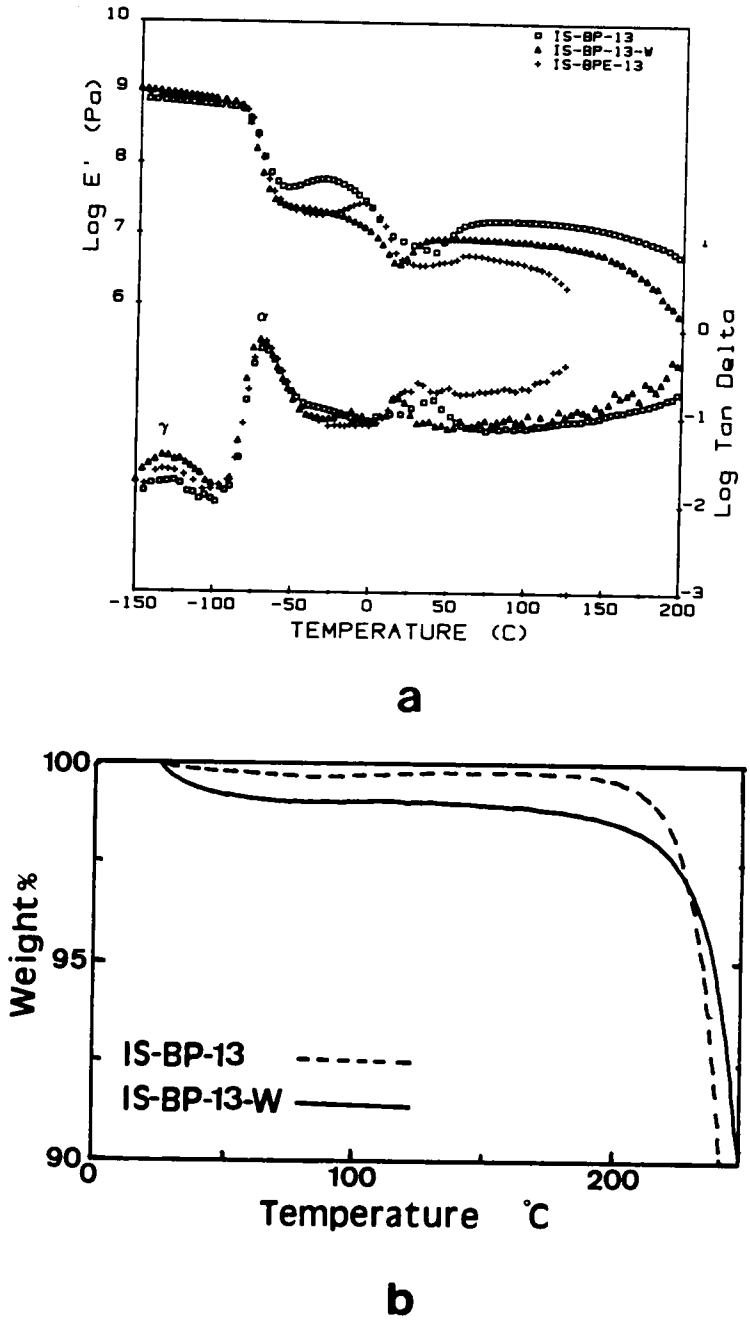

Figure 90. Dynamic mechanical and thermogravimetry spectra of "wet" and dry ionene polymers: (a). Dynamic mechanical spectra of the ionene polymers. (b). TGA thermograms of "wet" and "dry" IS-BP-13 ionene polymer.

6.4.3. Effect of Conformational Changes in the Hard and Soft Segments

6.4.3.1. DMA and DETA Behavior of Ionene Elastomers at the "Jump"

A possible explanation for the "jump" is a conformational change in the polymer chains especially in the ionene hard segments. As shown in Figure 90, the "jump" is reduced greatly when the rigid BP hard segments in the ionene system is replaced by the more flexible BPE hard segments other factors being the same. In fact, there is no "jump" observed in the DMA spectra of samples IS-BPE-18 and IS-BPE-25 (recall Figure 83 on page 239). Some published results of DMA studies on other ionene elastomers also support the possibility of conformational changes in the hard segments[136,137]. Recently, Yamshita et. al.[136] studied a polybutadiene (PB) ionene elastomer with aliphatic ionene hard segments. The ion content of the butadiene ionene was 0.013 ions per butadiene unit. There was no modulus "jump" observed in the DMA spectrum of this ionene elastomer. However, there is a transition observed at 40°C in the tanδ spectrum which was explained due to ion clustering[136]. Another study on crosslinked polyurethane (PU) ionenes has been conducted by Sasaki et. al[137]. In these PU ionenes, the soft segment was PTMO segment with one MDI unit at both ends. The PTMO segment length was in the range from 1,000 to 2,000 and the hard segment was either dichloro xylene or dibromo hexane. Again, no modulus "jump" was observed. Since the hard or soft segments in the PB or PU ionenes differ to those in the IS-BP or IB-NS ionene system, these implies that the "jump" is caused by the latter hard segments. As expected, there is no "jump" observed because the conformational change in the PB or PU systems is different or absent than in the IS-BP or IB-NS systems.

The relationship between the dynamic modulus "jump" (ΔE^* or $\Delta E'$) and the changes in the conformational entropy ΔS can be deduced as following. In the Rheovibron measurements, the modulus E^* is determined by

$$E^* = \frac{f L}{dL\, A} \tag{23}$$

where L is the sample length, A is the cross section area of the sample, f is the force monitored by the stress gage, and dL is the amplitude of the sinusoidal displacement. During the DMA experiment, dL is very small and a constant, thus, both L and A can be consider as constants. At the modulus "jump", the changes in modulus causes a change in force, or

$$\Delta f = \frac{\Delta E^* \ A \ dL}{L} \tag{24}$$

During the "jump", the change in mechanical energy, ΔW, is equal to $\Delta f dL$. therefore, value of ΔW can be related to the modulus "jump" as

$$\Delta W = \Delta f \, dL = \frac{\Delta E^* A \, dL^2}{L} \tag{25}$$

According to rubber elasticity theory, the value of ΔW at the modulus "jump" temperature, T_j, should be equal to the change in conformational entropy as follows:

$$\Delta W = \Delta f \, dL = - T_j \Delta S \tag{26}$$

or

$$\frac{\Delta E^* A \, dL^2}{L} = - T_j \Delta S \tag{27}$$

As Eq.(27) shows, if this treatment applies, the modulus "jump" is directly correlated with the changes in the conformational entropy (ΔS) when other factors are constant. Based on statistical thermodynamics, the conformational entropy at a given temperature is determined by the number of conformation of a polymer chain Ω by:

$$\Delta S = k \ln \Delta\Omega = k \ln \frac{\Omega_2}{\Omega_1} \tag{28}$$

where k is Boltzmann constant, Ω_1 is the number of conformations before the transition, and Ω_2 is the number of conformations after the transition. If the polymer chains or segments change from

a random arrangement to a ordered arrangement, the conformation entropy of the chains or segments will reduce, and ΔS will have a negative value. Therefore, the modulus will increase, since the polymer chains in a ordered arrangement gives a higher energy state than a random arrangement.

In the IS-BP ionene systems, the possible conformations of the BP hard segments are two rings rotating to each other around the C-C bond connecting two rings. In the BPE hard segment, however, the rotation can occur in the C-C bonds between the ring and the CH_2 units as well as the C-C bond between two methylene units. Therefore, the number of potentially available conformations in the BPE units is much larger than those in BP units. In the BP hard segment, the two bulky $CF_3SO_3^-$ counter ions which are almost twice as large as a benzene ring, are likely closer than in the BPE units. Any change in the conformational behavior of the BP hard segment is also expected to be limited by the steric hindrance by the counter ions. In contrast, the two counter ions are farther away from the BPE units and they should less affect conformational changes. Due to the rigid nature of the BP hard segments and its steric hindrance, the BP units would be much easier to lock into a fixed conformation than the BPE units. At T_j, the BP hard segments might be locked into a fixed conformation which causes a large change in the conformational entropy, as a result, the modulus jumps. However, the BPE units are likely not as easily locked into a fixed conformation because of its flexible nature and the change in the magnitude of the ΔS would be much smaller than for the BP units. Hence, the "jump" is also much smaller. This analogy can also be applied to the dihalide ionenes. For example, the IB-NS ionenes should have a higher "jump" than the IC-NS ionene other factor being constant because of the size of the bromide ions are larger than the chloride ions. Therefore, the bromide ionene hard segments might have a larger change in conformational entropy than for the chlorine ionene hard segments. If so, the "jump" in the IB-NS sample should be higher than in the IC-NS sample. The experimental results support this assumption. For sample IC-NS-21, the magnitude of the "jump" is about half that of sample IB-NS-18. Since the PTMO segment length in these two samples is close, the lower "jump" of IC-NS-21 is tentatively explained by the above mechanism, although at this stage it is still a speculation, believed due to the smaller size of Cl^- counter ions.

Since the ionene hard segments are highly polar groups, if there is a conformation change in the hard segment, the dielectric thermal analysis (DETA) might be able to detect these changes. It is well known that the DMA is sensitive to both long range and local motions of either polar or non-polar polymer chains. However, the DETA is more sensitive to the motions that concern only the motion of polar groups[138]. For example, Nielsen[139] found that the glass transition (α relaxation) of a linear PMMA polymer has a higher magnitude than the β relaxation by DMA. However, in the DETA $\tan\delta_E$ spectra, the β peak has a much higher intensity than the α peak. It is generally accepted that the β relaxation is due to the local scale motion of the polar side group [138].

Figure 91 on page 259 shows the $\tan\delta$ and $\tan\delta_E$ spectra of sample IB-NS-18 obtained by utilizing both the DMA and DETA methods respectively. In Figure 91a, three major relaxations, α, β_1, and β_2, have been observed on the DMA $\tan\delta$ spectra. The α transition is the glass transition of the PTMO segments, β_1 is due to the crystal melting of the PTMO segments, and β_2 is believed to be related to the "jump" transition which is being discussed.

In the DETA $\tan\delta_E$ spectra, there are two major relaxation peaks observed and designated as β_{E1} and β_{E2} . There is also a α_E relaxation which results form the glass transition of the PTMO segments in the $\tan\delta_E$ spectra, however, it is not shown in Figure 91b because of the very low intensity of this peak due to the long range motion of the less but still polar PTMO soft segments. For a PTMO homopolymer, the α_E peak intensity is of the order of 0.2 [140]. However, the intensity of β_{E1} and β_{E2} shown in Figure 91b is in a order of 10! The β_{E1} could be the β_1 transition which shifts to a higher temperature because of the difference between two experimental methods and the a higher frequency of the DETA measurements. However, the β_{E2} relaxation seems to clearly result from the "jump".

By carefully inspecting the DMA $\tan\delta$ spectra in Figure 59 on page 184 and Figure 83 on page 239, the author has found that the β_2 relaxation occurs at a lower temperature than the temperature where E′ starts to jump. In contrast, the α relaxation (T_g transition) occurs at a higher temperature than the temperature where E′ begins to drop. At the glass transition (α transition), the mobility of polymer chains increase, therefore, E′ decreases. Due to these chain motions, more

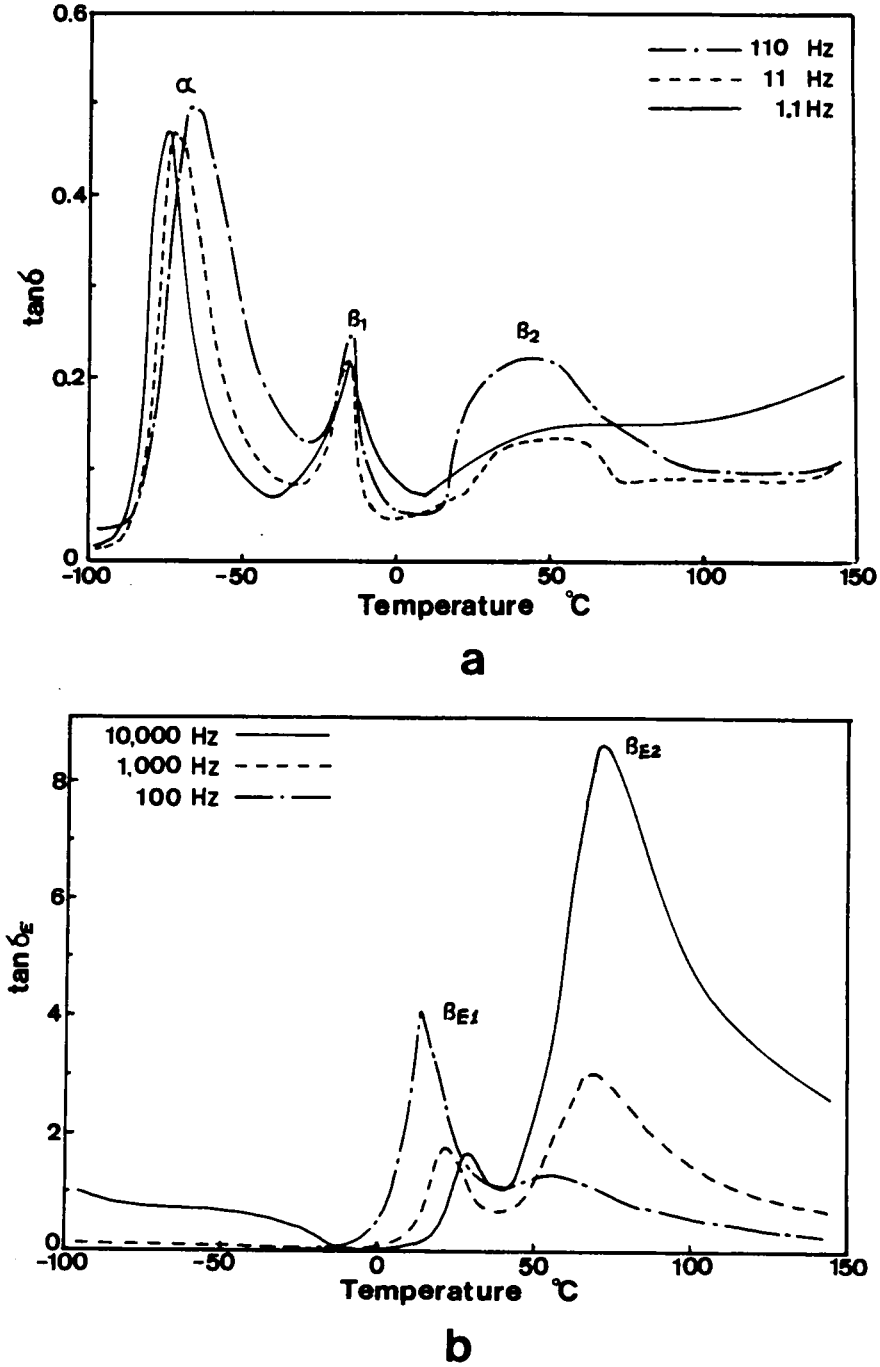

Figure 91. The DMA and DETA spectra of the IB-NS-18 ionene elastomer: (a).The tanδ spectra obtained by DMA. (b).The tanδ_E spectra obtained from the DETA.

mechanical energy is dissipated into the system, and there results a tanδ peak in the DMA spectra. That is why the temperature of the tanδ peak is higher than the temperature of the E′ drop. Since the tanδ β_2 relaxation occurs at a temperature lower than the temperature of the E′ "jump" (T_j), thereby, the β_2 relaxation suggests that there is some kind of local motion that occurs before the "jump".

Another important feature shown in the tanδ_E spectra (Figure 91b) is the frequency dependency of the β_{E1} and β_{E2} peak intensities. The intensity of β_{E1} decreases with an increase of frequency, while the magnitude of β_{E2} increases with frequency. The frequency dependence of β_{E1} may result from local motions of less polar groups or segments such as some local motion of PTMO units in the polymer backbone. Since the intensity of the β_{E2} peak increases with frequency, this might be due to motions of highly polar groups or segments, in this case, the motions of the ionene hard segments. If it is the case, the DMA and the DETA data suggest that there are some local motions on the PTMO segments occurring at temperature lower than T_j. These motions allow the ionic hard segments to change their conformation from a lower energy state to a higher energy state which results in the modulus "jump". This speculation is supported by the earlier observation of the relationship between the PTMO T_m and the T_j of the IS-BP ionenes. In these systems, the difference between the T_m and T_j is a constant (recall section 6.3.1.4). As will be discussed in the next section, the SAXS - temperature behavior of sample IB-NS-18 can also be indirectly correlated with this speculation.

6.4.3.2. Temperature Dependence of X-ray Scattering Behavior.

If there is a conformational change in the ionene hard segments, some rearrangements in the ionic domains would be expected. By utilizing both SAXS and WAXS techniques, these changes might be able to be detected.

The SAXS profiles of sample IS-BP-25 show almost no change in the shape of the SAXS profile in a temperature range from 25°C to 80°C (the T_j of this sample is ca. 50°C). No recogni-

zable changes in the "d" spacing was observed which may be due to the broadness of the SAXS scattering peaks (recall Figure 85 on page 242 and Figure 87 on page 246). Also, the WAXS patterns of the IS-BP ionene polymers show no distinctive changes in the same temperature range as the SAXS measurements.

However, distinct changes in both the SAXS and WAXS have been observed for the IB-NS ionene polymers. Figure 92a shows the temperature dependence of the scattering peak of sample IB-NS-18. As the temperature increases, the scattering peak shifts toward a higher scattering angle. In other words, the "d" spacing (interdomain spacing) decreases with an increase of temperature and levels off at ca. 70°C. When the sample is re-cooled to ambient, the scattering peak shifts back to its original position. Figure 92b shows the relationship between the "d" spacing and the temperature. It clearly shows that there is change ("d" spacing transition") in the "d" spacing - temperature curve of the IB-NS-18. This "d" spacing transition occurs at the same temperature range as the modulus "jump". When the PTMO segment length increases, the "d" spacing transition disappears. There is no "d" spacing transition and the modulus "jump" is also absent for samples with PTMO segment length greater than 3,400. The temperature dependence of the the "d" spacing in the IB-NS ionene systems is quite similar to the modulus "jump" of these materials.

The WAXS results for sample IB-NS-18 and IB-NS-14 also show some very distinct changes which support the assumption of local rearrangement. Figure 93 on page 263 shows the WAXS patterns of sample IB-NS-18. At ambient temperature, the WAXS patterns show only an amorphous halo. When the sample is heated and held at 90°C for the WAXS experiment, several sharp rings appear in the WAXS pattern. These rings suggest some type of distinctive ordered structure is formed. Interestingly, when the sample has been cooled down to ambient, those sharp rings disappear, and the amorphous halo appears again! The heating and cooling WAXS experiments have been repeated on the same sample for three times, the same patterns have been obtained each time!

Based on the SAXS and WAXS data, a possible rearrangement of hard segments in the ionic domains is again postulated as shown in Figure 94 on page 265. This rearrangement could be due

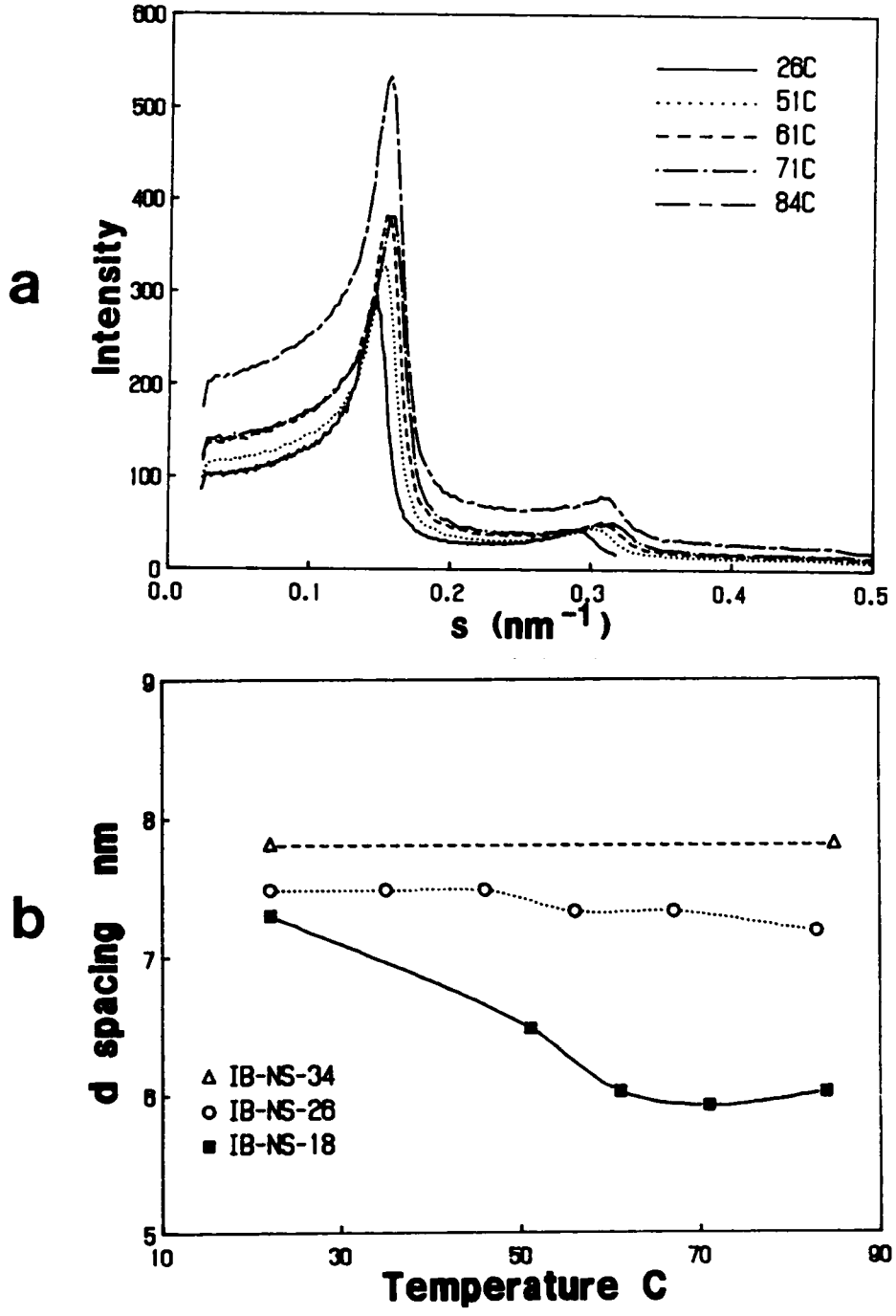

Figure 92. **Temperature-"d" spacing dependence of the IB-NS ionene polymers:** (a).SAXS profiles of sample IB-NS-18. (b). Temperature - "d" spacing dependence of the IB-NS ionene polymers.

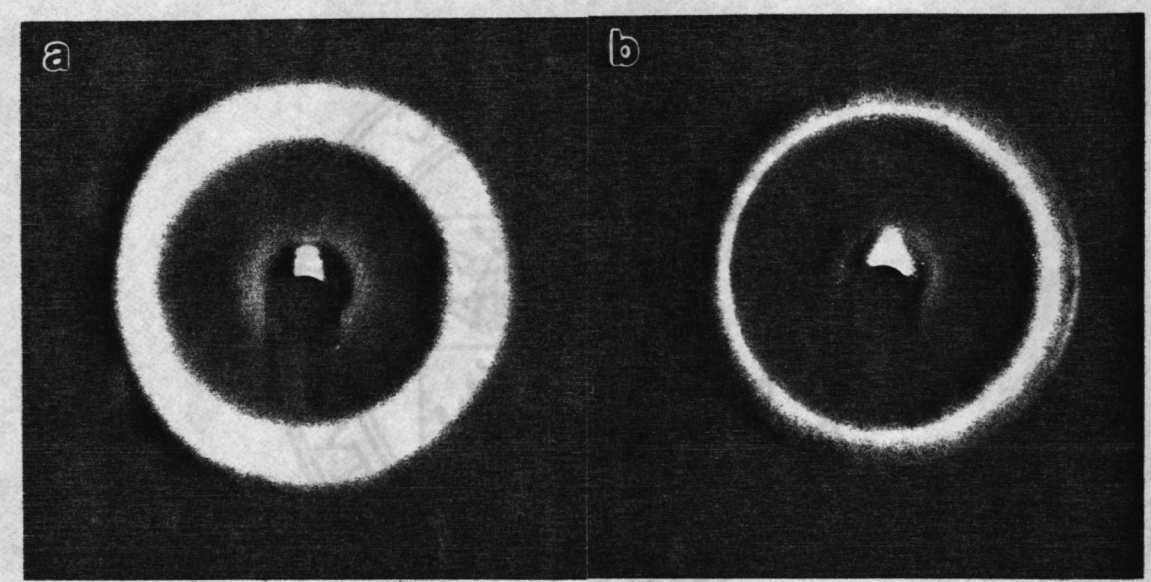

Figure 93. WAXS patterns of sample IB-NS-18: (a). T = 25°C. (b). T = 80°C.

to the balance between the electrostatic energy introduced by the ionic hard segments and the thermal brownian energy associated with the PTMO soft segments. In these ionene systems, the coulombic force between the hard segments - which have the same charge - on the same ionene polymer chain is repulsive. This coulombic force will try to keep the hard segments in the same chain away from each other. As a result, the PTMO soft segments between the ionic hard segments will be stretched (refer to section 6.2.3, 6.3.3.1, Table 16 on page 224 and Table 17 on page 244). When the soft segment is stretched, its conformational entropy will be reduced, and the segment would desire to coil up to increase the entropy thereby working against the coulombic forces. At a temperature below T_j, the thermal energy of the chain is low, and the chain is more stretched. Therefore, the "d" spacing is larger. Also, the hard segments might pack somewhat randomly in the ionic domains. Their more random lower energy arrangement could result from the conformation of both hard and soft segments and even be influenced by the molecular weight distribution of the soft segments. Thus, the resulting WAXS pattern shows an amorphous halo. When the temperature increases, the thermal energy of the chain increases. At a critical temperature, the soft segments gain sufficient thermal brownian motion (energy), which cause the β_2 relaxation on the DMA spectra and begin to promote the soft segment to recoil. Therefore, the end-to-end distance of the PTMO segments is reduced, and the the "d" spacing decreases. The thermal energy of the hard segments also increases with temperature. The higher thermal energy allows the hard segments to possibly undergo a conformational change from a lower energy state to a higher energy state. This conformational change may subsequently lead to a relatively ordered arrangement of hard segments in the ionic domains which is a higher energy state. If this ordered arrangement of ionic hard segments results, the β_{E2} relaxation occurs and the sharp rings would appear in the higher temperature WAXS pattern.

Another possible cause for the conformational change in the ionene hard segments is the change in dielectric constant of the PTMO segments in two different states (solid state at $T < T_m$ and liquid state at $T > T_m$). Related to this is the recognition of two possible conformation isomers of the BP hard segment; the "anti-conformation" and the "skew conformation" (refer to Figure 95 on page 268). In the former; the two rings of the BP unit are co-planer, and two bulky $CF_3SO_3^-$

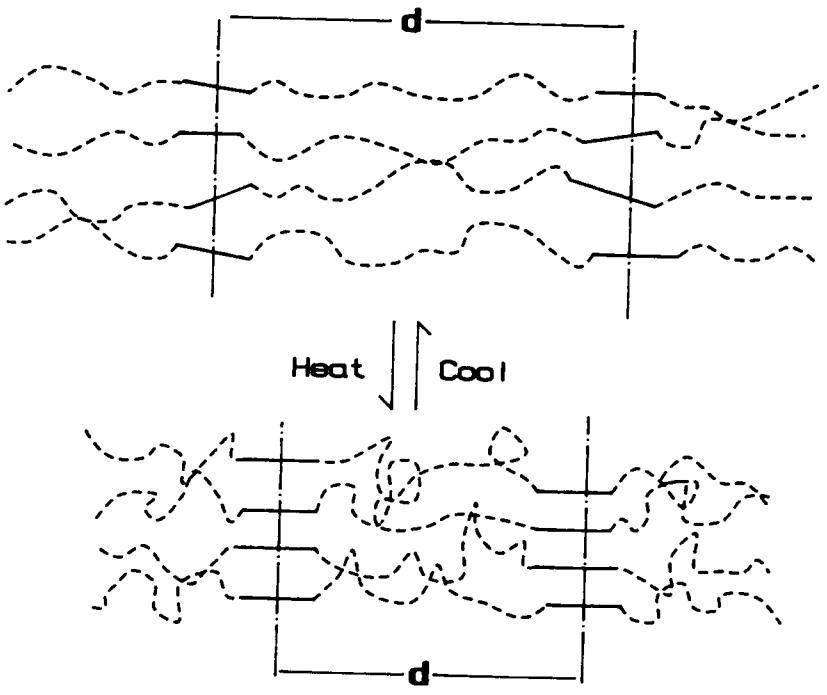

Figure 94. Illustration of the ionic domain rearrangements.

counter ions are on opposite sides of the two rings. This may be the lowest energy state of the BP unit because the distance between two ions is a maximum. The "skew conformation", is more important in polar media than in non-polar media, because the "skew conformation" has a considerable dipole moment and solvation is know to reduce the potential energy of a dipole thereby stabilizing this form relative to the "anti-conformation"[22]. In the solid state, the "anti-conformation" of the BP hard segments tend to be preferred over the "skew-conformation" at temperature below the T_m of the PTMO segment. When the temperature is higher than the T_m of the PTMO segments, the ionic domains can be considered to be dispersed in a polar medium. As temperature reaches T_j, the energy of the hard segments may be sufficient to overcome the rotational barrier of the transition from the "anti" to the "skew" conformations. Therefore, the population of the "skew" isomers increases drastically. In the "anti-conformation", the bulky $CF_3SO_3^-$ counter ions tend to stay away from each other because of the common charge. The repulsion force between the counter ions are reduced in the "skew" form because two triflic acid anions are not on the same plane. Also, the distance between two BP units in a ionic domain is expected to be smaller in the "skew-conformation" than in the "anti-conformation". If this speculation is truly the case, the ionic domains become more compact when the hard segments have the "skew conformation", thereby, raising the modulus of the sample because of stronger interchain interactions. The similar analogy can also be applied on the dihalide hard segments. In the ionic domain of the IB-NS ionenes, the the distance between two dihalide hard segments would be expected different form two Br^- ions being on opposite sides of the benzene ring to the form of two counter ions and the ring being co-planer. If the conformation of the dihalide hard segments changes from the former to the latter (the co-planer), the hard segments in the ionic domains become closer, and results in the modulus "jump".

The basis of the foregoing discussions is based on the fact that the PTMO matrix may serve as a polar medium at elevated temperatures. Although there is no direct supporting experimental evidence to these latter speculations at this time, there is an indirect support from an early study on the T_g of aliphatic ionenes by Eisenberg and co-workers[81]. In their study, the T_g of aliphatic ionenes had been studied by using different solvents as plasticizers. Eisenberg and co-workers found

that the T_g of a 6,8 bromine ionene suddenly increased as the dielectric constant of the plasticizers increased to a critical value (refer to Figure 11 on page 37). They suggested that the change was caused by a conformational change of the aliphatic ionene.

6.4.5. Correlation between the "Jump" and the Structural Parameters

The experimental evidence to date indicates that the magnitude of the "jump" is directly related to the ionic content. The higher the ionic content or shorter PTMO segment length is, the higher the "jump" will be. The counter ion size also strongly influences the "jump". The ionene polymers with larger counter ions has a higher "jump". The most important factor is the type of hard segment. When a rigid hard segment has been replaced by a more flexible hard segment, the "jump" disappears. Since the coulombic force plays an important role in these ionene systems, there the electronegativity of counter ions and the distance between two counter ions in a hard segment should contribute to the "jump". The higher electronegativity of the ion should cause a stronger coulombic interaction and thus the "jump" is expected to be higher. However, if two ions in a hard segment are further apart, the hard segment has more conformations because of less steric hindrance due to the counter ions, thus, ΔS becomes smaller, and the "jump" would be lower.

Based on the above speculations, a correlation between the "jump" with the structural parameters has been established as follows:

$$\frac{E_j}{E_o} = f(C, D, q, \frac{1}{d})$$

where, E_j is the E′ after "jump" and E_o is the value of E′ at ambient temperature, C is the ion content, D is the diameter of the counter ion, q is the electronegativity of the counter ion, and d is the distance between the two positive charged nitrogen atoms in a hard segment. This distance determines the distance between two counter ions in a hard segment. Based on the above parameters, a correlation between the relative "jump" and the structural parameters is plotted in

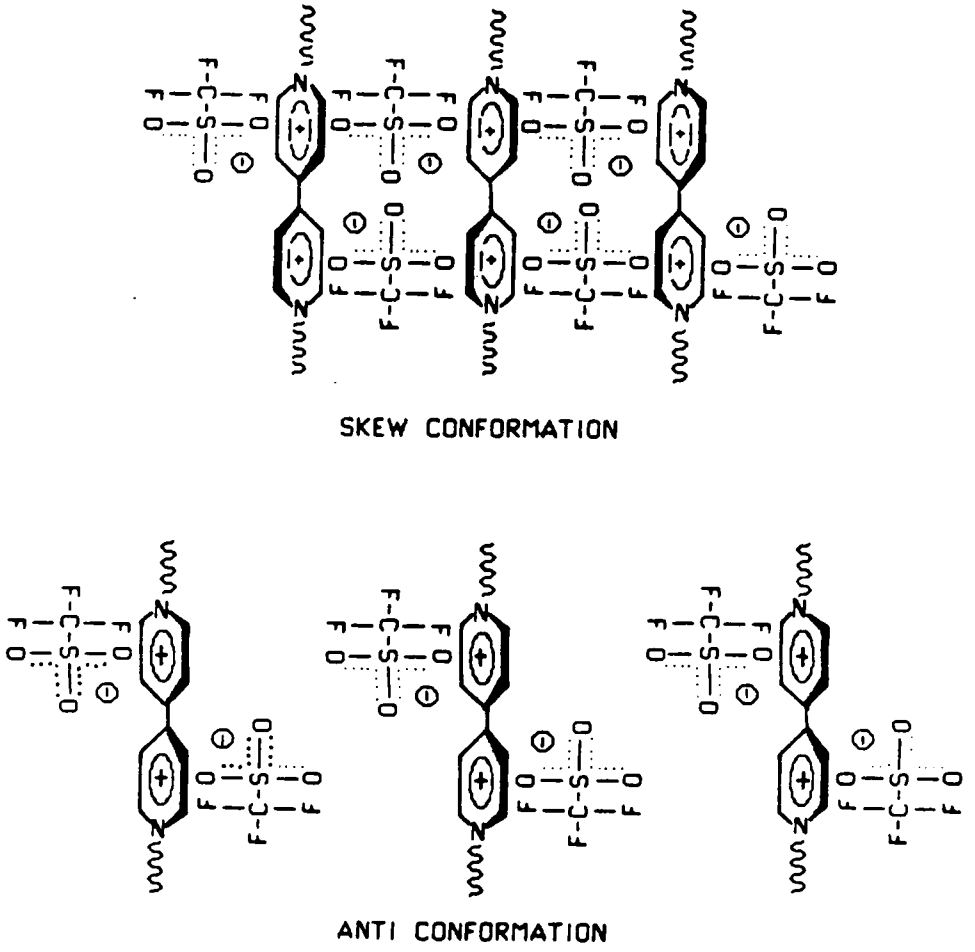

Figure 95. Conformational interchange of the BP hard segments (Ref. 22).

Figure 96 on page 270. A statistically based linear correlation between the relative "jump" with the structural parameters has been established. The linear correlation coefficient is 0.97! This indicates that the experimental data fit the correlation very well. When the BP hard segments have been replaced by the BPE units, the linear relationship between the relative "jump" and the structural parameters no longer holds. This supports the assumption of a conformational change in the hard segments. It is important to point out that this correlation is only a pure speculation. It needs more experimental and theoretical work for support.

6.4.5. Summary and Recommendations

6.4.5.1. Summary

According to the experimental evidence, the unusual modulus "jump" of these novel ionene elastomers is highly reversible and it is not caused by the adsorption - desorption of water. More likely, this "jump" is due to the some type of conformational change in the ionic hard segments which results some rearrangements of the hard segments in the ionic domains. These changes are caused by the changes in the balance between the electrostatic and thermal energy of the ionene polymer chains. A correlation between the "jump" and some structural parameters has been established based on the experimental evidence to date. However, the reader should keep in mind that this correlation is a pure speculation. No definitive conclusions have been reached and further work is needed.

6.4.5.2. Recommendations

In future studies, spectroscopy methods such as FT-IR, solid state NMR, SANS, and SAXS (synchrotron) could be applied to study the temperature dependent behavior of these ionene sys-

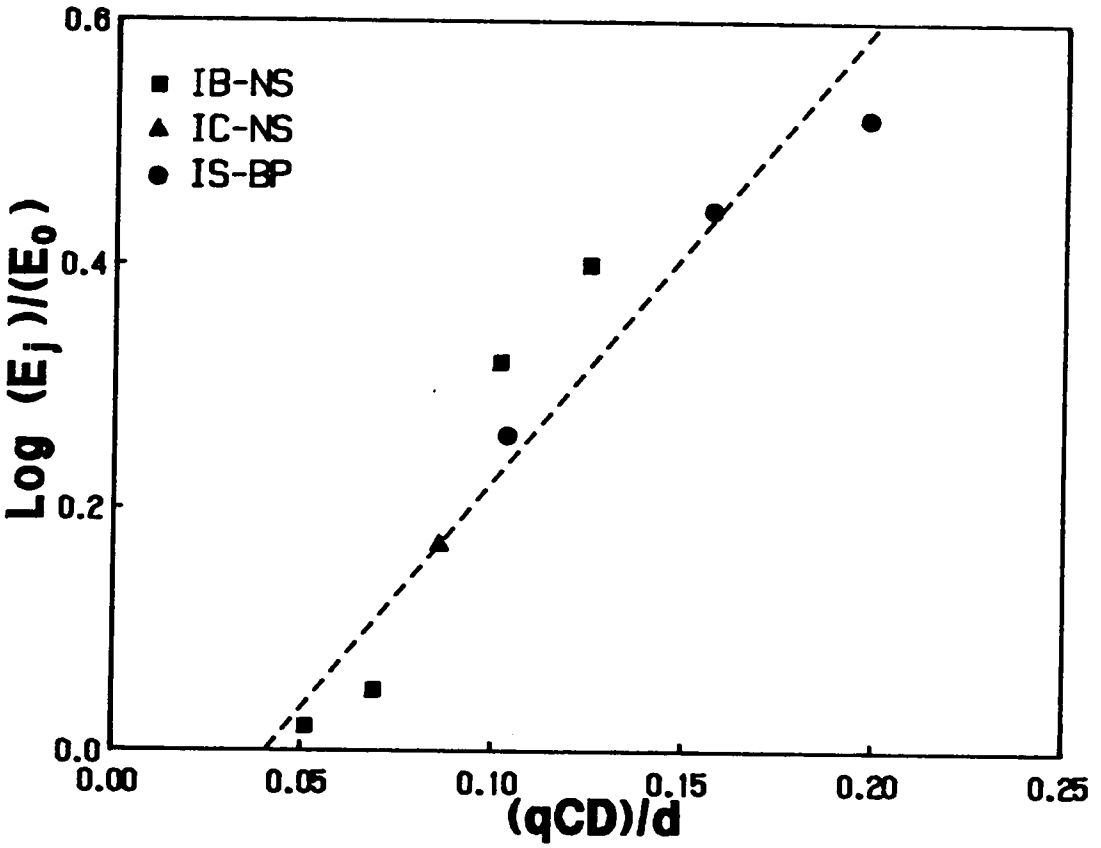

Figure 96. Relationship between the "jump" magnitude with some molecular parameters: The linear correlation coefficient is 0.97.

tems. Both SAXS and SANS could be used to study the changes in the morphological structures and the arrangements of the ionene hard segments in the ionic domains, while solid state NMR and FT-IR could detect the conformational change in both soft and hard segments. However, there may be some difficulties in the application of the FT-IR and NMR techniques because of the low ionene content in these materials.

Another approach would be to study model systems, for example, using 1,2-dipyridine ethylene as the hard segment in the IS ionene systems instead of the BP or BPE units (other parameters being constant). Due to the conjugated π bonds between the pyridinium rings and the ethylene units, 1,2-dipyridine ethylene would be a very rigid units. Therefore, conformational change should be more difficult than in both BP and BPE units. However, the distance between two counter ions in the 1,2-dipyridine ethylene hard segment should be greater than in the BP units, hence, the steric hindrance in the 1,2-dipyridine ethylene units would be expected to be smaller than in the BP units. As a result, the "jump" of this PTMO-1,2-dipyridine ethylene ionene might well be higher than in the IS-BPE system and might be even higher than in the IS-BP system if the "jump" is due to the conformational change in the hard segment.

Another way to study the steric hindrance of the counter ions is to use ion exchange method to change the size of counter ion, i.e, using Br^- counter ions exchange with the $CF_3SO_3^-$ anions in the IS-BP system, or using the I^- counter ions to replace the Br^- ions in the IB-NS systems by utilizing diiodo xylene instead of dibromo xylene in the polymerization.

Besides using different hard segments in the ionene systems, a model compound synthesized by trimethylamine, $(CH_3)_3N$, and dibromo xylene could be also used to study the conformation changes of dihalide hard segments in the IB-NS ionene system. In this compound, the dihalide content would be much higher than in the ionene system discussed here, which which would allow the possible use of FT-IR, WAXS, NMR, and thermal analysis methods to study the conformational change of the dihalides.

6.5. CONCLUSIONS AND RECOMMENDATIONS

6.5.1. Conclusions

The segmented PTMO ionene elastomers display many of the characteristics common to the segmented and block polymer thermoplastic elastomers. These features are due to the microphase separated domain structure in these materials. The microphase separation is promoted by the strong ionic interactions rather than the segment - segment incompatibility.

For the PTMO-dihalide ionene elastomers, the polymers tend to degrade or possibly depolymerize when exposed to higher temperature as noted by a decrease in properties that are not recovered with time in the melt or solid form. Therefore, these systems are not thermally processable. However, the PTMO-dipyridinium (IS-BP) ionene elastomers can be thermal processing, although they do show some loss in properties with molding. Due to the limited amount of materials, the cause of the time dependent recovery behavior of the IS-BP systems still remains unknown and further investigations are required.

The bulk properties of these ionene elastomers change with the ion content, type of counter ion, and the hard segment architecture. When these parameters vary, the level of ionic interaction in the ionene elastomers is changed, hence the bulk properties are altered. For example, when the PTMO segment length decreases, the ionic content increases which results in a rise in the level of ionic interaction and the Young's modulus. When a spacer group is added into the ionic hard segment, the mechanical properties of the polymer decrease which reflect the decrease in the ionic interaction.

Due to the strong ion clustering, a rod-like morphology has been observed by both TEM and SAXS in some of the ionene systems having a higher ion content. It is the first time that the results of these two methods agree with each other for an ionomer system. It has been demonstrated that the microphase separation can promote a continuous long range ordered structure with a relatively low volume fraction of one component (< 10 vol%). This has not been predicted by any existing

theories of ion clustering in ionomers or the usual knowledge form morphological studies of block/segmented polymers. As expected, the morphology of these ionene elastomers is altered with ion content. When the ion content in the ionene system decreases, the long range ordered structure disappears as well as the rod-like structure.

A very unique phenomenon, a highly reversible modulus "jump", has been observed on these ionene materials which has not been reported before. This "jump" is directly related to the ion content, type of counter ion and the hard segment. Based on experimental evidence, the "jump" is tentatively speculated to be caused by a conformational change in the ionene hard segments. However, further investigations are needed to support or disprove this speculation.

6.5.2. Future Work and Recommendations

In this study, the general structure properties of segmented PTMO based ionene elastomers have been studied. However, there are some remaining questions such as the thermal processibility, ion clustering behavior, the mysterious modulus "jump", etc.

The thermal processibility of these novel ionene elastomers is a very critical property for their future applications, therefore, a detailed study on the thermal molding and recovery behavior of these materials is needed. In the future investigation, the spectroscopic techniques such as solid state NMR, SAXS (synchrotron) and SANS techniques as well as further thermal and mechanical analysis are suggested. Solid state NMR could monitor changes in the molecular structure of the polymer due to the depolymerization - repolymerization process and the possible decomposition process. Both SAXS and SANS could be utilized to monitor the ion clustering process after thermal molding. Thermal and mechanical measurements could monitor the changes in bulk properties of these materials caused by the thermal processing.

In some of these ionene elastomers, a rod-like morphological structure has been observed which has not been predicted by any existing theories of ion clustering. Therefore, further morphological studies on these ionene systems would contribute to the theory of ion clustering

greatly. In the future studies, the SAXS and SANS would be the major techniques. One of the focal point is the scattering in the very low angle region which would help to clear the controversy in the current theories of ion clustering. Also, scattering studies on deformed ionene systems would give some additional information on the type of ionic domains.

For the future investigations of the modulus "jump" of these ionene elastomers, a detailed discussion on the experimental approaches has been given in section 6.4.5.2. Besides the experimental approaches, theoretical calculations on the possible conformations of the ionene hard segments can also provide a background to identify the source of the "jump".

There are also several interesting features of these ionene systems such as photochromic properties and solvent dependent properties as noted in this study. These features might be of interest to develop some future applications of these ionene elastomers, therefore, a systematic investigation on these phenomena are recommended.

Besides the PTMO soft segments, some other polymers can also be utilized as soft segments to change the properties of the ionene polymers. For example, if polydimethylsiloxane (PDMS) is used as a soft segment in the ionene systems, the low temperature properties and the thermal stability of the ionene systems might be improved greatly.

LITERATURE CITED

1. J. E. McGrath, J. Chem. Education, **58**, 914(1981)
2. A. Noshay and J. E. McGrath, "Block Copolymers: Overview and Critical Survey", Academic Press, New York, 1977
3. J. C. Saam, D. J. Gordon, and S. Lindsey, Macromolecules, **3**, 1(1970)
4. J. W. Dean, Polymer Letters, **8**, 677(1970)
5. S. Varshney and P. Baiaj, Advances in Chem. Ser., **203**, 179(1981)
6. W. G. Davies and D. P. Jones, ACS Polym. Preprints, **11**(1), 447(1970)
7. P. Chaumont, G. Beinert, J. Herz, and P. Rempp, Polymer, **22**, 663(1981)
8. A. V. Tobolsky and A. Rembaum, J. Applied Polym. Sci., **3**, 307(1964)
9. F. C. Baines, J. H. Grezlak, and A. V. Tobolsky, J. Polym. Sci.: PartA-1, **7**, 3297(1969)
10. E. Zaganiris and A. V. Tobolsky, J. Applied Polym. Sci., **14**, 1997(1970)
11. F. J. T. Fildes and A. V. Tobolsky, J. Polym. Sci.: Part A-1, **10**, 151(1972)
12. J. H. Grezlak and G. L. Wilkes, J. Applied Polym. Sci., **19**, 769(1975)
13. J. V. Crivello, J. L. Lee and D. A. Conlon, J. Polym. Sci. Polym. Chem. Ed., **24**, 1197(1986)
14. J. V. Crivello, J. L. Lee and D. A. Conlon, J. Polym. Sci. Polym. Chem. Ed., **24**, 1251(1986)
15. R. D. Lundberg, in "Encyclopedia of Polymer Science and Engineering", 2nd Ed., Vol. 8, 1984, P383
16. S. Kohjiya, T. Ohtsuki, and S. Yamashita, "Abstracts of IUPAC 6th International Symposium on Cationic Polymerization and Related Processes", Ghent, Belgium, 1983, P181
17. T. Hashimoto, S. Kohjiya and S. Yamashita, Nippon Gomu Kyokaishi, **60**(1), 27(1987)
18. S. Yamashita, T. Hashimoto, T. Yoshida, and S. Kohjiya, Nippon Gomu Kyokaishi, **60**(1), 34(1987)
19. T. P. Klun, L. A. Wendling, J. W. C. Van Bogart, and A. F. Robbins, J. Polym. Sci. Polym. Chem. Ed., **25**, 87(1987)

20. C. M. Leir and J. E. Stark, submit to J. Appl. Polym. Sci.

21. K. Hohjiya, T. Hashimoto, S. Yamashita, and M. Irie, Chemistry Letters, 1497(1985)

22. B. Lee, Ph.D Dissertation, Virginia Polytechnic Institute and State University, 1987

23. A. Rembaum, W. Baumgartner, and A. Eisenburg, J. Polym. Sci. Polym. Letters, **6**, 159(1968)

24. G. E. Molau, in "Block Polymers", S. L. Aggarwal ed., Plenum Press, New York, 1970, p79

25. E. Halfand, Accts. Chem. Res., **8**, 295(1975)

26. D. J. Meier, J. Polym. Sci.: Part C, **26**, 81(1969)

27. D. J. Meier, ACS Polym. Preprints, **11**, 400(1970)

28. D. J. Meier, in "Block and Graft Copolymers", J. J. Burke and V. Weiss ed., Syracuse University Press, 1973, p105

29. E. Helfand, Macromolecules, **8**, 552(1975)

30. E. Helfand and Z. R. Wasserman, Macromolecules, **9**, 879(1976)

31. S. Krause, Macromolecules, **3**, 84(1970)

32. S. Krause, ACS Polym. Preprints, **11**, 568(1970)

33. S. Krause, in "Block and Graft Copolymers", J. J. Burke and V. Weiss ed., Syracuse University Press, 1973, p143

34. S. Krause, Macromolecules, **11**, 1288(1978)

35. S.Krause, J. Polym. Sci. Polym. Phys., **23**, 129(1985)

36. T. Hashmoto, K. Nagtoshi, A. Todo, H. Hasegawa, and H. Kawai, Macromolecules, **7**, 364(1974)

37. T. Hashimoto, A. Todo, H. Itoi, and H. Kawai, Macromolecules, **10**, 377(1977)

38. T. Hashmoto, M.Shibayama, and H. Kawai, Macromolecules, **13**, 1237(1980)

39. T. Hashimoto, M. Fujimura, and H. Kawai, Macromolecules, **13**, 1660(1980)

40. T. Hashmoto, Y. Tsukahara, and H. Kawai, Macromolecules, **14**, 708(1981)

41. T. Hashimoto, Y.Tsukahara, and H. Kawai, J. Polym. Sci. Polym. Letters ed., **18**, 585(1980)

42. T. Hashmoto, M. Shibayama, M. Fujimura, and H. Kawai, Memoirs of the Faculty of Engineering, Kyoto University, **XLIII**, Part 2, 184(1981)

43. G. York, MS Thesis, Virginia Polytechnic Institute and State University, 1987

44. P. J. Flory, in "Principles of Polymer Chemistry", Cornell University Press, 1953

45. D. Tyagi, J. E. McGrath, and G. L. Wilkes, Polym. Eng. Sci., **20**, 1371(1986)

46. A. Eisenburg, Maxcromolecules, **3**, 147(1970)

47. C. Geraldine Bazuim, and A. Eisenburg, Ind. Eng. Chem. Prod. Res. Dev., **20**, 271(1981)

48. C. T. Meyer and M. Pineri, J. Polym. Sci. Polym. Phys., **16** , 569(1978)

49. A. Neppel, I. S. Butler, and A. Eisenberg, Macromolecules, **12**, 948(1979)

50. A. Neppel, I. S. Butler, and A. Eisenberg, J. Polym. Sci. Polym. Phys., **17**, 2145(1979)

51. F. C. Wilson, R. Longworth, and D. J. Vaughan, ACS Polym. Preprints, **9**, 505(1968)

52. C. L. Marx, D. F. Caulfield, and S. L. Cooper, Macromolecules, **6**, 344(1973)

53. W. J. MacKnight, W. P. Taggart, and R. S. Stein, J. Polym. Sci.: Symp., **45**, 113(1974)

54. D. J. Yarusso and S. L. Cooper, Macromoelcules, **16**, 1871(1983)

55. M. Fujimura, T. Hashimoto, and H. Kawai, Macromoelcules, **15**, 1361(1982)

56. E. G. Knapick, J. A. Hirsch, and P. Ander, Macromolecules, **18**, 1015(1985)

57. D. J. Yarusso and S. L. Cooper, Polymer, **26**, 371(1985)

58. E. J. Roche, R. S. Stein, T. P. Russell, and W. J. MacKnight, J. Polym. Sci. Polym. Phys. ed., **18**, 1497(1980)

59. A. F. Galambos, W.B. Stockton, J. K. Koberstein, A. Sen, R. A. Weiss, and T. P. Russell, Macromolecules, **20**, 3091(1987)

60. Y. S. Ding, R. A. Register, S. L. Cooper, S. R. Hubbard, and K. O. Hodgson, Polym. Mat. Sci. Eng. Proc., **58** 990(1988)

61. C. L. Marx, J. A. Koutsky, and S. L. Cooper, J. Polym. Sci. Polym. Letters, **9**, 167(1971)

62. P. J. Phillips, Polymer Letters, **10**, 443(1972)

63. D. Graiver, M. Litt, and E. Baer, J. Polym. Sci. Polym. Phys., **17**, 3573(1979)

64. D. L. Handlin, W. J. MacKnight, and E. L. Thomas, Macromolecules, **14**, 795(1981)

65. D. L. Handlin, Ph.D Dissertation, University of Massachusetts, 1983

66. Y. Minoura, M. Mitoh, A. Tabuse and Y. Yamada, J. Polym. Sci.: A-1, **7**, 2753(1969)

67. M. Morton, Y. Kesten, and L. J. Fetters, Applied Polym. Sym., **26**, 113(1975)

68. J. C. Saam and F. W. Gordon Fearon, Polym. Preprints, **11**, 455(1970)

69. J. C. Saam and F. W. Gordon Fearon, Ind. Eng. Chem. Res. Develop., **10**, 10(1971)

70. B. Wang and S. Krause, Macromolecules, **20**, 2201(1987)

71. J. C. Saam and F. W. Gordon Fearon, in "Colloidal and Morphological Behavior of Block and Graft Copolymers", G. E. Molau ed., Plenum Press, New York, 1971, p75

72. J. C. Saam, A. H. Word, and F. W. Gordon Fearon, ACS Polym. Preprints, **13**, 524(1972)

73. C. F. Gibbs, E. R. Littmann, and C. S. Marvel, J. Amer. Chem. Soc. **55**, 753(1935)

74. M. Watanabe, N. Toneaki, Y. Takizawa, and I. Shinohara, J. Polym. Sci. Polym. Chem. ed., **20**, 2669(1982)

75. Y. Takizawa, H. Aiga, M. Waranabe, and I. Shinohara, J. Polym. Sci. Polym. Chem. Ed., **21**, 3145(1983)

76. V. Hadek, H. Noguchi and A. Rembaum, Macromolecules, **4**, 494(1971)

77. D. Casson and A. Rembaum, Macromolecules, **5**, 74(1972)

78. T. Buruiana, I. Bestiuc, and A. Caraculacu, Die Angew. Makromol. Chem., **147**, 99(1987)

79. T. Buruiana, I. Bestiuc, V. Popescu, and A. Caraculacu, Die Angew. Makromol. Chem., **134**, 165(1985)

80. L. Dominquez, W. H. Meyer, and G. Wegner, Makromol. Chem. Rappid Commun., **8**, 151(1987)

81. A. Eisenberg, H. Matsuura, and T. Yokoyama, Polymer J., **2**, 117(1971)

82. T. Tsutsui, T. Sato, and T. Tanaka, Polymer Journal, **5**, 332(1973)

83. A. Takahashi, M. Kawaguchi, T. Kato, M. Kuno, and S. Matsumoto, J. Macromol. Sci. Phys., **B17**, 747(1980)

84. S. Smith and A. J. Hubin, J. Macromol. Sci.- Chem., **A7**, 1399(1973)

85. S. J. Clarson, K. Dodgso, and J. A. Semlyen, Polymer, **26**, 930(1985)

86. S. Krause, M. Iskandar, and M. Iqbal, Macromolecules, **15**, 105(1982)

87. B. Lee, MS Thesis, Virginia Polytechnic Institute and State University, 1985

88. D. Tyagi, Ph.D Dissertation, Department of Chemical Engineering, Virginia Polytechnic Institute and State University, 1986

89. A. Rudin and D. Burgin, Polymer, **16**,291(1975)

90. G. L. Lee, O. K. Johannson, O. L. Flaningam, and P. Hahn, ACS Polym. Preprints, **10**, 1311(1969)

91. J. V. Crivello, Personal communication.

92. T. Hashimoto, Y. Tsukahara, and H. Kawai, Macromolecules, **16**, 648(1983)

93. B. Morese-Seguela, M. St-Jacques, J. M. Renaud, J. M., and J. Prud'homme, Macromolecules, **13**, 100(1980)

94. S. Krause and M. Iskandar, Adv. Chem. Ser., **176**, 205(1979)

95. J. M. G. Cowie, D. Lath, and I. J. McEwen, Macromolecules, **12**, 52(1979)

96. J. P. Pascault and Y. Camberlin, J. Polym. Sci. Polym. Chem. ed., **21**, 415(1983)

97. J. P. Pascault and Y. Camberlin, J. Polym. Sci; Polym. Phys. ed., **22**, 1835(1984)

98. J. P. Pascault and Y. Camberlin, Polymer Communications, **27**(8), 230(1986)

99. H. E. Bair, Polym. Eng. Sci., **10**, 247(1970)

100. P. Bajaj and S. K. Varshney, J. Polymer, **21**, 201(1980)

101. S. L. Malhotra, T. L. Bluhm, and Y. Deslandes, European Polymer Journal, **22**, 391(1986)

102. G. Odian, in "Principles of Polymerization", John Wiley & Sons, New York, 19 , pp271-281

103. D. T. Turner and H. B. Lee, Macromolecules, **10**, 221, 226, and 231 (1977)

104. E. Abuin and E. A. Lissi, J. Macromole. Sci. Chem., **A11**(2), 287(1977)

105. J. N. Cardenas and K. F. O'Driscoll, J. Polym. Sci. Polym. Chem., **15**, 1883(1977)

106. J. N. Cardenas and K. F. O'Driscoll, J. Polym. Sci. Polym. Chem., **15**, 2097(1977)

107. J. Dionisio, H. K. Mahabadi, K. F. O'Driscoll, E. Abuin, and E. A. Lissi, J. Polym. Sci. Polm. Chem., **17**, 1891(1979)

108. J. Dionisio and K. F. O'Driscoll, J. Polym. Sci. Polym. Chem., **18**,241(1980)

109. S. Smith and J. E. McGrath, Personal Communication.

110. H. Alter, J. of Applied Polym. Sci., **9**, 1525(1965)

111. O. E. Otterstedt, J. E. A. Otterstedt, J. Ekdahl, and J. Backman, J. Applied Polym. Sci., **34**, 2575(1987)

112. M. Morton, J. M. McGrath, and P. C. Juliano, J. Polym. Sci.: Part-C, **26**, 99(1969)

113. M. Enyiegbulam and D. J. Hourston, Polymer, **19**, 727(1970)

114. S. Bagrodia and G. L. Wilkes, J. Biomed. Mater. Res., **10**, 101(1976)

115. G. L. Wilkes, S. Bargrodia, Z. Ophir, and J. A. Emerson, J. Appl. Phys., **49**(10), 5060(1978)

116. A. K. Fritzsche and F. P. Price, ACS Polym. Preprints, **11**, 462(1970)

117. M. R. Tant, PhD Thesis, Virginia Polytechnic Institute and State University, 1986

118. M. R. Tant and G. L. Wilkes, J. Macromol. Sci.-Rev. Macromol. Chem. Phys., **C28**(1), 1(1988)

119. A. H. Willbourn, Trans. Faraday Soc., **54**, 717(1958)

120. P. W. Atkins, "Physical Chemistry", Oxford University Press, Oxford, 1978, p472

121. L. N. Venkateshwaran, personal communication.

122. A. W. Agar, R. H. Alderson, and D. Chescoe, "Principles and Practice of Electron Microscope Operation", North-Holland Publishing Company, Amsterdam, 1974

123. J. W. Cowley, "Diffraction Physics", North-Holland Publishing company, Amsterdam, 1975

124. H. P. Erickson, "advances in Optical and Electron Microscopy", R. Barer and V. E. Crosslett, ed., Vol. 5, Academic Press, New York, 1973, pp163-189

125. B. L. Misell, "Practical Methods in Electron Microscopy", Vol. 7, A. M. Glauert, ed., North-Holland Publishing Company, New York, 1978

126. E. L. Thomas and E. J. Roche, Polymer, **20**, 1413(1979)

127. E. J. Roche and E. L. Thomas, Polymer, **22**, 333(1981)

128. E. L. Thomas, in "Structure of Crystalline Polymers", H. I. Hall, ed., Elservier Applied Science Publishers, New York, 1984, pp 79-124

129. R. E. Burge and G. H. Smith, Proc. Phys. Soc., **79**, 673(1962)

130. H. P. Erikson and A. Klug, Phil. Trans. Roy. Soc. London, **B 261**, 105(1971)

131. J. A. Ibers, D. H. Templeton, B. K. Vainshtein, G. E. Bacon, and K. Lonsdale, in "International Tables for X-ray Crystallography", Vol. III, 201(1962)

132. C. L. Marx, J. A. Koutsky, and S. L. Cooper, J. Polym. Sci. Polym. letters, **9**, 167(1971)

133. M. Pineri and A. Eisenberg, ed., "Structure and Properties of Ionomers", NATO ASI Ser., D. Reidel Publishing Company, Dordrecht, 1987. pp453-456

134. G. Broze, T. Jerome, Ph. Teyssie, and b. Gallo, J. Polym. Sci. Polym. Letters, **19**, 415(1981)

135. E. L. Thomas, in "Encyclopedia of Polymer Science and Engineering", 2nd ed., John Wiley & Sons, N.Y., 1987, pp644-687

136. S. Yamashita, M. Itoi, S. Kohjiya, and A. Kidera, J. of Applied Polym. Sci., **35**, 1927(1988)

137. N. Sasaki and T. Yokoyama, Kobunshi Ronbunshu, **44**(12), 867(1987)

138. J. J. Aklonis and W. J. MacKnight, "Introduction to Polymer Viscoelasticity", 2nd Ed., John Wiley and Sons, New York, 1983, pp189-211

139. L. E. Nielsen, "Mechanical Properties of Polymers", Reinhold, New York, 1962, p. 178

140. N. G. McCrum, B. E. Read, and G. Williams, "Anelastic and Dielectric Effects in Polymeric Solids", John Wiley & Sons, New York 1967, pp 561-565

Appendix A

Estimation of the volume percentage occupied by the ionene domains.

The volume fraction of ionene domains in IB-NS-18 has been estimated by assuming the hexagonal packed rod-like domains or the lamellar domains. In these estimations, the length of the domains is assumed to be the same as the height of the unit volume. Other parameters used for the estimation of the volume percentage of ionene domains in IB-NS-18 ionene are defined as following:

d = interdomain spacing

D = domain size (diameter of domain or lamellar thickness) which is assumed to be the length of an ionene unit.

L^2 = unit area which is defined as $L^2 = (10d)^2$

V = unit volume which equals to L^2H

H = height of unit volume

V_h = volume of an ionene domain

f_h = volume fraction of ionene domains

n = number of rods or lamellae per unit volume

n = 126 for hexagonal packed rod-like domains in a unit area

n = 10 for lamellar domains in a unit area

For hexagonal packed domains:

$$f_h = \frac{V_h n}{V} = \frac{\pi/4 D^2 nH}{L^2 H}$$

For lamellar domains:

$$f_h = \frac{V_h n}{V} = \frac{DLHn}{L^2 H}$$

The calculation results are listed in the following table.

Ionene Domain Size	Ionene Domain Vol%	
nm	Hexagonal	Lamellar
1.1	2.8	16.9
1.5	5.3	23.1

The vita has been removed from the scanned document